CLASS I MAJOR HISTOCOMPATIBILITY COMPLEX RESTRICTED EPITOPES IN
ONCOLYTIC VIRUS INFECTION AND THERAPY

by

Youra Kim

Submitted in partial fulfilment of the requirements
for the degree of Doctor of Philosophy

at

Dalhousie University
Halifax, Nova Scotia
August 2021

TABLE OF CONTENTS

LIST OF TABLES

LIST OF FIGURES

ABSTRACT

Cancer immunotherapies (re)educate the body's natural defenses to recognize and attack malignant cells. The consequent anti-tumor immunity is highly specific, long-lasting, and often dependent on CD8 T cells, the presence of which in the tumor microenvironment correlates with a favorable cancer prognosis. CD8 T cell activity requires T cell receptor-mediated recognition of antigenic peptides (i.e., epitopes) bound to class I major histocompatibility complex (MHC-I). The sequences of the MHC-I-bound peptides can be used to study cognate, antigen-specific T cells or design peptide vaccines to develop immunity against certain epitopes. However, despite recognizing the important role of CD8 T cells in immunotherapies, the identities of the epitopes dictating anti-tumor CD8 T cell responses have remained largely elusive.

This thesis aims to address this knowledge gap by elucidating the MHC-I-restricted epitopes in the context of an oncolytic virus (OV)-based cancer immunotherapy. In addition to their direct tumor-destructive effects, OVs activate anti-tumor CD8 T cells and overturn tumor-associated immune evasion mechanisms. OV-mediated increase in tumor MHC-I expression is of particular relevance to this thesis and lays the foundation for our pursuit of discovering therapy-modulated MHC-I-bound peptides that direct anti-tumor immunity.

In this work, the latest advances in mass spectrometry were utilized to investigate the array of tumor MHC-I-bound peptides (i.e., MHC-I peptidome) following oncolytic reovirus treatment, either as a monotherapy or as a combination therapy with immune checkpoint blockade. Within the therapy-modulated MHC-I peptidome, immunogenic epitopes were identified and administered as peptide vaccines to enhance OV efficacy. Furthermore, an immunoinformatics approach was used to discover MHC-I-restricted epitopes of reovirus and the corresponding anti-viral CD8 T cells were characterized. These viral epitopes were then used to antigenically reprogram the tumor MHC-I peptidome, resulting in viral peptide-presenting cancer cells as targets of anti-viral CD8 T cells, for the repurposing of anti-viral immunity. Overall, the elucidation of the MHC-I-restricted epitopes of tumors and reovirus provided an insight on the anti-tumor and anti-viral CD8 T cell responses during reovirus administration, and yielded information that can be exploited to further potentiate CD8 T cell immunity of OV therapy.

LIST OF ABBREVIATIONS AND SYMBOLS USED

7AAD	7-amino-actinomycin D
α	Alpha
ACK	Ammonium-chloride-potassium
ACN	Acetonitrile
ACT	Adoptive cell transfer
Ad	Adenovirus
ANN	Artificial neural network
ANOVA	Analysis of variance
APC	Antigen-presenting cell
ATP	Adenosine triphosphate
β	Beta
B2M	β_2 microglobulin
BCR	B cell receptor
BiTE	Bispecific T-cell engager
BP	Biological process
BSA	Bovine serum albumin
CALR	Calreticulin
CAR	Coxsackievirus and adenovirus receptor
CAR-T	Chimeric antigen receptor T cell
CCAC	Canadian Council on Animal Care
CCL	Chemokine (C-C) motif ligand
CD	Cluster of differentiation
cDNA	Complementary DNA
CEA	Carcinoembryonic antigen
CNBr	Cyanogen bromide
ConA	Concanavalin A
C_T	Cycle threshold
CTL	Cytotoxic T lymphocyte
CTLA-4	Cytotoxic T-lymphocyte associated protein 4

Ctrl	Control
CTV	CellTrace Violet
CXCL	Chemokine (C-X-C) motif ligand
°C	Degrees Celsius
d	Day
d.p.i.	Days post infection/injection
Da	Dalton
DAF	Decay accelerating factor
DAMP	Damage-associated molecular pattern
DC	Dendritic cell
DCT	Dopachrome tautomerase
DEMHCP	Differentially expressed MHC-I-associated peptide
DMSO	Dimethyl sulfoxide
DNA	Deoxyribonucleic acid
DRiPs	Defective ribosomal products
dsRNA	Double-stranded RNA
e.g.	For example
E1A	Early region 1A protein
EC	Endothelial cell
ECM	Extracellular matrix
EGFR	Epidermal growth factor receptor
ELISA	Enzyme-linked immunosorbent assay
ER	Endoplasmic reticulum
ERAD	ER-associated protein degradation
ERAP	ER aminopeptidase
ERK2	Extracellular signal-regulated kinase 2
FACS	Fluorescence-activated cell sorting
FBS	Fetal bovine serum
FcγR	Fc gamma receptor
FDA	Food and Drug Administration
FDR	False discovery rate

γ	Gamma
g	Gram
xg	gravity
GITR	Glucocorticoid-induced TNFR family-related gene
GM-CSF	Granulocyte-macrophage colony-stimulating factor
GO	Gene ontology
gp100	Glycoprotein 100
GPI	Glycosylphosphatidylinositol
GzmB	Granzyme B
h	Hour
HER2/neu	Human epidermal growth factor receptor 2
HLA	Human leukocyte antigen
HMGB1	High mobility group box 1
HPV	Human papillomavirus
HRP	Horseradish peroxidase
HSV	Herpes simplex virus
HVEM	Herpesvirus entry mediator
i.e.	In other words
i.p.	Intraperitoneal
i.t.	Intratumoral
IAC	Immuno-affinity chromatography
ICAM-1	Intercellular adhesion molecule 1
ICB	Immune checkpoint blockade
ICD	Immunogenic cell death
ICI	Immune checkpoint inhibitor
ICOS	Inducible co-stimulator
ICOSL	ICOS ligand
ICS	Intracellular cytokine stain
IFN	Interferon
IL	Interleukin
IP	Immuno-precipitation

iPDL1	PD-L1 inhibitor (soluble PD-1 extracellular domain fused with immunoglobulin G1 Fc fragment)
irAEs	Immune-related adverse events
ISG	Interferon-stimulated gene
ISO	Isotype control antibody
ITIM	Immunoreceptor tyrosine-based inhibitory motif
JAK	Janus kinase
JAM-A	Junctional adhesion molecule A
kDa	Kilodalton
KLH	Keyhole limpet hemocyanin
KLRG1	Killer cell lectin-like receptor G1
L	Liter
LAG-3	Lymphocyte activation gene-3
LC	Liquid chromatography
LCMV	Lymphocytic choriomeningitis virus
LDLR	Low-density lipoprotein receptor
LFQ	Label-free quantitation
μg	Microgram
μL	Microliter
MAE	Mild acid elution
MAGE-A1	Melanoma-associated antigen A1
MCP-1	Monocyte chemoattractant protein-1
MDSC	Myeloid-derived suppressor cell
MFI	Mean fluorescence intensity
mg	Milligram
MHC	Major histocompatibility complex
MHC-I	Class I MHC
min	Minutes
mL	Milliliter
mm	Millimeter
mM	Millimolar

MMR	Measles-mumps-rubella
MOI	Multiplicity of infection
MOSE	Mouse ovarian surface epithelial
mRNA	Messenger RNA
MS	Mass spectrometry
MS/MS	Tandem MS
MV	Measles virus
N	Normality (equivalent per liter)
NAb	Neutralizing antibody
NDV	Newcastle disease virus
NFκB	Nuclear factor kappa-light-chain-enhancer of activated B cells
NK	Natural killer
nm	Nanometer
NT	Non-treated
OV	Oncolytic virus
OVA	Ovalbumin peptide (SIINFEKL)
%	Percent
PAMP	Pathogen-associated molecular pattern
PBMC	Peripheral blood mononuclear cell
PBS	Phosphate-buffered saline
PD	Protein Discoverer
PD-1	Programmed cell death protein 1
PD-L1	Programmed death-ligand 1
PEG	Polyethylene glycol
PEP	Peptide
PeptiCRAd	Peptide-coated conditionally replicating adenovirus
PFA	Paraformaldehyde
PFU	Plaque-forming unit
pg	Picogram
PKR	Protein kinase R
PLC	Peptide-loading complex

pMHC	Peptide-MHC
ppm	Parts per million
Pro-A	Protein-A
PRR	Pattern recognition receptor
PSFM	Position-specific frequency matrices
PSM	Peptide spectrum match
REO	Reovirus
REO-IMM	Reovirus-immunized
RIG-I	Retinoic acid-inducible gene I
RNA	Ribonucleic acid
RT	Room temperature
RT-qPCR	Real-time quantitative polymerase chain reaction
σ	Sigma
s	Second
s.c.	Subcutaneous
S/N	Signal to noise
scFv	Single-chain variable fragment
SD	Standard deviation
SPE	Solid phase extraction
SPS-MS3	Synchronous precursor selection with three-stage MS
STAT	Signal transducer and activator of transcription
TAA	Tumor-associated antigen
TAM	Tumor-associated macrophage
TAP	Transporters associated with antigen processing
TB	Tumor-bearing
T_{CM}	Central memory T cell
TCR	T cell receptor
T_{EM}	Effector memory T cell
TFA	Trifluoroacetic acid
TGF	Transforming growth factor
Th	T helper

TIGIT	T cell immunoglobulin and ITIM domain
TIL	Tumor-infiltrating lymphocyte
TIM3	T cell immunoglobulin and mucin-domain containing-3
TLR	Toll-like receptor
TME	Tumor microenvironment
TMT	Tandem mass tag
T_N	Naïve T cell
TNBC	Triple-negative breast cancer
TNF	Tumor necrosis factor
TNFR	TNF receptor
TRAIL	TNF-related apoptosis-inducing ligand
Tregs	Regulatory T cells
TRP-2	Tyrosinase-related protein 2
TSA	Tumor-specific antigen
T-Vec	Talimogene laherparepvec
U	Unit
U.S.	United States
UCLA	University Committee on Laboratory Animals
VEGF	Vascular endothelial growth factor
VEGFR	VEGF receptor
VISTA	V-domain Ig suppressor of T cell activation
vol	Volume
VSV	Vesicular stomatitis virus
VV	Vaccinia virus
WES	Whole exome sequencing
$\leq$	Less than or equal to
$\geq$	Greater than or equal to

ACKNOWLEDGEMENTS

"Good things happen in your life when you surround yourself with positive people."
– Roy T. Bennett

When I reflect on my blessings, I know I could not have achieved all that I've done without the support of the amazing people in my life. First and foremost, I would like to thank my supervisor, Dr. Shashi Gujar. Your faith in me and accepting me as a student (even though I had absolutely ZERO immunology background) truly changed my life. Thank you for your unwavering support and all the opportunities you've provided to help foster my growth as an academic. I have a tremendous amount of respect for you as a mentor and scientist, and I'm grateful for all that you've taught me and will continue to teach me. I've still got a lot to learn, and I look forward to our future endeavours.

I'm also grateful to my supervisory committee members, Drs. David Waisman, Jun Wang, and Paola Marcato, for your guidance, support, and insightful comments and questions. My eagerness to impress you all kept me on my toes and motivated me. I would also like to thank Dr. Patrick Lee who always awed me with his scientific mind. Your enthusiasm for research was truly infectious.

Thank you to my friends and colleagues who made Halifax feel like a second home. You've provided me with good times both in and outside the lab, and I appreciate you all teaching me how to be a better team player. Thank you for getting me to come out of my shell and giving me some of the best experiences of my late 20s. To my beloved family, I appreciate your patience and support for the past seven years. Thank you for being my pillar of strength and getting me through this chapter of my life. I hope I made you all proud.

CHAPTER 1: INTRODUCTION

Certain viruses exhibit a tropism for malignant cells and cause cancer cell lysis, a process termed oncolysis[1]. Reports of naturally acquired viral infections leading to tumor regression date back to the mid 1800s and much progress has been made in the field of oncolytic virus (OV) therapy over the past century[2], culminating in the approval of talimogene laherparepvec (T-Vec; herpes simplex virus type 1) for the treatment of melanoma by the U.S. Food and Drug Administration (FDA) in 2015[3]. OVs can be naturally tumor selective, owing to defective signaling pathways in tumors that make them susceptible to viral infections, or engineered to discriminately target cancer cells[1,4,5]. As such, the main advantage of OV therapy, compared to conventional cancer treatments like chemotherapy and radiation, is the assured specificity against tumors with minimal damage to healthy cells[6,7]. The highly favorable safety profiles of OVs also make them promising candidates for combination therapies[8–10]. Furthermore, mounting preclinical and clinical evidence support the role of the immune system during OV therapy, with cytotoxic and immunostimulatory activities of OVs promoting immune-mediated tumor eradication[1,11,12]. The modulation of the tumor immune microenvironment by OVs is key to the generation of anti-tumor immunity which provides a highly specific, long-term protection against cancer at both local and distant sites. To this end, all three fields of virology, cancer biology, and immunology in the context of OVs must be studied for the effective application of this multifaceted therapeutic platform. The following subchapters will provide a comprehensive overview of these topics, building up to the overarching objective of this thesis: the identification and characterization of the immunogenic signals of oncolytic reovirus infection and therapy. Taken together, this work aimed to further our

understanding of both anti-tumor and anti-viral immune responses during oncolytic reovirus therapy, specifically in terms of class I major histocompatibility complex (MHC-I)-restricted epitopes for CD8 T cell activity.

1.1 FACTORS TO CONSIDER IN CHOOSING THE OPTIMAL OV THERAPY

Over the past 150 years, numerous viruses have been studied for their oncolytic potential and the list continues to grow[2]. Observations of virus-induced cancer remissions led scientists to postulate that certain viruses can destroy tumors but only under the right circumstances (i.e., in patients with compromised immune systems) and for a short-lived remission[2]. Thus, during the 1950s and 1960s when there were tremendous advances made in the field of virology, a renewed interest in viruses as oncolytic agents and the pursuit to find the ideal OV were cultivated[2]. The most extensively researched OVs include adenovirus (Ad), herpes simplex virus (HSV), measles virus (MV), vesicular stomatitis virus (VSV), Newcastle disease virus (NDV), and reovirus, all of which are under various stages of clinical investigation[1,13]. While there is no one perfect OV, the most optimal OV for a particular therapeutic application must be sought after in a context-dependent manner.

1.1.1 Biosafety of OV Therapy

One of the most important factors to assess during OV administration is safety – to protect against uncontrolled replication, damage to healthy tissues, and shedding and transmission[6,7]. Such consideration was lacking in early clinical studies where sera or tissue extracts from patients with ongoing hepatitis infection were used to treat patients with Hodgkin's disease, some of whom succumbed to viral hepatitis[2]. With more stringent ethical standards nowadays, typically just mild flu-like symptoms are observed as adverse events. Severe adverse events have been observed but were fortunately rare occurrences

and not life-threatening[6]. For instance, oncolytic HSV caused hypotension, tachycardia, and encephalitis[14,15], and Ad caused pleural effusion and liver dysfunction in clinical trials[16]; but these severe adverse events were managed by withdrawal of OV treatment. Further measures taken to ensure safety include the use of viruses with no or low pathogenicity in humans. These can be viruses that have natural hosts in animals other than humans, such as rat parvovirus[17], or viruses that are attenuated by serial passage in cultured cells, such as HSV[18]. In addition, genetic modifications of OVs can be used to further attenuate pathogenicity, increasing their oncolytic potential by enhancing their specificity for tumors. Deletion of virulence genes, such as ICP-34.5 in HSV[19] or thymidine kinase in vaccinia virus (VV)[20], results in replication-selective viruses that target malignant cells. Viruses with large genomes are more amenable to genetic manipulation, albeit at the cost of replication speed, for not only targeting modifications but also the expression of immunomodulatory factors[1], which will be discussed in more detail below.

Biosafety, as well as therapeutic efficacy, will also depend on the dosage of the virus. Due to their replicative potential, OVs can proliferate upon administration which can produce variability in effective doses[1]. Thus, small doses may be sufficient in providing significant results and avoid dose-limiting toxicity. In fact, high viral doses carry the risk of viral shedding and transmission. Shedding viruses have been detected in the serum, urine, and saliva of patients treated with high doses of Ad, HSV, or reovirus[6,16,21]. Fortunately, viral shedding was observed in just a few limited cases and with highly attenuated viruses, so infection control issue was not a cause for concern. Overall, OV therapy is generally safe with only rare reports of severe adverse events, owing to breakthroughs in recombinant

DNA technology, but there is still much to be investigated before OVs can be widely applied as an anti-cancer therapeutic.

1.1.2 OV Delivery Platform

Like any standard anti-cancer drug, the pharmacokinetics of OVs must be evaluated for effective administration in clinics[1,4]. Pharmacokinetics, referring to the movement of the virus through the body, will greatly depend on the route of infection. The three most common methods of OV administration are intratumoral, intravenous, and intraperitoneal deliveries[4,6]. When OVs are directly injected into tumors, the concentration of OVs at the tumor site can be precisely controlled and less off-target effects will be observed[6,22]. However, the complex procedure of intratumoral delivery creates challenges for accessing deep tumors and repeat dosing. For intravenous delivery, OVs are injected into the peripheral vein and travel to the target site via the circulatory system. This convenient and rapid administration route is advantageous in targeting tumor metastases[23], and it has even been recently shown that some intravenously delivered OVs can bypass the blood-brain barrier and reach central nervous system tumors[24]. The widespread viral dissemination following intravenous delivery, however, requires OVs to be highly tumor-selective. Elimination of OVs by host anti-viral immune responses involving pre-existing neutralizing antibodies (NAb) or virus-specific memory T cells is another concern with intravenous administration[25] (discussed further in *Chapter 1.4*). For intraperitoneal delivery, injection of OVs into the peritoneal cavity will lead to OVs being absorbed by the veins in the peritoneum to enter the circulatory system, though at a slower rate than through intravenous injection, or directly target tumors in the abdominal cavity[6]. Although it is relatively easy to administer, intraperitoneal delivery is used less frequently in clinics

and is rather limited to animal studies. Ultimately, the choice of delivery route will depend on the type and location of the tumor.

As suboptimal delivery would reduce therapeutic efficacy, various strategies can be employed to circumvent barriers to virus dissemination[25,26]. These are particularly important for systemic therapy where naked purified virions in the bloodstream are vulnerable to host defense mechanisms. One of the simplest methods to achieve better propagation is repeat dosing[6,13,27]. A single shot of OV is highly unlikely to result in complete therapeutic efficacy, so a long-term repeat dosing regimen is required, as is the case with any anti-cancer treatment. While the administration of multiple doses of virus may trigger a stronger anti-viral immune response, certain viruses have naturally adapted strategies to evade immune detection, such as through cell carriage by blood cells that protects against NAb[28,29]. Similarly, the same strategy can be exploited in the laboratory where carrier cells are infected *in vitro* with OVs and then systemically injected. Cells that have been used in this "Trojan horse" delivery approach include T cells for MV[30], cytokine-induced killer cells for VV[31], teratocarcinoma cells for HSV[32], an immortalized monocyte cell line for MV[33], and mesenchymal progenitor cells for Ad[34]. Of note, immortalized cell lines must be treated with γ-irradiation to ablate tumorigenicity. Furthermore, chemical modification strategies can be used to shield OVs from neutralizing immunity[25,35]. OVs can be camouflaged from immune surveillance through viral surface modifications with polyethylene glycol (PEG) or charged polymers, or packaging in nanoparticles or liposomes, prolonging blood circulation time and increasing cellular uptake by cancer cells[25]. The final hurdle that systemically delivered-OVs must overcome to access tumors is the layer of blood vessel endothelium and extracellular matrix (ECM)[1]. Virus penetration

can be aided by pre-treatment with vasoactive compounds (e.g., histamine or nitroglycerin) or proteolytic enzymes (e.g., hyaluronidase or collagenase)[36–38]. Genetic modification can also be used to engineer OVs to express ECM-degrading enzymes[39]. All in all, therapeutic efficacy of OVs is highly dependent on efficient delivery, which is contingent on administration route, dose, and use of carrier cells or sheathing agents.

1.1.3 OV Tumor Cell Entry Mechanisms

OVs exhibit specific cell entry mechanisms and tropism toward cancer cells. The interaction between cancer cellular receptors and virus surface proteins determines how different OVs recognize and enter particular cancer cells[1,40,41]. For example, VSV G glycoprotein (VSV-G) binds low-density lipoprotein receptor (LDLR), and then the VSV-G/LDLR complex gets internalized via clathrin-mediated endocytosis[42,43]. An OV can also have multiple virus-receptor associations that occur over several steps to facilitate entry. For instance, the lower part of reovirus sigma-1, an outer capsid protein, first binds to cell surface monosaccharides like sialic acid in a low-affinity interaction; then, the head of sigma-1 binds to junctional adhesion molecule A (JAM-A) in a high-affinity attachment, continuing on to clathrin-mediated endocytosis[44,45]. HSV glycoprotein gB binds heparan sulfate proteoglycans and HSV glycoprotein gD binds nectin or herpesvirus entry mediator (HVEM), ultimately resulting in envelope fusion with host plasma membrane[40,46,47]. For Ad, the viral fiber knob binds coxsackievirus and adenovirus receptor (CAR) for the initial attachment, followed by endocytosis of the Ad-CAR complex involving other capsid proteins and integrins[48]. Furthermore, a particular OV can utilize multiple entry mechanisms depending on host cell type. It was recently determined that reovirus penetrates neurons via macropinocytosis as opposed to clathrin-dependent endocytosis

required for the infection of non-neuronal cells[49]. This cell type-specific entry mechanism emphasizes the need to understand virus entry in order to tailor OVs to better target cancer cells. It is important to note that the abovementioned cellular receptors are expressed on not only cancer cells but also normal cells. Normal cells, however, have intact anti-viral mechanisms that would clear the virus; while aberrant expression of oncogenes and tumor suppressor genes, as well as defective anti-viral responses, in cancer cells favor OV replication[1,40]. The tendency for these receptors to be overexpressed by cancer cells also drives the selectivity of OVs towards certain tumor types. For example, HVEM and nectin are highly expressed by melanoma and carcinoma cells, thereby making these tumor types more suitable for HSV treatment[50,51]. Likewise, intercellular adhesion molecule 1 (ICAM-1) and decay accelerating factor (DAF), used by coxsackievirus for internalization, are overexpressed by multiple myeloma, melanoma, and breast cancer cells[52–54]. In sum, the interaction between OV surface proteins and tumor cellular receptors mediate virus attachment and internalization by cancer cells, in a manner which is unique to each OV and critical in determining tumor-specific tropism.

1.2   MECHANISMS OF OV ACTION

There are at least three major mechanisms through which OVs mediate tumor eradication: direct oncolysis, vascular collapse, and anti-tumor immunity (Figure 1.1)[1,5,55]. Virus infection of cancer cells with subsequent oncolysis is a direct cytotoxic effect of OVs. On the other hand, destruction of vascular supply and immune cell recruitment and activation are indirect anti-tumor activities of OVs. Direct oncolysis was initially thought to be the only anti-tumor mechanism of OVs but it has become abundantly clear that anti-tumor immunity is an indispensable aspect of OV therapeutic efficacy, resulting in a paradigm

shift from oncolytic virotherapy to oncolytic virus immunotherapy[56]. The multimodal approach of OVs to target and destroy malignant cells will be reviewed in this subchapter.

1.2.1 Oncolysis

Whether it is a cancer cell or a healthy cell, host cell lysis is a common outcome of viral infection[57]. Once replication and assembly are completed, progeny virions are released from the host cell through budding or lysis, which are processes that kill the cell by slowly consuming or bursting the cell membrane, respectively[58]. Unlike healthy cells which possess functional anti-viral mechanisms that clear the virus, cancer cells have aberrant signaling pathways that fail to prevent virus-induced cell death[1]. The expression of oncogenes or loss of tumor suppressor genes that leads to elevated metabolism, dysregulation of cell cycle and sustained proliferation in cancer cells (classic hallmarks of cancer[59]) creates a niche which is conducive to viral replication and is often intricately linked to anti-viral mechanisms[60,61]. For instance, Ras GTPases, the mutated forms of which are overexpressed in 20-30% of human cancers[62], support viral protein synthesis by blocking protein kinase R (PKR), which is a negative regulator of viral gene translation[63,64]. Enhanced replication of oncolytic HSV[65], NDV[66], VSV[67], Ad[68], and reovirus[69] has been attributed to Ras signaling. Moreover, Ras transformation can also lead to defects in anti-viral cytokine, type I interferon (IFN), production and response[70,71], thereby allowing efficient viral spread. Activation of the Raf/MEK/ERK signaling cascade, one of the downstream pathways of Ras, downregulates type I IFN expression via inhibition of a viral RNA sensor called retinoic acid-inducible gene I (RIG-I)[72]. Since IFN and IFN-responsive genes oppose cancer cell growth – by inhibiting angiogenesis[73], inducing apoptosis[74], and stimulating immune responses[75] – it is no surprise that 65-70% of malignant cells have

impaired IFN signaling that renders them more susceptible to OV infection compared to normal cells[8,61,76].

Following productive viral replication, there are several modes of cancer cell death that can be induced[77,78]. These include apoptosis, necrosis, necroptosis, autophagic cell death, and pyroptosis[78]. Apoptosis is the process of programmed cell death characterized by membrane blebbing, chromatin condensation, and nuclear fragmentation; and it is regulated by proteases called caspases in a complex reaction cascade. Necrosis is accompanied by membrane rupture and leakage of intracellular contents, while necroptosis is a programmed form of necrosis that occurs in a regulated manner. Autophagy is a catabolic mechanism that degrades and recycles unnecessary or dysfunctional cellular components via the lysosomal machinery; elevated levels of autophagy can result in cell death. Pyroptosis is a caspase-1 dependent inflammatory form of programmed cell death. Each OV will induce primarily one form of cancer cell death[77]. For example, Ad has been reported to result in autophagic cell death in glioma cells[79] and HSV-2 causes pyroptosis in melanoma cells[80]. However, some OVs can also instigate multiple modes of cancer cell death, such as the concurrent induction of apoptosis and autophagy by NDV[81] and reovirus[82]. Specific genes encoded by the virus will dictate the type of cell death induced[77]. For instance, the early region 1A (E1A) protein of Ad type 5 promotes an accumulation of p53 and thus induces apoptosis[83]. Similarly, viruses can be genetically modified to express death pathway-modulating genes, which has been demonstrated with VV encoding apoptosis-inducing protein apoptin[84] or Ad expressing TNF-related apoptosis-inducing ligand (TRAIL)[85]. Knowing the mode of OV-induced cancer cell death is useful in determining which OV would be appropriate to target a particular type of malignancy; for

example, OVs that trigger necroptosis may be better suited to treat apoptosis-resistant cancers[77]. With the ultimate goal of cancer cell death in mind, it is pertinent to understand the mechanism through which OVs kill malignant cells to develop strategies to potentiate this effect.

1.2.2   Vascular Collapse

Due to tumor-mediated angiogenesis that ensures blood supply to support tumor progression and eventually metastasis, targeting the tumor vasculature with OVs has increasingly become an area of interest[86]. OVs can cause anti-vascular effects through three mechanisms: infection of tumor endothelial cells (ECs), immune response that results in clot formation, and expression of anti-angiogenic factors[8,86,87]. ECs line all blood vessels, but OVs such as VV and VSV have been shown to specifically infect and lyse tumor ECs without harming the normal vasculature[88,89]. While the exact mechanism for this tropism is unknown, the elevated proliferation rate of tumor ECs may explain the increased support for viral replication. In addition, viral infection can cause a neutrophil response, triggering clot formation that leads to ischemic cancer cell death[90,91]. This type of vascular disruption has been demonstrated with VSV where the virus not only directly infected and killed tumor ECs but also induced intratumoral coagulation via neutrophils, which express elastase and cathepsin G that promote fibrin deposition[88,92]. Lastly, OVs can express anti-angiogenic factors either naturally or through genetic engineering. Some viral proteins may cause a downregulation of angiogenic proteins and cytokines; for example, Ad E1A protein interacts with p300, a transcriptional co-activator of hypoxia-inducible factor 1 alpha, and inhibits the synthesis of vascular endothelial growth factor (VEGF)[93]. Genetic manipulation allows certain OVs to carry and deliver anti-angiogenic factors. Ad

expressing soluble VEGF receptor (VEGFR)[94], as well as VV encoding VEGFR-1-Ig fusion protein[95], that binds VEGF was effective in decreasing mean vessel density and tumor volume. Similar results were demonstrated with Ad expressing short hairpin RNA against interleukin (IL)-8[96], a cytokine that promotes EC proliferation and survival, and HSV encoding endostatin and angiostatin[97], which are angiogenesis inhibitors. Such anti-vascular agents can also be applied in conjunction with OVs as a combination therapy, which has been shown with HSV and copper chelator ATN-224[98] or reovirus and VEGFR inhibitor sunitinib[99]. Of note, some viruses express pro-angiogenic factors to support virus replication and spread, as exemplified by parapoxvirus which encodes a homolog of VEGF[100]. Viral genes that encode or upregulate the expression of angiogenic factors should be deleted before these viruses are used as oncolytic agents. On the whole, the principles that govern the advantages of using OVs to target tumors (i.e., specificity, expression of virus-encoded proteins, induction of immune response) also apply for the tumor vasculature, and limiting tumor perfusion via OV-mediated anti-vascular effects provides an effective means to inhibit tumor progression.

1.2.3   *Anti-tumor Immunity*

From first being proposed in 1909 by Paul Ehrlich, immunologic control of neoplasia has become a firmly established principle in oncology[101]. According to the cancer immunoediting hypothesis, the dynamic relationship between the immune system and tumors involves three phases: elimination, equilibrium, and escape[101]. The immune system recognizes and eliminates tumor cells; however, some tumor cell variants with low immunogenicity may evade immune detection, enter a period of latency, and eventually give rise to an outgrowth of malignant cells that have escaped immunological restraints.

Thus, it is pertinent to recognize the role of the immune system throughout tumor development, and accordingly, immune cells are an important component of the tumor microenvironment (TME)[102]. The TME, which is composed of not only cancer cells and immune cells but also vascular ECs, cancer-associated fibroblasts, extracellular matrix, and secreted factors, can be grouped based on immune status as inflamed tumors (presence of immune cell infiltrate), immune-excluded tumors (immune cells stuck in the surrounding stroma), and immune deserts (devoid of immune cell infiltrate)[102]. Further mutations and selective pressures drive the emergence of tumor-mediated immunosuppressive mechanisms such as the secretion of anti-inflammatory cytokines (e.g., IL-10, transforming growth factor beta [TGFβ]) or recruitment of immunosuppressive immune cells (e.g., myeloid-derived suppressor cells [MDSCs], tumor-associated macrophages [TAMs], regulatory T cells [Tregs])[101,103–105]. OVs overturn this tumor-associated immunosuppression and mediate a 'cold-to-hot' tumor modulation, promoting the generation of anti-tumor immune responses[106,107]. The specific mechanisms through which OVs achieve this feat and cancer eradication from the resultant anti-tumor immunity will be explored in this subchapter.

1.2.3.1 OV-mediated Innate Immune Responses

The first line of defense against infections is the innate immune system, comprised of chemical/physical barriers, complement cascade, and inflammatory response mediated by white blood cells[108,109]. Despite being oncolytic agents, OVs are nonetheless pathogens and will trigger an innate immune response directed against the virus. Depending on the kinetics and strength of these responses, innate immunity can be detrimental or beneficial to the efficacy of OV therapy[11,110,111]. Since OVs selectively replicate in tumors, the

ensuing immune responses alter the cytokine milieu and immune cell composition within the TME, contributing to the establishment of anti-tumor immunity. Innate immunity is triggered upon the recognition of pathogen-associated molecular patterns (PAMPs) by surface or intracellular host pattern recognition receptors (PRRs) of tissue-resident immune cells, resulting in the induction of cytokine production and the recruitment of innate immune cells (e.g., neutrophils, granulocytes, natural killer [NK] cells, antigen-presenting cells [APCs])[112]. One of the key cytokines produced in response to viral infection is type I IFNs, IFNα and IFNβ, which establish an anti-viral state and limit viral spread[108]. Following type I IFN exposure, NK cells produce and secrete IFNγ which inhibits angiogenesis and induces apoptosis; and dendritic cells (DCs) upregulate the expression of class I MHC molecules and co-stimulatory molecules for more effective antigen presentation[75]. Secretion of other pro-inflammatory cytokines (e.g., IL-1β, IL-6, IL-12, tumor necrosis factor alpha [TNFα]) by innate immune cells not only initiates vascular and cellular reactions of inflammation but also makes the TME less immunosuppressive[108].

The newly recruited innate immune cells also contribute to the reversion of tumor-associated immunosuppression and carry out direct anti-tumor effects[107]. Neutrophil infiltration of OV-treated tumors (e.g., VSV-treated colorectal CT26 tumors[88]) has been demonstrated and as mentioned above, leads to neutrophil-mediated tumor vasculature collapse and subsequent ischemic cancer cell death[90,91]. Direct cytolytic activity of infiltrating neutrophils has also been shown where neutrophils isolated from HSV-2 (FusOn-H2)-treated EC9706 esophageal squamous cell carcinoma killed cancer cells *ex vivo* more effectively than neutrophils harvested from untreated tumors[91]. Moreover, NK cells play a prominent role in the elimination of virus-infected cells and cancer cells; and

are thus, unsurprisingly, crucial for the success of OV therapy[113]. Various studies support OV-mediated recruitment of NK cells into the TME, such as reovirus-treated prostate tumors[114], coxsackievirus B3-treated lung adenocarcinomas[115], and MV-treated gliomas[116]. Augmented cytolytic activity of NK cells has also been demonstrated in the context of OV infection. For instance, higher levels of IFNγ and TNFα were produced by NDV-stimulated NK cells, which then effectively lysed NDV-infected tumor cells[117]. Similar results were observed with H-1 parvovirus and pancreatic ductal adenocarcinoma and colon carcinoma cells[118,119]. In addition, there is ample evidence of crosstalk between NK cells and DCs that mediates innate and adaptive anti-tumor immune responses in OV therapy[113]. The interaction between OV-infected tumor cells, NK cells, and DCs was shown with reovirus where DCs primed with reovirus-infected melanoma lysates (DC-MelReo) released type I IFNs and induced NK cell cytotoxicity more efficiently as compared to NK cells stimulated with reovirus-infected tumor cells[120]. Direct infection of DCs by OVs (e.g., Maraba virus MG1) can also cause DC maturation and strengthen NK cell-activating capacity[121]. Furthermore, OV-modulated changes in DC function can have their own implications. As specialized APCs with notable roles in the initiation and regulation of innate and adaptive immune responses, DCs are indispensable for the development of OV-mediated anti-tumor immunity[122]. OV-driven accumulation, activation/maturation, and increased co-stimulatory molecule expression of DCs contribute to enhanced DC function and subsequent anti-tumor immune responses[122]. Macrophages are another type of innate immune cells which can be modulated by OVs. Broadly classified as either classically activated M1 or alternatively activated M2 macrophages that display pro-inflammatory or suppressive/regulatory phenotypes, respectively,

macrophages serve a wide range of functions and are one of the most prevalent cell types in the TME[123]. TAMs have an M2 phenotype, but due to the plastic nature of macrophage polarization, TAMs can adopt an M1 phenotype with tumoricidal functions in response to changing environmental conditions like viral infections. Such 're-education' of TAMs by OVs was evident following treatment of mammary carcinomas 4T1 and TSA, as well as colon carcinoma MC38, with Ad expressing chemokine (C-C motif) ligand (CCL)-16 in combination with toll-like receptor (TLR)-9 ligand CpG and anti-IL-10 receptor antibody[124]. OVs can also promote the recruitment of M1 macrophages, the presence of which in the TME correlates with effective anti-tumor immune responses, that perform tumoricidal activity via nitric oxide and TNFα or phagocytosis[125]. Ultimately, through the action of various innate immune cells, anti-tumor immune responses can be rapidly initiated at early stages of OV therapy, not only directly eradicating cancer cells but also setting up the stage for the generation of adaptive anti-tumor immunity.

1.2.3.2 OV-mediated Adaptive Anti-tumor Immune Responses

Following innate immune responses, the second line of defense, adaptive immunity, is initiated. Adaptive immune responses are carried out by lymphocytes – B cell for humoral immunity and T cells for cell-mediated immunity – that mount a highly specific response against 'non-self' entities[109]. Specificity is dictated through antigens that are recognized in their native forms by B cell receptors (BCR) or as digested peptides presented via MHC (human leukocyte antigen [HLA] in humans) by T cell receptors (TCR)[109]; antigen presentation by MHC proteins is discussed more thoroughly in *Chapter 1.5*. The generation and action of adaptive anti-tumor immunity occur in several steps: (1) release of tumor antigens by dying cancer cells, (2) antigen processing and presentation by APCs, (3)

priming and activation of effector T cells in secondary lymphoid organs, (4) trafficking and infiltration of T cells into the TME, (5) recognition of cancer cells by T cells via TCR/peptide-MHC interaction, and (6) T cell-mediated killing of cancer cells[126,127]. OVs contribute to this cancer-immunity cycle by promoting the release of tumor antigens through oncolysis, creating an acute inflamed environment that recruits and activates immune cells, and restoring antigen presentation by tumor cells to allow T cell recognition[8,9]. Accordingly, mounting evidence supports the generation and role of OV-induced anti-tumor immunity which causes regression of treated as well as distant, untreated tumors, with this abscopal effect being one of the key advantages of OV therapy[8,128,129]. In addition, immunological memory – the ability of long-lived, memory B and T cells to rapidly respond to previously encountered antigens[109] – provides continual protection against cancer recurrence. Cure by OV therapy prevents re-implantation with the same cancer cell type where this anti-tumor protection is conferred by the immune system, as demonstrated by adoptive transfer of T cells from cured mice or tumor rechallenge with immune cell depletion[130–132]. Thus, by hindering metastatic spread and relapse, anti-tumor immune response is increasingly being considered more important than the direct oncolytic effect of OVs.

With the ability to promote the generation of anti-tumor immune responses and cause the release of damage-associated molecular patterns (DAMPs), it is then apropos that OVs are regarded as bona fide inducers of immunogenic cell death (ICD)[77]. Cancer cells undergoing ICD are characterized by the temporospatial expression and emission of DAMPs that bind to their cognate receptors on immune cells, triggering a sequence of events that ultimately lead to the activation of anti-tumor T cells[133,134]. The four major

hallmarks of ICD include pre-apoptotic exposure of calreticulin (CALR) on the outer surface of the plasma membrane[135], secretion of adenosine triphosphate (ATP)[136], production of type I IFNs[137], and post-apoptotic release of high mobility group box 1 protein (HMGB1)[138]. The immunostimulatory and immunomodulatory effects of DAMPs influence each step along the antigen presentation and T cell activation pathway (i.e., from DC recruitment [ATP], antigen uptake [CALR] and processing [HMGB1], DC maturation and cytokine profile for CD8 T cell priming [ATP], to T cell recruitment [type I IFNs]), culminating in the activation of tumor antigen-specific CD8 T cells. Numerous studies to date have reported the ICD-inducing capacity of certain OVs. For example, T-Vec induces the expression of ICD hallmarks in melanoma cell lines[139], and NDV was established to induce ICD in lung cancer[140], melanoma[141], and glioma[132]. Thus, some OVs are able to promote the generation of anti-tumor immunity through the induction of tumor ICD; and regardless of the specific type of cell death pathway triggered, OV-induced cancer cell death can be broadly classified as ICD with the consequent anti-tumor immune responses contributing greatly to tumor remission.

Much of the efforts to understand anti-tumor immune responses are focused on CD8 T cells, as will be the case in this thesis. CD8 T cells, also referred to as cytotoxic T lymphocytes (CTLs), are the ultimate effector cells that inhibit and kill malignant cells, and the correlation between tumor progression control and infiltration of CTLs in tumors is well established for various cancer types[142–145]. Upon tumor antigen recognition by cognate TCRs, CD8 T cells release pre-formed effector molecules, perforin and granzymes, that activate the apoptotic pathway in the target cancer cells. Other mechanisms through which CTLs act include secretion of cytokines IFNγ and TNFα, and induction of apoptosis

following the ligation of Fas ligand on the surface of activated CD8 T cells with Fas on target cells[109]. These anti-tumor effects of CD8 T cells have been shown to be enhanced following OV therapy. Numerous studies have reported increased CD8 T cell infiltration of tumors due to OV administration, such as Ad in an immunocompetent mouse model of CMT-93 rectum carcinoma[146]; VSV in triple-negative breast cancer (TNBC)[147]; VV in 4T1 mammary carcinoma[148] and MC38 colon adenocarcinoma[149]; and alphavirus M1 in B16F10 melanoma, RM-1 prostate cancer, and GL261 glioma[23], attributing to elevated levels of T cell-recruiting chemokines CCL3 and CCL5, and chemokines (C-X-C motif) ligand (CXCL) family chemokines such as CXCL9, CXCL10, and CXCL11[8,12,56,111]. Similar effects were observed in patient biopsies after T-Vec treatment[3,150,151]. More importantly, these newly recruited CD8 T cells exhibit activation signatures that can overcome the immunosuppression of the TME. For instance, alphavirus M1-recruited CD8 T cells expressed high levels of activation markers CD69 and CD44[23], indicating newly activated T cells with intact functional capacity. Thus, CD8 T cells are the main mediators of anti-tumor immunity, and there is ample evidence to support that OVs are able to quantitatively and qualitatively improve anti-tumor CD8 T cell responses[9,111,131,132,152,153].

1.3   COMBINING OVS WITH CANCER IMMUNOTHERAPIES

Like most cancer therapeutics, it has become clear that OV therapy alone is insufficient to achieve clinical success. Due to the genetic and phenotypic heterogeneity of tumors, it is improbable that an OV can kill all cancer cells within a tumor mass or in widespread disseminated malignancies[8–10,56,154]. Thus, combining multiple therapies is becoming a routine strategy to enhance treatment efficacy. While OVs have been used in combination with conventional cancer treatments like chemotherapy[155] or radiation[156], the greatest

therapeutic gains are obtained when OVs are used as the foundation of combination therapies with other immunotherapeutic agents[157]. OV contribution to the cancer-immunity cycle – from efficient priming against tumor antigens, increased trafficking and infiltration of CD8 T cells into the TME, to circumventing tumor-mediated immunosuppression – addresses some of the challenges faced by other cancer immunotherapies as stand-alone treatments[8,9]. The interplay between an OV, the TME, and the immune system also provides multiple points of interaction to be targeted by combinatorial approaches for optimal manipulation of the immune response to attack cancer[10]. This subchapter will provide an overview of the various strategies in which OVs are administered in *cis-* or *trans*-combination as a single therapeutic with OVs encoding transgenes or a separate therapeutic in (a)synchronous administrations with other cancer immunotherapeutic agents, respectively. Ultimately, OVs act as a potent immunological adjuvant in the context of a multimodal treatment regimen to ensure the generation of robust and durable anti-tumor immune responses.

1.3.1 *Cytokines and Chemokines*

The TME is a highly immunosuppressive milieu due to factors secreted by cancer cells, stromal cells, and immune cells that support tumor growth[105,107,158]. By turning tumors 'hot' and shifting the cytokine balance from immunosuppressive to immunostimulatory, OVs can tilt the immune system in favor of a pro-inflammatory anti-tumor profile[106,159]. To best achieve this, OVs are genetically modified to express transgenes encoding cytokines. Such *cis*-combination of OVs and cytokines has been reported for several interleukins, interferons, chemokines, and growth factors[160]. As a case in point, IL-2, which is important in the proliferation and cytolytic activity of effector T cells, has been incorporated in the

VV backbone (VV-IL-2) for the treatment of MC38 murine colon cancer[161]. The IL-2 construct in this particular study was modified to remain membrane-bound, via a glycosylphosphatidylinositol (GPI) anchor with a rigid peptide linker, thereby avoiding the severe side effects and toxicity associated with systemic IL-2. Similarly, Wang et al. re-designed IL-12, which not only improves NK and T cell priming and activation but also has direct anti-tumor activity of promoting anti-angiogenesis, where Ad expressing non-secreting IL-12 was curative against Syrian hamster models of pancreatic cancer without systemic toxicity[162]. IL-12 has also been incorporated in oncolytic Maraba MG1 virus, in the context of an infected cell vaccine model, and shown to recruit activated NK cells, leading to prolonged survival of B16F10 peritoneal tumor-bearing mice[163]. IL-15, which has many overlapping functions (e.g., NK and T cell activating) as IL-2 but is less toxic, has been inserted into several OV vectors, including but not limited to NDV[164], Ad[165], and VSV[166]. Notably, Kowalsky et al. demonstrated that VV encoding a superagonist IL-15, a fusion protein of IL-15 and IL-15 receptor alpha (IL-15/IL-15Rα), improved survival in MC38 colon and ID8 ovarian cancer models[167]. The therapeutic potency of this OV was attributed to increased tumor infiltration of activated CD8 T cells, which conferred protection against tumor rechallenge.

Interferons, naturally produced and secreted by host cells as a defensive response to viruses[108], have also been combined with OVs. While the idea of coupling an anti-viral cytokine with an OV is paradoxical, IFNs are highly immunostimulatory cytokines that will enhance OV-mediated indirect induction of anti-tumor immunity despite the cost of impairing direct oncolysis[75]. For instance, therapeutic effects of Ad engineered to express IFNα have been demonstrated in both subcutaneous and peritoneal carcinomatosis models

of pancreatic cancer in Syrian hamsters[168]. Increased treatment efficacy against mesotheliomas using IFNβ-encoding MV has also been reported, where the administration of this novel oncolytic MV augmented innate immune cell tumor infiltration and anti-angiogenesis[169]. Similarly, VSV-IFNβ has exhibited success in the treatment of mesothelioma[170] and non-small cell lung cancer[171]. VSV armed with IFNγ has also been shown to enhance anti-tumor immune responses in 4T1 mammary adenocarcinoma and CT26 colon carcinoma, resulting in delayed tumor growth, reduced lung metastases, and prolonged survival[172]. Efficacy was T cell-dependent and mediated by increased secretion of other pro-inflammatory cytokines (e.g., IL-6, TNFα, monocyte chemoattractant protein-1 [MCP-1]), activation of DCs, and recruitment of T cells to tumors.

Tumor infiltration of not only T cells but also other immune cells can be driven by chemokine-armed OVs. As previously mentioned (see *Chapter 1.2.3.2*), OV administration (e.g., VV[148,149], M1[23], Ad[146]) stimulates high expression of CXCL9, CXCL10, and CXCL11 in infected tumors, prompting greater accumulation of intratumoral T cells. As such, VV has been genetically engineered to express CXCL11, which increased intratumoral trafficking of endogenous, as well as adoptively transferred, T cells[173]. If, however, OV infection alone drives high intratumoral levels of chemokines, then no added benefits from the *cis*-combination of OV and chemokine may be observed, as was the case for CXCL9-encoding VSV[174]. For the recruitment of DCs and NK cells, CCL5 is another chemokine whose chemotactic activity has been coupled with OVs. The administration of CCL5-expressing Ad in JC mammary adenocarcinoma and EL4 lymphoma was shown to enhance the intratumoral recruitment of DCs, as well as macrophages, NK cells, and CD8 T cells, and the tumor-infiltrating DCs displayed a higher maturation profile (e.g., higher

levels of IFNγ and IL-12 secretion)[175]. In addition, Li et al. presented elevated levels of NK cells in tumors treated with CCL5-expressing VV[176]. Of note, this study was performed in immunodeficient mice implanted with HCT-116 colon cancer using NK cells engineered to overexpress CCR5, the receptor for CCL5, due to endogenously low levels of CCR5 that would not respond to the virus-delivered CCL5. Regardless of this enforced CCR5-CCL5 interaction, the principle of combining OVs and chemokines to direct immune trafficking into the TME remains strongly supported.

A discussion on OV-based cytokine expression cannot leave out granulocyte-macrophage colony-stimulating factor (GM-CSF). T-Vec, the only OV approved by the U.S. FDA, is HSV type 1 genetically engineered to express GM-CSF[3,151], thus bringing notable attention to this cytokine. GM-CSF serves important functions in granulocyte differentiation, monocyte migration, and APC maturation for enhanced antigen presentation[177]. Incorporation of GM-CSF in not only T-Vec but also other OV vectors (e.g., Pexa-Vec) has resulted in elevated DC recruitment and maturation, boosted CD8 T cell priming, and reduction in immunosuppressive cells such as MDSCs and Tregs[178,179]. Notably, GM-CSF has also been administered in *trans*-combination with OVs. Samson et al. described improved survival in glioma-bearing mice due to intravenous administration of reovirus and GM-CSF, along with another immunotherapy, immune checkpoint blockade[24]. As is also the case for the other cytokines/chemokines outlined above, the expression of GM-CSF by OVs is highly effective in trafficking immune cells and improving immune effector function in the TME, and the combined effect of these two immunomodulatory modalities establishes an 'inflamed' tumor.

1.3.2   *Co-stimulatory Molecules*

Co-stimulatory molecules provide one of the crucial signals in the activation of lymphocytes, influencing T cell fate and differentiation[180]. They are especially important for the differentiation of naïve T cells into effector cells, where antigen stimulation in the absence of a co-stimulatory signal can induce T cell anergy[180]. Agonistic antibodies targeting co-stimulatory molecules have shown potential to enhance immunity[181] and thus, combining OVs with these agonists may augment therapeutic efficacy. As a case in point, the combination of anti-4-1BB antibody and VV has been studied in mouse models of breast and colon cancer[182]. 4-1BB signaling increases the cytotoxic activity and survival of activated CD8 T cells. Following this *trans*-combination therapy, reduced tumor growth and elevated tumor trafficking of CD8 T cells, NK cells, and neutrophils were observed. Higher levels of CD11b+ and CD11c+ myeloid cells in the tumor-draining lymph nodes were detected as well. Another example of a *trans*-combination of an OV and a co-stimulatory agonist involves OX40, which not only promotes the expansion, survival, and generation of memory T cells but also inhibits Tregs[183]. As described by Scherwitzl et al., IL-12-expressing Sindbis virus vector administered in CT26 colon cancer or MyC-CaP prostate cancer upregulated OX40 expression on CD4 T cells, providing the rationale for including an OX40 agonist[183]. The triple combination therapy of VV, cytokine, and anti-OX40 antibody resulted in enhanced tumor infiltration and effector function of T cells displaying an altered transcriptomic and metabolic profile.

Furthermore, OVs and co-stimulatory agonists can be combined in *cis*, where transgenes encoding the ligands for the co-stimulatory molecules are incorporated in the OV vector, ensuring the expression of the agonist within the tumor. To illustrate, Rivera-Molina et al. engineered Ad encoding the ligand for glucocorticoid-induced TNFR family-

related gene (GITR), showed the expression of the ligand on the surface of human and murine glioma cells post infection, and documented increased therapeutic efficacy in murine glioma models[184]. Prolonged survival of glioma-bearing mice, elevated levels of central memory CD8 T cells, and protection against tumor rechallenge were reported. Inducible co-stimulator (ICOS) has also been exploited for immunotherapeutic intervention. After first noting the upregulation of ICOS in NDV-treated B16F10 melanoma, Zamarin et al. generated ICOS ligand-expressing NDV (NDV-ICOSL) to target ICOS directly within tumors[185]. Administration of NDV-ICOSL in a bilateral flank B16F10 tumor model resulted in intratumoral expansion of activated CD8 T cells and tumor regression in both the virus-injected and the distant, untreated tumors. Therapeutic efficacy was further enhanced by the addition of immune checkpoint blockade therapy. This study, as well as the aforementioned work by Scherwitzl et al., highlights the main advantage of combining OVs and co-stimulatory agonists: upregulated expression of co-stimulatory molecules induced by OV infection. The ensured presentation of agonist targets allows maximal utilization of the co-stimulatory axes for optimal differentiation and function of anti-tumor T cells during OV therapy.

1.3.3 Tumor Antigens

As the signal that dictates the specificity of immune responses, tumor antigens are vital to anti-tumor immunity[109] and stimulating their cognate T cells by peptide vaccines is another immunotherapeutic avenue in which OVs can be integrated. OVs can be utilized for not only effective delivery and expression of tumor antigens but also as adjuvants to arouse otherwise immunosuppressed tumor antigen-specific T cells[9,10,186]. Such oncolytic vaccines (i.e., OVs engineered to express tumor antigens) have been reported for VSV

encoding E7 (human papillomavirus [HPV] type 16 E7 protein)[187], DCT (dopachrome tautomerase)[188], OVA (ovalbumin as a surrogate tumor antigen)[189], and gp100 (glycoprotein 100)[190]; as well as VV encoding CEA (an oncofetal glycoprotein called carcinoembryonic antigen)[191], 5T4 (another oncofetal glycoprotein)[192], and HER2/neu (human epidermal growth factor receptor 2)[193]. To illustrate in more detail the effective use of oncolytic vaccines, Kottke et al. and Pulido et al. described the anti-tumor efficacy of a virally expressed epitope library, where the expression of a cDNA library derived from normal prostate tissues or melanoma cell lines covered a broad range of tumor antigens[194,195]. These VSV-expressed cDNA libraries resulted in the rejection of established prostate and melanoma tumors, attributed to an induction of Th17 CD4 T cell response. The ability to target multiple tumor antigens makes virally expressed epitope libraries an attractive therapeutic strategy that is applicable against various cancer types.

Another novel oncolytic vaccine platform involves coating viruses with tumor-specific peptides for efficient tumor antigen delivery. This technology was developed using Ad where tumor peptides are adsorbed onto the negatively-charged viral capsid, thus negating the need to genetically modify the virus[196]. This peptide-coated conditionally replicating adenovirus (PeptiCRAd), loaded with either OVA, tyrosinase-related protein 2 (TRP-2) and gp100, or melanoma-associated antigen A1 (MAGE-A1), was demonstrated to promote the expansion of antigen-specific CD8 T cells and mature, antigen-presenting DCs, as well as eradicate established tumors[196]. Multivalent PeptiCRAd, expressing both TRP-2 and gp100, exhibited the greatest anti-tumor efficacy, even displaying an abscopal response in a bilateral flank B16F10 tumor model[196].

Most vaccines require multiple doses for optimal efficacy and production of long-lasting immunity. This poses a challenge for oncolytic vaccines since the more intense anti-viral immune responses against the viral vector, which can prematurely clear the virus, may overpower the tumor antigen-specific immune response[186,197]. The balance between the immune response against the virus versus the immune response against the tumor antigen can be skewed towards the latter by a heterologous prime-boost strategy[197]. Here, two viral vectors encoding the same tumor antigen are administered one after the other to prime then boost a stronger memory immune response against the tumor antigen; the second viral vector, on the other hand, will trigger a relatively weaker primary immune response. In one example, gp100-expressing Ad was used to prime and gp100-expressing lymphocytic choriomeningitis virus (LCMV) was used to boost gp100-specific CD8 T cell responses in both a prophylactic and therapeutic setting (i.e., protect against B16F10 challenge and reduce the growth of established tumors, respectively)[198]. Many different combinations of recombinant OVs are possible (e.g., Ad-DCT to prime and Maraba-DCT to boost, VSV-DCT to prime and Ad-DCT to boost, Sindbis-E7 to prime and VV-E7 to boost) for the generation of potent tumor antigen-specific immunity[197]. Ultimately, the use of oncolytic vaccines to establish immune responses against tumor antigens highlights the important role OVs can play in the development of the next-generation of cancer peptide vaccines.

1.3.4 *Bispecific T-cell Engagers (BiTEs)*

Immunological synapse – the interface between a target cell and a lymphocyte – can be forced using bispecific T-cell engagers (BiTEs)[157,199]. A BiTE is an artificial fusion protein consisting of two single-chain variable fragments (scFv), one that binds CD3 on T cells and another that binds an antigen on tumor cells[199]. By forming a link between a T cell and

a cancer cell, the BiTE-induced synapse allows T cells to exert cytolytic activity on tumors irrespective of TCR/peptide-MHC interaction. BiTE therapy, however, may be limited by the short circulating half-life of BiTEs, on-target/off-tumor toxicity if target antigen is also expressed on normal cells, and the reliance on the intratumoral presence of functional T cells[157]. Arming OVs with BiTEs can address these obstacles. As shown by Fajardo et al., Ad encoding an epidermal growth factor receptor (EGFR)-specific BiTE (Ad-EGFR-BiTE) was capable of producing BiTEs that enhanced T cell function and bystander killing effect in an *in vitro* co-culture assay with human cancer cells and peripheral blood mononuclear cells (PBMCs)[200]. They also demonstrated increased T cell tumor infiltration and anti-tumor efficacy in two human tumor xenograft models following intratumoral or intravenous administration of Ad-EGFR-BiTE, along with a systemic administration of human PBMCs. Similar improvements in bystander effect and anti-tumor efficacy were observed in response to VV armed with ephrin-A2-targeting BiTE[201] and Ad encoding BiTE specific for epithelial cell adhesion molecule EpCAM[202]. Overall, combining BiTEs and OVs by genetic engineering supports the sustained production and expression of BiTEs within the TME. The reversal of tumor-associated immunosuppression by OVs can also aid in the enhanced T cell activity upon BiTE-mediated cancer cell-T cell ligation.

1.3.5 *Adoptive Cell Therapy (ACT)*

Adoptive cell therapy (ACT) involves the transfer of immune cells into patients to enhance anti-tumor immune responses[203]. There are three types of ACTs engaging T cells: [1] tumor-infiltrating lymphocyte (TIL) therapy where naturally occurring anti-tumor T cells are harvested from a patient, activated and expanded *ex vivo*, and infused back into the patient; [2] engineered TCR therapy where T cells isolated from a patient are engineered

to express a tumor antigen-specific TCR and then activated and expanded prior to reinfusion; and [3] chimeric antigen receptor (CAR)-T cell therapy where T cells are engineered to express a recombinant antigen receptor composed of a scFv specific against an antigen on the surface of cancer cells and co-stimulatory signaling domains that sustain the activation and proliferation of the engineered T cells following reinfusion[203]. The main advantage of CAR-T cells is that they recognize and kill cancer cells independently of peptide processing and presentation by tumor MHC[203].

The success of ACTs depends on T cell trafficking to and survival in the TME. Thus, it would be advantageous to combine OV therapy with ACT due to OV-mediated events that improve T cell recruitment and effector function, as well as extended anti-tumor T cell priming by tumor antigens released by oncolysis[9,157]. Indeed, Nishio et al. utilized a *trans*-combination of CCL5 and IL-15-expressing Ad and neuroblastoma antigen GD2-specific CAR-T cells to show the increased migration, proliferation, and function of CAR-T cells in a neuroblastoma TME, resulting in reduced tumor growth and improved survival in the tumor-bearing mice[204]. Similar findings have been reported in numerous preclinical studies combining various OVs and CAR-T cells specific for HER2/neu, EGFR, and mesothelin[10,152,157]. Furthermore, OVs can also enhance the function of endogenous T cells to augment ACT efficacy. As described by Walsh et al., VSV oncolytic vaccine (engineered to express a peptide derived from a mutated ERK2 protein) combined with ACT of transgenic CD8 T cells specific against the same ERK2 peptide resulted in complete and durable tumor regression of CMS5 fibrosarcoma[205]. This anti-tumor efficacy was attributed to rapid destruction of tumor mass by the transferred T cells and long-term

protective memory response by endogenous T cells. Thus, the full potential of the immune system can be exploited by the combination therapy of OV and ACT.

1.3.6 Immune Checkpoint Blockade (ICB)

Immune responses are maintained under control by inhibitory immune checkpoint molecules[180]. The interaction between an inhibitory immune checkpoint, expressed on APCs and cancer cells, and its cognate receptor, expressed on lymphocytes, is similar to that of co-stimulation except the result in this case is immunosuppression. This immune checkpoint signaling is essential to maintain self-tolerance (i.e., prevent autoimmunity) and moderate immune responses during infection (i.e., prevent excessive inflammatory tissue damage)[180]. Cancer cells, however, utilize immune checkpoints as one of the main strategies of tumor immune evasion[105,181]. Thus, immune checkpoint blockade (ICB) therapies, where antibodies specific for immune checkpoints (i.e., immune checkpoint inhibitors [ICIs]) inhibit receptor-ligand interactions thereby allowing T cell activation, are being recognized for their capacity to reinvigorate anti-tumor immune responses and have shown promise in clinical settings[181,206,207]. The most extensively studied immune checkpoints are cytotoxic T-lymphocyte associated protein 4 (CTLA-4), programmed cell death protein 1 (PD-1), and programmed death-ligand 1 (PD-L1). CTLA-4 is expressed on T cells – constitutively on Tregs or upregulated on effector T cells upon activation – and competes with the co-stimulatory molecule CD28 to bind CD80 and CD86 on APCs, where receptor-ligand engagement inhibits T cell expansion[180]. PD-1 is found on the surface of activated T cells, as well as Tregs, B cells, NK cells, and myeloid cells, and binding its ligand PD-L1 (or PD-L2) inhibits T cell proliferation and function and induces T cell apoptosis[180]. Other immune checkpoints under investigation include T cell

immunoglobulin and mucin-domain containing-3 (TIM3), lymphocyte activation gene-3 (LAG-3), T cell immunoglobulin and ITIM domain (TIGIT), and V-domain Ig suppressor of T cell activation (VISTA)[180].

As with most cancer therapies, ICB is not without its challenges. There are some patients in whom ICB fails to achieve successful therapeutic outcomes, particularly if the tumors exhibit a low mutational burden or lack TILs[208–210]. The incorporation of OVs to ICB therapeutic regimen can address the shortcomings and thus numerous OV-ICB combinations are underway in preclinical and clinical studies[211]. By turning tumors 'hot' and driving the infiltration of T cells into tumors, OVs increase the sensitivity of TILs to ICIs[106,211]. Likewise, OV-mediated upregulation of immune checkpoint molecules on cancer cells also provides the target for ICB therapy[106,211]. As exemplified by Zamarin et al. using a bilateral flank B16F10 tumor model, combination therapy of NDV and anti-CTLA-4 antibody increased the recruitment of activated CD4 and CD8 T cells into distant, untreated tumors, resulting in complete regression and protection against rechallenge[128]. Similar findings were observed following the administration of NDV and anti-PD-1 or anti-PD-L1, where the PD-1/PD-L1 axis was targeted in this case after noting NDV-induced PD-L1 upregulation in treated and untreated, distant tumors[212]. Enhanced anti-tumor efficacy can also be obtained by targeting multiple immune checkpoint signaling pathways in a triple combination therapy of an OV and two ICIs (e.g., IL-12-expressing HSV combined with anti-CTLA-4 antibody and anti-PD-1 antibody in glioblastoma[213]). Furthermore, PD-1 blockade can affect other immune cells besides T cells to potentiate therapeutic efficacy. Combination therapy of reovirus and PD-1 blockade not only prolonged survival in B16 melanoma-bearing mice but also improved NK cell-mediated

killing of reovirus-infected cancer cells and reduced Treg-mediated suppression of CD8 T cell anti-tumor activity[214]. On the whole, OV-mediated enhanced sensitization to ICB is best illustrated by Bourgeois-Daigneault et al. using Maraba rhabdovirus as a neoadjuvant (i.e., therapy delivered before the main treatment)[215]. In this study, animals in which the primary TNBC tumors were treated with Maraba prior to surgical resection responded well (60-90% complete response) to anti-PD-1 blockade therapy of the secondary, rechallenge tumor; on the other hand, ICB was ineffective against tumor rechallenge in animals that did not receive neoadjuvant Maraba therapy before primary tumor resection. This therapeutic model exemplifies the course of treatment in real clinical settings (from primary tumor, OV therapy, tumor resection, secondary tumor, to ICB) and highlights how the OV-ICB combination can be harnessed for maximum therapeutic efficacy.

As opposed to the *trans*-combination of OV and ICB described thus far, *cis*-combination (i.e., OVs genetically modified to express ICIs) is also possible and provides an additional benefit of the efficient delivery of ICIs to the TME. This enhanced tumor localization of ICIs will minimize one of the major side-effects of ICB – off-target toxicity resulting in immune-related adverse events (irAEs) such as colitis, hepatitis, type 1 diabetes, and myocarditis[181,216]. VV co-expressing GM-CSF and a PD-L1 inhibitor (VV-iPDL1/GM) was generated by Wang et al. and shown to be capable of producing high levels of functional PD-L1 inhibitor (iPDL1; soluble PD-1 extracellular domain fused with immunoglobulin G1 Fc fragment) that bound to PD-L1 of treated and distant B16F10 or MC38 tumors, as well as tumor-infiltrating immune cells[131]. Enhanced anti-tumor activities against the primary and distant, untreated tumors were due to VV-iPDL1/GM-mediated increase in tumor infiltration of CD8 T cells showing higher activation capacity (i.e.,

express higher levels of IFNγ, TNFα, and CD107a upon stimulation) and decrease in the level of immunosuppressive cells in the TME. Most important of all, VV-iPDL1/GM activated CD8 T cell responses against neoepitopes (i.e., peptides derived from tumor-specific mutant antigens) identified in MC38 cancer cells, thus emphasizing the role of CD8 T cells in anti-tumor immunity. Another form of ICI encoded by OVs is anti-CTLA-4 scFv that blocks CTLA-4 signaling[217]. Recombinant NDV or influenza A virus expressing this CTLA-4 inhibitor was effective against B16F10 melanoma in reducing the growth of established tumors and increasing overall survival, as well as contributing to an abscopal effect[218,219]. Collectively, whether it is through OV-induced upregulation of immune checkpoints on cancer cells, enhanced tumor immune infiltration or targeted delivery of ICIs to the TME, OV and ICB combination forms an ideal complementary partnership for cancer immunotherapy.

1.4   THE ROLE OF ANTI-VIRAL IMMUNITY DURING OV THERAPY

Upon virus detection, a series of immunological events involving soluble mediators and immune cells of both innate and adaptive immunity will be triggered to restrict viral replication and spread[11,108,109,111]. *Chapter 1.2.3.1* described how some of the initial immune responses (i.e., innate immunity) to OV recognition can contribute to the development of anti-tumor immunity. The current subchapter will focus on immune responses directed towards the virus and present the detrimental, as well as fortuitously beneficial, outcomes of this anti-viral immunity. There is mounting evidence that OV therapeutic efficacy is hindered by the presence of pre-existing anti-viral immunity due to prior exposure (e.g., previous immunizations, natural infections by viruses found ubiquitously in the environment) or repeat administration of OV therapy[220]. Even if pre-

existing immunity is absent, the immune system will eventually facilitate viral clearance, generally keeping the therapeutic window during which an OV can exert its anti-tumor effects to the first 1-2 weeks after administration[11]. Thus, anti-viral immunity is one of the biggest obstacles faced by OV therapy, especially for systemic delivery, that can adversely impact treatment outcome at several stages: prior to cell entry by humoral immunity (i.e., neutralizing antibodies, complement proteins); and upon cell infection by interferons that inhibit viral replication or by immune cells that destroy virus-infected cells.

1.4.1   *Neutralizing Antibodies*

Neutralizing antibodies (nAbs) are secreted by activated B cells and as the name implies, they act to subdue the offending pathogen and render them non-infectious[221,222]. By blocking the virus-host cell interaction, nAbs prevent OV entry into cancer cells and thus negate therapeutic effects[26,111]. As a case in point, Chen et al. demonstrated decreased anti-tumor activity of Ad against LNCaP prostate cancer xenograft model in the presence of Ad nAbs, for which >85% of the human population is seropositive[223,224]. Similarly, nAbs cause a challenge for OVs like MV in previously vaccinated patients (the MMR [measles-mumps-rubella] vaccine is widely used around the world to immunize children[225]) or T-Vec (>90% of adults in the U.S. are estimated to have been exposed to HSV-1[226]). Antibody responses against ubiquitous viruses can be acquired during early childhood and increase with age, as exemplified by the prevalence of reovirus-specific antibodies in a cohort of young children in Nashville, Tennessee[227]. Levels of pre-existing nAbs can further increase after clinical exposure to OVs. Accordingly, numerous strategies have been employed to circumvent nAbs in OV therapy[26,220]. In addition to the use of cell carriers or liposomes described in *Chapter 1.1.2* to shield OVs from nAbs, another

approach is to switch serotypes, which are variations of a virus that differ in their surface antigens and thus trigger different antibodies[1]. With more than 50 distinct serotypes, Ad is particularly amenable to serotype switching[1]. Most OV research on Ad is based on serotype 5, but Hemminki et al. generated a serotype 3 oncolytic Ad (Ad3-hTERT-E1A; rendered oncolytic by placing its replication under the control of a tumor specific promoter) and showed its anti-tumor efficacy even in the presence of nAbs against Ad serotype 5[228]. Serotype switching, however, is not a feasible approach for monotypic viruses such as MV. Rather, a proof-of-concept study by Xu et al. demonstrated that UV-inactivated MV can act as a decoy virus to sequester pre-existing anti-MV antibodies prior to the addition of active oncolytic MV[229]. Alternatively, modifications to the viral coat proteins can deter neutralization. For instance, surface deglycosylation of VV to block TLR-2 activation was shown to decrease anti-VV nAb production[230]. Escaping humoral immunity was also achieved by replacing the envelope glycoprotein of VSV with the non-neurotropic envelope glycoprotein of LCMV for the treatment of brain cancer; while this "pseudotyping" was intended to inhibit neurotropism, it also resulted in an abrogation of nAb response and thus allowed a multi-dosing regimen of this recombinant OV[231–233]. Of note, non-neutralizing antibodies (i.e., binding antibodies) against viruses are also produced upon infection, which instead of affecting infectivity will hinder virus activity by triggering an immune response against the pathogen-antibody complex[222].

1.4.2 Complement System

The complement system consists of soluble proteins circulating in the blood and other body fluids that act as PRRs or effector molecules for the detection or destruction of microorganisms[109,234]. Even in the absence of anti-viral antibodies, the complement

cascade can facilitate viral clearance by directly causing virolysis; other modes of complement-mediated viral inactivation are aggregation and phagocytosis[235]. As such, inhibition of the complement system has been coupled with OV therapy to augment systemic delivery of OVs[25,26,220]. Using cobra venom factor pre-treatment to deplete complement protein levels, Wakimoto et al. presented increased infection of glioma xenografts by oncolytic HSV-1 following intravascular administration[236]. The authors also highlighted how HSV infection can activate different complement pathways in a species-specific manner, which is highly relevant to the translation of OV therapy from preclinical rodent models to human clinical trials. Monoclonal antibodies against complement components have also been used to inhibit complement activity; specifically, inhibition of complement C5 significantly enhanced *in vitro* infection and oncolysis of MC38 cancer cells by VV[237]. In addition, certain viruses have naturally acquired complement subversion mechanisms such as the expression or secretion of immune-modulating molecules. For example, glycoprotein C of HSV-1 binds complement protein C3b which prevents C5 activation[238]; and vaccinia virus complement control protein is a virulence factor secreted by VV that binds and inactivates complement components C4b and C3b[239,240]. VV is also unique in producing two distinct infectious virions, intracellular mature virus and extracellular enveloped virus, during its replication cycle; and it has been documented that the extracellular enveloped virus form is resistant to neutralization by complement factors due to the incorporation of host proteins within its membrane[29]. While some of these findings were reported in viral infection models rather than in OV therapy models, they still provide a valuable insight on the role of the complement system that are applicable to OV systemic delivery.

1.4.3 Anti-viral Cytokines

If a virus has somehow managed to bypass the obstacles of systemic delivery and gain entry into its target cell, it will face another roadblock of interferons that will limit viral replication and spread[1,8,241]. While the type I IFN pathway is defective in about 65-70% of cancer cell lines, making them more permissive to OV infection, the degree of impairment can vary and still affect OVs[76]. Also, the remaining 30% of cancer cell lines have intact IFN response pathways and IFNs can be produced by other cell types in the TME. Thus, IFNs pose a major impediment to OV therapy, and the correlation between upregulated levels of IFN signaling and resistance to OV therapy supports the use of IFN modulators in combination with OVs[241]. To illustrate, JAK/STAT inhibition with ruxolitinib was shown to increase the oncolytic efficacy of IFNβ-expressing VSV in a murine lung cancer model[171,242]. Another group demonstrated that ruxolitinib pre-treatment increased the susceptibility of malignant peripheral nerve sheath tumors to HSV infection due to reduced interferon-stimulated gene (ISG) expression, resulting in augmented viral replication and HSV-mediated anti-tumor CD8 T cell responses[243]. Other pharmacological inhibitors targeting different parts of the IFN pathway that have been used to potentiate various OV therapies include histone deacetylase inhibitors (prevent ISG transcription)[244], dimethyl fumarate (block nuclear translocation of NF-κB)[245], and microtubule-destabilizing agents (disrupt IFN mRNA translation and reduce protein secretion)[246]. Moreover, the B18R gene of VV, which encodes a type I IFN-binding protein, has been incorporated into the HSV-1 genome, culminating in the secretion of IFN-binding decoy receptors that allowed the recombinant virus to retain its oncolytic activity in the presence of high IFN levels *in vitro* and exhibit greater therapeutic effects in Hepa1-6 tumors *in vivo*[247]. Altogether, as the

success of OV therapy is dependent on dysfunctional IFN signaling in cancer cells, therapeutic approaches to dampen IFN-induced anti-viral state in the TME is essential to overcome IFN-mediated tumor resistance to OV therapy.

1.4.4 Cell-mediated Responses

Non-specific uptake of viruses by the reticuloendothelial system significantly reduces the systemic availability of OVs[26], with reports of as high as 90% of Ad being sequestered from the blood by Kupffer cells (i.e., macrophages in the liver)[248]. In addition to phagocytosis of viral particles, macrophage-mediated suppression of viral replication or destruction of infected cells further contributes to premature viral clearance[26]. Thus, systemic delivery of OVs can benefit from macrophage depletion, which can be achieved by an intravenous administration of liposomes containing clodronate (dichloromethylene-diphosphonate; only phagocytic cells take up liposomes and succumb to apoptosis following intracellular clodronate exposure)[26,111,249,250]. This clodronate-liposome was shown to deplete over 80% of peripheral macrophages (in spleen and blood) of rats harboring syngeneic gliomas, resulting in a 5-fold increase in intratumoral oncolytic HSV-1 titers[251]. As the liposomes cannot cross the blood-brain barrier, microglia (i.e., brain-resident macrophages) remained unaffected; the selective depletion of peripheral macrophages is favorable as intratumoral macrophages can play an essential role in the anti-tumor effects of OVs. Moreover, combining macrophage depletion and anti-coagulant treatment with warfarin was reported to potentiate Ad oncolytic activity in a mouse model of human hepatocellular carcinoma[252]. Macrophage depletion in this particular study was established by Ad pre-dosing, where a high dose of Ad was first administered to cause rapid necrosis of Kupffer cells prior to the delivery of a second therapeutic Ad dose; and

warfarin treatment was included to prevent blood factor-mediated Ad transduction of hepatocytes (off-target toxicity). In addition to increased intratumoral spread and persistence of Ad, reduced tumor growth and prolonged survival in tumor-bearing mice were attained by "de-targeting" Ad from Kupffer cells and hepatocytes.

NK cells are another class of innate immune cells that play a prominent role in host defense against viral infections. The rapid recruitment and activation of NK cells in response to viruses, either infectious or therapeutic, are well documented; and NK cells destroy virally infected cells through the production of IFNγ, secretion of cytolytic granules, or expression of death receptor ligands[253,254]. However, given their capacity to also facilitate tumor clearance, NK cells in the context of OV therapy may be detrimental (anti-viral) or supportive (anti-tumor) of OV efficacy, which could depend on the stage of treatment[220]. As suggested by Alvarez-Breckenridge et al., NK cell depletion in the early phase of therapy can benefit virus replication and intratumoral spread while NK cell activation at later stages can support anti-tumor immunity[255]. The same authors showed that oncolytic HSV induced NK cell infiltration of gliomas which resulted in reduced intratumoral viral titers and therapeutic efficacy; depletion of NK cells using NK antigen-specific antibodies reversed these effects[256]. Another study used the immunosuppressive cytokine TGFβ to suppress NK cells during oncolytic HSV therapy of glioblastoma[257]. TGFβ pre-treatment was shown to temporarily inhibit NK cells, as well as macrophages, leading to decreased intracranial infiltration of these innate immune cells, increased viral titers, and improved therapeutic responses. Oncolytic HSV has also been genetically modified to express E-cadherin, a ligand for an NK inhibitory receptor called KLRG1, to block cytolytic NK cell activity during anti-glioblastoma therapy[258]. In addition to NK

inhibition, E-cadherin also facilitated cell-to-cell infection and thus potentiated viral spread. Consequently, this recombinant OV-mediated inhibition of NK cells and increased viral infectivity prolonged survival in glioma-bearing mice.

Cells of adaptive immunity can also contribute to rapid anti-viral responses, specifically in the form of memory B cell and memory T cells during secondary viral challenge[109,221,259]. Following an infection, lymphocytes proliferate and differentiate into effectors cells that eliminate the pathogen through their effector functions (e.g., antibody secretion by B cells, cytotoxic activity by CD8 T cells)[221,260,261]. When the pathogen is cleared, most effector cells die during the contraction phase, leaving about 10% that persist long-term[109,260–262]. These memory cells differentiate back into effector cells for a prompt and efficient response to reinfection by the same pathogen. Memory B cells are critical to the nAb-mediated responses to viruses; since the half-life of antibodies in serum is short (hours to days), memory B cells need to maintain and/or rapidly produce nAbs[263]. Equally important are virus-specific memory CD8 T cells that facilitate viral clearance by eliminating virus-infected cells via their cytotoxic mechanisms[260,261] (see *Chapter 1.2.3.2*). In relevance to OV therapy, virus-specific memory T cells have been shown to be a part of TILs[264,265]. Simoni et al. determined that human colorectal and lung tumors were infiltrated by a heterogenous population of CD8 T cells, some specific for putative neoepitopes and others specific for common virus epitopes (e.g., Epstein-Barr virus, cytomegalovirus, influenza virus)[264]. Another group analyzed the intratumoral TCR repertoire in ovarian and colorectal cancer and demonstrated tumor infiltration by "bystander" virus-specific T cells[265]. With the potential to expand rapidly upon detection of OVs in tumors, these virus-specific memory T cells and their role in OV therapy require further elucidation. Overall,

the coordinated efforts of innate and adaptive immunity mount a robust anti-viral response that will impede OV therapy, and thus a better understanding of the OV-immune system interaction is required to strategize maximal OV delivery and therapeutic effect.

1.4.5 Potential Benefits of Anti-viral Immunity

Contrary to existing dogma, anti-viral immunity may provide unforeseen benefits for OV therapy. We and others have postulated such anti-tumor benefits of anti-OV immunity (Figure 1.2) and evidence continues to emerge in support of this paradigm shift[110,266–269]. Namely, the strong cytokine and cellular responses triggered by OVs overturn tumor-associated immunosuppression and promote the influx of immune cells into the TME, ultimately contributing to the generation of anti-tumor immunity[107,159]. In addition, the selective nature of OVs indicates that a virally infected cell is a virally infected cancer cell, which is then subjected to anti-viral immune responses. The outcome of anti-viral immunity may then depend on temporospatial dynamics, much like the aforementioned dual role of NK cells in OV therapy: detrimental if directed at OVs in systemic circulation leading to premature viral clearance, but beneficial if initiated in the TME. To skew towards the latter, immunomodulatory interventions aimed at anti-viral immunity should be implemented when appropriate. In one example, a bispecific adaptor protein that binds both Ad-specific nAbs and polysialic acid on tumor cells was included in Ad therapy of MC38 colon cancer[270]. This molecular retargeting of nAb-coated Ad to tumor cell surface significantly delayed tumor growth and prolonged survival in tumor-bearing mice only in the presence of pre-existing anti-viral immunity. Even without intervention, nAbs may help OVs[271–273]. As described by Berkeley et al., nAb-coated reovirus was amenable to cell carriage by monocytes[272]. nAb-OV complexes were internalized by monocytes, which

delivered functional, replicative reovirus to melanoma cells in an *in vitro* assay, resulting in oncolysis. In another study investigating the cell carriage potential of CD11b+ cells for reovirus systemic delivery, cytokine conditioning with GM-CSF to improve carrier function was most effective when pre-existing nAbs were present[271].

Pre-existing anti-viral adaptive immunity, specifically CD8 T cell-mediated response, has also been reported to potentiate OV therapy[267,274–276]. First, it has been observed that there is a correlation between anti-viral and anti-tumor T cell induction in Ad-treated cancer patients, where anti-tumor T cells (i.e., anti-survivin T cells) were absent in the absence of anti-viral T cells[179]. The authors suggested that the generation of anti-tumor T cells was dependent on Ad providing the necessary danger signal strong enough to break tumor-associated immunologic tolerance and on Ad-mediated oncolysis promoting epitope spreading. Moreover, Ricca et al. showed that anti-viral immunity may actually be a driving force behind OV therapeutic efficacy[267]. Despite the fact that intratumoral spread of NDV was attenuated by pre-existing anti-viral immunity, OV therapeutic efficacy (i.e., tumor clearance, abscopal effect, survival) was augmented in mice that were immunized with NDV prior to B16F10 tumor inoculation and intratumoral NDV administration. When the splenic CD8 T cells from these NDV-immunized, tumor-bearing mice were co-cultured with either non-treated B16F10 cells (to examine anti-tumor response) or NDV-treated MB49 cells (to examine anti-viral response), greater level of IFNγ production was observed due to B16F10 stimulation, thus confirming the establishment of potent anti-tumor immunity. Furthermore, in a different study investigating the contribution of anti-viral and anti-tumor CD8 T cell responses during oncolytic HSV therapy, it was determined that the former was enough to cause a significant

tumor growth reduction in the absence of the latter (administration of HSV in a tolerized tumor-associated antigen model of breast cancer allowed such an analysis)[277]. It was hypothesized that the presentation of OV-derived peptides by tumor MHC molecules was sufficient for tumor cell lysis by anti-viral CD8 T cells, which would not be subjected to immunologic tolerance mechanisms or exhaustion due to chronic stimulation like the anti-tumor counterparts[278]. The feasibility of redirecting anti-viral immunity towards cancer cells has been corroborated by multiple groups using various strategies to deliver viral peptides to tumors for the activation of anti-viral T cells (e.g., intratumoral injection of peptides, antibody-peptide epitope conjugates, PeptiCRAd platform)[274–276]. As such, rather than regarding anti-viral immunity as an impediment to OV therapy, strategies to harness the immunologic potential should be considered.

1.5 ANTIGEN PROCESSING AND PRESENTATION IN CANCER IMMUNOTHERAPY

All the discussion thus far on immunity requires a certain level of understanding of antigen presentation. Otherwise, how can one distinguish anti-tumor versus anti-viral immune responses or specifically target the former using immunomodulatory interventions? The specificity of an immune response is dictated by an antigen, which simply put is a substance that is capable of stimulating lymphocytes; an epitope (also known as the antigenic determinant) refers to the distinct part of the antigen that is being recognized[109,279,280]. In T cell immunology, an antigen must be in the form of peptides bound to major histocompatibility complex (MHC); peptides are derived from endogenous proteins for class I MHC presentation to activate CD8 cytotoxic T cells (Figure 1.3) or exogenous proteins for class II MHC presentation to activate CD4 helper T cells[279,281]. For the purpose

of this thesis with my focus on CD8 T cell immune responses during OV infection and therapy, only MHC-I antigen presentation pathway will be discussed here.

The general interest of cancer immunotherapies on stimulating anti-tumor CD8 T cell responses necessitates the identification of tumor-associated antigens (TAAs) or tumor-specific antigens (TSAs)[282–284]. TAAs are self-antigens that are expressed at elevated levels on cancer cells; examples include Her2/neu, MAGE-A1, mesothelin, and survivin[284]. On the other hand, TSAs are expressed only on cancer cells and can be organized into several categories, including but not limited to oncofetal (expressed by cancer cells and fetal tissues)[285,286], cancer-testis (expressed by cancer cells and adult reproductive tissues)[287,288], oncoviral (encoded by cancer-causing viruses such as HPV)[289–291], or neoantigen (arise from genetic mutations [e.g., single nucleotide variations, insertions/deletions, transcript splice variants] which generate novel peptide sequences)[292–296]. Importantly, the knowledge of antigen identity can be exploited to manipulate the cognate CD8 T cell responses during cancer immunotherapies. The following subchapters will describe how an antigen is processed and presented through the MHC-I pathway, as well as recent advances in the field of epitope discovery.

1.5.1   Class I MHC (MHC-I) Pathway

The MHC-I pathway is an elaborate, multi-step process that occurs in a few intracellular compartments, culminating in the surface expression of stable peptide-MHC complexes to be recognized by cognate TCRs (Figure 1.4)[279–281]. MHC-I molecules are expressed on the surface of all nucleated cells. As they present peptide fragments of cytosolic proteins, MHC-I molecules report on the intracellular state of cells to CD8 T cells[297]. Under physiological conditions, MHC-I-bound self-antigens do not activate CD8 T cells.

However, during pathological conditions, MHC-I-bound non-self, foreign antigens that arise from viral infections or cellular transformations serve as antigenic determinants and stimulate CD8 T cells[298]. Thus, the array of MHC-I-bound peptides (or ligands), collectively termed the MHC-I peptidome (or ligandome), is vital for CD8 T cells to distinguish either self or non-self entities and react once the latter is detected[298,299].

1.5.1.1 MHC-I Structure and Polymorphism

MHC-I molecules are heterodimers comprised of two non-covalently linked polypeptide chains, a polymorphic heavy α chain and a constant β_2 microglobulin (B2M)[281,300]. The α_1 and α_2 domains fold to form the peptide-binding groove, while the transmembrane α_3 domain interacts with the CD8 co-receptor on T cells. Within the peptide-binding groove, a peptide is sandwiched between two α helices lying on a β-pleated sheet. The coupling of the α chain and B2M occurs in the endoplasmic reticulum (ER) with the aid of chaperone proteins[301]. MHC-I is unstable without a bound peptide, so an empty MHC-I will dissociate and be degraded by the ER-associated protein degradation (ERAD) pathway[302,303].

MHC-I is polygenic, meaning that the α chain locus contains several genes[281]. Specifically, there are HLA-A, HLA-B, and HLA-C genes in humans, and H2-K, H2-L, and H2-D genes in mice[300]. MHC-I is also highly polymorphic, which means that multiple variants (i.e., alleles) of each gene exists within the population[281]. With over 200 alleles identified for the HLA-A gene, 500 for HLA-B, and 100 for HLA-C, the HLA system displays the highest level of polymorphism known[300,304,305]. As a result of this polygeny and polymorphism, each person has their own set of HLA alleles (i.e., HLA haplotype) with the corresponding distinct set of HLA-bound peptides; variations arising from polymorphism particularly affect the amino acid residues in the peptide-binding groove

and thus dictate the binding specificity of each MHC allotype[306,307]. Furthermore, the identity of MHC alleles is just as important as the sequence of the bound peptides in mediating antigen recognition by T cells[308]. That is, a T cell that recognizes an antigen bound to a specific MHC allotype will not react against the same antigen bound to another MHC allotype[281]. This process of MHC restriction is due to not only the polymorphic amino acid residues in the peptide-binding groove but also the unique conformation of the bound peptide in different MHC molecules, both of which will influence the interaction of the peptide-MHC complex with the TCR[308].

1.5.1.2 Antigen Processing

MHC-I antigen presentation requires cytosolic proteins to be broken down into short peptide fragments, usually 8-11 amino acids in length[279]. Protein turnover (i.e., degradation of older proteins and replacement with newly synthesized proteins) is a continuous process mediated by the proteasome and it is well established that this multi-catalytic proteinase complex produces peptides for MHC-I molecules[309,310]. Of note, it is not just older proteins from which peptides originate as defective ribosomal products (DRiPs) also give rise to MHC-I peptides[311]. DRiPs are prematurely terminated or misfolded polypeptides resulting from defective transcription or translation, and make up about 30% of newly synthesized proteins[311]. Proteins are marked for degradation by ubiquitylation, and the attached ubiquitin is recognized by the 19S cap subunit of the proteasome, which deubiquitinates and unfolds the proteins[281,309]. Proteins then enter the 20S core barrel with the catalytic subunits β1, β2, and β5 that have distinct proteolytic activities, and are broken down into 3-15mer oligopeptides that are released back into the cytosol[312]. In response to pro-inflammatory cytokines during viral infections, IFNγ-inducible variants of the β subunits

called LMP2 (PSMB9), LMP7 (PSMB8), and MECL-1, as well as an 11S cap that replaces the 19S cap, make up a modified form of the proteasome termed the immunoproteasome[312–317]. Compared to the constitutive proteasome, the immunoproteasome not only has different cleavage site specificity due to the different proteolytic subunits but also has a more efficient proteolytic capacity, allowing the cell to handle the increased level of misfolded proteins that result from immune stress or IFNγ exposure[279,313,314,316,318].

1.5.1.3 Peptide Loading on MHC-I

The cleaved peptides leaving the (immuno)proteasome are then transported from the cytosol into the ER via transporters associated with antigen processing (TAP)1 and TAP2[319]. TAP1/2 complex is a part of the larger multi-subunit peptide-loading complex (PLC) that coordinates peptide translocation, editing, and loading onto MHC-I molecules[281,320]. TAP1/2 heterodimer forms a channel in the ER membrane through which peptides pass and exerts a certain level of selectivity; that is, TAP1/2 preferentially translocates 9-16mer peptides that have aromatic, hydrophobic or positively charged C-terminal residues[321–324]. Next, ER aminopeptidase (ERAP)1 and ERAP2 trim the N-terminal residues to create 8-11mer peptides that fit in the peptide-binding groove[325,326]. Other components of the PLC, meanwhile, stabilize the empty MHC-I molecule awaiting its ligand[301]. A newly synthesized MHC-I α chain is first associated with calnexin until B2M binds[327]. Then the partially folded MHC-I molecule, which is stabilized by chaperone proteins calreticulin[328] and ERp57[329,330], binds tapasin that interacts with the TAP1/2 complex[331,332]. Once a peptide bind, the PLC dissociates from the stable peptide-MHC complex which is transported to the cell surface via the Golgi apparatus[281,333]. Eventually, peptide-MHC complexes are internalized via clathrin-independent endocytosis[334–336],

much like the other plasma membrane proteins that are constitutively recycled by endocytosis as a part of protein turnover[337].

Binding of a peptide is dependent on its sequence. Anchor residues, usually at positions 2 and 9, secure the peptide through a series of hydrogen bonds and ionic interactions with the residues of the peptide-binding groove[338–341]. Typically, polymorphic amino acids line the pockets of the peptide-binding groove into which the amino acid side chains of the bound peptide are inserted[342–344]. As a consequence, the anchor residues of all peptides that bind the same MHC allele are similar[345–347]. To allow a broad range of peptides to bind a specific MHC allele, other secondary anchor residues also contribute to binding[348]. Based on the amino acid sequence, peptides exhibit different degrees of MHC-I binding affinity (further described in *Chapter 1.5.2.1*), which may serve as an indicator of peptide-MHC complex stability and immunogenicity[349–353]. Low affinity peptides may be replaced for ones with higher affinity due to the peptide editing function of the PLC, ensuring that optimal peptide-MHC complexes reach the cell surface[354–357]. Moreover, while peptides are typically linear epitopes (i.e., sequential amino acids), longer conformational epitopes (i.e., non-sequential amino acids) are possible by folding the antigen[281,358]. Conformational epitopes not only explain why longer MHC-I peptides are observed but also may yield epitopes with increased antigenic potency due to enhanced stabilization of the peptide-MHC complex via secondary anchor residues[281].

1.5.1.4 Cross Presentation

Cross presentation is a special instance where exogenous proteins are presented by MHC-I molecules instead of class II MHC[281,359]. Performed with particular efficiency by APCs, especially DCs[360,361], cross presentation explains how anti-viral or anti-tumor cytotoxic

CD8 T cells become primed[362,363]. That is, intracellular pathogens that do not infect DCs or antigens released from dying cancer cells must be presented via MHC-I molecules of DCs to prime CD8 T cells. After DCs acquire extracellular antigens via micropinocytosis, endocytosis, or phagocytosis, antigen processing is proposed to occur through either a cytosolic pathway or a vacuolar pathway[360,361]. In the cytosolic pathway, antigens are released from endocytic compartments into the cytosol and broken down by the proteasome, as per the usual MHC-I antigen processing pathway[364]. The cleaved peptides either enter the ER or re-enter the phagosome to be loaded on MHC-I molecules[364,365]. On the other hand, in the vacuolar pathway, antigens remain in the endocytic compartments and are degraded by lysosomal enzymes, thereby possibly generating epitopes with different cleavage specificities, before being loaded on MHC-I molecules in the phagosome[366–368]. In both pathways, how MHC-I molecules and the PLC end up in the endocytic compartments is unclear; it could be MHC-I being recycled from the cell surface[334–336] or newly synthesized MHC-I being recruited by CD74[369]. Though there are still many questions left to be answered, cross presentation by DCs is without a doubt an integral part of anti-viral and anti-tumor CD8 T cell priming that sheds further light on the role of antigens in immune responses.

1.5.1.5 Defects in Tumor MHC-I Pathway

Given the critical role of CD8 T cells in anti-tumor immunity, cancer cells exhibit aberrations in the MHC-I antigen presentation pathway to evade immune detection[105,370,371]. Since MHC-I molecules without bound peptides are unstable and thus not expressed on the cell surface[303], defects in any component of the antigen processing pathway (e.g., proteasome subunits, TAP1/2, chaperone proteins) have detrimental effects[325,355,356,370,372–

[374]. The most extensively studied antigen presentation dysfunction is regarding the MHC-I molecule. Aberrant expression of MHC-I, α chain and/or B2M, has been reported in many different cancer types[333,370,375]. Downregulation can occur at varying degrees, such as different expression levels within the heterogenous tumor mass or between primary and secondary tumors, all of which can change over time as the cancer progresses[376–378]. Defects in MHC-I expression can be due to a mutation or deletion of MHC-I genes, as well as transcriptional regulation (e.g., epigenetic silencing) or post-transcriptional regulation (e.g., microRNAs that inhibit translation)[379–385]. Clinical implications of reduced tumor MHC-I expression include decreased TILs, resistance to cancer immunotherapies, and poor prognosis[386–391]. Thus, elucidating the underlying mechanisms through which cancers circumvent antigen presentation will aid in the design of immunomodulatory interventions to restore MHC-I expression and improve therapeutic outcome.

1.5.2   Methods of Epitope Identification

High-throughput prediction and identification of MHC-I peptides are possible due to advances in bioinformatics and proteomics technologies[392]. The knowledge generated from such comprehensive analyses on CD8 T cell epitopes can be applied to generate personalized anti-tumor or anti-viral vaccines, as well as lead to the discovery of novel biomarkers[393–396]. Another highly useful and informative application of T cell epitopes is the synthesis of peptide-MHC multimers (e.g., tetramer, pentamer, dextramer) for the detection and enumeration of antigen-specific T cells by flow cytometry[397]. Two possible ways to identify MHC-I peptides are (1) *in silico* analyses to predict T cell epitopes and (2) immuno-precipitation (IP) and mass spectrometry methods to isolate and identify MHC-bound peptides. In both cases, a final validation step to confirm the immunogenicity of the

MHC-I peptides is necessary as not all predicted or identified peptides stimulate cognate CD8 T cells[398]. The specific techniques, along with the advantages and disadvantages, of each approach will be discussed in this subchapter.

1.5.2.1 In Silico Prediction Algorithms

Computational strategies can be applied to generate epitope prediction algorithms – specifically, to predict MHC-I binding affinities of peptides[399]. MHC-I allele-specific peptides identified using these bioinformatics tools are candidate CD8 T cell epitopes that are likely to be immunogenic; as such, this procedure has been termed reverse immunology[392]. The most useful application of this strategy is in vaccine formulation where viral genomes can be analyzed to discover virus-specific T cell epitopes[400–402]. MHC-I ligands can be predicted using methods based on peptide binding motifs. Peptides that bind a specific MHC allotype share anchor residues with similar properties (see *Chapter 1.5.1.3*) and thus a particular peptide sequence pattern (i.e., motif) can be determined for each MHC allele[346,403,404]. *In silico* tools, such as SYFPEITHI which is a database of over 7000 class I and II MHC binding peptides amassed from published works[405], scan the whole protein sequence to find peptides which fit these motifs. Quantitative matrices then assign an arbitrary value to the amino acids at each position, based on the frequency at which the residue is found at anchor positions or in other MHC-bound peptides in the database[406]. The total value represents the score for the epitope, with higher scores indicating better MHC binding affinities. Similarly, artificial neural networks (ANNs; e.g., NetMHC) can be trained to predict peptide-MHC binding[407–409]. These machine learning algorithms build complex, non-linear models that analyze the interactions among amino acids, based on multiple properties such as hydrophobicity and

charge, to classify peptides as binders or non-binders of MHC molecules[406]. High-accuracy predictions resulting from the new generation of epitope discovery platforms produce better vaccines and precision medicine in an efficient and high-throughput manner.

1.5.2.2 Isolation of Naturally Processed MHC-I Peptides

The field of MHC-I peptidomics represents a dynamic new frontier in immunotherapy and vaccine development. In this approach, peptides are eluted from MHC complexes and subjected to MS[397,410]. The elucidation of naturally processed and presented MHC-I peptides, as opposed to predicted peptides, narrows the search space to find immunogenic epitopes. The two main principles of this approach are MHC-I peptide isolation and identification. Peptide-MHC complexes can be isolated by mild acid elution (MAE) or immuno-affinity chromatography (IAC)[397,411]. As initially described by Sugawara et al. in 1987, MAE involves the treatment of cells with citric acid (pH 3.0)[412]. The acid treatment causes B2M to dissociate from MHC-I, reducing the peptide binding capacity of the complex and thus releasing the associated peptide. The outcome of MAE is specifically MHC-I peptides since MAE does not affect class II MHC molecules[413]. One of the main advantages of MAE is that cells remain viable after acid treatment so multiple processing of the sample with continuous regeneration of peptide-MHC complexes can result in high MHC-I peptide yields[414]. The low number of purification steps and the absence of detergents to lyse cells also make this approach favorable[415]. However, a huge pitfall of MAE is the excessive level of contaminant peptides that are not directly eluted from MHC-I molecules. According to Fortier et al., only about 40% of peptides resulting from MAE are true MHC-I peptides whereas the rest are other cell surface peptides[411,416]. Thus, a more specific approach to isolating MHC-I peptides such as IAC may be preferred.

The fundamental principles of affinity chromatography as used in biochemistry can also be utilized for the separation and purification of MHC-I peptides (Figure 1.5)[417]. In this pull-down assay, peptide-MHC complexes are isolated using anti-MHC antibodies immobilized on beads (hence, this technique is also referred to as immuno-precipitation [IP])[410]. Following a purification step to get rid of other unbound proteins (i.e., washing the column), peptide-MHC complexes are dissociated and then eluted peptides are separated and analyzed by MS[410]. Due to the specificity of the anti-MHC antibodies, only true MHC-I peptides are isolated[418–420]. In addition, a variety of sample types are supported by this method, such as cell line lysates, homogenized tissues, biological fluid samples, and frozen samples, making IAC the most commonly used method in MHC-I peptidomics[397]. However, IAC is not without its drawbacks. It is a highly labor intensive and time-consuming process that occurs over multiple days. Modified protocols to streamline the method have been demonstrated (e.g., automated 96-well format)[421] but they are not yet widely used. There are so many other parameters that must be taken into consideration as well depending on the specific needs of each experiment; for example, variations in the detergent for lysate preparation, antibody immobilization technique, purification protocol, and MS data identification method have been reported[397]. Furthermore, the high amount of starting material (usually between 10^8 and 10^{10} cells) and anti-MHC antibodies (specific for different MHC alleles and in-house hybridoma needed for production) required also deter many researchers from pursuing MHC-I peptidomics[422–424]. Nevertheless, high rewards offset the high costs. The elucidation of MHC-I peptidome means the discovery of CD8 T cell targets. This information is especially invaluable in vaccine development, aimed to generate potent immune responses against specific tumor

or pathogenic antigens. Additionally, MHC-I peptidome provides an insight on the underlying mechanism of therapeutic efficacy (i.e., antigens that stimulate anti-tumor T cells in response to immunotherapy).

1.6 RATIONALE AND OBJECTIVES

It is well established that oncolytic reovirus triggers a robust anti-tumor, as well as anti-viral, immunity. Yet the underlying antigenic signals that drive these immune responses have remained elusive even though such information has invaluable use towards the manipulation of CD8 T cell activity to enhance therapeutic efficacy. Thus, the objectives of this thesis were to identify the MHC-I-restricted epitopes of reovirus and reovirus-treated cancer cells and elucidate the corresponding anti-viral and anti-tumor CD8 T cell responses, respectively. The work reported herein is the first to characterize therapy-induced changes to the tumor MHC-I peptidome in response to reovirus – either as a monotherapy (*Chapter 3*) or a combination therapy with immune checkpoint blockade (*Chapter 4*) – and to conduct a genome-wide epitope mapping of reovirus (*Chapter 5*). To achieve this feat, a multidisciplinary approach combining immunology, bioinformatics, and proteomics was designed and utilized.
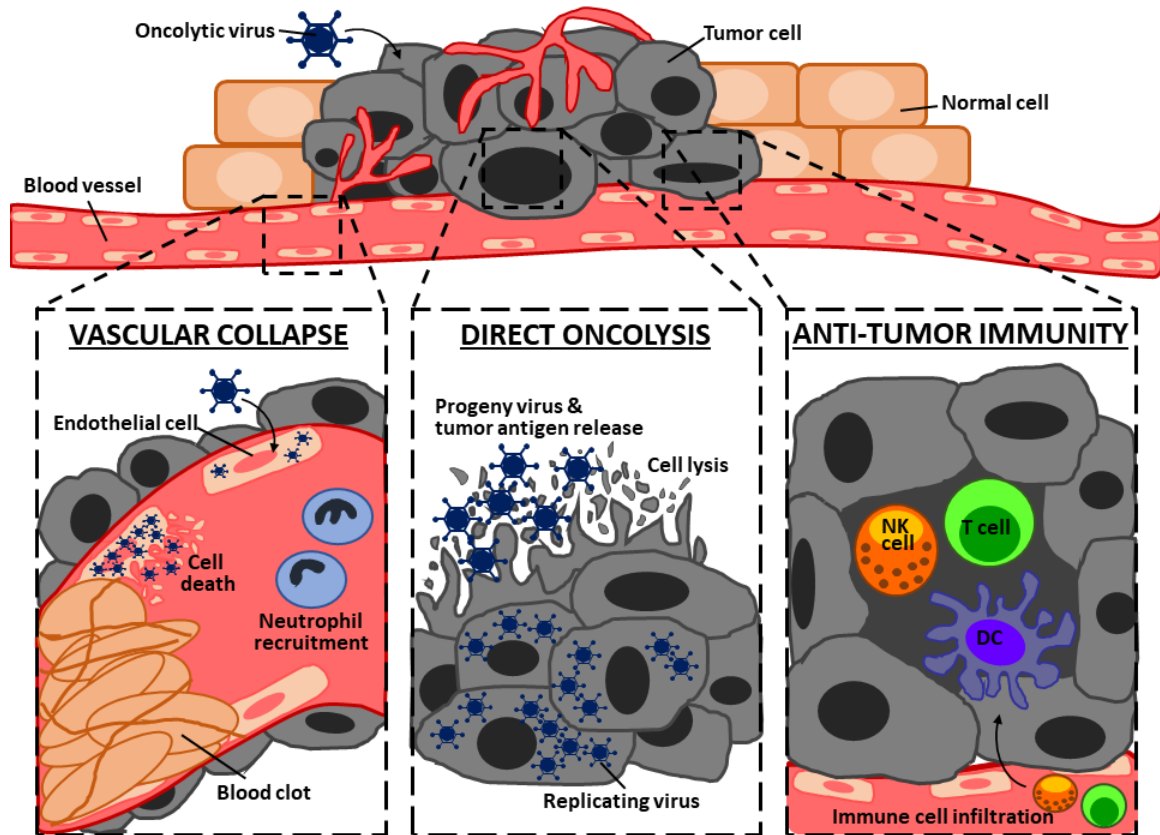
Figure 1.1. *Anti-cancer mechanisms of oncolytic viruses.*

Oncolytic viruses (OVs) cause tumor destruction through a multi-pronged approach involving direct oncolysis, vascular collapse, and anti-tumor immunity. OVs preferentially infect and replicate in cancer cells, leading to cancer cell lysis (i.e., oncolysis) and release of viral progeny particles that spread to infect neighboring cancer cells. OVs attack the endothelial cells lining the tumor vasculature and promote neutrophil-dependent blood clot formation that triggers vascular collapse. OVs also promote the recruitment and activation of innate and adaptive immune cells in the tumor microenvironment, resulting in the generation of highly specific and durable anti-tumor immunity. Figure adapted from Lee and Gujar, *Nat. Rev. Urol.* 2018, 15, 4, 235-250[425].
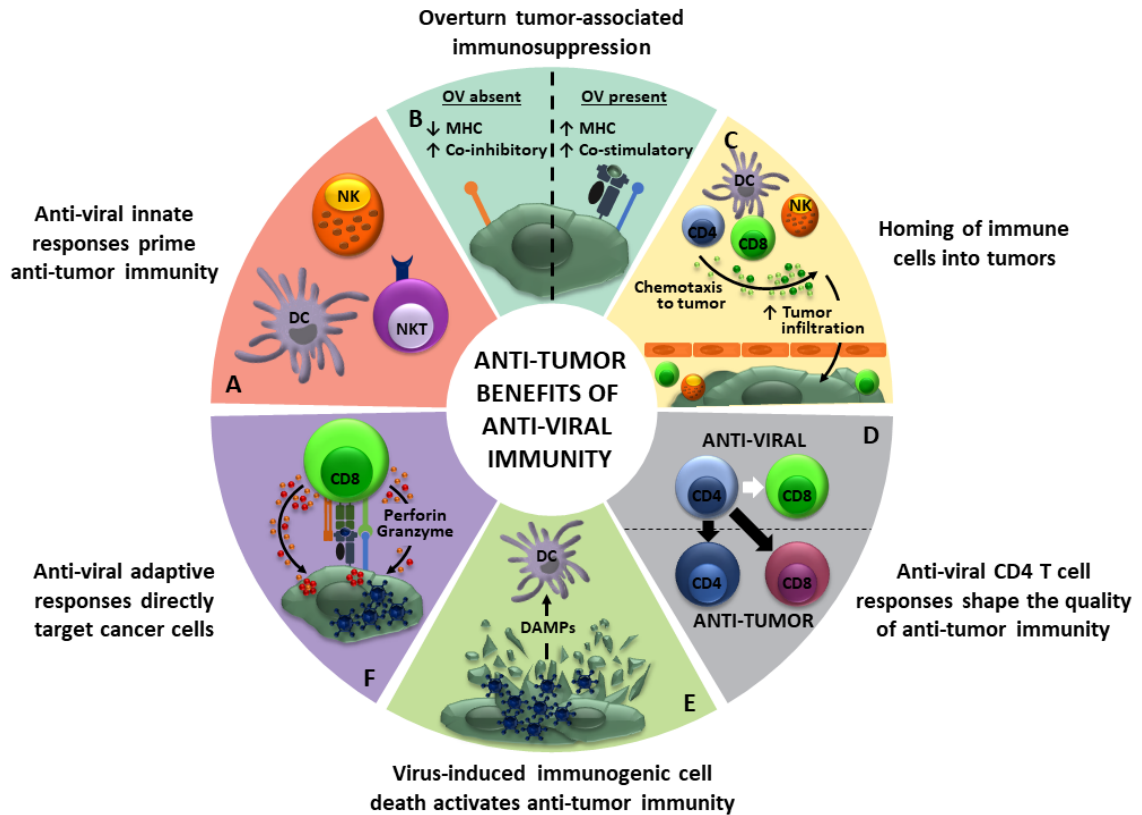
Figure 1.2. *Anti-tumor benefits of anti-viral immunity during OV cancer therapy.*

(A) Anti-viral pro-inflammatory responses activate innate immune cells (e.g., dendritic cells [DC], natural killer cells [NK], and NK T cells). **(B)** OVs overturn tumor-associated immune evasion mechanisms, specifically restoring antigen processing and presentation and inducing the expression of co-stimulatory molecules. **(C)** Anti-viral pro-inflammatory responses promote the recruitment of immune cells into tumors. **(D)** Anti-viral CD4 T cells can aid the activation of anti-tumor CD4 and CD8 T cells. **(E)** OV-mediated oncolysis releases damage-associated molecular patterns (DAMPs) that recruit and activate DCs, promoting the generation of anti-tumor immunity. **(F)** Anti-viral CD8 T cell responses can directly target virus-infected cancer cells. Figure from Gujar and Pol, et al., *Trends Immunol.* 2018, 39, 3, 209-221[110].
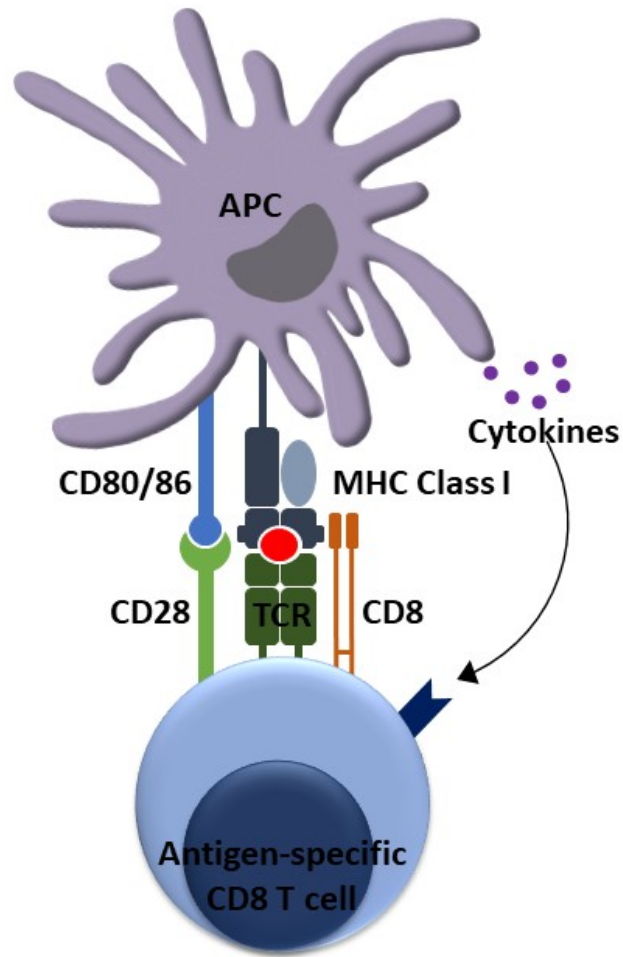
Figure 1.3. *Three signals required for CD8 T cell activation.*

CD8 T cell activation requires three signals from antigen-presenting cells (APCs): [1] an antigenic peptide bound to a class I major histocompatibility complex (MHC) molecule which is recognized by the T cell receptor (TCR), [2] co-stimulation (ligation of CD28 on T cells with CD80 or CD86 on APCs), and [3] pro-inflammatory cytokines. MHC-I ligands define the specificity of CD8 T cell responses.
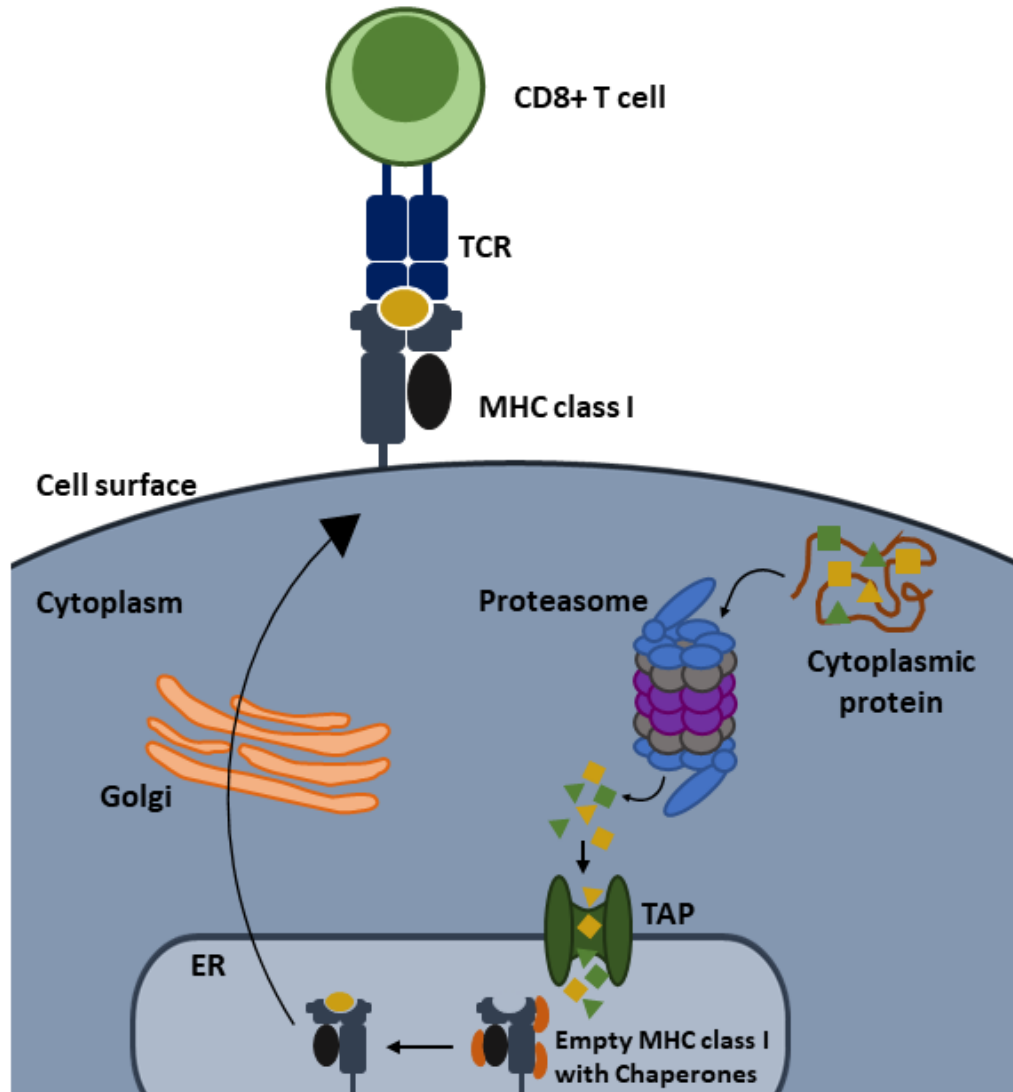
Figure 1.4. *Antigen processing and presentation through the MHC-I pathway.*

Proteins of cytoplasmic origin are degraded by the proteasome into short peptide fragments (3-15 amino acids in length). Peptides are translocated by transporters associated with antigen processing (TAP) into the endoplasmic reticulum (ER), where they are further trimmed (8-11mer peptides) and then loaded into the peptide-binding groove of MHC-I molecules with the help of chaperone proteins. Stable peptide-MHC complexes then migrate to the cell surface via the Golgi apparatus and are presented for recognition by CD8 T cells via the T cell receptor (TCR).
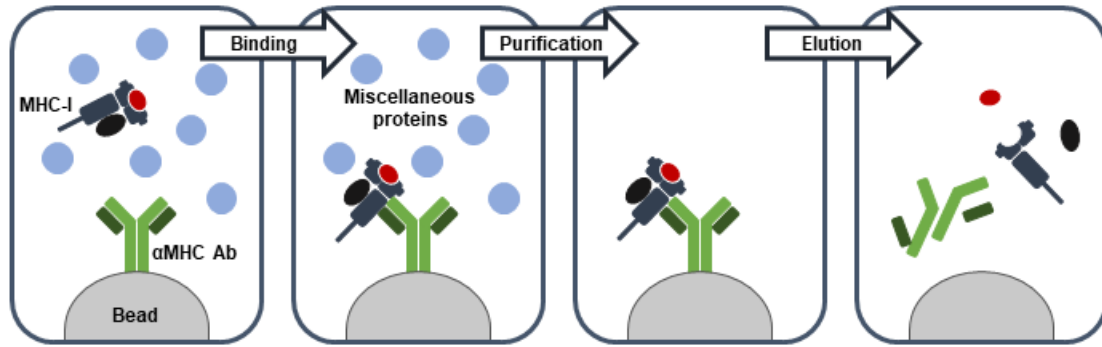
Figure 1.5. *MHC-I peptide isolation by immuno-affinity chromatography.*

Antibodies specific against MHC-I molecules (αMHC Ab) immobilized on a solid support (e.g., beads) are used to isolate peptide-MHC complexes. Unbound, miscellaneous proteins are removed by a purification step. Peptides are eluted from the MHC-I molecule and then separated from the mixture using molecular weight cut-off filters or reverse-phase chromatography.

CHAPTER 2: MATERIALS AND METHODS

2.1   CELL LINES AND REAGENTS

Mouse ovarian surface epithelial cell line (MOSE, clone ID8) was obtained from Dr. Edith Lord (University of Rochester, Rochester, NY)[426], mouse MCA205 fibrosarcoma cell line from Dr. Guido Kroemer (INSERM, Villejuif, France)[427], and mouse EL4 T lymphoma cell line from Dr. David Hoskin (Dalhousie University, Halifax, NS, Canada). All three cell lines were grown at 37 °C, 5% CO_2 in DMEM containing 10% (vol/vol) fetal bovine serum (FBS), 1X sodium pyruvate, 1X nonessential amino acids, and 1X Antibiotic-Antimycotic (all obtained from Invitrogen, Carlsbad, CA). Reovirus (serotype 3, Dearing strain) was available by in-house production – cultured, amplified, and isolated using a previously established protocol[428]. TMT10plex isobaric label reagent set plus TMT11-131C label reagent, and Imject Freund's Complete and Incomplete Adjuvant were purchased from Thermo Fisher Scientific (San Jose, CA). Recombinant mouse IFNγ (carrier-free) was purchased from BioLegend (San Diego, CA). For validation experiments of tumor MHC-I ligands (*Chapters 3 and 4*), peptides were purchased from JPT Peptide Technologies (Berlin, Germany) and lyophilized peptides were resuspended in phosphate-buffered saline (PBS; Invitrogen). Peptide vaccination experiment (*Chapter 3*) utilized keyhole limpet hemocyanin (KLH)-conjugated peptides[429] from JPT Peptide Technologies. Reovirus peptides (*Chapter 5*) were purchased from ProImmune, Inc. (Sarasota, FL) and Genscript USA, Inc. (Piscataway, NJ) and resuspended in dimethyl sulfoxide (DMSO). SIINFEKL peptide from ovalbumin ($OVA_{257-264}$) was purchased from AnaSpec (Fremont, CA) and resuspended in PBS. Peptide-MHC tetramers (H2-K^b $S3_{21-28}$, VCPNYVML, PE-conjugated) were synthesized and provided by the NIH Tetramer Core Facility at Emory

University (Stone Mountain, GA). Ficoll-Paque Premium media was purchased from VWR (Radnor, PA). The following reagents were used for T cell functional assays: concanavalin A (ConA; Sigma-Aldrich, St. Louis, MO), Brefeldin A (Sigma-Aldrich), Foxp3/ Transcription Factor Staining Buffer Set (eBioscience, San Diego, CA), and anti-mouse IFNγ DuoSet ELISA kit (R&D Systems, Minneapolis, MN). Other reagents used for flow cytometry include 7-amino-actinomycin D (7AAD) viability staining solution (BioLegend), Fixable Viability Dye eFluor 780 (eBioscience), and CellTrace Violet Cell Proliferation Kit (Invitrogen). The antibodies listed in Table 2.1 were all reactive against mouse unless otherwise specified and used at the concentrations recommended by the manufacturer.

2.2 ANIMAL EXPERIMENTS

2.2.1 Ethics Approval

All *in vivo* experimental procedures were approved by the University Committee on Laboratory Animals (UCLA) at Dalhousie University, Halifax, NS, Canada in accordance with the Canadian Council on Animal Care (CCAC) guidelines. Six to eight weeks old female wildtype C57BL/6 mice were obtained from Charles River Laboratories (Montreal, QC, Canada) and kept in group housing.

2.2.2 Reovirus Infection in Non-TB Mice

For the analysis of immune checkpoint expression (*Chapter 4*) and anti-viral immune responses (*Chapter 5*), mice were injected with 5 x 10^8 plaque forming units (PFU) of reovirus, intraperitoneal (i.p.). Cells were harvested from the peritoneum (site of injection) and spleen (lymphoid organ) at 7 days post injection (d.p.i.) unless otherwise stated.

2.2.3 Establishment of Tumor Models and Treatment in TB Mice

For the ID8 tumor model, mice were injected with 3 x 10^6 cells in PBS, i.p., and then injected with reovirus (5 x 10^8 PFU, i.p.) at day 35 post tumor implantation; tumor nodules in the peritoneum and spleens were collected at 7 d.p.i. for MHC-I peptidome analysis and validation (*Chapter 3*). For the analysis of TILs (*Chapter 4*), ID8 TB mice were injected with reovirus (5 x 10^8 PFU, i.p.) at day 28 post tumor implantation and cells were collected from the peritoneum and spleen at 7 d.p.i..

For the MCA205 and EL4 tumor models, mice were injected with 5 x 10^5 cells in the right hind flank, subcutaneous (s.c.), and injected with reovirus (5 x 10^8 PFU, intratumoral [i.t.]) at 10-14 days post tumor implantation (at tumor volume of approximately 20 mm³, calculated as length x width x height). For MHC-I peptidome analysis of MCA205 tumors (*Chapter 4*), mice were injected as follows with the frequency of treatment shown in the figure schematics: reovirus (5 x 10^8 PFU, i.t.), anti-mouse PD-1 antibody (250 µg/mouse, i.p.), rat IgG2a isotype control antibody (250 µg/mouse, i.p.); for the validation of the MHC-I peptides, spleens were harvested from MCA205 TB mice following the same treatment regimen as the one used to collect MHC-I IP samples. For the analysis of anti-viral immune responses (*Chapter 5*), cells from tumors and spleens were harvested at 7-10 days post reovirus injection, and lymphocytes were isolated by Ficoll-Paque density gradient centrifugation (400 xg for 40 min). For the establishment of EL4 tumors in reovirus-immunized mice (*Chapter 5*), mice were first injected with reovirus (5 x 10^8 PFU, i.p.), implanted with EL4 cells (5 x 10^5 cells, s.c.) at 7 d.p.i., and tumors and spleens were harvested at 18 days post tumor implantation. All subcutaneous and intratumoral injections were performed while mice were anesthetized with isoflurane (3

L/min, O$_2$ at 2 L/min). TB mice were euthanized upon reaching set timepoints, ulceration, >15 mm in one dimension, or other signs of morbidity.

2.2.4   Peptide Vaccination (Chapter 3)

Mice were immunized with a pool of KLH-conjugated peptides (GIIRFLIGF, INYVVAHV, STLSHVVL, and RSYRFMVM; total 200 µg/mouse) resuspended in PBS and emulsified in a 1:1 ratio with complete Freund's adjuvant, injected subcutaneously in the right hind flank. A booster of the peptides emulsified in incomplete Freund's adjuvant was administered 14 days later. At 21 days post booster, mice were implanted with ID8 cells (3 x 10^6 cells, i.p.) and then injected with a therapeutic regimen of reovirus (3 doses of 5 x 10^8 PFU each) at day 14, 16, and 18 post tumor implantation. ID8 TB mice were monitored for the onset of ascites development and euthanized when abdominal distension was equal to that of a near-term female.

2.3   MHC-I ISOLATION BY IMMUNO-PRECIPITATION

2.3.1   Cyanogen Bromide-activated Sepharose 4B-based Pulldown Assay (Chapter 3)

MHC-I peptide immuno-precipitation was conducted as previously described[430]. In brief, 1 x 10^8 ID8 cells for each treatment group (non-treated, IFN-γ treated [100 units/mL], and reovirus-treated [multiplicity of infection 10] for 24 h), and 1 g of pooled tumor tissue or spleens for each treatment group (PBS- and reovirus-treated ID8 TB mice tumors and spleens, PBS- and reovirus-treated naïve mice spleens) were harvested, flash frozen, and stored at -80 °C until processing. Samples were lysed in PBS containing 0.4% CHAPS and cOmplete, Mini protease Inhibitor Tablets (Roche, Indianapolis, IN). MHC-I proteins were precipitated from the cell lysates using 2 mg of anti-MHC-I antibody (both H2-D^b and H2-K^b for mouse) coupled to 80 mg of cyanogen bromide (CNBr)-activated Sepharose 4B

resin (Uppsala, Sweden). Following overnight incubation in 10 mL glass tubes at 4 °C, bound MHC-I proteins and peptides were washed with 40 mL of PBS, then 30 mL of Milli-Q water, and peptides were eluted from the antibody-resin by acid treatment (8 times with 200 µL of 0.2% trifluoroacetic acid [TFA]). Eluates were purified by ultrafiltration through 3 kDa molecular weight cut-off filters (Millipore, Cork, Ireland), and then the filtrates were lyophilized and desalted using home-made Stage-tips packed with Empore C18 extraction material (Sigma-Aldrich) as previously described[431], then lyophilized.

2.3.2   Protein A Sepharose 4B-based Pulldown assay (Chapter 4)

Tumor samples were collected following the treatment regimens shown in the figure schematics, flash frozen, and stored at -80 °C until processing as previously described[421,432–434]. For each treatment group, 1 g of tumor tissue was cut in small fragments and mixed with 10 mL of lysis buffer comprised of 0.25 % sodium deoxycholate (Sigma-Aldrich), 0.25 mM iodoacetamide (Sigma-Aldrich), 1 mM EDTA (Thermo Fisher Scientific), 1:200 cOmplete, Mini protease Inhibitor Tablets (Roche), and 1% octyl-β-glucopyranoside (Sigma-Aldrich) in PBS. The lysates were processed with a tissue homogenizer (three 20 s intervals, on ice), shaken gently on a rotator for 30 min at 4 °C, sonicated (three 20 s intervals, on ice), and shaken again for 30 min at 4 °C. Lysates were cleared by centrifugation at 4 °C, 3300 xg for 50 min, and then pre-cleared of endogenous antibodies using Protein-A Sepharose 4B (Pro-A) beads (Invitrogen). MHC-I complexes were immuno-affinity purified from the lysates using the B22.249 and Y3 antibodies (1 mg/g of tissue each), covalently bound to Pro-A beads with dimethyl pimelimidate dihydrochloride (Sigma-Aldrich) and incubated overnight at 4 °C on a rotator. The samples were passed through Poly-Prep columns (BioRad Laboratories, Hercules, CA) and the

bead-bound MHC-I proteins and peptides were washed 4 times with 2 mL of 150 mM NaCl in 20 mM Tris-HCL, pH 8.0; 4 times with 2 mL of 400 mM NaCl in 20 mM Tris-HCL, pH 8.0; 4 times with 2 mL of 150 mM NaCl in 20 mM Tris-HCL, pH 8.0; and then 2 times with 2 mL of 20 mM Tris-HCL, pH 8.0 using a vacuum manifold. MHC-I molecules and their bound peptides were eluted 8 times with 200 µL of 0.2% TFA. The eluates were purified by solid phase extraction (SPE) with 60 mg Oasis HLB cartridges (Waters, Milford, MA). Peptides were eluted from SPE with 30% acetonitrile (ACN), lyophilized, and desalted using home-made Stage-tips packed with Empore C18 extraction material (Sigma-Aldrich) as previously described[431], then lyophilized.

2.4   MHC-I ANALYSIS BY MASS SPECTROMETRY

Label-free MHC-I peptides were solubilized in 12 µL of 1% formic acid and analyzed by LC–MS/MS as previously described[435]. For TMT-labeled peptidomics, lyophilized peptides were first solubilized in 100 µL of 30% ACN in 50 mM HEPES (pH 8.5) and 10 µL of TMT reagents at a final concentration of 20 µg/mL in anhydrous ACN for 1 h at room temperature (RT), quenched with 0.5% hydroxylamine (Sigma-Aldrich), combined, and purified by SPE with 10 mg Oasis HLB cartridges (Waters). Lyophilized TMT-labeled peptides were resuspended in 6 µL of 1% formic acid and analyzed by LC-SPS-MS3[434].

MHC-I peptides were identified using a previously described targeted search strategy[435]. Briefly, MHC-I peptides were predicted from all mouse proteins for the H2-D^b and H2-K^b alleles using NetMHC with a rank cut-off of 2% and these peptides were used to create a FASTA database. MS data were searched using Sequest with "no cleavage" enzyme specificity with an MS1 tolerance of 5 ppm and MS2 tolerance of 0.5 Da. False discovery rates were controlled to 5% using Percolator. Searches were implemented in

Protein Discoverer (PD) version 2.2 (Thermo Fisher Scientific). Label-free quantitation was also implemented in PD version 2.2 using the Minora peak alignment algorithm. All peptides were normalized based on the summed peptide intensity for the entire sample. For TMT-labeled MHC-I peptides, the summed reporter ion S/N for all spectral matches (PSMs) for each peptide was used for relative quantitation and normalized within each channel using the summed S/N for all compared peptides. Averages of the technical duplicates for each experimental group were used for analysis. Reovirus-induced MHC-I peptides (*Chapter 3*) were determined as those with mean $\log_2$[fold change] ≥ 1, compared to control, and p values ≤ 0.05 (adjusted using Benjamini-Hochberg multiple hypothesis correction). Therapy-modulated MHC-I peptides (*Chapter 4*) were those with mean $\log_2$[fold change] ≥ 1 or ≤ -1, compared to control. Gene ontology (GO) enrichment analysis for biological processes (BPs) was completed for the source proteins of MHC-I peptides using the PANTHER Classification System with the *Mus musculus* reference list.

2.5   QUANTITATIVE PROTEOMICS

2.5.1   Sample Preparation

Reovirus-infected ID8 cells (multiplicity of infection [MOI] 1 or 10) were harvested at five timepoints over 48 hours. Cells were scraped into 2 mL of lysis buffer containing 2% SDS, 150 mM NaCl, 50 mM Tris (pH 8.5), 5 mM DTT, and 1 tablet of protease inhibitor (Sigma-Aldrich) per 10 mL of buffer. Samples were homogenized with an Omni homogenizer (Omni International, Kennesaw, GA) with 3 cycles of 12 s, with cooling on ice between cycles, plus sonication with probe sonication. Samples were incubated at 56 °C for 30 min, cooled, then cysteines were alkylated using 14 mM iodoacetamide, and protein was purified by methanol-chloroform precipitation. Proteins were dried then resolubilized in

1.5 mL of 8 M urea, 50 mM Tris, pH 8.8 then protein content in the samples was measured using a BCA assay (Thermo Fisher Scientific). An aliquot of 100 µg of protein was diluted to 1.5 M urea, digested for 4 h with trypsin (Promega, Madison, WI) then again overnight (both at a ratio of 1:100 trypsin:protein) at 37 °C. The pH of the digest was adjusted to < 3 using formic acid and peptides were desalted using 60 mg solid phase Oasis HLB extraction cartridges (Waters) then lyophilized. Peptides were resuspended in 100 µL of 100 mM HEPES, 30% ACN and 10 µL of TMT10 reagents (Thermo Fisher Scientific) pre-aliquoted at a concentration of 20 µg/mL in anhydrous ACN. The reaction was quenched with 0.5% hydroxylamine (Sigma-Aldrich), mixed equally, desalted using a 60 mg solid phase Oasis HLB extraction cartridge (Waters), and lyophilized.

2.5.2 Data Acquisition and Analysis

Peptides were fractionated using an Onyx monolithic 100 x 4.6 mm C18 column (Phenomenex, Torrance, CA) using a flow rate of 800 µL/min, with a gradient of 5−40% ACN (10 mM ammonium formate, pH 8) applied over 60 min using an Agilent 1100 pump (Agilent Technologies, Santa Clara, CA). Twelve fractions were collected and desalted using home-made Stage-tips packed with Empore C18 extraction material (Sigma-Aldrich) as previously described[431], then lyophilized and subjected to LC-SPS-MS3 as described previously[436]. Mass spectrometry data files were converted to mzXML using a modified version of ReadW.exe. MS2 spectra were searched against the mouse Uniprot database (downloaded August, 2011) using Sequest (Ver28)[437] concatenated with a reovirus protein sequence database. TMT was set as a fixed modification (229.162932) on lysine residues and peptide N-termini, and carbamidomethylation (15.99492) as a fixed modification on cysteine. The allowable precursor mass tolerance was 10 ppm and product ion mass

tolerance was 1 Da. False positive rates were controlled using the target-decoy approach[438] with a concatenated reversed database employing linear discriminant analysis to distinguish correct and incorrect peptide identifications based on XCorr, ΔCN, peptide length, and charge state. Peptides were grouped into proteins and their multiplied linear discriminant analysis probabilities were used to sort proteins and filter to a 1% maximum false discovery rate. The sum of all reporter ion summed signal to noise (S/N) values for peptides matching each protein was used for protein quantitation.

2.6 EXPERIMENTAL DESIGN AND SAMPLE PROCESSING

MHC-I IP were performed in technical duplicates and/or analyzed by MS in technical triplicates. All *in vitro* experiments for flow cytometry analysis were completed in technical triplicates in at least three independent experiments (mean ± SD shown for bar graphs and representative data from one experiment shown for histograms, unless otherwise stated). T cell activation assays to validate the immunogenicity of MHC-I peptides were performed using splenocytes pooled from 2-3 biological replicates. Validation screens in *Chapters 3* and *4* were performed for the individual peptides without replicates due to the limited amount of synthetic peptide available. For the comparison of ID8 and MCA205 cancer cells (*Chapter 4*), cells were infected with reovirus at MOI of 0, 10, 100, 1000, and 10000 for 24 or 48 h *in vitro*. Stimulation with mouse IFNγ at 100 units/mL (U/mL) was included as a positive control. Cells were collected for antibody staining (flow cytometry analysis) by trypsinization. For peptide-pulsing of cancer cells (*Chapter 5*), cancer cells were incubated with the peptides at the concentrations indicated in the figures for 4 h at 37 °C. For co-culture assays, the supernatant of peptide-pulsed cancer cells was removed and splenocytes were added for 24 h in fresh media. Cancer cells

were stained with 0.5 µM CellTrace Violet (CTV) in PBS for 20 min at 37 °C prior to peptide-pulsing. To assess the activation of antigen-specific T cells following co-culture, the effector (splenocytes) to target (cancer cells) ratio was 10:1; to assess cytotoxicity against peptide-pulsed cancer cells, it was 40:1.

For immune cell analysis following *in vivo* experiments, cells were collected and analyzed for each mouse independently. Cells were harvested via a flush of the peritoneum with PBS-EDTA (1% vol/vol), and spleens were mechanically disrupted using the end of a syringe plunger. Harvested cells were filtered through a 40 µm cell strainer, treated with red blood cell-lysing ammonium-chloride-potassium (ACK) buffer (Thermo Fisher Scientific) and then washed in flow cytometry running buffer (PBS-EDTA with 1% FBS; FACS buffer). For TB mice, tumor and spleen samples were subjected to Ficoll-Paque density gradient centrifugation instead of the ACK step.

2.7   T CELL FUNCTIONAL ASSAY

For splenocytes containing CD8 T lymphocytes and antigen-presenting cells, spleens were harvested from mice and mechanically disrupted using the end of a syringe plunger. Cells were filtered through a 40 µm cell strainer and treated with red blood cell-lysing ACK buffer (Thermo Fisher Scientific). The resulting single-cell suspension of splenocytes was cultured in RPMI 1640 containing 1% (vol/vol) Glutamax, 10% FBS, 1X sodium pyruvate, 1X nonessential amino acids, and 1X Antibiotic-Antimycotic (all obtained from Invitrogen) for *ex vivo* stimulation with peptides. Splenocytes (1 x 10^6 cells/well in a 96-well plate) were cultured in the presence of peptide (10 µg/mL) and purified anti-mouse CD28 antibody (1 µg/mL) for 24 h (48 h if samples were used for ELISA). For intracellular IFNγ staining for flow cytometry analysis, cells were treated with Brefeldin A (2 µg/mL) at 18

h post peptide stimulation and incubated for an additional 6 hours. Control groups included splenocytes cultured with no peptide, splenocytes cultured with anti-mouse CD28 antibody only, and splenocytes cultured with 2 µg/mL of ConA.

2.8 ENZYME-LINKED IMMUNOSORBENT ASSAY (ELISA)

Supernatants were collected from T cell functional assays to be assessed for the concentration of secreted IFNγ using the IFNγ ELISA kit (R&D Systems) following the manufacturer's instructions. In brief, Nunc Maxisorp Immuno Plate (Thermo Fisher Scientific) were coated with the rat anti-mouse IFNγ capture antibody diluted in PBS to the recommended concentration and incubated overnight at 4 °C. Plates were washed 3 times with a wash buffer (0.05% [vol/vol] Tween 20 in PBS) and blocked with 1% BSA in PBS for 90 min at RT. After washing the plates 3 times with wash buffer, samples and serial dilutions of recombinant mouse IFNγ in reagent diluent (0.1% BSA and 0.05% Tween 20 in Tris-buffered saline) were added and incubated overnight at 4 °C. Plates were washed with wash buffer and then biotinylated goat anti-mouse IFNγ detection antibody diluted in reagent diluent were added for 2 h at RT. Plates were washed, streptavidin-HRP was added for 20 min at RT in the dark, plates were washed again, and substrate solution (tetramethylbenzidine, Thermo Fisher Scientific) was added for 20 min at RT in the dark. Stop solution (2N H_2SO_4) was added and the absorbance was measured at 450 nm using a microplate reader. IFNγ concentrations were quantified in relation to the standard curve and the cut-off formula used was (mean + 3 x standard deviation) of the negative controls[439].

2.9 ANTIBODY STAINING FOR FLOW CYTOMETRY

2.9.1 Extracellular Surface Marker Staining

All antibody staining were done in FACS buffer for 25 min at 4 °C in the dark unless otherwise stated, washed with FACS buffer and pelleted by centrifugation (500 xg for 5 min at 4 °C) between each step, fixed with 1% paraformaldehyde (PFA) for 15 min at RT, and resuspended in FACS buffer prior to analysis. Immune cell samples were blocked with anti-CD16/32 antibody prior to extracellular surface marker staining. All flow cytometry data were collected using FACS Canto II and LSR Fortessa flow cytometers (BD Bioscience), and analysis was conducted using FACSDiva (BD Bioscience) and FCS Express V6 software (DeNovo Software).

2.9.2 Intracellular Staining

To measure intracellular reovirus for assessing infectivity (*Chapter 4*), cells were fixed with 1% PFA and then permeabilized in 1% Triton X-100 (Sigma-Aldrich; vol/vol in PBS) for 15 min at RT. Cells were incubated with rat anti-reovirus polyclonal primary antibody (1:500) in 0.1% Triton X-100 for 25 min at 4 °C, followed by goat anti-rat secondary antibody (1:500) in 0.1% Triton X-100 for 25 min at 4 °C. Intracellular cytokine staining (IFNγ or granzyme B; *Chapters 4 and 5*) was performed after the extracellular surface marker staining step. The Foxp3/transcription factor staining buffer set was used following the manufacturer's instructions. Briefly, cells were fixed and permeabilized (fix/perm buffer), washed with permeabilization buffer, and then incubated with the intracellular protein-binding antibody in permeabilization buffer.

2.9.3 Viability Staining

To measure cell death for assessing oncolysis (*Chapter 4*), cells were washed with PBS and then stained with Annexin V in Annexin V binding buffer (10 mM HEPES, 150 mM NaCl, 2.5 mM $CaCl_2$ in PBS) for 5 min at RT. Without a wash step, 7AAD in Annexin V

binding buffer was added and incubated for an additional 15 min at RT. Data for these live samples were acquired using the flow cytometer. To assess cytotoxicity against peptide-pulsed cancer cells (*Chapter 5*), cells were stained with the Fixable Viability Dye eFluor 780 in PBS for 15 min at RT and then fixed with 1% PFA.

2.9.4   Tetramer Staining

PE-conjugated peptide-MHC tetramers were used to stain virus-specific T cells. A 1:10 working stock in PBS was prepared and used for up to 3 months at a time. Peptide-MHC tetramers were used at a final dilution of 1:1000 in FACS buffer. After cells were blocked with anti-CD16/32 antibody, cells were incubated with MHC tetramers for 20 min at RT. Samples were then stained for extracellular surface markers and then fixed, with minimal vortexing at all stages once MHC tetramers were added.

2.10   REAL-TIME QUANTITATIVE POLYMERASE CHAIN REACTION (RT-QPCR)

RNA extractions were performed using standard TRIzol methodology and Purelink RNA Mini Kit (Invitrogen) following the manufacturer's instructions. Purified RNA was quantified and diluted to 2 μg for the synthesis of complementary DNA (cDNA) using Superscript II (Invitrogen). cDNA was amplified and quantified using the CFX96 touch RT-PCR instrument (BioRad Laboratories) and murine gene-specific primers listed in Table 2.2 (primer sequences were obtained from our previous publications and all primers were purchased from Invitrogen). qPCR data were collected and analyzed using the Livak and Schmittgen's $2^{-\Delta\Delta CT}$ method[440], where fold change was calculated by first normalizing the cycle threshold (C_T) of the indicated gene against the *Gapdh* reference gene, followed by a comparison against the respective controls.

2.11 *IN SILICO* EPITOPE PREDICTION AND PEPTIDE-MHC BINDING VALIDATION (*CHAPTER 5*)

Through the Class I ProImmune REVEAL & ProVE Rapid Epitope Discovery System[441], an overlapping (offset by 1 amino acid) PEPscreen® peptide library was generated. It was comprised of reovirus-derived 8mer and 9mer peptides restricted to H2-K^b and H2-D^b MHC-I alleles, respectively, predicted using the SYFPEITHI epitope prediction algorithm[405] on the whole reovirus genome. Peptides with SYFPEITHI score ≥ 20 for H2-K^b and ≥ 21 for H2-D^b were synthesized and screened by ProImmune REVEAL® MHC-peptide binding assay. MHC-binding score for each peptide is calculated in comparison to a positive control peptide with a high binding affinity, and peptides with a score $\geq 45\%$ of the positive control are considered good binders.

2.12 STATISTICAL ANALYSIS

Statistical analyses of all MHC-I and proteomic data in *Chapter 3* were performed in R. F-tests were performed on the quantitative MHC-I and proteome data using the *genefilter* package. Histogram ridge plots were generated using *ggridges*, position-specific frequency matrices (PSFM) were calculated using *peptools,* sequence logos were generated using *ggseqlogo,* and heatmaps were generated using *pheatmap* R packages.

All other statistical analyses were done in GraphPad Prism 6.0 software (GraphPad Software Inc). All results were expressed as the mean ± standard deviation (SD) unless otherwise stated. The number of animals used in each experiment is indicated in the figure legends. One-way analysis of variance (ANOVA) with Bonferroni post-test or a two-tailed Student's *t*-test with 95% confidence interval was used for statistical analysis where indicated. *p* values were corrected for multiple hypothesis (adjusted p-values) using

Benjamini Hochberg for MHC-I peptide analysis in *Chapter 3*. Data for Kaplan-Meier survival curves were analyzed by log-rank (Mantel-Cox) test[442,443]. Statistical significance is represented as follows: ns = $p > 0.05$, *$p \leq 0.05$, **$p \leq 0.01$, and ***$p \leq 0.001$.

Table 2.1. *Antibodies used for flow cytometry, MHC-I IP, and ICB therapy.*

Target	Clone	Conjugated fluorochrome	Company
Annexin V		FITC	BioLegend (San Diego, CA)
CD16/32	2.4G2	Non-conjugated	Bio X Cell (Lebanon, NH)
CD19	1D3	BV510	BD Biosciences (San Jose, CA)
CD19	1D3	APC	BD Biosciences (San Jose, CA)
CD28	37.51	Non-conjugated	BioLegend (San Diego, CA)
CD3	17A2	PE-Cy7	BioLegend (San Diego, CA)
CD3	17A2	FITC	BioLegend (San Diego, CA)
CD3ε	145-2C11	PE	BioLegend (San Diego, CA)
CD4	RM4-5	FITC	BioLegend (San Diego, CA)
CD44	IM7	FITC	BioLegend (San Diego, CA)
CD62L	MEL-14	BV650	BD Biosciences (San Jose, CA)
CD62L	MEL-14	APC	BioLegend (San Diego, CA)
CD8a	53-6.7	PerCP-Cy5.5	BioLegend (San Diego, CA)
CTLA-4	UC10-4F10-11	APC-R700	BD Biosciences (San Jose, CA)
F(ab')2-goat anti-rat IgG (H+L)		FITC	eBioscience (San Diego, CA)
Granzyme B	GB11	FITC	BioLegend (San Diego, CA)
H2-D^b	B22.249	Non-conjugated	In-house
H2-D^b	28-14-8	FITC	eBioscience (San Diego, CA)
H2-K^b	Y3	Non-conjugated	In-house
H2-K^b	AF6-88-5	APC	BioLegend (San Diego, CA)
H2-K^b bound to SIINFEKL (MHC-ova)	25-D1.16	PE	BioLegend (San Diego, CA)
IFNγ	XMG1.2	APC	eBioscience (San Diego, CA)
PD-1	29F.1A12	Non-conjugated	Bio X Cell (Lebanon, NH)
PD-1	29F.1A12	PE-Cy7	BioLegend (San Diego, CA)
PD-L1	10F.9G2	PE	BioLegend (San Diego, CA)
Rat IgG2a isotype control	2A3	Non-conjugated	Bio X Cell (Lebanon, NH)
Reovirus (Rat)	Polyclonal	Non-conjugated	In-house
TIGIT	1G9	BV650	BD Biosciences (San Jose, CA)
TIM3	RMT3-23	APC	BioLegend (San Diego, CA)

Table 2.2. *Sequences of mouse gene-specific primers used for RT-qPCR.*

Gene	Forward sequence (5' to 3')	Reverse sequence (5' to 3')
Gapdh	TGGCAAAGTGGAGATTGTTG	AAGATGGTGATGGGCTTCCC
Cxcl10	GTTGAGATCATTGCCACGATGAAA	CTGCTGTCCATCCATCGCA
Ddx58	AGACGGTTCACCGCATACAG	AAGCGTCTCCAAGGACAGTG
Ifnb	CCCTATGGAGATGACGGAGA	ACTTGAGGTGGTCGTCTGTC
Il1b	GCCCATCCTCTGTGACTCAT	AGGCCACAGGTATTTTGTCG
Tlr3	TCCTGCTGGAAAACTGGATGG	AGCCTGAAAGTGAAACTCGCT

CHAPTER 3: THERAPY-INDUCED MHC-I LIGANDS SHAPE NEO ANTI-TUMOR CD8 T CELL RESPONSES DURING ONCOLYTIC VIRUS-BASED CANCER IMMUNOTHERAPY

Parts of this work appear in the following publication:

Murphy JP, Kim Y (co-first author), Clements DR, Konda P, Schuster H, Kowalewski DJ, Paulo JA, Cohen AM, Stevanovic S, Gygi SP, Gujar S. 2019. Therapy-induced MHC I ligands shape neo-antitumor CD8 T cell responses during oncolytic virus-based cancer immunotherapy. *Journal of Proteome Research*. 18 (6): 2666-2675.

3.1   AUTHOR CONTRIBUTIONS

JPM and YK contributed equally. JPM conceived the original idea, designed and performed the experiments, and analyzed the data for Figures 3.1-3.3 and Supplementary Figures 3.1-3.3. YK designed and performed the experiments, and analyzed the data for Figures 3.4-3.6. YK drafted the manuscript with input from JPM and SG. DRC contributed to sample preparation for Figure 3.1 and manufactured reovirus. PK developed the targeted database search strategy and contributed to the interpretation of the results. JAP ran the proteomics samples on the mass spectrometer in the SPG laboratory at Harvard University. AMC provided mass spectrometry assistance in the Dalhousie Proteomics Core Facility. HS and DJK contributed to the MHC-I immuno-precipitation methodology. SS provided the antibodies for the MHC-I immuno-precipitation. SG supervised and acquired funding for the project. All authors provided critical feedback of the manuscript.

3.2   ABSTRACT

Oncolytic viruses (OVs), known for their cancer-killing characteristics, also overturn tumor-associated defects in antigen presentation through the class I MHC pathway and induce protective neo anti-tumor CD8 T cell responses. Nonetheless, whether OVs shape the tumor MHC-I ligandome remains unknown. Here, we investigated if an OV induces the presentation of novel MHC-I-bound tumor antigens (termed tumor MHC-I ligands). Using comparative mass spectrometry (MS)-based MHC-I ligandomics, we determined differential tumor MHC-I ligand expression following treatment with oncolytic reovirus in a murine ovarian cancer model. *In vitro,* we found that reovirus changes the tumor ligandome of cancer cells. Concurrent multiplexed quantitative proteomics revealed that the reovirus-induced changes in tumor MHC-I ligand presentation were mostly independent of their source proteins. In an *in vivo* model, tumor MHC-I ligands induced by reovirus were detectable not only in tumor tissues but also the spleens (a source of antigen-presenting cells) of tumor-bearing mice. Most importantly, therapy-induced MHC-I ligands stimulated antigen-specific IFNγ responses in anti-tumor CD8 T cells from tumor-bearing mice treated with reovirus. These data show that therapy-induced MHC-I ligands may shape the underlying neo anti-tumor CD8 T cell responses. As such, they should be considered in strategies promoting the efficacy of OV-based cancer immunotherapies.

3.3   INTRODUCTION

Therapy-induced anti-tumor immune responses correlate with better cancer outcomes and thus are highly desired in clinics[444–446]. Immunotherapies, administered either alone or in combination with conventional therapies, focus on promoting anti-tumor CD8 T cell responses as the presence of CD8 T cells predicts better clinical outcomes from many of

the commonly occurring cancers[145,447]. Furthermore, immunotherapies like immune checkpoint blockade with anti-PD-1 and anti-CTLA-4 antibodies promote neo CD8 T cell expansion, which otherwise remain undetectable in non-treated cancer patients[144,444,448]. These therapy-induced CD8 T cell responses can recognize and target cancer cells and also establish protection against relapse[142,144,449]. As the activation of CD8 T cells is defined by the epitopes presented in class I MHC molecules (also known as MHC-I ligands), the tumor MHC-I ligandome shapes anti-tumor CD8 T cell responses. The potential role of therapy-driven MHC-I ligandome changes is poorly understood.

Reovirus, in its natural form, preferentially replicates in and kills cancer cells and is thus considered an oncolytic virus (OV) leading to several clinical trials for its use in cancer treatment. Reovirus also induces potent anti-tumor CD8 T cell immune responses, in part by overturning several tumor-associated immune evasion mechanisms[9,110,425,428,450–455]. This is manifested by a localized release of cytokines within the tumor microenvironment, leading to the activation and recruitment of various innate and adaptive immune cells[12,456]. In addition, antigen-presenting cells that ingest cell debris released during oncolysis may activate tumor antigen-specific CD8 T cells[12,457]. We have previously demonstrated that reovirus OV therapy enhances the expression of proteins involved in antigen processing (e.g., TAP1, TAP2) and presentation (e.g., MHC-I, β_2 microglobulin) in tumors of various cancer types[130,458]. Furthermore, using cancer cells expressing ovalbumin as a surrogate tumor-associated antigen, we have demonstrated reovirus-mediated enhancement of tumor antigen-specific CD8 T cell immunity[130]. This robust OV-mediated anti-tumor CD8 T cell immunity can be further invigorated by genetically

engineering OVs to express immunostimulatory transgenes[3], adding immune checkpoint inhibitors[24,215], or combining with chemotherapeutic drugs[459].

Our laboratory has recently reported MHC-I ligandome changes in response to the chemotherapeutic drug, doxorubicin[434]. Although both preferential tumor replication and increased antigen presentation by OVs are well established, whether OVs also change the tumor MHC-I ligandome has not been explored. Here, we used MHC-I immuno-precipitation and LC-MS/MS with label-free quantitation to determine oncolytic reovirus-induced MHC-I ligands. We found that oncolytic reovirus induces new MHC-I ligands in tumor cells *in vitro* and *in vivo*, and in spleens (a source of antigen-presenting cells) of tumor-bearing animals. Quantitative proteomic analysis of virus-infected cancer cells revealed that reovirus-induced changes within the tumor MHC-I ligandome occur mostly independent of their source proteins. Most importantly, IFNγ-based T cell activation assays showed that these therapy-induced tumor MHC-I ligands are immunogenic. Together, these findings highlight the importance of considering the effect of therapies such as OVs on the tumor MHC-I ligandome. The data provide rationale for exploiting the OV-induced tumor MHC-I ligands for cancer immunotherapies due to OV's preferential replication in tumors.

3.4   RESULTS AND DISCUSSION

3.4.1   *Oncolytic Reovirus Induces the Expression of Otherwise Low-abundant MHC-I Ligands in Mouse Ovarian Cancer Cells in Vitro*

On the basis of our previous findings that reovirus (type 3 Dearing strain) initiates CD8 T cell anti-tumor immunity[130,458], we first sought to determine whether reovirus infection differentially modifies MHC-I ligandome constituents in cancer cells grown *in vitro*.

Mouse ID8 ovarian cancer cells (C57BL/6 background; H2-D^b and H2-K^b MHC-I alleles) were untreated (NT), treated with interferon gamma (IFNγ; a known inducer of MHC-I expression, used as a positive control), or infected with reovirus at a multiplicity of infection (MOI) of 10 for 24 hours. MHC-I peptides were then isolated by MHC-I immuno-precipitation (IP), measured by LC-MS/MS, identified using our recently developed targeted database search approach[435], and quantified by label-free quantitation (Figure 3.1A). This resulted in a dataset of 1,542 unique H2-D^b-specific peptides and 1,346 unique H2-K^b-specific peptides, totalling 2,888 unique MHC-I peptides matching to 3,766 protein accessions. Of these, we obtained label-free quantitation data for 1,393 (90%) and 1,227 (92%) unique H2-D^b- and H2-K^b-specific peptides, respectively (Figure 3.1B). The majority of the MHC-I ligands identified by our method had NetMHC[408,409]-predicted binding affinities ≤0.5% rank and thus were considered strong binders, confirming the robustness of our MHC IP and search strategy (Supplementary Figure 3.1A). In a reference search, not targeted towards MHC-I ligands, we observed 407 unique peptides with NetMHC % rank >2 and some of these were found at a higher abundance following reovirus or IFNγ treatment. However, these arose from commonly observed proteins by proteomics (such as AHNAK, TUBB, and S100A11) or derived from reovirus proteins (Supplementary Figure 3.1B). These peptides are thus likely degradation products or those with weak MHC-I binding affinity but could be investigated further for immunogenicity. Quantitative datasets have been made available at Mendeley Data (DOI: 10.17632/t5xb48z959.1).

We observed vast changes in MHC-I ligands in response to both IFNγ and reovirus, many reaching a level of relative quantitation (above noise) that were as great as the MHC-

I peptides derived directly from virus source proteins (Figure 3.1C). Using IFNγ to control for overall increases in antigen presentation machinery allowed us to determine MHC-I peptides specifically induced by reovirus infection. As such, we observed 274 virus-induced (normalized $\log_2$[reovirus/NT] ≥ 1, adjusted p value ≤ 0.05) MHC-I ligands which were not induced by IFNγ, representing 8.3% of the total MHC-I peptides identified in the experiment (Figure 3.1D). As expected, gene ontology (GO) enrichment analysis using the PANTHER Classification System[460,461] of the source proteins of these specific virus-induced MHC-I ligands were enriched in viral defense biological processes (BPs), as well as DNA replication, cell cycle, and proteolysis regulation (Figure 3.1D). These include proteins such as DDX60, ISG15, and NF-κB and many other proteins involved in the cell cycle (Figure 3.1D). Interestingly, we identified 400 virus-induced MHC-I ligands that are also induced by IFNγ treatment (Figure 3.1E). PANTHER analysis of source proteins of these IFNγ/reovirus-induced MHC-I ligands revealed enriched GO BP terms such as telomere maintenance, G1/S transition, and ubiquitin-dependent catabolic process (Figure 3.1E) exemplified by MHC-I peptides from GVIN1, IFI47, and OASL2 (Figure 3.1E). The comparison between virus-induced and IFNγ/virus-induced MHC-I ligands indicates that some changes in the MHC-I ligandome constituents are virus-specific, independent of the viral enhancement of antigen presentation. Previous studies have reported changes to the self MHC-I peptidome due to virus infections possibly through IFN signaling[462]. However, the unique changes in the MHC-I repertoire apart from antigen presentation differences we observed here may offer therapeutic advantages if the preferential targeting of OV in tumors can be harnessed.

3.4.2 Virus-induced Alterations in the Tumor MHC-I Ligandome are Largely Independent of Their Source Proteins

MHC-I peptide presentation is proposed to correspond to source protein abundance[419]. We therefore next determined whether reovirus-induced alterations in the tumor MHC-I ligands are due to changes at the proteome level. To explore the MHC-I ligand and proteome relationship quantitatively, we performed 10-plex tandem mass tag (TMT)-based quantitative proteomics[463] on virus-infected ID8 cells over a 48-hour time course with two MOI of reovirus (1 and 10) (Figure 3.2A). In total, we quantified 6,561 proteins and observed temporally distinct patterns of protein expression following k-means clustering (Figure 3.2A). GO annotation analysis using PANTHER of Cluster 1, which contained proteins that increased due to reovirus infection, showed enrichment of proteins involved in virus response, interferon response, and antigen processing (Figure 3.2B). Similar to the reovirus proteins that we identified (e.g., Lambda1, Mu1; Figure 3.2C), virus response proteins (e.g., APOL9B, CCL5, GBP4, OAS1A; Figure 3.2D) and antigen presentation proteins (e.g., B2M, H2-D1, TAP1, TAP2; Figure 3.2E) all showed increased relative intensity over time in response to reovirus. These data confirm the results from our previous work showing the effect of reovirus on antigen presentation in ID8 cells[458]. The remaining proteins (five of the six clusters, representing most of the dataset) showed only minor changes, or decreases, in relative intensity over time (Figure 3.2A). Proteomics data have been submitted to the PRIDE repository, accession #PXD013066.

To match peptides to potential source proteins, we matched MHC-I peptides to all potential protein accessions from the UniProt database and then determined whether any of those proteins were in our proteomics dataset (Figure 3.3A). This resulted in 1,022

(66%) and 912 (68%) H2-D^b and H2-K^b peptides, respectively, with successful matches to the proteome dataset (Figure 3.3B). These matches equated to 1,070 and 1,022 peptide-accession combinations for H2-D^b- and H2-K^b-specific peptides, respectively. Comparison of the log$_2$(fold change) in MHC-I peptide abundance against the log$_2$(fold change) in protein abundance at 48 hours revealed poor correlation between MHC-I peptide presentation and protein abundance (Figure 3.3C). For example, AALDFKNV from the protein SMC4 was induced 29-fold but showed no difference at the source protein level (Figure 3.3D). Although most MHC-I peptides indeed showed no protein-level changes, a small fraction of the MHC-I peptides did increase both at the MHC-I peptide and source protein levels (Figure 3.3C). For example, AALTGTHVL from APOL9B was increased 9.2- and 290-fold at the MHC-I peptide and protein levels, respectively (Figure 3.3D).

The general lack of correlation between the MHC-I peptide and source protein levels in our data somewhat contrasts with previous studies on peptide presentation and protein abundance. However, our data concern differential measurements rather than overall abundance, which suggests that external effects on protein abundance, such as those affected by virus infection, are not represented by the MHC-I ligandome changes. These data suggest that virus-induced differences in protein cleavage and peptide trimming, as opposed to the synthesis of new proteins, may play a greater role in MHC-I peptide generation during viral infections. To investigate this, we analyzed source protein sequences of reovirus-induced MHC-I peptides compared to unchanged peptides. We observed only minor differences in the frequency of amino acid residues ten positions upstream or downstream of these MHC-I peptides, between induced or all other MHC-I peptides in the dataset (Supplementary Figure 3.2A). There was also no observable

84

difference in the distance to the source protein N- or C-terminus between the induced, unchanging, or repressed MHC-I peptides (Supplementary Figure 3.2B). Altogether, our data suggest that MHC-I ligand differences from reovirus infection are not caused by differential protein abundance or peptide cleavage. MHC-I peptide presentation is complex and factors such as protein synthesis rates, turnover, and proteostasis should be investigated in further studies to determine how antigen presentation is governed.

3.4.3   *In Vivo, Reovirus Induces Tumor MHC-I Ligands That are Exclusive to Tumor-bearing Mice*

Although it has been observed that OVs elicit anti-tumor immunity, whether induced antigens drive this immune response remains unexplored. Further, a major characteristic of OVs is their preferential replication in tumors as a result of their ability to hijack the active replicative machinery of cancer cells[61]. Having established that reovirus alters the MHC-I ligandome in an *in vitro* setting, we next sought to understand whether the virus preferentially alters the MHC-I ligandome in tumors and whether this is reflected in MHC-I ligands of immune cells. To do this, spleens and/or tumors were collected from non-treated or reovirus-treated mice, either naïve or ID8 tumor-bearing (TB), and analysed by MHC-I IP and LC-MS/MS with label-free quantitation (Figure 3.4A). In this experiment, we quantified 2,447 and 1,681 H2-D^b and H2-K^b peptides, respectively, matching to 6,170 protein accessions in the search database (Figure 3.4B). Consistent with recently reported differences in tissue-specificity of mouse MHC-I ligands[464], we observed only partial overlap with the *in vitro* experiment whereby 1,071 (20% of the 5,199 total peptides between the two experiments) of the *in vitro*-identified MHC-I peptides were not quantified *in vivo* (Supplementary Figure 3.3A). Importantly, preferential tumor replication of

reovirus was indeed reflected in the MHC-I ligandome. We observed a far greater differential MHC-I abundance in the TB mice (both in the spleen and the tumor) than in the naïve mice. For example, 2.9- and 7.8-fold more H2-D^b peptides were induced by reovirus in the spleen and tumor, respectively, of TB mice (normalized log$_2$[reovirus/NT] $\geq$ 1.0, adjusted p value $\leq$ 0.05) (Figure 3.4B). H2-K^b peptides showed this same effect whereby 6.4- and 14-fold more peptides were induced in the TB mice by reovirus at the spleen and tumor, respectively, than in the naïve mice (Figure 3.4B). To further illustrate the preferential reovirus infection in tumors, we directly compared reovirus-induced MHC-I ligands across the experiment. Of the MHC-I peptides that were significantly induced (normalized mean log$_2$[reovirus/NT] $\geq$ 1.0, adjusted p value $\leq$ 0.05) at the tumor, approximately 50% were also induced in the spleen of TB mice but very few of these were induced in the naïve mice (Supplementary Figure 3.3B). Representative label-free quantitation data for several of these MHC-I peptides induced in both the spleen and tumor, tumor-only, or reovirus-derived are exemplified in Figure 3.4C. These data suggest that TB mice display a reovirus-induced tumor MHC-I ligandome that is not found in reovirus-treated naïve mice, PBS-treated naïve mice, or PBS-treated TB mice.

3.4.4 *Reovirus-induced Tumor MHC-I Ligands Contain Biologically Active Anti-tumor CD8 T Cell Epitopes*

Having determined the preferential reovirus-induced MHC-I ligand changes in the ID8 tumor, we next investigated whether these therapy-induced MHC-I ligands elicit anti-tumor CD8 T cell responses. To do this, we chose 16 *highly* virus-induced tumor MHC-I ligands (normalized log$_2$[reovirus/NT] $\geq$ 3.0, adjusted p value $\leq$ 0.05) across a range of NetMHC % rank (but all $\leq$ 2% rank) and peptide spectrum matches (PSMs), and excluding

those that were also induced in the naïve spleen (Figure 3.5A). These highly induced peptides were essentially absent in the untreated tumors and 13 of them were also induced in the spleen of TB mice (Figure 3.5B). These 16 peptides were synthesized and their capacity to elicit CD8 T cell responses in splenocytes of untreated and reovirus-treated TB mice was measured by IFNγ ELISA. We observed no IFNγ response in splenocytes from reovirus-treated TB mice in the absence of any of the peptides or with anti-CD28 co-stimulation alone. In a validation screen, four of these peptides (GIIRFLIGF, INYVVAHV, STLSHVVL, and RSYRFMVM) produced strong responses (>150 pg/mL) in splenocytes of reovirus-infected TB mice, nearly equalling IFNγ production of the concanavalin A positive control (Figure 3.5C). Taken together, these data strongly suggest that reovirus-induced tumor MHC-I ligands can activate CD8 T cells. Although these MHC-I peptides are non-mutated self peptides, they are absent without infection and thus may be immunogenic. These results support findings that the breadth of anti-tumor CD8 T cell immune response is majorly dictated by tumor-associated antigens[465,466]. Most importantly, our data show that OV-induced MHC-I ligands may shape the therapy-induced neo anti-tumor CD8 T cell responses.

3.4.5 Peptide Vaccination with Reovirus-induced Tumor MHC-I Ligands Increases OV Therapeutic Efficacy

To demonstrate the therapeutic potential of the immunogenic virus-induced tumor MHC-I ligands, we used a peptide vaccination approach. We hypothesized that immunization with the tumor MHC-I ligands will generate anti-tumor T cell responses, which will attack cancer cells expressing the cognate MHC-I ligands following reovirus administration. Most peptide-based vaccines to date consist of multiple peptides that result in a more

effective immune response; thus, we created a vaccine pool of the top four most immunogenic virus-induced tumor MHC-I peptides (GIIRFLIGF, INYVVAHV, STLSHVVL, and RSYRFMVM). As per the experiment schematic shown in Figure 3.6A, we had four treatment groups of ID8 TB mice: [1] untreated (PBS→PBS), [2] peptide vaccine alone (PEP→PBS), [3] reovirus alone (PBS→REO), and [4] both peptide vaccine and reovirus (PEP→REO). The PBS→PBS and PEP→PBS groups succumbed to peritoneal carcinomatosis by day 40 post tumor inoculation (Figure 3.6B, gray and green lines). Reovirus treatment alone delayed ascites development as compared to the untreated group, which supports our previous findings in the ID8 model (Figure 3.6B, red line). Most importantly, the combination treatment of peptide immunization and reovirus resulted in a significantly delayed ascites development and prolonged survival in TB mice relative to the untreated control or either treatment alone (Figure 3.6B, blue line). Thus, immunization with the reovirus-induced tumor MHC-I ligands was shown to augment reovirus therapeutic efficacy. As the ID8 model is quite aggressive with a highly immunosuppressive tumor microenvironment and a sudden onset of ascites, anti-tumor immune responses may need to be further strengthened by additional boosters of peptide immunization or inclusion of more immunogenic epitopes in the vaccine regimen. Nevertheless, our data support that virus-induced MHC-I ligands are the driving force behind anti-tumor immunity, which can be potentiated by peptide-based vaccines.

3.5   CONCLUSIONS

Similar to the already proposed implications for cancer neoepitopes[144,448], our data suggest that another promising strategy to enhance anti-tumor CD8 T cell immunity could be to exploit the OV therapy-induced tumor MHC-I ligandome. The exclusive identification of

virus-induced MHC-I peptides in TB mice demonstrates the potential for therapy-induced human HLA-ligand-based vaccines to be developed and used in combination with OVs currently being tested in clinical trials. Finally, induced MHC-I ligands may be valuable not only for OV-based cancer therapies but other treatments that induce neo anti-tumor CD8 T cell responses (e.g., doxorubicin, and checkpoint inhibitors such as anti-PD-1 and anti-CTLA-4 antibodies[144]) ultimately leading to next generation cancer immunotherapies.

3.6 ACKNOWLEDGEMENTS
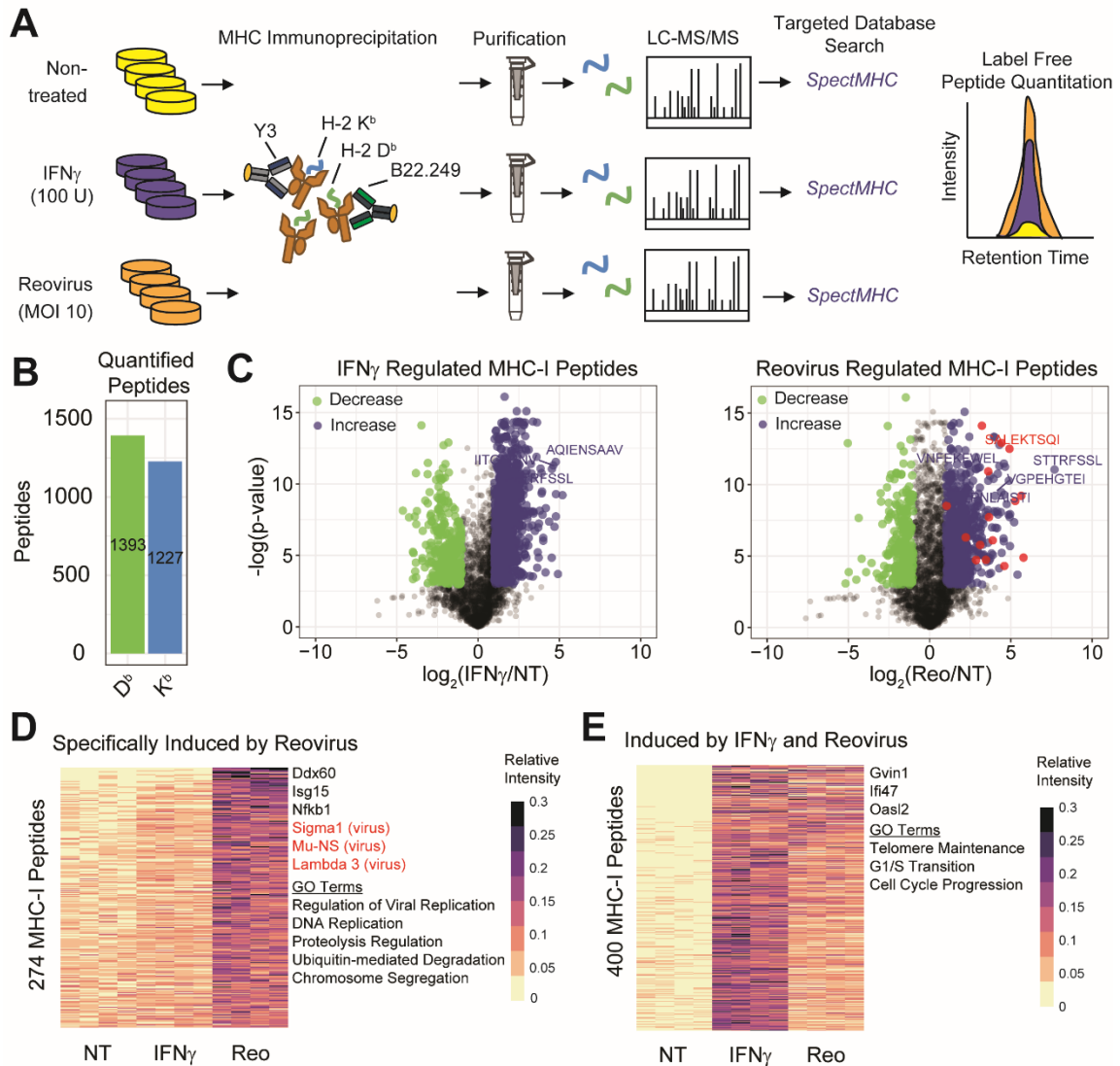
Figure 3.1. *Delineation of the reovirus-induced tumor MHC-I ligandome in vitro.*

(A) Schematic of the experimental setup. ID8 MOSE ovarian carcinoma cells (1×10^8) were treated for 24 hours with IFNγ, reovirus (MOI 10) or left untreated. MHC-I peptides were immuno-precipitated with antibodies specific to the H2-K^b and H2-D^b C57BL/6 mouse MHC-I alleles and analyzed by mass spectrometry. Spectra were then identified with SpectMHC and compared across samples by label-free quantitation. **(B)** Total number of unique peptides specific to the H2-D^b and H2-K^b mouse alleles that were quantified across the experiment. **(C)** Volcano plots of the IFNγ and reovirus quantitative

comparisons. Shown are the -log(p value) based on F-tests (y-axis) versus the $\log_2$(fold change) of reovirus or IFNγ-treated/control (x-axis). Induced (blue dots) or repressed (green dots) peptides are those with normalized $\log_2$(fold change) $\leq$ -1 or $\geq$ 1 and p values $\leq$ 0.05 (adjusted using Benjamini-Hochberg multiple hypothesis correction). Peptides derived from reovirus source proteins are shown in red. **(D)** MHC-I peptides that are specifically induced by reovirus (mean $\log_2$[fold change] $\geq$ 1 and p values $\leq$ 0.05) and not by IFNγ including several examples and enriched GO terms (biological process) pertaining to the source proteins. **(E)** MHC-I peptides that are induced by both reovirus and IFNγ (mean $\log_2$[fold change] $\geq$ 1 and p values $\leq$ 0.05) including several examples and enriched GO terms (biological process) pertaining to the source proteins.
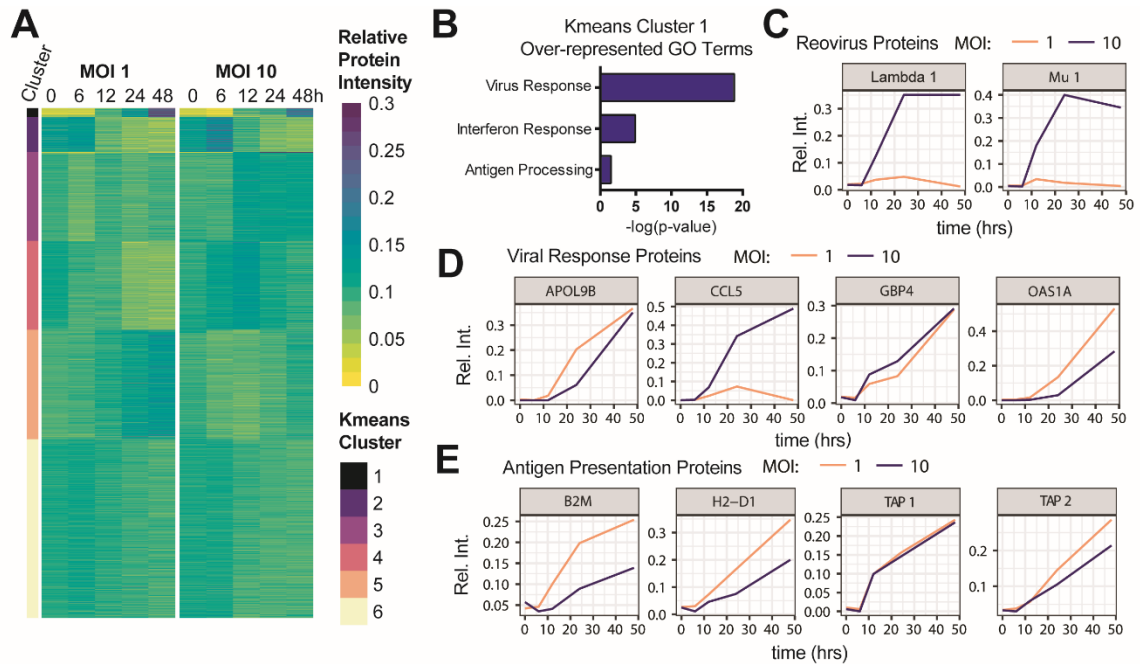
Figure 3.2. *Summary of temporal quantitative proteomics of reovirus-infected ID8 cells.*

(A) ID8 cells were harvested at five timepoints over 48 hours of reovirus infection at MOI 1 or MOI 10 followed by multiplexed, quantitative proteomics using tandem mass tags (TMT). Shown is a heatmap with six k-means clusters (colored alongside) of the multiplexed relative temporal proteomics dataset (n=6,561 proteins). **(B)** Enriched GO terms (derived using PANTHER) in k-means Cluster 1 (highly upregulated by reovirus) from A. **(C)** Temporal relative intensity from the proteomics dataset of reovirus proteins Lambda 1 and Mu 1 during the 48-hour course of infection (MOI 1 and 10, five time points each). **(D)** Temporal relative intensity from the proteomics dataset of representative viral response proteins (APOL9B, CCL5, GBP4, and OAS1A) during the 48-hour course of infection (MOI 1 and 10, five time points each). **(E)** Temporal relative intensity from the proteomics dataset of representative antigen presentation proteins (B2M, H2-D1, TAP1, and TAP2) during the 48-hour course of infection (MOI 1 and 10, five time points each).
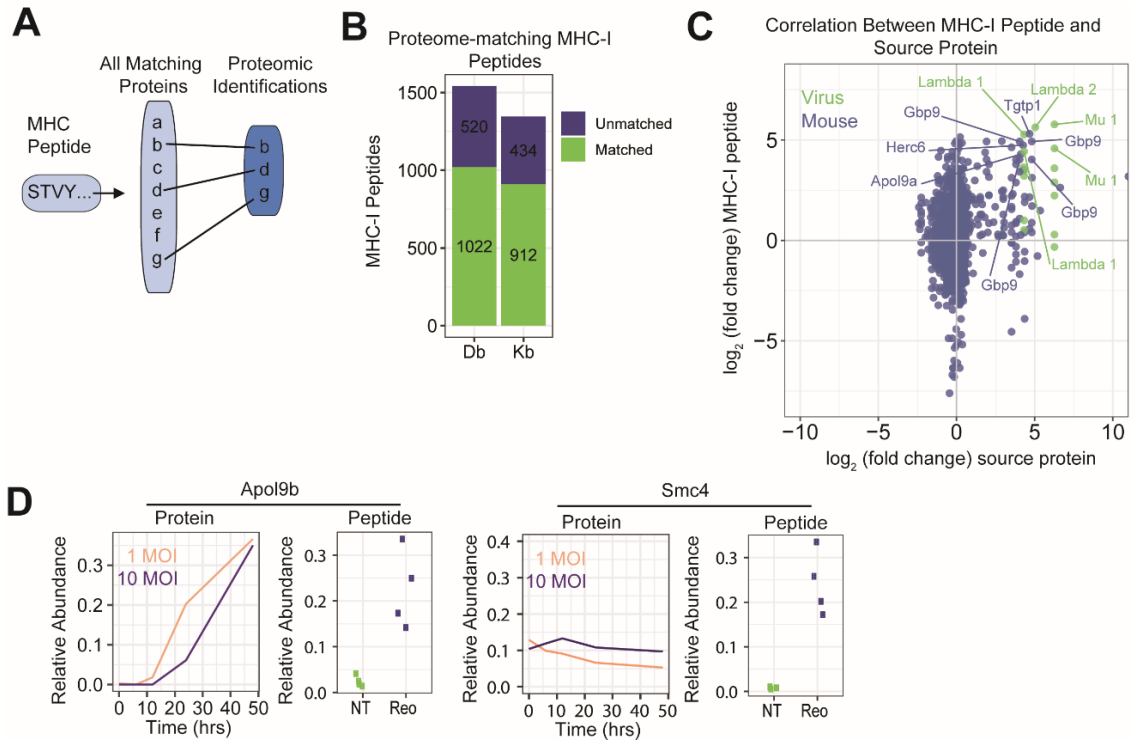
Figure 3.3. *Matching MHC-I peptide and source proteome quantitation during reovirus infection in ID8 cells.*

(A) MHC-I peptides were matched to all mouse protein accessions from the UniProt database and then these accessions were considered source proteins if they appeared in the proteomics dataset shown in Figure 3.2. Some peptides match multiple source proteins. **(B)** Number of MHC-I peptides from the dataset in Figure 3.1, for which protein matches were found (matched) or not found (unmatched) in the quantitative proteomics dataset (both H2-D^b [Db] and H2-K^b [Kb] specific MHC-I peptides). **(C)** Correlation of log$_2$(fold change) of Reovirus/Control between MHC-I peptides from the MHC-I ligandome analysis from Figure 3.1 and their matching source proteins from the proteomics dataset. Data are compared at 48 hours of reovirus infection. **(D)** Representative examples of MHC-I peptides for which log$_2$(fold change) of Reovirus/Control are correlated (APOL9B) and uncorrelated (SMC4) at the MHC-I peptide and source protein levels.
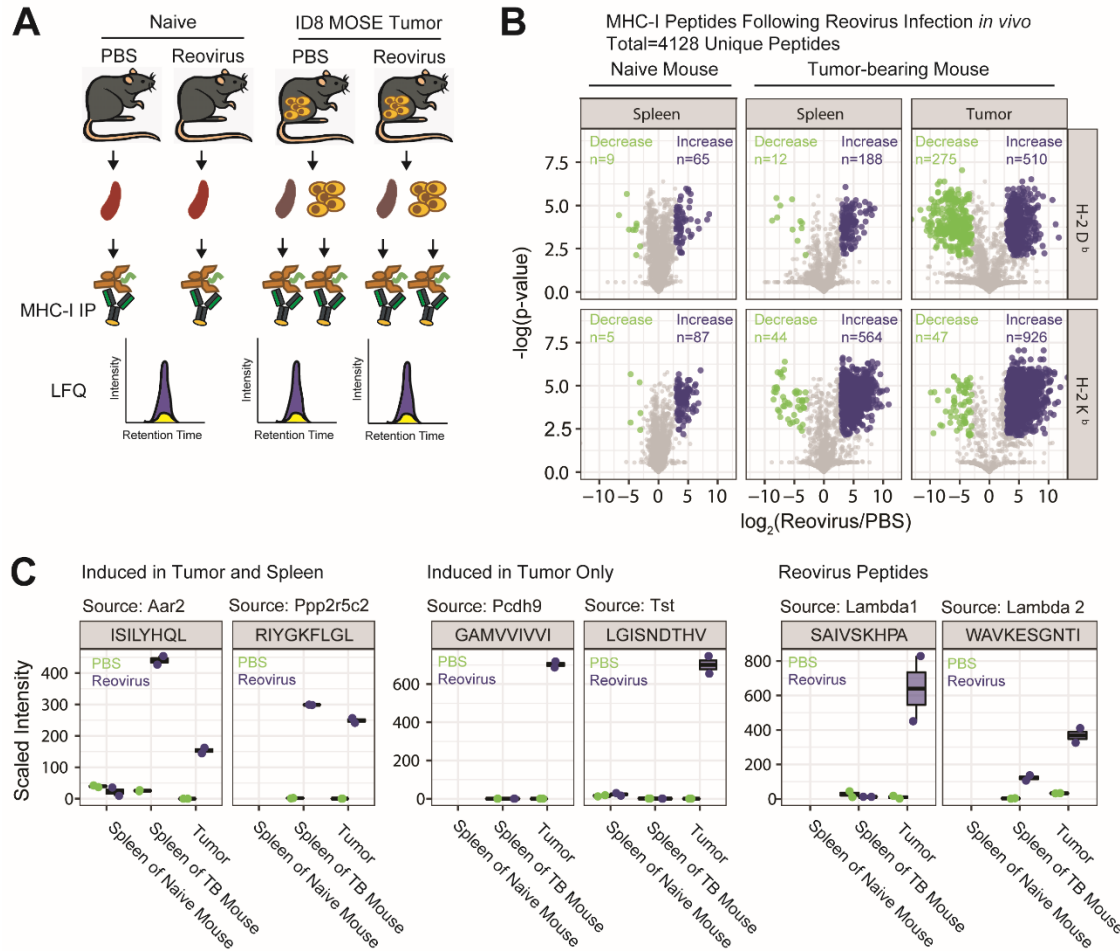
Figure 3.4. *Discovery of tumor MHC-I ligands in tumor and immune cells in vivo.*

(A) Experimental setup for *in vivo* MHC-I ligandome monitoring. Naive mice or those harbouring ID8 MOSE tumors were injected with either PBS or reovirus (5×10^8 plaque forming units, intraperitoneally). Spleens and tumors (spleens only from naïve mice) were harvested at 7-10 days post injection and MHC-I peptides were compared by immuno-precipitation and LC-MS/MS with label-free quantitation. **(B)** Volcano plots for the number of increased (blue dots) and decreased (green dots) MHC-I peptides ($\log_2$[fold change] $\leq$ -1 or $\geq$ 1 and *p* values ≤ 0.05) in the naïve mice spleens, tumor-bearing mouse spleens, and tumors. The -log(*p* value) is based on F-tests implemented in the R package genefilter and adjusted using Benjamini-Hochberg multiple hypothesis correction. **(C)**

Representative examples of the MHC-I peptide intensities increased by reovirus across tumors or spleen of the tumor-bearing mice, but not in naïve mice. Shown also are intensities of example MHC-I peptides derived from reovirus source proteins quantified in the experiment.
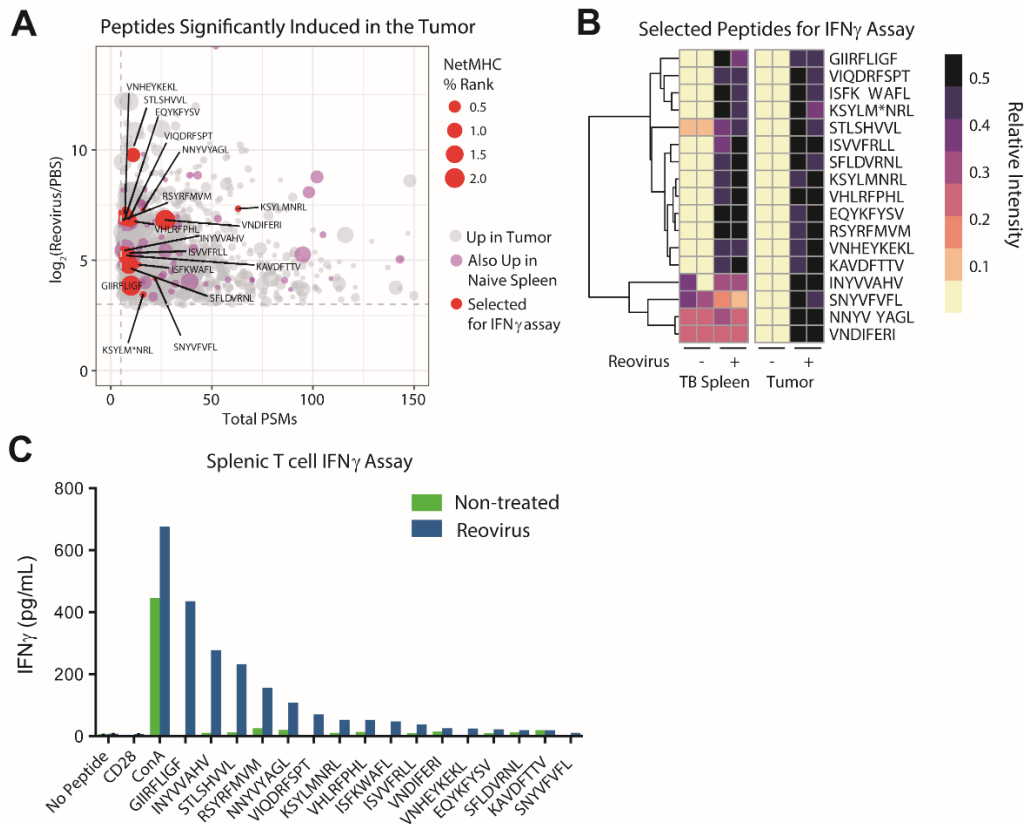
Figure 3.5. *Immunogenicity testing of reovirus-induced tumor MHC-I peptides.*

(A) Distribution of mean $\log_2$[fold change], number of PSMs identified (as an indication for MHC-I abundance), and NetMHC % rank for significantly induced peptides at the tumor from the data in Figure 3.4, showing the MHC-I peptides chosen (randomly) for validation by IFNγ assay. Any MHC-I peptides also induced by reovirus in the naive spleen (shown in purple) were excluded from being chosen for validation assays. **(B)** Heatmap of relative intensity in the tumor and spleen of tumor-bearing mice of MHC-I peptides selected for validation assays (from the data in Figure 3.4). *=oxidized methionine **(C)** MHC-I peptides from B were incubated with splenocytes collected from reovirus-infected and non-treated tumor-bearing mice. All incubations were done in the presence of CD28 co-stimulation, and concanavalin A (ConA, 2 μg/mL) was used as a positive control. IFNγ production (y-axis) was determined by ELISA.
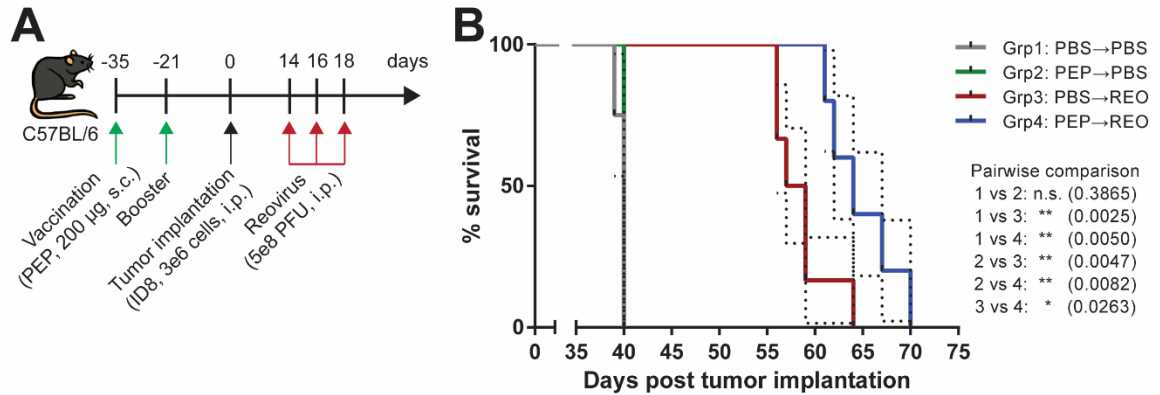
Figure 3.6. *Vaccination with reovirus-induced MHC-I ligands to potentiate anti-tumor immune responses.*

(A) Schematic diagram of the peptide vaccination and reovirus treatment regimen. A pool of the top four immunogenic virus-induced MHC-I ligands in complete Freund's adjuvant and incomplete Freund's adjuvant was used to vaccinate and boost mice, respectively. Following ID8 tumor implantation, mice were treated with a therapeutic regimen of reovirus and monitored for survival. **(B)** Survival analysis of the four treatment groups with Kaplan-Meier curves. Log-rank (Mantel-Cox) test for pairwise comparisons. Dotted lines represent standard error of the mean and treatment groups had n=3-6 mice each. PEP: peptide pool, s.c.: subcutaneous, i.p.: intraperitoneal, PFU: plaque forming unit, PBS→PBS: untreated, PEP→PBS: peptide vaccine alone, PBS→REO: reovirus alone, PEP→REO: peptide vaccine combined with reovirus

97
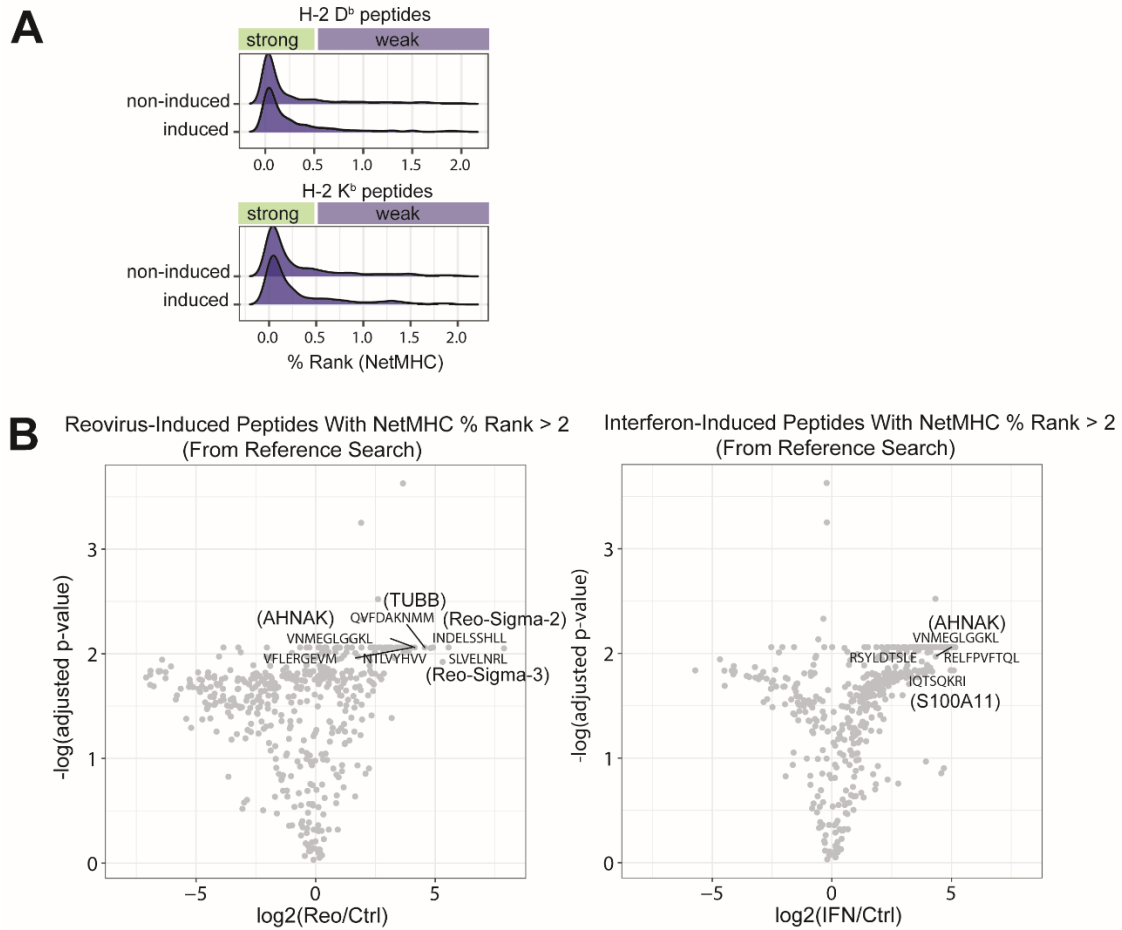
Supplementary Figure 3.1. *Characteristics of MHC-I peptides in the in vitro MHC-I ligandome experiment.*

(A) Predicted binding affinity of identified peptides (NetMHC % rank). Strong binders are <0.5% rank and weak binders are 0.5% to 2% rank. **(B)** Differential MHC-I ligand quantitation for peptides with NetMHC rank greater than 2% resulting from a no-enzyme mouse-reovirus database search.
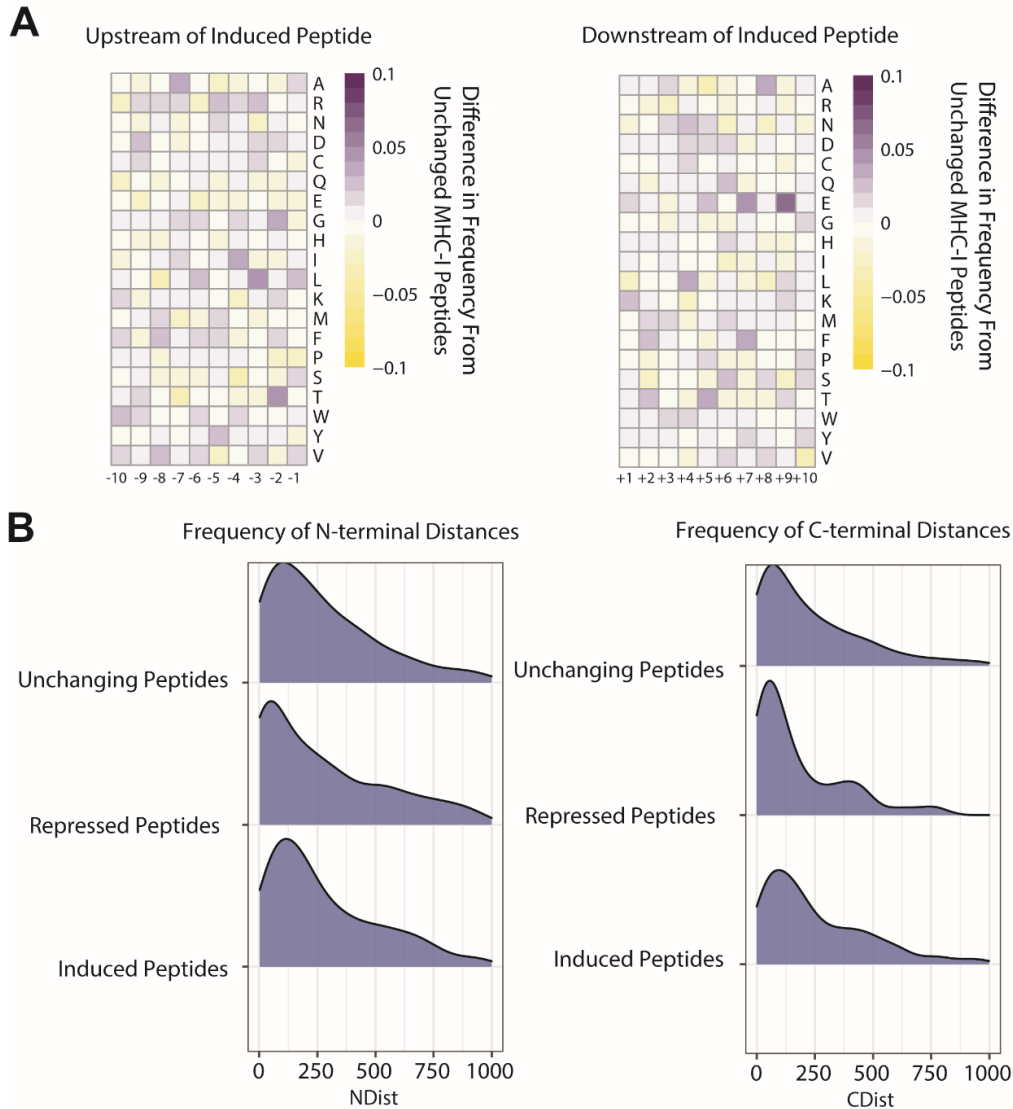
Supplementary Figure 3.2. *Characteristics of upstream and downstream sequences of reovirus-induced MHC-I peptides in vitro.*

(A) Heatmaps displaying the difference in frequency (from a position specific frequency matrix) of the upstream (-10 amino acid residues) and downstream (+10 amino acid residues) between the reovirus-induced MHC-I peptides compared to all other MHC-I peptides. **(B)** Comparison of the frequency of MHC-I peptides at different distances (in amino acid residues) to the N- or C-terminus compared between reovirus-induced, repressed, and unchanged MHC-I peptides.
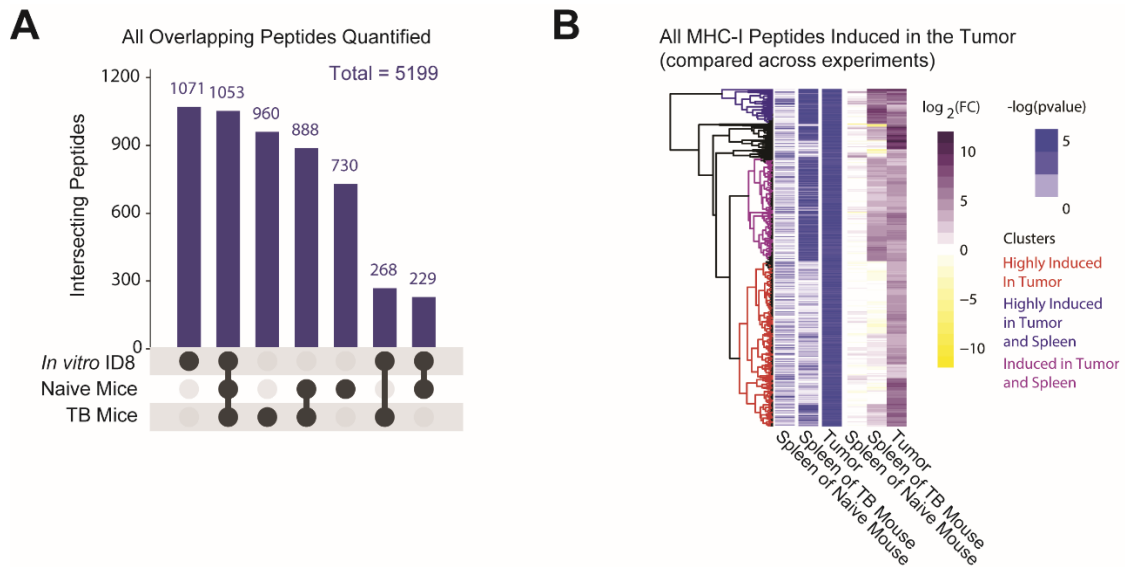
Supplementary Figure 3.3. *Peptide overlap between experiments.*

(A) Overlap in the number of peptides quantified between the *in vitro* experiment and across naïve and tumor-bearing mouse comparisons. **(B)** MHC-I peptides that were increased ($\log_2$[fold change] ≤ 3 or ≥ 3 and *p* values ≤ 0.05) at the tumor and their corresponding mean $\log_2$[fold change] across the spleen of the tumor-bearing mice and naïve mice.

3.7   SUMMARY OF CHAPTER 3 AND TRANSITION TO CHAPTER 4

Our MS-based analysis of MHC-I ligands revealed reovirus-induced changes in the MHC-I peptide repertoire of ID8 mouse ovarian cancer cells, resulting in the presentation of novel MHC-I peptides. Similar changes in the MHC-I ligand landscape were observed in tumors and spleens isolated from reovirus-treated ID8 TB mice. We also demonstrated that some of these reovirus-induced MHC-I ligands exhibit tumor-specific immunoreactivity, capable of stimulating T cell responses exclusively in reovirus-treated TB mice; and when they were administered as peptide vaccines, delayed ascites development was observed due to enhanced OV efficacy. In the following chapter, we moved on to investigate reovirus-induced MHC-I ligands of another cancer model to determine the idiosyncrasies of tumor MHC-I ligandomes. We also adopted a combinatorial therapy approach of reovirus and immune checkpoint blockade because A) combination therapies are necessary and on the rise in the immunotherapy field and B) we hypothesized that the complementary actions of the two treatment strategies will enhance the immunoediting of the tumor MHC-I ligandome.

CHAPTER 4: IMMUNE CHECKPOINT BLOCKADE AUGMENTS CHANGES WITHIN ONCOLYTIC VIRUS-INDUCED CANCER MHC-I PEPTIDOME, CREATING NOVEL ANTI-TUMOR CD8 T CELL REACTIVITIES

4.1   AUTHOR CONTRIBUTIONS

YK designed and performed the experiments, analyzed the data, and wrote the manuscript with input from JPM and SG. PK contributed to Figures 4.1E and 4.1F, manufactured reovirus, and developed the targeted database search strategy. PK and JPM contributed to the interpretation of the results. JAP ran the TMT-labeled MHC-I peptidome samples on the mass spectrometer in the SPG laboratory at Harvard University. SG supervised and acquired funding for the project. All authors provided critical feedback of the manuscript.

4.2 ABSTRACT

The combination cancer immunotherapies with oncolytic virus (OV) and immune checkpoint blockade (ICB) re-instate otherwise dysfunctional anti-tumor CD8 T cell responses. One major mechanism that aids such re-instatement of anti-tumor CD8 T cells involves the availability of new class I major histocompatibility complex (MHC-I)-bound tumor epitopes following therapeutic intervention. Thus, therapy-induced changes within the MHC-I peptidome hold the key to understanding the clinical implications for therapy-re-instated CD8 T cell responses. Here, using mass spectrometry-based immuno-affinity methods and tumor-bearing animals treated with OV and ICB (alone or in combination), we captured the therapy-induced alterations within the tumor MHC-I peptidome which were then tested for their CD8 T cell response-stimulating activity. We found that the oncolytic reovirus monotherapy drives up- as well as down-expression of tumor MHC-I peptides in a cancer type and oncolysis susceptibility dependent manner. Interestingly, the combination of reovirus+ICB results in higher numbers of differentially expressed MHC-I-associated peptides (DEMHCPs) relative to either monotherapies. Most importantly, OV+ICB-driven DEMHCPs contain biologically active epitopes that stimulate interferon-gamma responses in cognate CD8 T cells capable of mediating clinically desired anti-tumor attack and cancer immunoediting. These findings highlight that the therapy-induced changes to the MHC-I peptidome contribute towards the re-instated anti-tumor CD8 T cell attack established following OV+ICB combination cancer immunotherapy.

4.3 INTRODUCTION

Immunotherapies aim to (re)educate the immune system to recognize and eliminate cancer cells, and unlike conventional anti-cancer therapies, the resulting anti-tumor immune

response can provide a highly specific and long-lasting protection[143,444]. These cancer immunotherapy approaches often focus on overturning the immunosuppression mediated through diverse immune evasion mechanisms within the tumor microenvironment (TME). In particular, cancer immunotherapy approaches based on the blockade of inhibitory immune checkpoints, such as PD-1, CTLA-4 and PD-L1, have shown promise in clinical settings and are being recognized for their capacity to re-instate antigen-specific CD8 T cell attack on cancers. Such therapy-induced anti-tumor CD8 T cell response is shaped by a spectrum of tumor antigens (i.e., it is polyclonal), can act on existing cancer cells, and maintain antigen-specific memory response against tumor challenge or relapse[142–144,445]. Thus, it is not surprising that 'hot' tumors – those with a higher density of tumor-infiltrating cytotoxic CD8 T cells – respond better to immune checkpoint blockade (ICB) and correlate with better clinical outcomes as compared to 'cold' tumors which show low or no immune cell infiltration in the TME[106,142,143,145]. Based on these observations, strategies that can make tumors 'hot' and prime them for ICB therapies are being pursued in an attempt to design broadly applicable and effective cancer immunotherapies.

One way to make tumors 'hot' ahead of ICB therapies involves the use of oncolytic viruses (OVs) which were originally discovered for their capacity to preferentially infect and kill cancerous cells without causing similar effects on normal cells. In the last decade, it has become clear that in addition to their direct tumoricidal effects, OVs overturn a myriad of tumor-associated immune evasion mechanisms and promote the induction of potent anti-tumor immune responses[1,4,12,467]. For instance, the type I interferon-driven response to viral infection restores the expression of proteins involved in antigen processing and presentation in various cancer cells[130,457,458]. OVs also support the

recruitment and activation of CD8 tumor-infiltrating lymphocytes (TILs), as well as other immune cells, via a localized release of cytokines in the TME[151,468,469]. This tumor immune infiltration-driving action of OVs makes them a suitable candidate for making tumors 'hot' and supports their use in combination with ICBs. Interestingly, the biological activities of OV monotherapy-induced anti-tumor CD8 T cell responses are dampened via the actions of immune checkpoints such as PD-1 and require rescuing via ICB to sustain their anti-tumor functions. Thus, during OV+ICB combination therapy, OVs and ICBs overcome the limitation faced by each monotherapy: OVs make tumors 'hot' and suitable for ICBs, and ICBs potentiate OV-induced CD8 T cell responses[144,445,447]. To this end, previous studies have shown the enhanced efficacy of OVs through (a)synchronous administrations of ICBs[128,151,214,470–473], and OVs have emerged as a strategically complementary partner for ICB therapies[9,152].

CD8 T cells are the main mediators of OV+ICB combination therapy[128,151,214,471,472]. The antigenic targets of CD8 T cells are complexes of peptides associated with class I major histocompatibility complex (MHC-I) molecules found on the surface of all nucleated cells[279,283]. These MHC-I-bound peptides are derived from the proteolysis of intracellular proteins, where those that originate from normal tissue are non-immunogenic while ones from viral proteins or abnormal tissue (mutated or overexpressed tumor-associated antigens) are immunogenic[279,283]. As such, the repertoire of peptides presented by MHC-I molecules, termed the MHC-I peptidome, reflects the health state of a cell. The MHC-I peptidome can be analyzed by a mass spectrometry (MS)-based approach using immuno-affinity (IP)-purified peptide-MHC-I complexes[432–434]. Many cancer types, however, have a defective antigen processing and presentation machinery,

thereby complicating the elucidation of the tumor MHC-I peptidome landscape[474]. We have recently shown that oncolytic reovirus can correct tumor-associated antigen presentation defects and promote the expression of MHC-I peptides on tumors that can induce new anti-tumor CD8 T cell responses. Currently, whether OV+ICB combination therapy affects the tumor MHC-I peptidome and subsequently shapes the repertoire of immunogenic anti-tumor CD8 T cells remain poorly understood.

The current study used MHC-I immuno-precipitation and liquid chromatography with tandem MS (LC-MS/MS) for label-free or tandem mass tag (TMT)-based multiplexed quantitation to analyze the tumor MHC-I peptidome following OV+ICB combination treatment. We found that oncolytic reovirus-mediated changes to the MHC-I peptidome *in vivo* are cancer type-specific, where differentially expressed MHC-I-associated peptides (DEMHCPs) displayed quantitative and qualitative variance in a tumor model-dependent manner. The addition of ICB to reovirus therapy showed potential therapeutic value since a greater change to the MHC-I peptidome was observed due to the combination therapy compared to either monotherapy alone. These DEMHCPs were capable of inducing antigen-specific CD8 T cell responses in reovirus+ICB-treated tumor-bearing (TB) mice, but not in non-treated TB mice. Such therapy-induced changes within the MHC-I peptidome and inherent changes in CD8 T cell activity may improve anti-tumor immunity and hold biological as well as therapeutic importance[475].

4.4   RESULTS

4.4.1   *Oncolytic Reovirus-induced Alteration of the Tumor MHC-I Peptidome is Dictated by Cancer Type and Susceptibility to OV*

Based on our previous findings that reovirus induces the presentation of novel MHC-I peptides in the MOSE ID8 ovarian peritoneal carcinomatosis model[433], we investigated reovirus-induced changes in the tumor MHC-I peptidome of a solid tumor model of MCA205 fibrosarcoma. There are a few reasons why we chose the MCA205 model. Unlike ID8 cancer cells which express low basal levels of MHC-I molecules that are upregulated in response to reovirus infection (Figure 4.1A), MCA205 cancer cells express constitutively high levels of MHC-I molecules that remain unaffected by reovirus infection (Figure 4.1B). We reasoned that MCA205 provides a good model to examine reovirus-mediated changes to the MHC-I peptidome without the need to account for changes to the MHC-I expression as a possible confounding variable. Moreover, MCA205 and ID8 models show differential susceptibility to reovirus infection *in vitro* (Figure 4.1C & 4.1D). Consequently, reovirus infection of MCA205 cells resulted in low level of oncolysis, as measured by Annexin V+,7AAD+ dead cells (Figure 4.1E), at both 24 and 48 hours post infection; ID8 cells, on the other hand, were previously shown to be highly susceptible to oncolysis[458]. Differences were also observed in mRNA levels of several markers that are known to be involved in anti-viral responses, where MCA205 cells expressed higher basal levels of anti-viral response genes and lower basal levels of dsRNA sensor genes (Figure 4.1F). Contrasting response to reovirus infection in the two tumor models were also evident *in vivo*. While reovirus alters the TME and drives an increase in the levels of CD3 and CD8 TILs in both the ID8 and MCA205 models, it did so at a much higher level in the ID8 model (Figure 4.1G & 4.1H) as compared to the MCA205 model (Figure 4.1I & 4.1J). Thus, MCA205 fibrosarcoma cells additionally allow us to explore if reovirus exposure

drives changes in the MHC-I peptidome in cancer cells that are relatively resistant to infection by this OV.

To test this, C57BL/6 mice were implanted with MCA205 cells, and the resultant tumors were administered with reovirus as shown in Figure 4.2A. Tumors from PBS-treated (control) or reovirus-treated MCA205 TB mice were collected and processed for MS-based MHC-I peptidome analysis. In this initial investigation, our label-free quantitation resulted in a dataset of 1,508 unique H2-D^b-specific peptides and 1,314 unique H2-K^b-specific peptides, totalling 2,822 unique MHC-I peptides matching to 2,290 protein accessions (Figure 4.2B). The majority of the MHC-I peptides we identified displayed typical amino acid length distributions for MHC-I peptides (Figure 4.2C) and had NetMHC-predicted binding affinities less than 0.5% rank (Figure 4.2D), thus confirming the robustness of our MHC-I peptidome precipitation, analysis and detection protocol. Of these, 213 were DEMHCPs that were upregulated (log$_2$[reovirus/PBS] $\geq$ 1) in response to reovirus treatment, representing 7.5% of the total MHC-I peptides quantified in the experiment (Figure 4.2E). Here, we also investigated the downregulated DEMHCPs (log$_2$[reovirus/PBS] $\leq$ -1), which we hypothesized show reduced expression due to possible immunoediting by cognate CD8 T cells, and identified 168 downregulated DEMHCPs in response to reovirus treatment, representing 6.0% of the total MHC-I peptides (Figure 4.2F). These data showed that oncolytic reovirus modulates the expression of the MHC-I peptidome of cancer cells that are relatively resistant to infection and oncolysis.

One noticeable difference between the present study's MCA205 MHC-I peptidome dataset and our previously published ID8 MHC-I peptidome dataset[433] was the number of peptides induced by reovirus treatment. Similar numbers of peptides were quantified from

MHC-IP of MCA205 and ID8 tumors, and we even identified peptides that are common between the two datasets (Figure 4.2G). However, we observed that out of the 643 H2-D^b and 476 H2-K^b overlapping peptides, higher numbers of upregulated and downregulated DEMHCPs were identified for the ID8 model (Figure 4.2H), suggesting that reovirus-modulated changes to the MHC-I peptidome is relatively less evident in the MCA205 model. In addition, gene ontology (GO) enrichment analysis using the PANTHER Classification System[460] of the source proteins of upregulated DEMHCPs revealed that MCA205 DEMHCPs were enriched in cellular biosynthetic and metabolic biological processes (BPs) while ID8 DEMHCPs were enriched in viral defence BPs (Figure 4.2I). For the downregulated DEMHCPs, metabolism-related BPs were enriched in the MCA205 dataset while endocytosis-related BPs were enriched in the ID8 dataset (Figure 4.2J). Overall, the comparison of the MHC-I peptidome datasets of MCA205 fibrosarcoma and ID8 ovarian cancer cells identified OV-induced oncolysis and tissue origin as possible dictators of therapy-induced cancer MHC-I peptidome changes in response to oncolytic reovirus treatment.

4.4.2 Immune Checkpoint Blockade Further Augments the MHC-I Peptidome Changes Induced by Oncolytic Reovirus

Given the minimal changes to the MHC-I peptidome observed in the MCA205 tumors following reovirus treatment, we sought to improve this by adding ICB therapy. We reasoned that ICB is an ideal candidate for combination treatment with reovirus since virus infection induces an upregulation of immune checkpoint ligand/receptor expression on cancer cells and immune cells[476,477]. Here, we chose to perform blocking of programmed cell death protein 1 (PD-1), the expression of which is upregulated on CD3 and CD8 T

cells at the site of infection (i.e., peritoneum) and within the lymphoid organ orchestrating T cell response development (i.e., spleen) in response to reovirus injection (Figure 4.3A & 4.3B). Of note, programmed death-ligand 1 (PD-L1), on the other hand, is not upregulated on CD3 and CD8 T cells at the site of infection, despite an initial peak at 1 day post injection, (Figure 4.3C) nor on MCA205 cancer cells in response to reovirus infection *in vitro* (Figure 4.3D). Thus, PD-1 rather than PD-L1 was our target of choice for ICB. We hypothesized that ICB-mediated activation of otherwise suppressed T cells would result in cancer immunoediting with subsequent alteration of the MHC-I peptidome repertoire. To examine this, MCA205 TB mice were treated with reovirus and anti-PD-1 antibody as per the schematic shown in Figure 4.3E, and then tumors were harvested for MS-based MHC-I analysis. In this experiment, we utilized a TMT-based platform for a multiplexed quantitative analysis of MHC-I peptides[434]. We observed 2,288 unique H2-D^b-specific and 1,945 unique H2-K^b-specific peptides, matching to 1,308 protein accessions (Figure 4.3F). The amino acid length distribution (Figure 4.3G) and NetMHC-predicted binding affinities (Figure 4.3H) once again support our dataset as bona fide MHC-I peptides. Data are available via ProteomeXchange with identifier PXD024369.

Next, we compared each treatment group to the PBS-treated control group to identify MHC-I peptides that are upregulated (log$_2$[fold change] $\geq$ 1; Figure 4.4A) or downregulated (log$_2$[fold change] $\leq$ -1; Figure 4.4B). While there were some overlapping DEMHCPs in common between treatments, especially when comparing reovirus and isotype control antibody or anti-PD-1 antibody combination therapy (henceforth referred to as REO+ISO or REO+ICB, respectively), we focused on DEMHCPs that are unique to each treatment considering our interest in cancer immunoediting (Figure 4.4C & 4.4D).

We observed the highest number of DEMHCPs due to REO+ICB combination therapy, with 172 upregulated (Figure 4.4E) and 118 downregulated (Figure 4.4F), representing 4.1% and 2.8% of the total MHC-I peptides identified, respectively. These REO+ICB DEMHCPs exhibited a range of fold change levels and number of peptide spectrum matches (PSMs) (Figure 4.4G & 4.4H). GO enrichment analysis of the source proteins of the REO+ICB DEMHCPs revealed enriched BPs such as nucleic acid metabolic process, macromolecular modification, and organelle organization (Figure 4.4I & 4.4J). These are exemplified by MHC-I peptides from *Sf3b3*, *Pnkp*, *Gvin1*, and *Zfp729a* (Figure 4.4K). Altogether, these data show the unique changes to the MCA205 MHC-I peptidome with the identification of DEMHCPs specific to reovirus and ICB combination treatment. Most importantly, these results demonstrate that the use of ICB within a combinatorial treatment can augment therapy-induced MHC-I peptidome changes during oncolytic virus-based cancer therapies.

4.4.3   *Differentially Expressed MHC-I Peptides Observed Following Reovirus+ICB Combination Therapy Contain Biologically Active Anti-tumor CD8 T Cell Epitopes*

Not all MHC-I peptides present in a cell are antigenic and often are involved in homeostatic immunoregulation. Thus, to realize the role of MHC-I peptides as an antigenic epitope for CD8 T cell recognition, their capacity to stimulate antigen-specific CD8 T cells must be tested (Figure 4.5A). Hence, we next investigated the biological activity of the reovirus and ICB combination therapy-modulated DEMHCPs. We chose 22 upregulated and 21 downregulated DEMHCPs with number of PSMs greater than or equal to 2 (Table 4.1). These 43 peptides were synthesized and their capacity to elicit CD8 T cell stimulation in splenocytes of untreated (PBS control) or REO+ICB-treated TB mice was measured by an

interferon-gamma (IFNγ) ELISA validation screen. Out of the 22 upregulated DEMHCPs, 3 peptides produced a strong IFNγ response (greater than the cut-off of [mean + 3 x standard deviation] of the negative controls) in splenocytes of REO+ICB-treated TB mice (Figure 4.5B, arrows). Interestingly, 3 out of the 21 downregulated DEMHCPs also induced a strong response in splenocytes of REO+ICB-treated TB mice (Figure 4.5C, arrows). We also found a few peptides that elicited a positive IFNγ response in splenocytes of PBS-treated control TB mice; although above the cut-off values, these responses were very low (Figure 4.5B & 4.5C, chevron-double-down symbol). Furthermore, there was no correlation between the MHC-I peptide abundance fold change levels and IFNγ response (Figure 4.5D). If anything, the immunogenic peptides tend to have lower fold change levels. We also confirmed the immunogenicity of the peptides by staining the stimulated splenocytes for intracellular IFNγ to be analyzed by flow cytometry. Comparison of the ELISA and flow cytometric data from splenocytes of REO+ICB-treated TB mice showed a slight trend of positive correlation of immunogenicity (Figure 4.5E). Due to the low percentage of IFNγ+ antigen-specific CD8 T cells detected by flow cytometry, ELISA may be a more reliable measure of an immunogenicity screen. Nevertheless, these data strongly support that reovirus+ICB therapy-induced DEMHCPs can activate cognate CD8 T cells. As CD8 T cells are the main mediators of OV+ICB therapeutic effects, these therapy-induced DEMHCPs are of importance in the context of anti-tumor immunity and therapeutic efficacy.

4.5   DISCUSSION

Here, we present the first report on the oncolytic reovirus+ICB combination therapy-induced changes to the tumor MHC-I peptidome. Using a relatively OV-resistant cancer

model, we demonstrate that despite the low susceptibility of cancer cells, oncolytic reovirus changes the MHC-I peptidome of cancers, albeit at a lower magnitude than that in OV-susceptible ID8 ovarian cancer cells. Next, we found that the reovirus-induced modulation of MHC-I peptidome in OV-resistant cells can be further augmented via an addition of ICB agents within the OV therapeutic regimen. From the clinical perspective and in line with our previous reports on therapy-induced changes to the MHC-I peptidome repertoire[433,434], here we show that the combination therapy-induced DEMHCPs have therapeutic potential in activating cognate anti-tumor CD8 T cells. These analyses provide an insight on how tumors change in response to cancer immunotherapies and highlight immunological nuances that could be harnessed to overcome the adaptive therapy-resistance of cancers.

In this study, we initially evaluated reovirus-induced changes to the MHC-I peptidome of a solid tumor model MCA205 fibrosarcoma and observed a low number of upregulated DEMHCPs, as compared to our previously published dataset on the MOSE ID8 ovarian cancer model. Further investigation revealed that this disparity was not only quantitative but also qualitative, and possibly originated due to differential OV-susceptibility, basal antigen presentation capacity, 'hot' or 'cold' nature, and tissue of origin within the cancers studied. Thus, our findings highlight the importance of context-dependent considerations for MHC-I peptidome analyses where certain tumors may be more suitable for MHC-I peptidome characterization. This is especially important when examining therapy-induced changes to the MHC-I peptidome landscape. One should assess the status of the antigen processing and presentation machinery of the tumors and determine whether the particular therapy under consideration is able to restore (or at least influence) the antigen presentation pathway[478]. Baseline expression level of MHC-I

molecules may also contribute to the overall quantitative changes observed in the MHC-I peptidome. However, even with the low number of upregulated DEMHCPs identified, the MCA205 model nevertheless showed that reovirus treatment induced changes to the tumor MHC-I peptide repertoire and provided a rationale for including ICB therapy in hopes of increasing the number of DEMHCPs.

We also employed a newly optimized TMT-based multiplexing platform for MHC-I peptidome analysis previously developed by our group[434]. Multiplexing not only allows a comparison of 11 samples in a single experiment but also provides an accurate relative quantitation of low-abundance peptides[479]. Consequently, this high-throughput MHC-I peptidome discovery approach resulted in the identification of the antigenic targets for the combination therapy-modulated anti-tumor immunity. Contrary to what we expected, the addition of ICB to reovirus therapy did not significantly increase the number of DEMHCPs overall; that is, we observed less than 200 upregulated or downregulated DEMHCPs which is a relatively low number. In any case, the combination therapy resulted in the highest number of DEMHCPs, especially compared to that of reovirus monotherapy, and emphasized the potential therapeutic advantage of the reovirus and ICB combination therapy. Moreover, we also observed a high number of DEMHCPs due to reovirus and isotype control antibody combination treatment, providing further evidence to support the role of Fc gamma receptors (FcγR) in the activities of immunomodulatory antibodies as reviewed by Stewart et al.[480]. Previous studies have shown the FcγR-dependent activity of anti-mouse CTLA4 antibodies in mouse tumor models[217,481,482]. Thus, the change in the MHC-I peptidome we observed due to the reovirus and isotype control antibody treatment may be due to non-specific binding of the isotype control antibody to FcγR. This effect, as

well as the one observed due to REO+ICB combination therapy, was detected only in the presence of reovirus since the pro-inflammatory stimuli was necessary to drive the expression of FcγR-expressing, or PD-1-expressing, effector cells in the tumor. These results support the role for OVs as primers ahead of the administration of ICB treatment[106], and provide an additional rationale for the use of OV+ICB combinations for enhanced anti-cancer therapeutic efficacy.

Since most MHC-I peptides in cells carry an immune homeostatic function and thus are not immunogenic, we added an additional step in the MHC-I peptidome discovery pipeline and validated the immunogenicity of the DEMHCPs found in our study. In the context of cancer immunotherapies, wherein functionally active anti-tumor CD8 T cells act as the main mediators of therapeutic effects, discovery of biologically active MHC-I peptides is highly clinically relevant. Out of the 43 peptides tested in the T cell activation-based validation screen, we observed 6 that stimulated high IFNγ responses in cognate CD8 T cells. As expected, many MHC-I peptides identified by the immuno-purification and MS analysis approach failed to produce IFNγ responses, underlining the value in assessing antigen-specific T cell activity. In addition, our observation of the lack of correlation between immunogenicity and fold change level as measured by MS-based MHC-I peptidome analysis suggests that stringent filters should be carefully applied in the workflow which focuses on the identification of MHC-I peptides that are biologically active. A wide range of peptides should be represented, not only the highly upregulated or downregulated peptides, as there are other factors involved in determining immunogenicity besides MHC-I peptide abundance. Furthermore, our current data emphasize the need to consider the contribution of the downregulated DEMHCPs to the anti-tumor immune

response, unlike our previous studies that had investigated only upregulated DEMHCPs. As we hypothesized, one mechanism through which these DEMHCPs are likely downregulated is due to selective destruction, by cognate CD8 T cells, of tumor cells that express it. Thus, biologically active MHC-I peptides within downregulated DEMHCPs likely contribute towards cancer immunoediting and contain the target candidates for peptide vaccines. Consequently, biologically active peptides found within upregulated and downregulated DEMHCPs hold implications for therapy-induced anti-tumor CD8 T cell responses.

In conclusion, this study further supports biological and therapeutic implications for therapy-induced changes to the MHC-I peptidome following combinatorial treatment with two emerging immunotherapies – OV and ICB. The elucidation of such therapy-driven DEMHCPs provides an insight on the alterations to the TME in response to therapy as well as identifies immunogenic peptides that can be exploited for the development of next-generation cancer immunotherapies.

4.6   ACKNOWLEDGEMENTS
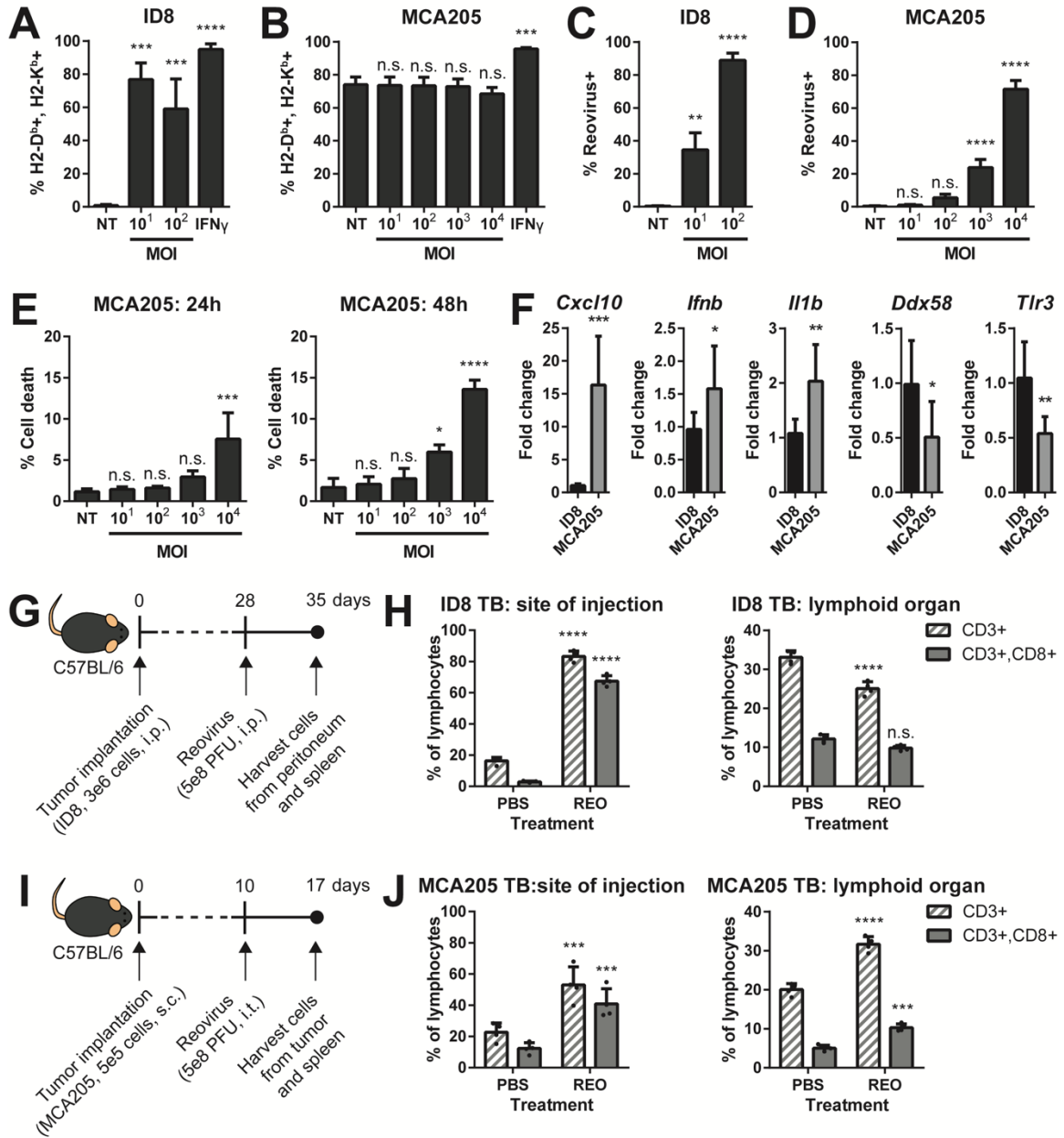
Figure 4.1. *Comparison of reovirus-modulated changes in ID8 and MCA205 models.*

MHC-I H2-D^b and H2-K^b expression levels in **(A)** ID8 and **(B)** MCA205 cancer cells *in vitro*. Cancer cells were infected with reovirus at various multiplicity of infection (MOI; 10-10,000) for 24 h, and H2-D^b+,H2-K^b+ cells were quantified by flow cytometry. Stimulation with IFNγ (100 units/mL [U/mL]) was included as a positive control. Reovirus infectivity in **(C)** ID8 and **(D)** MCA205 cells *in vitro*. Cancer cells were infected at various

MOIs for 24 h, and reovirus+ cells were quantified by flow cytometry. Reovirus-mediated oncolysis in **(E)** MCA205 cells *in vitro*. Cancer cells were infected at various MOIs for 24 and 48 h, and late apoptotic (Annexin V+,7AAD+) cells were quantified by flow cytometry. **(F)** Quantitative PCR analysis of anti-viral gene expression. Untreated ID8 and MCA205 cells were collected for RNA extraction and cDNA synthesis to measure the expression of *Cxcl10, Ddx58, Ifnb, Il1b,* and *Tlr3* by qRT-PCR using gene-specific primers. All values were first normalized to *Gapdh* and compared to ID8 control. Reovirus-mediated tumor immune cell infiltration in **(G & H)** ID8 and **(I & J)** MCA205 models *in vivo*. CD3 and CD8 T cell levels were measured by flow cytometry in tumor-bearing mice at both the site of injection (TME) and lymphoid organ (spleen). Statistical analysis was performed using a Student's *t* test or one-way ANOVA coupled with a Bonferroni post-test. Data are representative of three independent experiments. Asterisks shown immediately on top of the bars signify the *p* values obtained by comparing the respective data against the control group (non-treated [NT], ID8 or PBS). n.s. = $p > 0.05$, *$p \leq 0.05$, **$p \leq 0.01$, ***$p \leq 0.001$, ***$p \leq 0.0001$. i.p.: intraperitoneal; PFU: plaque-forming units; s.c.: subcutaneous; i.t.: intratumoral.
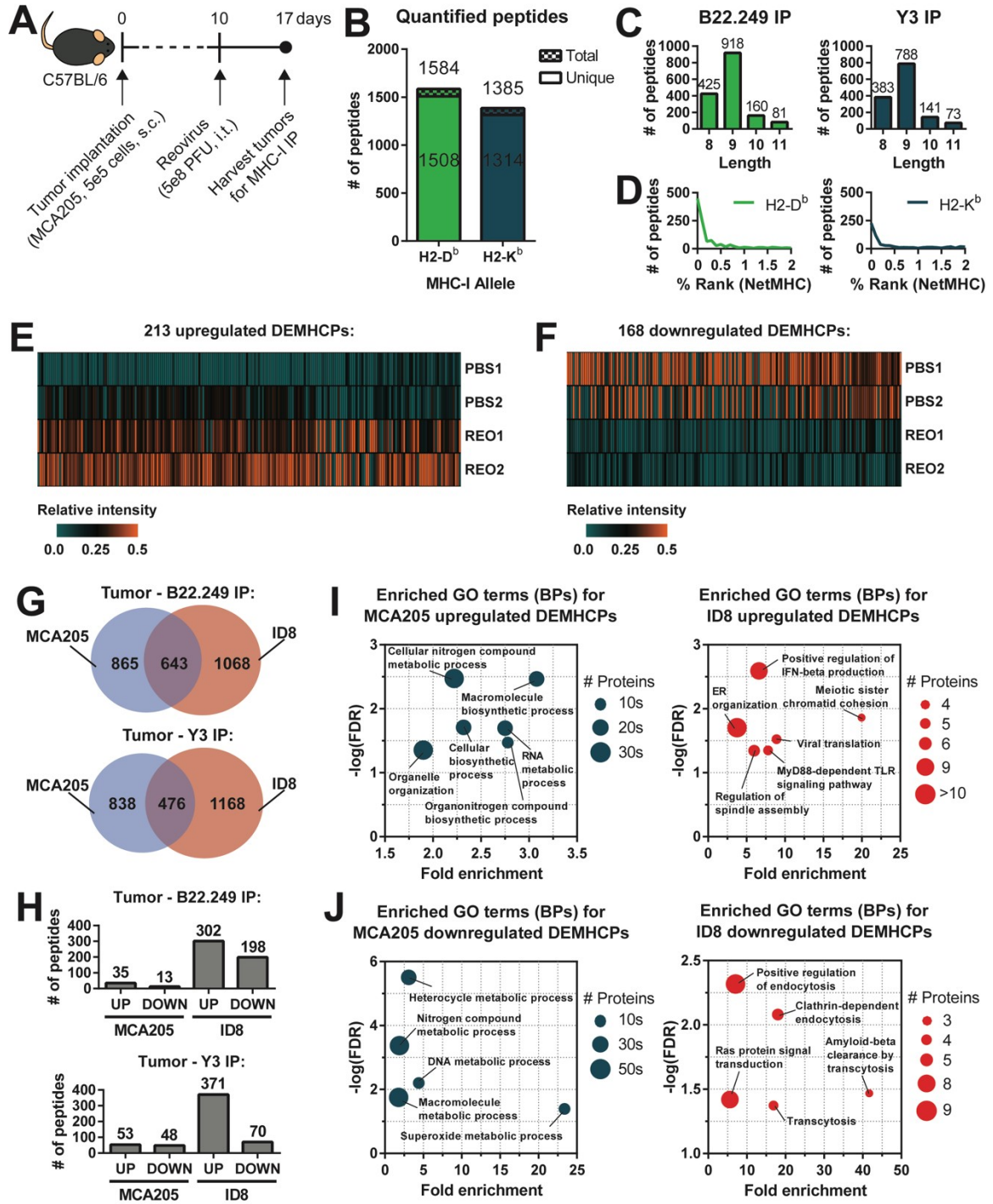
Figure 4.2. *Label-free quantitation of reovirus-modulated MCA205 MHC-I peptidome.*

(A) Experimental setup for MHC-I peptidome analysis of MCA205 tumors following reovirus treatment. MCA205 tumor-bearing mice were injected with either PBS or

reovirus, and tumors were harvested for MHC-I peptidome and mass spectrometry analysis with label-free quantitation. **(B)** Number of total and unique H2-D^b- and H2-K^b-specific peptides quantified in the experiment. **(C)** Length distribution of the quantified MHC-I peptides. **(D)** Predicted binding affinity (NetMHC % rank) of the quantified MHC-I peptides. Peptides that are <0.5% rank are considered strong binders whereas those that are 0.5-2% rank are weak binders. Relative intensities of H2-D^b- and H2-K^b-specific peptides that are specifically **(E)** upregulated ($\log_2$[reovirus/PBS] $\geq$ 1) or **(F)** downregulated ($\log_2$[reovirus/PBS] $\leq$ -1) by reovirus (REO) as compared to PBS-treated tumor-bearing control mice. **(G)** Number of distinct and overlapping H2-D^b (B22.249 IP) or H2-K^b (Y3 IP) peptides from the MCA205 and ID8 datasets. **(H)** Number of upregulated (UP) or downregulated (DOWN) MHC-I peptides observed for the MCA205 and ID8 models out of the overlapping peptides in common between the two datasets. **(I)** Enriched GO terms (BPs) in the source proteins of upregulated DEMHCPs. **(J)** Enriched GO terms (BPs) in the source proteins of downregulated DEMHCPs. s.c.: subcutaneous; PFU: plaque-forming units; i.t.: intratumoral; IP: immuno-affinity purification; BPs: biological processes; FDR: false discovery rate.
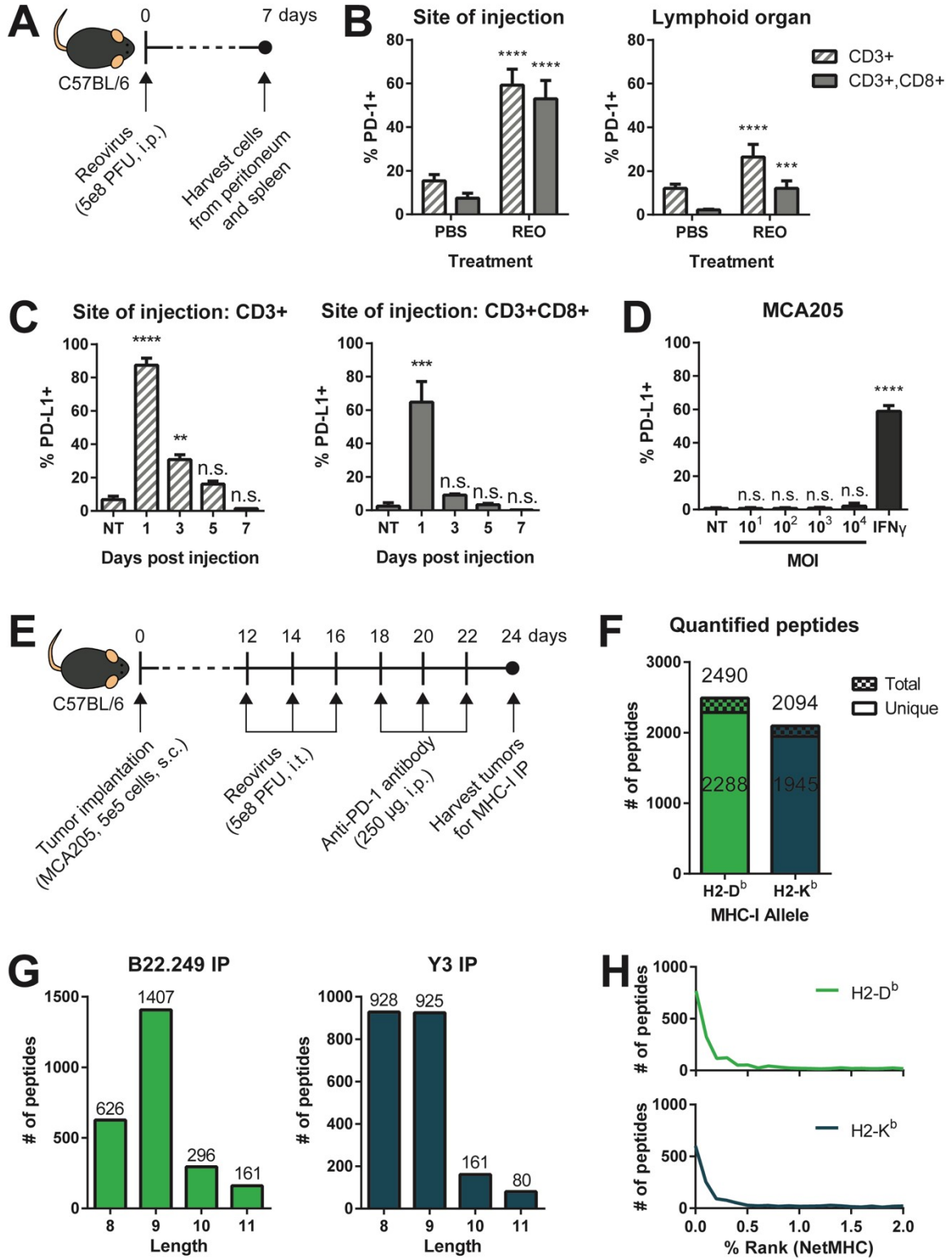
Figure 4.3. *TMT-based multiplexing platform analysis of reovirus and ICB combination-modulated MCA205 MHC-I peptidome.*

(A) Schematic of reovirus infection *in vivo* to analyze immune checkpoint expression. **(B)** Flow cytometry analysis of PD-1 expression on CD3 and CD8 T cells from the site of injection (peritoneum) and lymphoid organ (spleen) of C57BL/6 mice (n = 5) at 7 days post injection, compared to PBS-treated control mice. A two-tailed Student's *t* test with 95% confidence interval was performed. **(C)** PD-L1 expression on CD3 and CD8 T cells from the site of injection at 1, 3, 5, 7 days post injection were also quantified by flow cytometry. **(D)** PD-L1 expression level on MCA205 cancer cells *in vitro.* Cells were infected with reovirus at various MOIs for 24 h, and PD-L1+ cells were quantified by flow cytometry. Stimulation with IFNγ (100 U/mL) was included as a positive control. Data are representative of three independent experiments. One-way ANOVA coupled with a Bonferroni post-test was performed. **(E)** Experimental setup for MHC-I peptidome analysis of MCA205 tumors following reovirus and ICB combination treatment. IP-purified MHC-I peptides were analyzed by TMT-based multiplexed quantitation. **(F)** Number of total and unique H2-D^b- and H2-K^b-specific peptides quantified in the experiment. **(G)** Length distribution of the quantified MHC-I peptides. **(H)** Predicted binding affinity (NetMHC % rank) of the quantified MHC-I peptides. Asterisks shown immediately on top of the bars signify the *p* values obtained by comparing the respective data against the non-treated (PBS or NT) control group. n.s. = p > 0.05, *p ≤ 0.05, **p ≤ 0.01, ***p ≤ 0.001, ***p ≤ 0.0001. i.p.: intraperitoneal; PFU: plaque-forming units; s.c.: subcutaneous; i.t.: intratumoral; IP: immuno-affinity purification.

A Upregulated DEMHCPs

ICB
5
ISO
3
REO
5
0
0
0
6
0
3
10
1
1
0
0
1
0
0
1
1
172
75
64
REO
+ICB
REO
+ISO

C Upregulated DEMHCPs

# of peptides

H2-D^b
H2-K^b

180
160
140
120
100
80
60
40
20
0

3   5   5   64   172

ISO ICB REO REO REO
               +ISO +ICB

Treatment

E 172 REO+ ICB upregulated DEMHCPs:

PBS
ISO
ICB
REO
REO+ISO
REO+ICB

Relative intensity

0.0   0.2   0.4

B Downregulated DEMHCPs

ICB
1
ISO
0
REO
0
0
0
0
0
0
0
1
1
0
0
0
0
0
0
3
118
7
24
REO
+ICB
REO
+ISO
REO
8

D Downregulated DEMHCPs

# of peptides

H2-D^b
H2-K^b

120
100
80
60
40
20
0

0   1   8   24   118

ISO ICB REO REO REO
               +ISO +ICB

Treatment

F 118 REO+ ICB downregulated DEMHCPs:

PBS
ISO
ICB
REO
REO+ISO
REO+ICB

Relative intensity

0.0   0.15   0.3

G Upregulated DEMHCPs

$\log_2$(REO+ICB/PBS)

4
3
2
1
0

1   2   3   4   5   > 5

PSMs

H Downregulated DEMHCPs

$-\log_2$(REO+ICB/PBS)

2.0
1.8
1.6
1.4
1.2
1.0
0.8

1   2   3   4   5   > 5

PSMs

I Enriched GO terms (BPs) for REO+ICB upregulated DEMHCPs

$-\log$(FDR)

4

3

2

1

0

Cellular macromolecule metabolic process
Intracellular transport
Nucleic acid metabolic process
Establishment of organelle localization
Histone phosphorylation
Regulation of chromatin organization
Regulation of cellular component biogenesis

Proteins
4
8
>10

0   10   20   30

Fold enrichment

J Enriched GO terms (BPs) for REO+ICB downregulated DEMHCPs

$-\log$(FDR)

3

2

1

Cellular macromolecule metabolic process
Cellular process
Primary metabolic process
Macromolecule modification
Organelle organization
Nucleic acid metabolic process

Proteins
20s
30s
40s
>50

0   1   2   3

Fold enrichment

K IIVSFVNATL (Source: *Sf3b3*)

Rel. intensity

0.3
0.2
0.1

YVHVNRDTL (Source: *Pnkp*)

Rel. intensity

0.3
0.2
0.1
0.0

SAIHNSTKV (Source: *Gvin1*)

Rel. intensity

0.20
0.15
0.10
0.05
0.00

KAFHFPSL (Source: *Zfp729a*)

Rel. intensity

0.15
0.10
0.05
0.00

PBS ISO ICB REO REO REO
                    +ISO +ICB

Treatment

Figure 4.4. *Characterization of upregulated and downregulated DEMHCPs of reovirus and ICB combination therapy.*

Number of unique and overlapping **(A)** upregulated ($\log_2$[fold change] $\geq$ 1) or **(B)** downregulated ($\log_2$[fold change] $\leq$ -1) H2-D^b- and H2-K^b-specific DEMHCPs observed in the different treatment groups as compared to PBS control. Numbers of unique **(C)** upregulated or **(D)** downregulated DEMHCPs from each treatment group as compared to PBS control. Relative intensities of MHC-I peptides that are specifically **(E)** upregulated or **(F)** downregulated by reovirus and ICB combination therapy. Number of PSMs and fold change levels of the combination therapy **(G)** upregulated and **(H)** downregulated DEMHCPs. Enriched GO terms (BPs) in the source proteins of combination therapy **(I)** upregulated and **(J)** downregulated DEMHCPs. **(K)** Representative examples of MHC-I peptides that are upregulated or downregulated by combination therapy. DEMHCPs: differentially expressed MHC-I-associated peptides; PSMs: peptide spectrum matches; ISO: isotype control antibody; PD-1: anti-mouse PD-1 antibody; REO: reovirus; BPs: biological processes; FDR: false discovery rate.

A < MHC PEPTIDOME DISCOVERY PIPELINE >

IDENTIFICATION → ANALYSIS → VALIDATION

B Upregulated DEMHCPs

C Downregulated DEMHCPs

D Upregulated DEMHCPs   Downregulated DEMHCPs

E All DEMHCPs
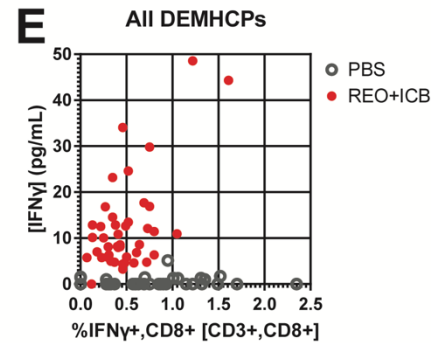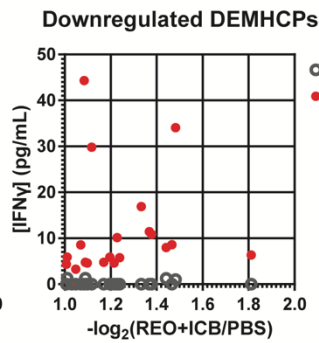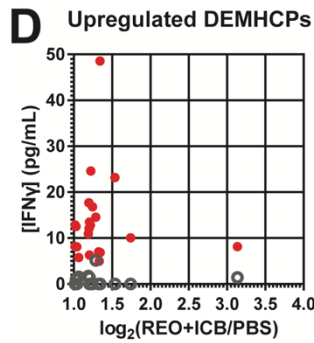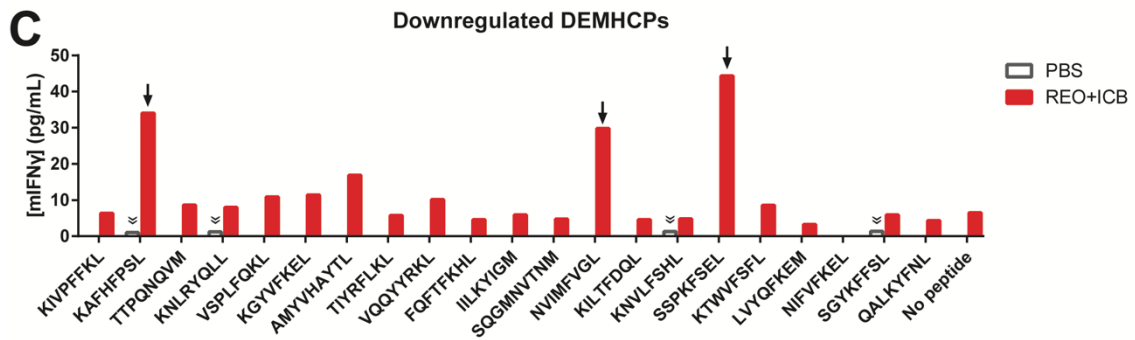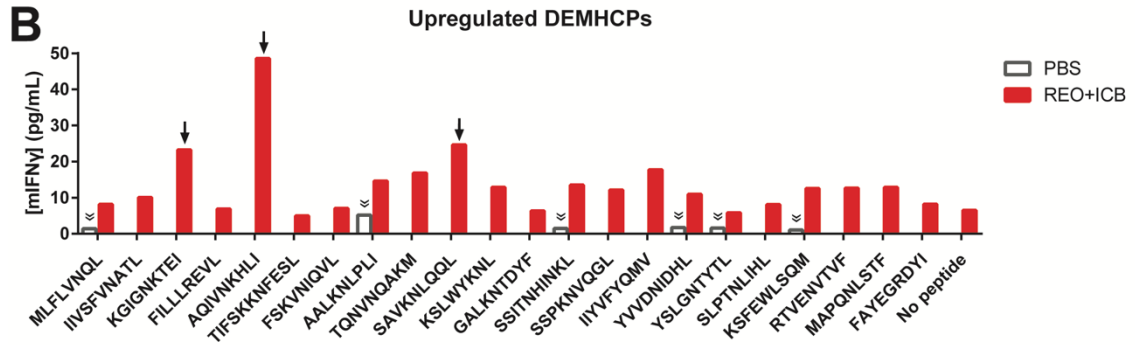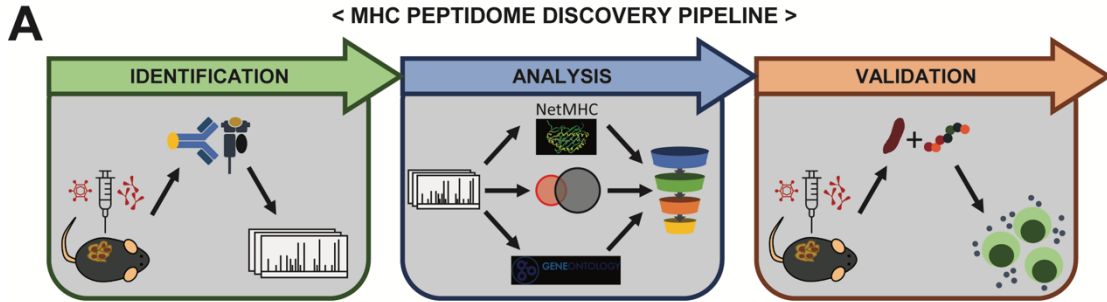
Figure 4.5. *Functional validation of reovirus and ICB combination therapy DEMHCPs as anti-tumor CD8 T cell epitopes.*

(A) Schematic diagram of the MHC-I peptidome discovery pipeline, from MHC-I peptide identification, analysis, to biological validation. Concentration of secreted IFNγ as measured by ELISA following *ex vivo* stimulation of splenocytes with **(B)** upregulated DEMHCPs or **(C)** downregulated DEMHCPs. Splenocytes from PBS- or reovirus and ICB (REO+ICB)-treated MCA205 tumor-bearing (TB) mice were cultured with the peptides for 24 h and then supernatants were collected for ELISA analysis. Arrows and chevron-double-down symbols indicate peptides that induced IFNγ levels greater than the cut-off value ([mean + 3 x standard deviation] of the negative controls – unstimulated splenocytes; 0 pg/mL for PBS and 17.77 pg/mL for REO+ICB). **(D)** Level of secreted IFNγ measured by ELISA and the corresponding fold change level measured by MHC-I analysis for each validated peptide. **(E)** Level of secreted IFNγ measured by ELISA and the corresponding intracellular IFNγ level measured by flow cytometry for each validated peptide. DEMHCPs: differentially expressed MHC-I-associated peptides; mIFNγ: murine interferon gamma.

Table 4.1. *Reovirus and ICB combination therapy DEMHCPs for immunogenicity validation.*

Sequence	Source protein gene	MHC allele	# PSMs	log$_2$(REO+ICB/PBS)
MLFLVNQL	Pcid2	Kb	4	3.14
IIVSFVNATL	Sf3b3	Db	3	1.74
KGIGNKTEI	Nsd3	Kb	4	1.54
FILLLREVL	Marchf6	Kb	3	1.34
AQIVNKHLI	Eif2b3	Kb	2	1.34
TIFSKKNFESL	Rpn2	Kb	2	1.33
FSKVNIQVL	Oasl2	Kb	3	1.32
AALKNLPLI	Acsl3	Kb	2	1.29
TQNVNQAKM	Maged1	Kb	2	1.24
SAVKNLQQL	Nprl3	Kb	3	1.22
KSLWYKNL	Il17rc	Db	2	1.22
GALKNTDYF	Nt5c3a	Kb	2	1.20
SSITNHINKL	Sema5a	Kb	3	1.20
SSPKNVQGL	Siglec1	Kb	2	1.20
IIYVFYQMV	Kifap3	Db	2	1.20
YVVDNIDHL	Cop1	Kb	3	1.19
YSLGNTYTL	Gpsm1	Kb	3	1.06
SLPTNLIHL	Ubr2	Kb	7	1.04
KSFEWLSQM	Dync1h1	Db	2	1.03
RTVENVTVF	Vat1	Kb	2	1.02
MAPQNLSTF	Dnajb11	Kb	2	1.02
FAYEGRDYI	H2-Q6	Kb	20	1.02
KIVPFFKL	Dync1h1	Kb	5	-1.81
KAFHFPSL	Zfp729a	Kb	2	-1.48
TTPQNQVDM	Chmp1b1	Db	2	-1.47
KNLRYQLL	Matr3	Kb	3	-1.44
VSPLFQKL	Mars1	Kb	6	-1.38
KGYVFKEL	Tlr7	Kb	2	-1.37
AMYVHAYTL	Psma3	Db	2	-1.33
TIYRFLKL	Fem1c	Kb	7	-1.24
VQQYYRKL	Prex1	Kb	2	-1.23
FQFTFKHL	Dnaja2	Kb	3	-1.21
IILKYIGM	Arl6ip1	Kb	2	-1.20
SQGMNVTNM	Ep300	Db	6	-1.17
NVIMFVGL	Srp54c	Kb	2	-1.12
KILTFDQL	Rpl18	Kb	5	-1.10
KNVLFSHL	Prkar1b	Kb	2	-1.09
SSPKFSEL	Wdr45	Kb	4	-1.08
KTWVFSFL	Cilp	Kb	4	-1.07
LVYQFKEM	Elf4	Kb	4	-1.05
NIFVFKEL	Rapgef6	Kb	2	-1.03
SGYKFFSL	Wipi2	Kb	3	-1.01
QALKYFNL	Sel1l	Kb	6	-1.01

MHC: major histocompatibility complex; PSM: peptide spectrum match; REO: reovirus; ICB: immune checkpoint blockade

4.7 SUMMARY OF CHAPTER 4 AND TRANSITION TO CHAPTER 5

In this chapter, we showed that oncolytic reovirus monotherapy upregulates, as well as downregulates, the expression of tumor MHC-I peptides in a cancer type and oncolysis susceptibility dependent manner. The combination of reovirus and ICB resulted in the highest number of DEMHCPs, among which we identified immunogenic epitopes with biologically active cognate CD8 T cells. Ultimately, these findings, as well as that of the previous chapter, highlighted that the therapy-induced changes to the MHC-I peptidome contribute towards the re-instated anti-tumor CD8 T cell attack established by the administration of immunotherapies. In the following chapter, we wanted to investigate the other robust immune response initiated following OV therapy: anti-viral immunity. Given the high immunogenicity of pathogens, we postulated that anti-viral immunity could make up the bulk of and/or overpower the immune response in the TME, in which case anti-viral T cell activity may be manipulated for therapeutic benefit. Thus, we sought to identify the targets of anti-viral T cells by performing reovirus genome-wide epitope mapping and study the cognate anti-OV T cell immune responses.

CHAPTER 5: REDIRECTING ANTI-VIRAL IMMUNITY TOWARDS CANCER BY ANTIGENIC REPROGRAMMING OF TUMOR MHC PEPTIDOME

This manuscript is in preparation, with the following contributors:

Kim Y, Holay N, Clements D, Konda P, Helson E, Gujar S

5.1   AUTHOR CONTRIBUTIONS

YK designed and performed the experiments, analyzed the data, and wrote the manuscript with input from SG. NH designed the flow cytometry panels for T cell differentiation and immune checkpoint markers. DC and EH contributed to Figure 5.1F and Table 5.1. PK manufactured reovirus. SG supervised and acquired funding for the project.

5.2 ABSTRACT

Overturning existing dogma, pre-existing anti-viral immunity has been reported to benefit oncolytic virus (OV)-based cancer immunotherapy. On this account, we sought to repurpose anti-viral immunity to enhance OV therapeutic efficacy by redirecting virus-specific CD8 T cells to target cancer cells. Our aim was to identify the antigenic determinants of anti-viral immunity and use this information to antigenically reprogram cancer cells to present viral peptides on their class I major histocompatibility complex (MHC-I). *In silico* prediction followed by biological validation was performed to identify the immunodominant CD8 T cell epitope of oncolytic reovirus, and MHC tetramers loaded with this virus epitope was used to analyze the distinct functional phenotype of reovirus-driven T cells. Reovirus was also shown to promote the 'cold-to-hot' transition of the tumor microenvironment (TME) in a murine tumor model, inducing an influx of CD3 and CD8 T cells which also included virus-specific CD8 T cells. Anti-viral T cells that infiltrated the TME were shown to maintain their functional phenotype, despite the expression of inhibitory immune checkpoints. To have this virus-specific T cell response target cancer cells, we increased the antigenicity of tumors through exogenous loading of synthetic viral peptides, which resulted in their presentation via tumor MHC-I and sensitized cancer cells to cytotoxic attack by virus-specific T cells *in vitro*. Thus, redirecting anti-viral immunity to target cancers can be achieved by the provision of viral peptides to tumors and represents a unique approach to potentiate OV therapy.

5.3 INTRODUCTION

By harnessing the innate properties of our own immune system to target tumors, cancer immunotherapies have galvanized oncology[444]. The efficacy of immunotherapies depends

on the generation and activation of anti-tumor CD8 T cells that recognize specific tumor peptides (i.e., antigens or epitopes) presented via class I major histocompatibility complex (MHC-I) molecules on the surface of cancer cells[142,143]. The presence of the resultant tumor-infiltrating lymphocytes (TILs), specifically the CD8 cytotoxic T lymphocytes (CTLs), correlates with better patient outcomes[106,142,145]. Despite recent advances in cancer immunotherapies, however, only a minority of patients show objective response to current immunotherapy regimens. Major impediments to therapeutic success include the lack of TILs and the immunosuppressive tumor microenvironment (TME), culminating in T cell exhaustion if there are any TILs. In addition, cancer cells display a low density of presented antigens due to defects in the antigen processing and presentation machinery, as well as reduced surface MHC-I expression. Difficulties in identifying immunogenic neoepitopes have also hindered the development of effective tumor-specific T cell therapy.

Oncolytic viruses (OVs) have emerged as a formidable cancer immunotherapeutic agent that can address these challenges[1,12]. Originally discovered for their tumor destructive effects, OVs are a highly immunostimulatory modality that promotes the induction of potent anti-tumor immune responses[1,4,12,467]. We have previously demonstrated this generation of anti-tumor immunity and subsequent long-term immune protection against tumor recurrence mediated by mammalian orthoreovirus type 3 Dearing strain (henceforth referred to as reovirus) in various murine tumor models[130,458,459]. The establishment of anti-tumor immunity was attributed to the ability of reovirus to overturn tumor-induced immunosuppression[130,458]. Specifically, the inflammatory response following reovirus administration restored the expression of MHC-I on cancer cells, thus allowing the presentation of otherwise obscure tumor-specific antigens. We recently

utilized a mass spectrometry-based approach to elucidate the reovirus-induced tumor MHC-I peptidome[433], which is the array of MHC-I bound peptides that define anti-tumor CD8 T cell responses.

While promoting the development of beneficial anti-tumor immunity, OVs as pathogens also trigger the host immune system to mount a detrimental anti-viral immune response. Neutralizing antibodies against OVs can prematurely clear the virus and prevent infection of tumor tissues. This poses as a significant hurdle for systemic administration of OVs, repeated therapeutic dosing, and treatment of patients with pre-existing immunity to OVs. Fortunately, contrary to this dogma, anti-viral immunity has been reported to actually potentiate OV therapy. Ricca et al. described enhanced therapeutic efficacy of Newcastle disease virus (NDV) in B16F10 melanoma tumor-bearing (TB) mice with pre-existing immunity against this OV, as compared to NDV-naïve TB mice[267]. Evidence of virus-specific memory CD8 T cells in human tumors has also been presented, highlighting the heterogeneity of TILs[264,265]. Multiple studies have used this fact to exploit pre-existing anti-viral immunity to target cancers by re-activating virus-specific memory T cells[274–276,483].

Here, we aimed to enhance the efficacy of reovirus-based cancer immunotherapy by repurposing anti-viral immunity to target cancer cells through reprogramming tumor antigenicity. We first performed a multidisciplinary analysis to catalog the repertoire of MHC-I-restricted reovirus-specific T cell epitopes and to characterize the phenotype and functionality of virus-specific CD8 T cells, in the presence and absence of the TME. We also demonstrated increased antigenicity of cancer cells through exogenous loading of viral peptides onto their MHC-I molecules, thereby rendering them susceptible to recognition

by anti-viral CD8 T cells. Thus, redirecting anti-viral immunity to tumors is possible through the manipulation of the tumor MHC peptidome to express virus epitopes.

5.4   RESULTS

5.4.1   *Reovirus Genome-wide Epitope Mapping Reveals an Immunodominant H2-K^b-restricted T Cell Epitope*

To repurpose anti-viral immunity for OV therapy, our first aim was to identify the immunogenic determinants of anti-viral immunity by *in silico* epitope prediction followed by immunogenicity assessment (Figure 5.1A). Specifically, an immunoinformatics (i.e., computational immunology) approach based on the SYFPEITHI epitope prediction algorithm[405] was utilized to analyze the 10 double-stranded RNA segments of the reovirus genome. Epitope mapping was completed for H2-K^b (8 amino acid long linear epitopes) and H2-D^b (9 amino acid long linear epitopes) MHC-I alleles for the C57BL/6 mouse background, generating an overlapping peptide library of 1,546 epitopes ($\geq$ SYFPEITHI score of 15) spanning long stretches of sequence within each protein. Limiting our analysis to epitopes with SYFPEITHI scores $\geq$ 20 resulted in the identification of 43 H2-K^b- and 75 H2-D^b-restricted epitopes, where 11 out of 12 reovirus proteins were represented (Figure 5.1B). These 118 CD8 T cell epitopes covered a wide range of SYFPEITHI scores from 20 to 29, with higher SYFPEITHI scores indicating greater predicted immunogenicity (Figure 5.1C).

In order to validate the immunogenicity of these predicted T cell epitopes, the abovementioned 118 reovirus epitopes were synthesized. First, the MHC binding affinity was analyzed by ProImmune REVEAL® MHC-peptide binding assay wherein binding scores greater than 45% represent high-affinity binders. Irrespective of SYFPEITHI scores,

42 out of 43 H2-K^b and 47 out of 75 H2-D^b epitopes were strong binders (Figure 5.1D). Subsequent analyses considered the REVEAL assay scores as the indicator of immunogenicity as opposed to the predicted SYFPEITHI scores. Next, the biological activity of these peptides was evaluated by a T cell activation assay. Following the *ex vivo* stimulation of splenocytes with peptides, interferon gamma (IFNγ) production by CD8 T cells was measured by flow cytometry (Figure 5.1E). Immunodominance hierarchy of reovirus epitopes was observed as shown for the top 15 most immunogenic peptides in Figure 5.1F (see Table 5.1 for the list of all 118 peptides). Interestingly, the level of IFNγ production by CD8 T cells was not dependent on the MHC binding affinity of the peptides. For example, a strong binder M1$_{388-396}$ (peptide sequence TGFINRHTI; MHC binding affinity of 103.4%) and a weak binder S2$_{263-271}$ (peptide sequence IRPGNRSLF; MHC binding affinity of 21.6%) both resulted in the activation of approximately 3.6% of IFNγ+,CD8+ T cells. These findings indicate that MHC binding affinity is not the sole criterion for immunogenicity. More importantly, we identified an immunodominant reovirus CD8 T cell epitope. S3$_{21-28}$ (peptide sequence VCPNYVML) is derived from the non-structural protein σNS, is a strong binder restricted to H2-K^b, and stimulates approximately 8% of IFNγ+,CD8+ T cells. With a two-fold higher IFNγ response compared to the next peptide in the immunodominance hierarchy, S3$_{21-28}$ serves as an ideal epitope to study anti-viral immune responses specific against reovirus.

5.4.2 Reovirus-specific CD8 T Cells Exhibit an Effector Memory Phenotype and Functional Activity, Despite Immune Checkpoint Receptor Expression

We used the immunodominant reovirus epitope (S3$_{21-28}$) as a representative to characterize the overall anti-viral CD8 T cell response. MHC-I tetramers loaded with the

immunodominant viral peptide (pMHC tetramers) were utilized to detect virus-specific CD8 T cells, specified as CD3+,CD19-,CD8+,Tetramer+, by flow cytometry (Figure 5.2A). First, we conducted a temporospatial analysis of reovirus-specific CD8 T cells from cells isolated from the peritoneum (site of injection) and spleen of C57BL/6 mice at 1, 3, 5, 7, and 10 days post infection (d.p.i.). Expansion of virus-specific CD8 T cells was observed as early as 5 d.p.i. in the spleen and 7 d.p.i. in the peritoneum (Figure 5.2B). The decrease in virus-specific CD8 T cells in the spleen after 5 d.p.i. is likely due to the migration of these cells to the site of infection, corresponding to the increased frequency of these cells in the peritoneum at this timepoint. The percentage of Tetramer+ cells in the peritoneum was highest at 10 d.p.i.; however, the absolute number of cells in the peritoneum was highest at 7 d.p.i., making analyses easier (i.e., many events must be acquired on the flow cytometer to visualize cells of low frequency). Thus, subsequent analyses of virus-specific CD8 T cells were performed at 7 d.p.i..

Next, we wanted to further delineate the phenotype of these virus-specific CD8 T cells by costaining for memory subset markers, distinguishing differentiation status. Upon antigen recognition, naïve T cells undergo differentiation into an effector state, characterized by a high proliferative and cytotoxic capacity[260–262]. The differentiation status of T cells can be based on the expression of CD44 (hyaluronic acid receptor) and CD62L (L-selection), with four defined subsets: naïve (T_N; CD44-,CD62L+), central memory (T_{CM}; CD44+,CD62L+), effector memory (T_{EM}; CD44+,CD62L-), and CD44-,CD62L-. In line with previous reports on acute viral infections[259–261,484], total CD8 T cells of the peritoneum (Figure 5.2C) and spleen differentiated into T_{EM} cells in response to reovirus at 7 d.p.i. (Figure 5.2D). At this timepoint, the frequency of T_{EM} cells of total CD8 T cells

was higher in the peritoneum than in the spleen. Moreover, virus-specific CD8 T cells of the peritoneum and spleen displayed an effector memory phenotype, in a more homogenous manner as compared to the total CD8 T cell population; that is, almost all Tetramer+ cells were T_{EM} (Figure 5.2D). Secondly, we also costained for inhibitory checkpoint receptors to further phenotypically characterize virus-specific CD8 T cells. We examined the expression of immune checkpoint receptors PD-1 (programmed cell death protein 1) and TIM3 (T cell immunoglobulin and mucin-domain containing-3), which play an important role in regulating autoimmunity and T cell exhaustion, respectively[447,485,486]. We observed that CD8 T cells upregulate the expression of PD-1 and TIM3 in response to reovirus at 7 d.p.i. (Figure 5.2E). The induced expression of these molecules on CD8 T cells was greater in the peritoneum than in the spleen (Figure 5.2F). Furthermore, while virus-specific CD8 T cells in the peritoneum and spleen were all PD-1+, approximately half of this Tetramer+ population was TIM3+. Other immune checkpoint receptors such as CTLA-4 and TIGIT were not expressed by CD8 T cells during reovirus infection (Supplementary Figures 5.1A & 5.1B).

We next wanted to analyze the functional capacity of these cells. Typically, the expression of inhibitory immune checkpoint receptors is strongly correlated with T cell exhaustion[447,486]. To examine whether the reovirus-driven T cell population is functionally active, we measured the expression of the cytotoxic molecule granzyme B (GzmB), a serine protease secreted along with perforin by CD8 T cells to induce apoptosis in the target cells. At 7 days post reovirus infection, approximately 50% of CD8 T cells and about 65% of virus-specific CD8 T cells in the peritoneum expressed GzmB (Figure 5.2G). Similar results were observed in the spleen but at a frequency less than that of the cells in the

peritoneum (Figure 5.2H). Therefore, despite the expression of inhibitory immune checkpoint receptors, reovirus-driven CD8 and virus-specific CD8 T cells displayed an effector memory phenotype and were functionally active, expressing cytotoxic molecule GzmB. Overall, reovirus infection induced a dramatic change in the phenotypes of the total CD8 T cell population, and more importantly, this change was greatly pronounced in virus-specific CD8 T cells.

5.4.3   Virus-specific CD8 T Cells Infiltrate Tumor Microenvironments

Our next aim was to determine the presence of anti-viral immunity in tumors and investigate whether the immunosuppressive TME can alter the phenotype and function of anti-viral CD8 T cells. We examined anti-viral immunity in the context of two syngeneic mouse models, EL4 T cell lymphoma and MCA205 fibrosarcoma. Upon injection of reovirus into established tumors (Figure 5.3A), we noted a difference in the level of TILs in the two tumor types. CD3 and CD8 TILs were already at relatively high levels in non-treated (PBS control) EL4 tumors, as compared to MCA205 tumors, and were unaffected by reovirus treatment (Figure 5.3B). On the other hand, both CD3 and CD8 TIL levels significantly increased in reovirus-treated MCA205 tumors, as compared to the levels observed in PBS-treated tumors (Figure 5.3C). More importantly, we detected virus-specific CD8 T cells in both the EL4 (Figure 5.3D) and MCA205 (Figure 5.3E) tumors, with generally a higher percentage observed in the latter compared to the former.

In terms of memory markers, we first recognized that intratumoral CD8 T cells in the absence of reovirus displayed a T_{EM} phenotype (Figure 5.3F), which contrasts with the CD8 T_N cells observed in non-TB, non-treated mice. Following reovirus exposure, total CD8 and virus-specific CD8 T cells in both tumor types maintain the T_{EM} phenotype

(Figure 5.3G & 5.3H). Similarly, CD8 T cells in non-treated tumors had a unique profile of immune checkpoint expression, already displaying high levels of PD-1 and TIM3 (Figure 5.3I). There was a slight difference between CD8 TILs of EL4 (Figure 5.3J) and MCA205 (Figure 5.3K) tumors. In reovirus-treated EL4 tumors, CD8 T cells shifted from PD-1+,TIM3+ to PD-1+,TIM3- phenotype, which was more pronounced in virus-specific CD8 T cells (Figure 5.3J). In contrast, CD8 TILs of reovirus-treated MCA205 tumors shifted from PD-1+,TIM3+ to PD-1-,TIM3+ cells; virus-specific CD8 T cells remained mostly PD-1 and TIM3 double-positive (Figure 5.3K). Overall, TIM3 expression, either alone or co-expressed with PD-1, was more apparent on MCA205 CD8 TILs. With respect to the functional capacity of these cells (Figure 5.3L), GzmB was expressed in CD8 TILs of non-treated EL4 (Figure 5.3M) and MCA205 (Figure 5.3N) tumors, with a higher basal level expression in the latter. Reovirus treatment resulted in increased GzmB expression in CD8 TILs of both tumor types but at a significantly higher level in the MCA205 than in the EL4 CD8 T cells (75% versus 20%); virus-specific CD8 T cells of both tumors were equally high in GzmB. In sum, despite being in an immunosuppressive TME, virus-specific CD8 T cells maintained an effector memory phenotype and functional activity, even with the expression of PD-1 and TIM3.

Furthermore, we also examined the immune cells in the secondary lymphoid organs, specifically the spleens, of these TB mice (Supplementary Figure 5.2A). Here, intratumoral injection of reovirus significantly increased the levels of CD3 and CD8 splenic T cells in both tumor models (Supplementary Figures 5.2B & 5.2C). Virus-specific CD8 T cells were also detected in these TB mice spleens (Supplementary Figures 5.2D & 5.2E). The trends observed in the TB mice spleens regarding memory marker

(Supplementary Figures 5.2F & 5.2G), immune checkpoint (Supplementary Figures 5.2H & 5.2I), and GzmB (Supplementary Figures 5.2J & 5.2K) expression on CD8 and virus-specific CD8 T cells were comparable to those observed in spleens of non-TB mice. This suggests that there was no apparent effect of the TME in altering the phenotype or function of CD8 T cells at these peripheral sites.

Thus far, our emphasis was on how acute viral infection can reprogram the tumor immune microenvironment towards one that is more virus-directed. Given that previous reports on anti-viral immune cells in tumors focused on memory immunity[274–276], we wanted to see if we can also detect reovirus-specific CD8 T cells in tumors without direct infection of tumors. Mice were immunized with reovirus (i.e., REO-IMM mice) prior to tumor implantation and pMHC tetramer quantification was performed once tumors developed (Supplementary Figure 5.3A). Even at 25 days post reovirus immunization and most importantly without intratumoral reovirus injection, virus-specific CD8 T cells were detected in non-treated EL4 tumors of REO-IMM mice (Supplementary Figure 5.3B). The level of Tetramer+ cells was comparable to that observed in reovirus-treated tumors at 7 d.p.i. (5.5% in REO-IMM versus 7% in REO). Thus, whether it was newly activated or pre-existing anti-viral immunity, reovirus-specific CD8 T cells infiltrated the TME.

5.4.4 *Reprogramming the Antigenicity of Tumor Cells Renders Them Susceptible to Virus-specific CTL Activity in Vitro*

Having shown the presence of virus-specific CD8 T cells in the TME, we next wanted to have these immune cells target cancer cells. To achieve this, we aimed to antigenically reprogram the tumor MHC-I peptidome landscape, resulting in the presentation of virus-specific peptides by cancer cells for subsequent recognition by anti-viral CD8 T cells. We

first showed that exogenously provided synthetic peptides are indeed taken up and presented by cancer cells. Here, we used the SIINFEKL-based system to measure MHC-I antigen presentation; MHC-I presentation of ovalbumin-derived SIINFEKL peptide (hereon referred to as Ova peptide) can be detected using anti-mouse H2-K^b bound to SIINFEKL (MHC-ova) antibody[487]. Pulsing EL4 (Figure 5.4A) and MCA205 (Figure 5.4B) cells with Ova peptide resulted in a concentration-dependent increase in MHC-ova expression. The mean fluorescence intensity (MFI) of MHC-ova was much higher in the EL4 cells relative to the MFI observed in MCA205 cells. Next, we demonstrated that the immunodominant reovirus epitope S3$_{21-28}$ (hereon referred to as Reo peptide) can be presented by EL4 (Figure 5.4C) and MCA205 (Figure 5.4D) cells, as indicated by the increased H2-K^b expression following peptide-pulsing. Since an antibody that detects H2-K^b bound to Reo peptide does not exist, we used H2-K^b expression as a surrogate measure of peptide-MHC presentation; Ova peptide, serving as a positive control, supported this assumption. Of note, we observed a significantly higher level of H2-K^b following Ova peptide-pulsing as compared to Reo peptide-pulsing in both cell lines. According to NetMHC[408,409], Ova peptide is a stronger MHC binder than Reo peptide – H2-K^b % rank 0.06 versus 0.4, respectively; thus, NetMHC-predicted binding affinity of the peptides can influence their MHC-I presentation following exogenous provision.

We then examined whether antigenically reprogrammed cancer cells were sensitized to recognition by anti-viral CD8 T cells using a cancer cells:splenocytes co-culture assay. Firstly, to confirm the presentation of Reo peptide-MHC complexes, we measured the activation (i.e., intracellular IFNγ expression) of virus-specific CD8 T cells within the co-cultured splenocytes (Figure 5.5A). Activated CD8 T cells were observed

when splenocytes from reovirus-treated mice were co-cultured with Reo peptide-pulsed EL4 (Figure 5.5B) or MCA205 (Figure 5.5C); CD8 T cells did not express IFNγ in response to the no peptide or Ova peptide-pulsed cancer cells. We did note that Reo peptide-pulsed EL4 cells resulted in higher percentage of IFNγ+,CD8+ cells compared to the levels observed with MCA205 cells. Secondly, we wanted to show that these newly activated virus-specific CD8 T cells attack the virus peptide-presenting cancer cells. The co-culture assay was modified where cancer cells were labeled with a fluorescent dye called CellTrace Violet (CTV) and the viability of the cancer cells was measured (Figure 5.5D); CTV labeling was necessary to distinguish cancer cells from immune cells. We observed a significant level of cell death in Reo peptide-pulsed EL4 cells compared to the control cells (Figure 5.5E). Ova peptide-pulsed EL4 cells showed a small increase in cell death level as well. The viability of Reo peptide-pulsed MCA205 cells, on the other hand, was unaffected by the co-culture assay (Figure 5.5F). Overall, better Reo peptide presentation, capacity to activate antigen-specific T cells, and susceptibility to cytotoxic attack by said T cells was demonstrated with the EL4 cell line. This suggests that certain cell lines are more suited to be targets of redirected anti-viral T cells. Ultimately, we showed that antigenic reprogramming is feasible, resulting in cancer cells that present viral peptide-MHC complexes which leaves them vulnerable to attack by virus-specific T cells.

5.5   DISCUSSION

Herein, we presented a T cell epitope mapping analysis of reovirus with the subsequent application of the immunodominant epitope to characterize and manipulate anti-viral immunity in the context of OV therapy. A multidisciplinary approach combining bioinformatics and immunology allowed us to identify the immunodominant reovirus-

specific epitope, which was used as a representative measure of anti-viral immunity via pMHC tetramer-based analyses. We showed that the total CD8 and virus-specific CD8 T cell populations display a unique profile of differentiation state, immune checkpoint receptors, and functional capacity in response to reovirus administration *in vivo*. Using two syngeneic tumor models, we demonstrated that virus-specific CD8 T cells infiltrate tumors and maintain the same phenotypes as those observed in naïve mice, despite being in an immunosuppressive TME. We then examined the feasibility of redirecting anti-viral immunity towards cancer cells by demonstrating that cancer cells can take up and present exogenous peptides via their MHC-I molecules and in doing so, can activate cognate virus-specific T cells and be subjected to the cytotoxic effect of these cells.

The elucidation of MHC-I epitopes has many useful benefits. The immunogenic MHC-I peptides identified can be used as peptide vaccines against pathogens or cancers[393–395,400–402]. T cell receptor (TCR)-transgenic mouse models can be developed[488,489]. The corresponding CD8 T cell responses can be characterized using pMHC tetramers[397], as was the case in this study. Utilizing *in silico* prediction algorithms enabled us to perform reovirus genome-wide T cell epitope mapping, which would have been difficult to achieve without computational analyses. However, there were some disadvantages to this approach. The 118 reovirus-specific peptides we selected (43 H2-K^b- and 75 H2-D^b-restricted epitopes) were those above an arbitrary SYFPEITHI score cut-off value of 20; if we had set this cut-off value to 15, it would have been 1,546 epitopes to validate. As confirmed by the ProImmune REVEAL® MHC binding assay, almost all 118 epitopes were strong MHC binders, with no distinction according to the SYFPEITHI scores. Thus, we may have limited ourselves to investigating only high MHC-binding epitopes. Binding

affinity predictions tell us about the interaction between a peptide and an MHC molecule and whether a stable enough complex will form and be presented on the cell surface[399,406]; it does not provide any information on the status of cognate TCRs. Peptides with low predicted binding affinities can still be presented and be immunogenic, which is supported by our data demonstrating that immunogenicity (i.e., IFNγ response) was not dependent on MHC binding affinity. If time and money allow, more epitopes covering a broader range of SYFPEITHI scores should be investigated. Nevertheless, our validation experiment established the immunodominance hierarchy of reovirus epitopes with the identification of the top immunogenic epitope $S3_{21-28}$ (peptide sequence VCPNYVML). An immunodominant virus epitope, if highly immunogenic enough, is advantageous to representatively measure the immune response against the whole pathogen[490–492].

The use of pMHC tetramers permits the study of T cells specific for a single epitope and when combined with multiparameter flow cytometry, we can analyze these cells for various physical characteristics[397,441,493]. Specifically, we chose to investigate the differentiation status, immune checkpoint receptors, and functional capacity, all of which have implications for the activation status of T cells during viral infection. We observed a rapid expansion of virus-specific CD8 T cells, reaching as high as 15% of the total CD8 T cell population. As these cells are specific for one epitope, this percentage was an impressively high number, especially since a T cell specific for any given antigen is estimated to occur at a frequency of $\sim 1/10^5$ T cells within the naïve CD8 T cell population[260,494]. Distinguishing the differentiation status of T cells was important as it allowed us to understand the differences observed between the T cells in the peritoneum and the spleen. That is, different T cell subsets – naïve versus antigen-experienced – are

found at different locations[260,262,495] and thus it could be that the other phenotypic markers are reflective of the differentiation state of the cells, rather than an environmental influence. In terms of immune checkpoint expression, our data were consistent with previous reports of PD-1 or TIM3 expression on CD8 T cells during acute viral infection where the expression of immune checkpoint receptors is induced during clonal expansion and is therefore associated with recent antigen exposure and activation, not exhaustion[476,477,496–499]. This is also supported by the fact that reovirus-driven CD8 and virus-specific CD8 T cells were functionally active, expressing GzmB. Thus, it is important to discern the role of immune checkpoints in a context-dependent manner (i.e., acute versus chronic conditions) and not assume that the expression of these molecules will always negatively affect T cell function[476,498,499]. Moreover, only a couple of the numerous immune checkpoints investigated were expressed on CD8 T cells in response to reovirus infection. The mechanism behind why certain immune checkpoints but not others are induced by reovirus can be an area for future research (e.g., different timepoints post infection, dose-dependent). Interestingly, we noted a heterogeneous expression of immune checkpoints and GzmB in what is supposed to be a homogenous Tetramer+ population. It remains to be determined whether this is due to TCR clonotype heterogeneity and what the implications are of having a diverse TCR repertoire for a particular virus epitope[500–502].

As reovirus is an oncolytic agent, it is important to study it in a cancer setting. First, we showed that intratumoral injection of reovirus can promote a 'cold-to-hot' transition of the tumor immune microenvironment. This effect was more greatly induced in the MCA205 tumors compared to the EL4 tumors, possibly because the latter is already immune-inflamed as indicated by two-fold higher levels of CD3 and CD8 T cells compared

to the former. Second and more importantly, we determined that virus-specific CD8 T cells can be detected in reovirus-treated tumors, as well as in non-treated tumors of reovirus-immunized mice. Our data support the work by Simoni et al. highlighting that TILs constitute a heterogenous population of cells that are not only specific for tumor antigens but also include cells that are specific for virus epitopes[264]. In addition to the difference in the level of TILs in the two tumor types, we also noticed that the percentage of Tetramer+ cells was higher in MCA205 tumors compared to that observed in EL4 tumors. Further investigation is necessary to determine if this discrepancy is related to the susceptibility to infection and oncolysis of the two tumors. Regardless, whether T cells were already present in the tumors (EL4) or newly recruited (MCA205), the effect of reovirus on tumor immune landscape was evident, especially for immune checkpoint and GzmB expression. CD8 T cells in non-treated tumors already expressed high levels of both PD-1 and TIM3, as expected for exhausted and functionally impaired TILs. Following reovirus administration, there was a shift towards PD-1+,TIM3- in CD8 TILs of EL4 tumors and PD-1-,TIM3+ in CD8 TILs of MCA205 tumors. It would be interesting to examine if this difference in expression is on the existing population of TILs (e.g., PD-1+,TIM3+ cells losing TIM3 expression) or due to an influx of anti-viral CD8 T cells with higher PD-1 expression. Moreover, the Tetramer+ population exhibiting two different phenotypes (PD-1+,TIM3+ and PD-1+,TIM3- in EL4 tumors while mostly PD-1+,TIM3+ in MCA205 tumors) suggests that the environment and/or susceptibility to reovirus infection can influence immune checkpoint expression on virus-specific T cells. As the basal levels of immune checkpoint receptors and GzmB of CD8 T cells differed between EL4 and MCA205 tumors, it is possible that these tumors harbor different mechanisms of immunosuppression

and thus contain distinct environmental factors that will affect anti-viral immunity. Therefore, our investigation of reovirus-specific CD8 T cells in two tumor models highlights the importance of studying anti-OV immunity in various tumor contexts.

After identifying the immunodominant reovirus epitope and characterizing the cognate CD8 T cells, we then sought to manipulate anti-viral immunity for OV benefit. We reasoned that targeting anti-viral immunity has several advantages over anti-tumor immunity. Anti-tumor T cells in the immunosuppressive TME are likely exhausted and dysfunctional[503,504]. In contrast, anti-viral T cells newly activated by viral infection will mount a robust immune response, which would be directed against non-self antigens and thus avoid the risk of autoimmunity; tumor antigens, on the other hand, are self antigens unless specified as neoantigens[278]. Thus, our aim was to repurpose anti-viral immunity and redirect it to attack cancer cells expressing the necessary target (i.e., virus epitope).

We first showed that cancer cells can present exogenously provided peptides via their MHC-I molecules. While the exact mechanism behind this effect is unknown (e.g., cross presentation as performed by professional antigen-presenting cells or peptide exchange where high MHC binding peptides replace low binders in MHC-I already at the cell surface)[360,505–507], we nevertheless demonstrated that the presentation of virus peptides by cancer cells leaves them vulnerable to attack by virus-specific T cells. Comparison between EL4 and MCA205 data suggests that the basal expression level of MHC-I molecules is an important factor to consider in this antigenic reprogramming. EL4 cells, which express higher basal level of MHC-I relative to MCA205 cells, exhibited higher levels of virus peptide-MHC presentation and susceptibility to anti-viral CTL-mediated cytotoxicity. It would be useful to delineate if the expression of other proteins (e.g.,

immune checkpoints) on EL4 and MCA205 cells contribute to the differences observed in cell death following the co-culture with splenocytes. Furthermore, the co-culture experimental setup employed in this study could benefit from using negatively isolated CD8 T cells instead of splenocytes to ensure that other immune cells within the splenocyte population do not have a confounding effect[508–510]. However, since we were pulsing the cancer cells with MHC-I-restricted peptides, which were removed from the supernatant before splenocytes were added, the results we observed should be unique to MHC-I-specific CD8 T cells. We also undoubtedly established that EL4 cells with reprogrammed antigenicity (i.e., expression of virus epitopes) are susceptible to anti-viral immune attack. To further enhance this effect and hopefully achieve 100% cell death, multiple virus epitopes should be utilized instead of targeting just the immunodominant epitope[511–513]. Lastly, the feasibility and efficacy of redirecting reovirus-specific T cells to target tumors should be examined *in vivo*. The therapeutic success of restimulating anti-viral memory T cell in tumors using virus epitopes has been demonstrated for Epstein-Barr virus, cytomegalovirus, and influenza[274–276,483]. This should also be possible for reovirus since it is ubiquitously found in the environment and thus almost all adults have pre-existing anti-reovirus immunity[227]. Even in the absence of anti-viral memory T cells, newly activated OV-specific T cells can still be exploited through antigenic reprogramming of the tumor MHC-I peptide repertoire. Ultimately, we believe that anti-viral immunity, generally thought to be detrimental to OV therapy, can be repurposed to target tumors and to accomplish this feat, a good understanding of the viral antigenic determinants and the cognate virus-specific T cells is necessary.

5.6 ACKNOWLEDGEMENTS
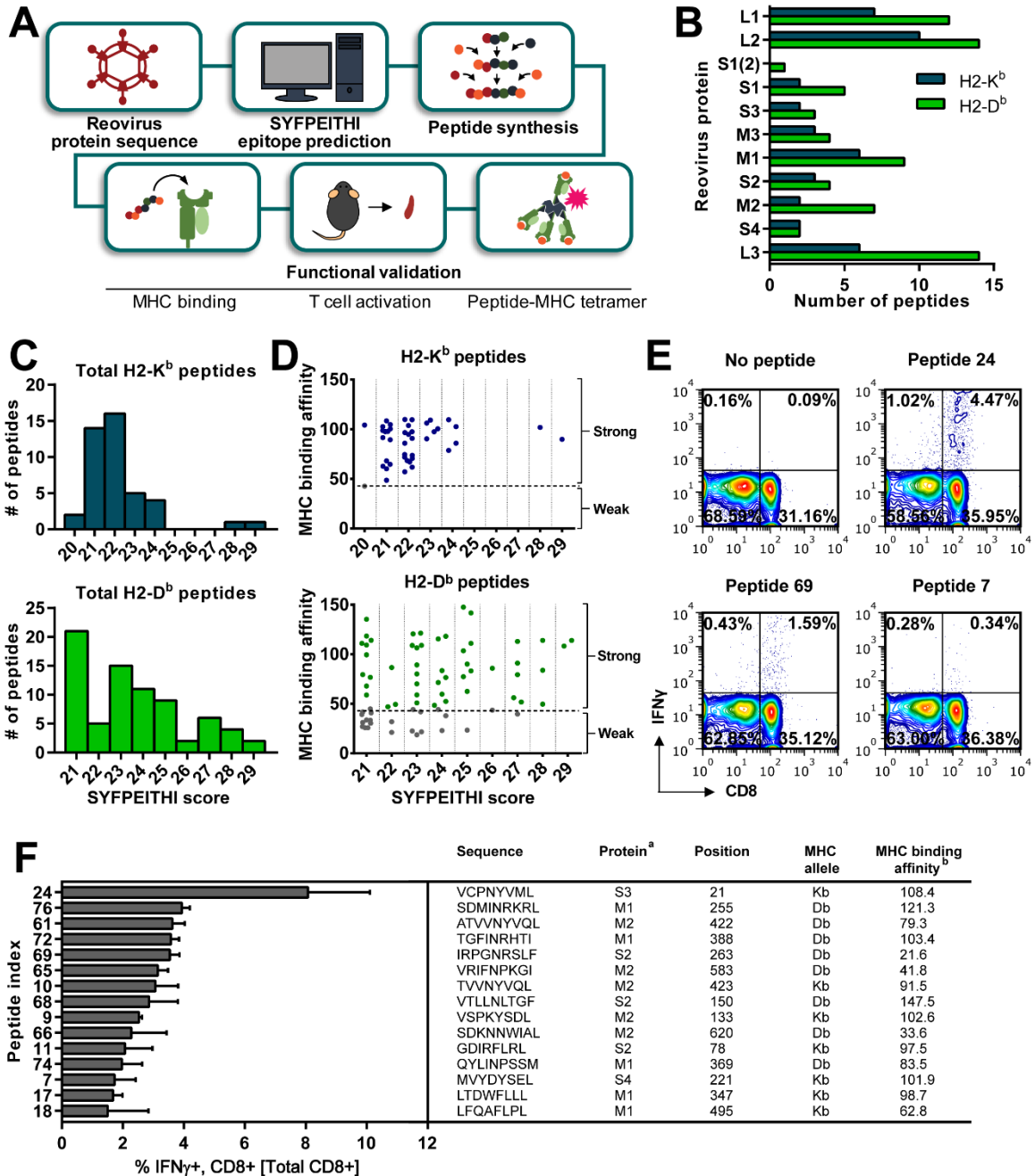
Figure 5.1. *Identification of an immunodominant H2-K^b-restricted reovirus T cell epitope.*

(A) A schematic representation of the identification and validation of reovirus-specific CD8 T cell epitopes via *in silico* prediction and T cell assays, respectively. **(B)** Reovirus peptides (43 H2-K^b- and 75 H2-D^b-specific epitopes) predicted using the SYFPEITHI

algorithm, represented across 11 reovirus proteins. **(C)** The distribution of SYFPEITHI scores of the 43 H2-K^b- and 75 H2-D^b-specific epitopes selected for validation. **(D)** MHC binding affinities of the selected epitopes determined by the ProImmune REVEAL® MHC binding assay. REVEAL scores greater than 45% were considered strong MHC binders. **(E)** Representative dot plots for IFNγ+,CD8+ T cell activation in response to *ex vivo* peptide stimulation followed by intracellular cytokine staining for flow cytometry. **(F)** Bar graph indicates the percentage of CD8 T cells that were positive for intracellular IFNγ, and the respective peptide sequence, protein structure and position, MHC allele, and MHC binding affinity are shown in the table for the top 15 immunogenic peptides. Reovirus proteins: Lambda 3 (L1), Lambda 2 (L2), Lambda 1 (L3), Mu 2 (M1), Mu 1 (M2), Mu NS (M3), Sigma 1 (S1), Sigma 1s (S1(2)), Sigma 2 (S2), Sigma NS (S3), Sigma 3 (S4)
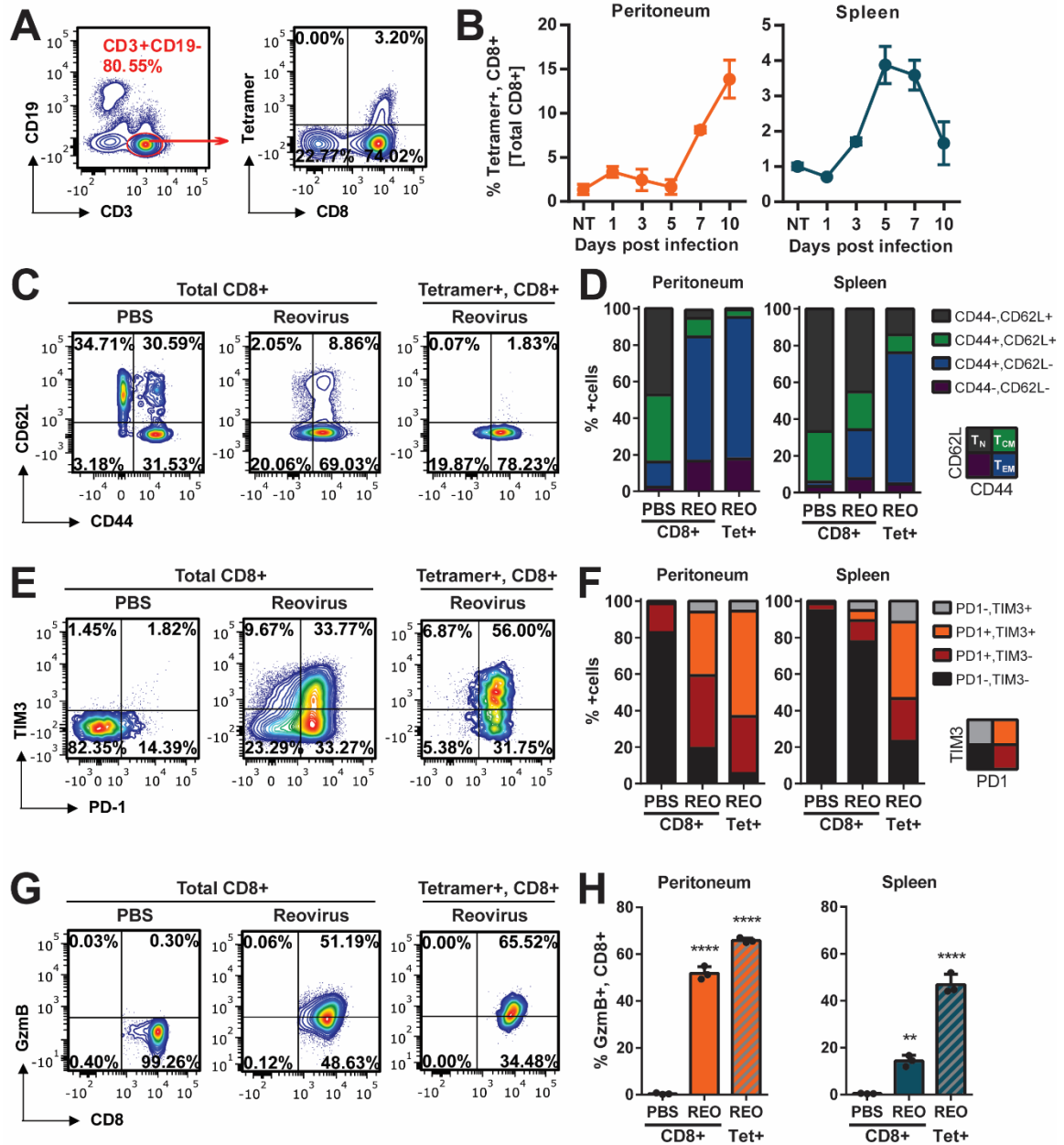
Figure 5.2. *Characterization of virus-specific CD8 T cell phenotype and function using pMHC tetramer.*

(A) Gating strategy for flow cytometric analysis of CD3+,CD19-,CD8+,Tetramer+ cells. pMHC tetramer was loaded with the immunodominant reovirus epitope $S3_{21-28}$ (peptide 24; VCPNYVML). **(B)** Temporospatial quantification of virus-specific (Tetramer+,CD8+) cells from the peritoneum and spleen of REO-infected mice during acute infection (n=2

mice at each timepoint). **(C)** Representative dot plots showing the differentiation status of CD8 and virus-specific T cells from the peritoneum of non-treated or REO-infected mice at 7 d.p.i.. **(D)** Bar graphs indicate the percentage of naïve (T_N: CD44-,CD62L+), central memory (T_{CM}: CD44+,CD62L+), effector memory (T_{EM}: CD44+,CD62L-), and CD44-,CD62L- T cell subsets within the total CD8 T cells and Tetramer+ cells of the peritoneum and spleen (n=12 mice each group). **(E)** Representative dot plots showing the immune checkpoint receptor expression of CD8 and virus-specific T cells from the peritoneum. **(F)** Bar graphs indicate the percentage of PD-1- and/or TIM3-expressing cells within the total CD8 T cells and Tetramer+ cells of the peritoneum and spleen (n=6 mice each group). **(G)** Representative dot plots showing the functional status (as indicated by GzmB expression) of CD8 and virus-specific T cells from the peritoneum. **(H)** Bar graphs indicate the percentage of GzmB+,CD8+ cells within the total CD8 and Tetramer+ cells of the peritoneum and spleen. One-way ANOVA with Bonferroni post-test was performed and p values < 0.05 were considered significant. PBS: non-treated, REO: reovirus, Tet: tetramer, GzmB: granzyme B
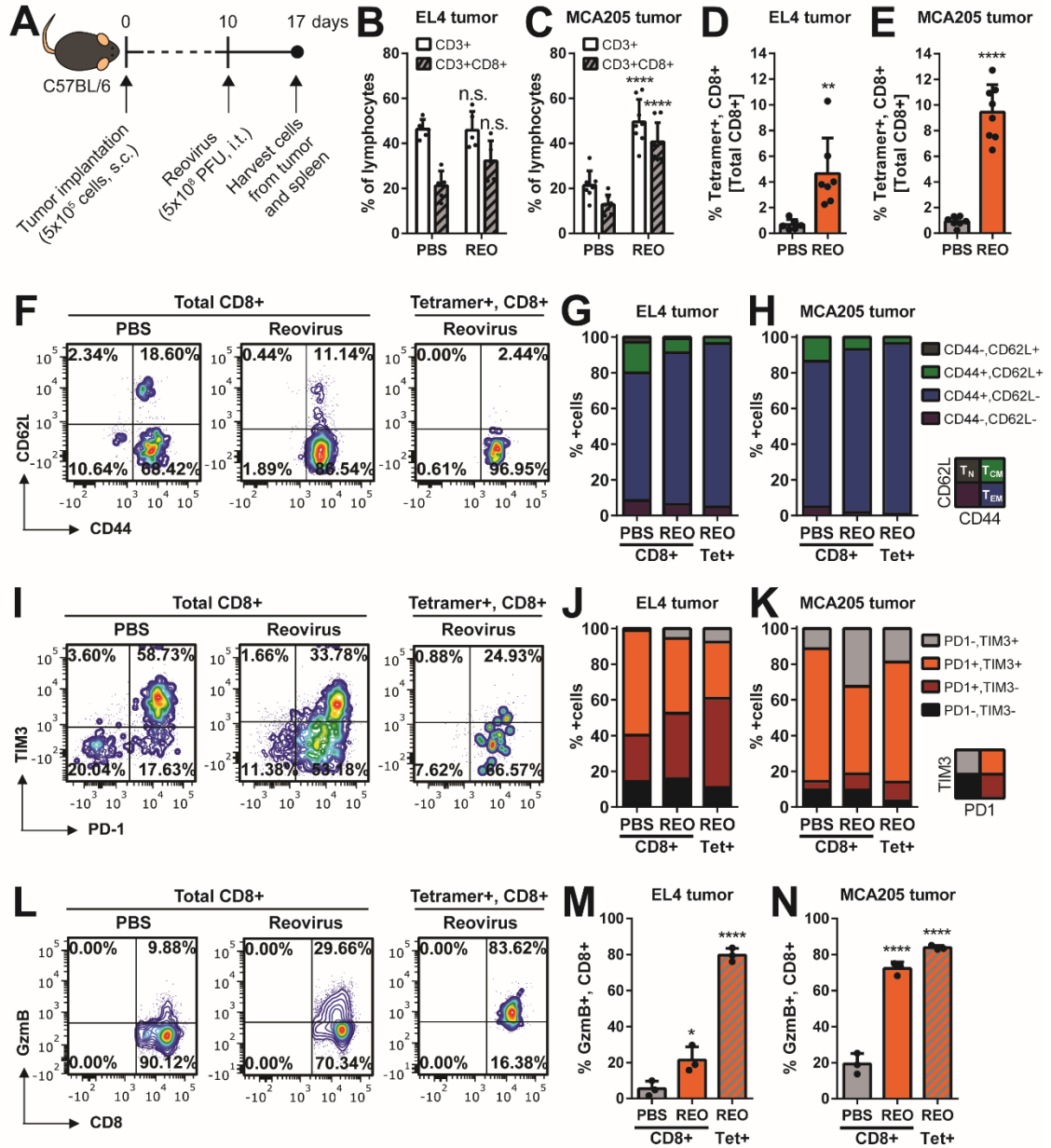
Figure 5.3. *Infiltration of the tumor microenvironment by virus-specific CD8 T cells.*

(A) A schematic diagram for establishing syngeneic tumor models with reovirus treatment.

Levels of CD3 and CD8 TILs in non-treated or REO-treated **(B)** EL4 and **(C)** MCA205

tumors. Percentage of Tetramer+,CD8+ T cells in non-treated or REO-treated **(D)** EL4 and

(E) MCA205 tumors. **(F)** Representative dot plots showing the differentiation status of

CD8 and virus-specific T cells from non-treated or REO-treated EL4 tumors. Bar graphs

indicate the percentage of naïve (T_N: CD44-,CD62L+), central memory (T_{CM}: CD44+,CD62L+), effector memory (T_{EM}: CD44+,CD62L-), and CD44-,CD62L- T cell subsets within the total CD8 T cells and Tetramer+ cells of non-treated or REO-treated **(G)** EL4 (n=5 mice each group) and **(H)** MCA205 (n=4 mice each group) tumors. **(I)** Representative dot plots showing the immune checkpoint receptor expression of CD8 and virus-specific T cells from non-treated or REO-treated EL4 tumors. Bar graphs indicate the percentage of PD-1- and/or TIM3-expressing cells within the total CD8 T cells and Tetramer+ cells of non-treated or REO-treated **(J)** EL4 (n=5 mice each group) and **(K)** MCA205 (n=7 mice each group) tumors. **(L)** Representative dot plots showing the functional status (as indicated by GzmB expression) of CD8 and virus-specific T cells from non-treated or REO-treated EL4 tumors. Bar graphs indicate the percentage of GzmB+,CD8+ cells within the total CD8 and Tetramer+ cells of non-treated or REO-treated **(M)** EL4 and **(N)** MCA205 tumors. Two-tailed Student's t test with 95% confidence interval or one-way ANOVA with Bonferroni post-test was performed, and p values < 0.05 were considered significant. s.c.: subcutaneous, i.t.: intratumoral, PFU: plaque-forming unit, PBS: non-treated, REO: reovirus, GzmB: granzyme B
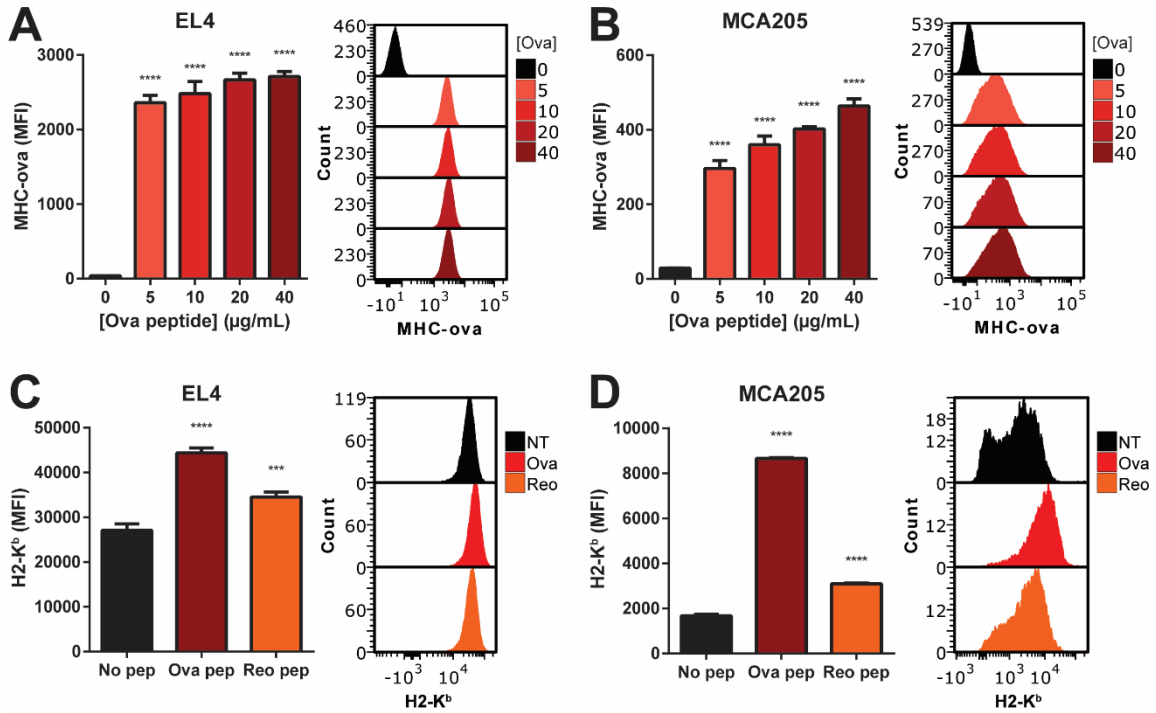
Figure 5.4. *Antigenic reprogramming of cancer cells to induce the expression of virus peptide-MHC complex in vitro.*

Exogenous peptide presentation by MHC-I molecules on **(A)** EL4 and **(B)** MCA205 cells pulsed with various concentrations of Ova peptide for 4 hours. Bar graphs show the MFI of MHC-ova expression with representative histograms displayed alongside. Presentation of exogenously provided reovirus-specific peptide by MHC-I on **(C)** EL4 and **(D)** MCA205 cells. Ova peptide-pulsing (at the same peptide concentration) was included as control. Bar graphs show the MFI of MHC-I (H2-K^b) expression with representative histograms displayed alongside. Ova: SIINFEKL peptide from ovalbumin protein, MFI: mean fluorescence intensity, NT: non-treated (No pep), Reo: immunodominant reovirus epitope (S3$_{21-28}$, peptide 24; VCPNYVML)
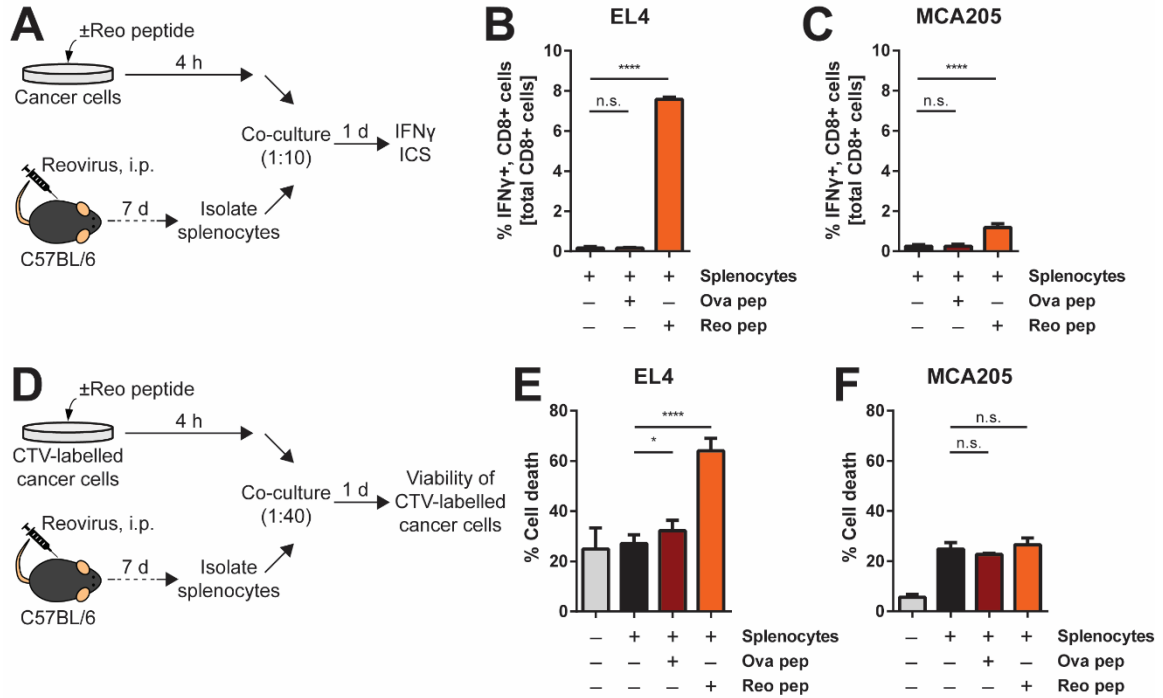
Figure 5.5. *Anti-viral CTL activity against virus peptide-presenting cancer cells.*

(A) A schematic diagram for the co-culture assay to assess the activation of cognate CD8 T cells by virus peptide-loaded cancer cells. Level of CD8 T cell activation (IFNγ response) following co-culture with virus peptide-loaded **(B)** EL4 and **(C)** MCA205 cancer cells. **(D)** A schematic diagram for the co-culture assay to assess cytotoxic immune activity against virus peptide-loaded cancer cells. Percentage of cell death in virus peptide-loaded **(E)** EL4 and **(F)** MCA205 cancer cell co-cultured with splenocytes from reovirus-treated mice. Ova: SIINFEKL peptide from ovalbumin protein, Reo: immunodominant reovirus epitope (S3$_{21-28}$, peptide 24; VCPNYVML), i.p.: intraperitoneal, h: hour, d: day, IFNγ: interferon gamma, ICS: intracellular cytokine stain, CTV: CellTrace Violet
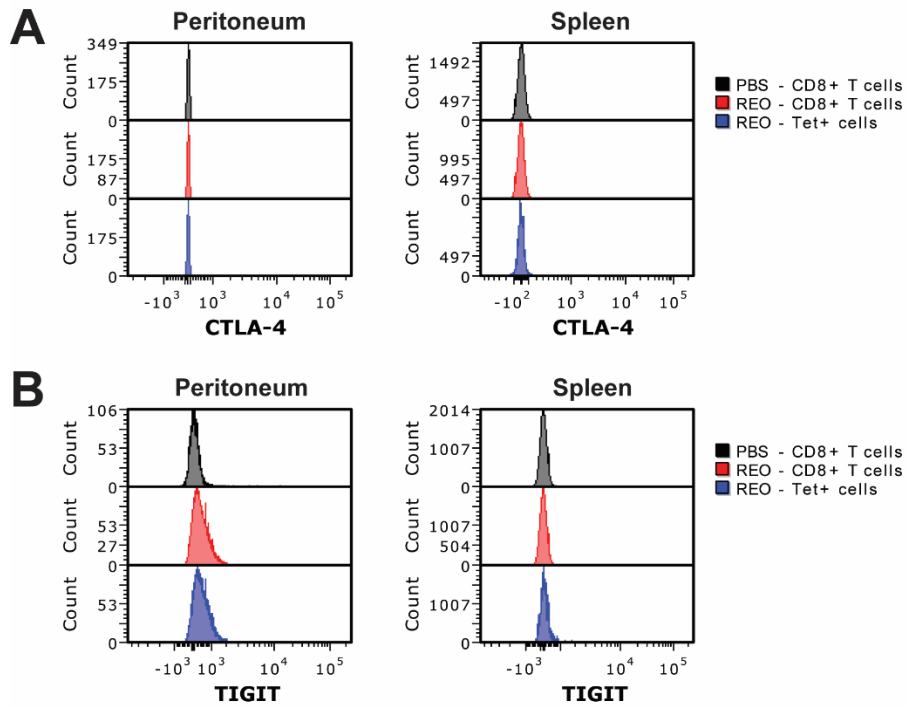
Supplementary Figure 5.1. *Lack of certain immune checkpoint receptor expression by virus-specific CD8 T cells.*

Flow cytometric analysis of total CD8 and Tetramer+ T cells in the peritoneum and spleen of non-treated (PBS) or reovirus-treated (REO) mice at 7 d.p.i. showed that these cells do not express **(A)** CTLA-4 and **(B)** TIGIT.
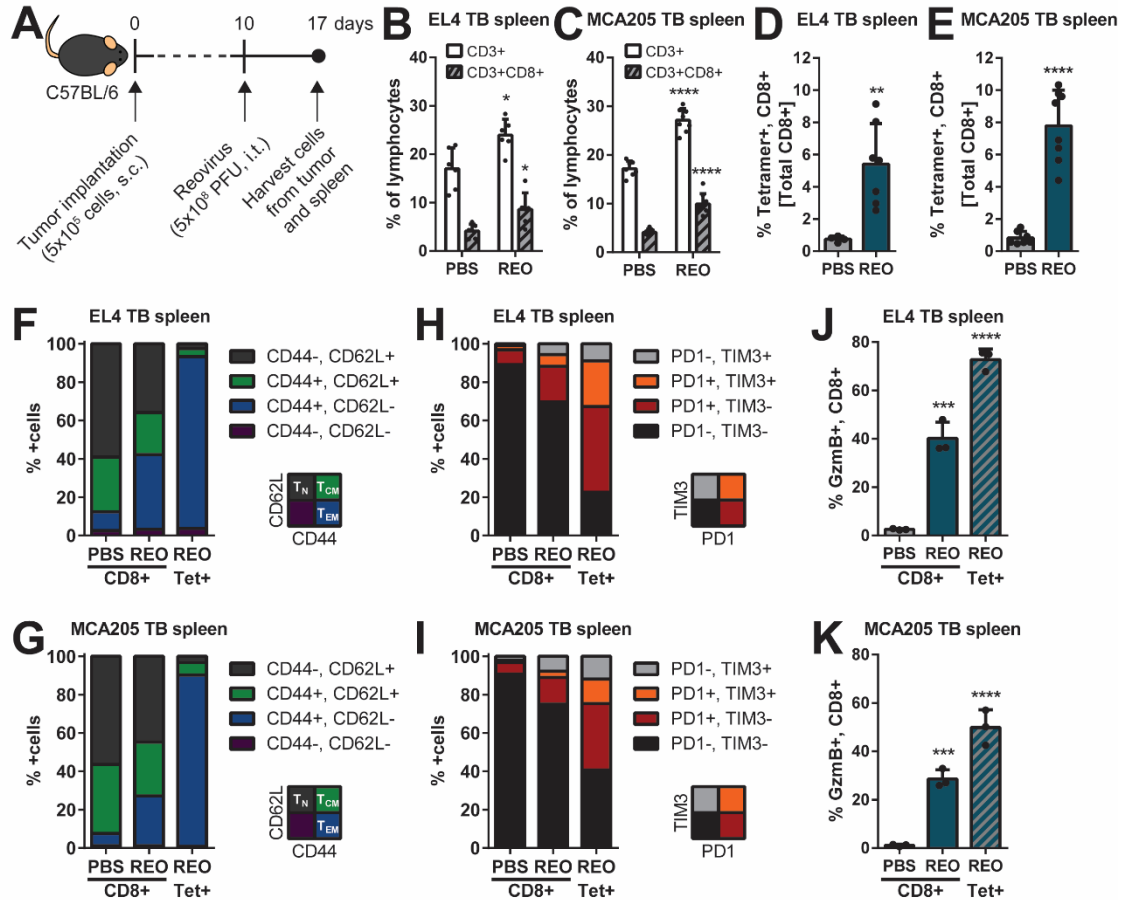
Supplementary Figure 5.2. *Characterization of virus-specific CD8 T cell phenotype and function in secondary lymphoid organs of tumor-bearing mice.*

(A) A schematic diagram for establishing syngeneic tumor models with reovirus treatment. Levels of CD3 and CD8 T cells in spleens of non-treated or REO-treated **(B)** EL4 and **(C)** MCA205 TB mice. Percentage of Tetramer+,CD8+ T cells in spleens of non-treated or REO-treated **(D)** EL4 and **(E)** MCA205 TB mice. Bar graphs indicate the percentage of naïve (T_N: CD44-,CD62L+), central memory (T_{CM}: CD44+,CD62L+), effector memory (T_{EM}: CD44+,CD62L-), and CD44-,CD62L- T cell subsets within the total CD8 T cells and Tetramer+ cells in spleens of non-treated or REO-treated **(F)** EL4 (n=5 mice each group) and **(G)** MCA205 (n=4 mice each group) TB mice. Bar graphs indicate the

160

percentage of PD-1- and/or TIM3-expressing cells within the total CD8 T cells and Tetramer+ cells in spleens of non-treated or REO-treated **(H)** EL4 (n=5 mice each group) and **(I)** MCA205 (n=7 mice each group) TB mice. Bar graphs indicate the percentage of GzmB+,CD8+ cells within the total CD8 and Tetramer+ cells in spleens of non-treated or REO-treated **(J)** EL4 and **(K)** MCA205 TB mice. Two-tailed Student's t test with 95% confidence interval or one-way ANOVA with Bonferroni post-test was performed, and p values < 0.05 were considered significant. s.c.: subcutaneous, i.t.: intratumoral, PFU: plaque-forming unit, PBS: non-treated, REO: reovirus, TB: tumor-bearing, GzmB: granzyme B
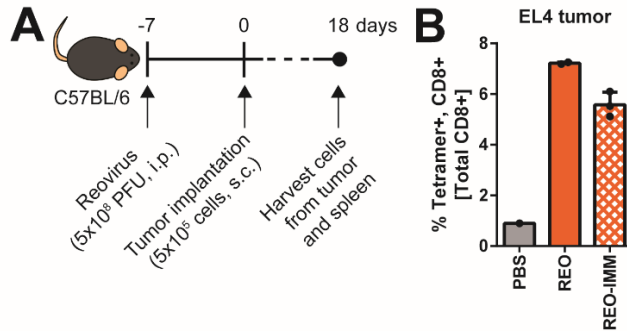
Supplementary Figure 5.3. *Presence of virus-specific memory T cells within tumors established in reovirus-immunized mice.*

(A) A schematic diagram for establishing EL4 tumors in mice previously immunized with reovirus. **(B)** Level of Tetramer+ cells in non-treated or reovirus-treated (7 d.p.i., included as control) EL4 tumors established in naïve mice, along with the level of Tetramer+ cells in non-treated EL4 tumors of REO-IMM mice (n=2 mice each group). i.p.: intraperitoneal, PFU: plaque-forming unit, s.c.: subcutaneous, PBS: non-treated, REO: reovirus, REO-IMM: reovirus-immunized

Table 5.1. *List of 118 peptides derived from reovirus proteins, as predicted by SYFPEITHI.* SYFPEITHI prediction for H2-K^b and H2-D^b MHC alleles. MHC binding affinity was determined by the ProImmune REVEAL® MHC binding assay. % IFNγ+,CD8+ was determined by intracellular cytokine staining for flow cytometry analysis (average of 3 independent experiments shown). Reovirus proteins: Lambda 3 (L1), Lambda 2 (L2), Lambda 1 (L3), Mu 2 (M1), Mu 1 (M2), Mu NS (M3), Sigma 1 (S1), Sigma 1s (S1(2)), Sigma 2 (S2), Sigma NS (S3), Sigma 3 (S4).

Peptide index	Sequence	Protein	Position	MHC allele	SYFPEITHI score	MHC binding affinity	%IFNγ+, CD8+
24	VCPNYVML	S3	21	Kb	21	108.42	8.09
76	SDMINRKRL	M1	255	Db	23	121.25	3.94
61	ATVVNYVQL	M2	422	Db	27	79.27	3.63
72	TGFINRHTI	M1	388	Db	25	103.39	3.58
69	IRPGNRSLF	S2	263	Db	23	21.58	3.55
65	VRIFNPKGI	M2	583	Db	23	41.84	3.15
10	TVVNYVQL	M2	423	Kb	21	91.48	3.08
68	VTLLNLTGF	S2	150	Db	25	147.46	2.86
9	VSPKYSDL	M2	133	Kb	24	102.57	2.53
66	SDKNNWIAL	M2	620	Db	21	33.59	2.28
11	GDIRFLRL	S2	78	Kb	22	97.50	2.08
74	QYLINPSSM	M1	369	Db	24	83.49	1.97
7	MVYDYSEL	S4	221	Kb	28	101.85	1.73
17	LTDWFLLL	M1	347	Kb	21	98.74	1.68
18	LFQAFLPL	M1	495	Kb	21	62.77	1.51
26	IADDYIHI	S1	343	Kb	20	42.67	1.43
28	LMYKYMPI	L2	1011	Kb	24	109.53	1.40
12	DCDDYPFL	S2	126	Kb	21	60.22	1.34
13	KHRVYQQL	S2	140	Kb	21	97.55	1.30
22	ICVGFDPL	M3	385	Kb	21	104.67	1.23
8	DTIKFGDL	S4	345	Kb	22	96.59	1.21
21	ADQSYFTL	M3	250	Kb	22	61.75	1.20
63	PADYNVRTL	M2	319	Db	24	22.94	1.17
100	WQIANPDKF	L2	1163	Db	23	70.02	1.11
15	KDDEYNQL	M1	114	Kb	22	57.08	1.10
4	NLWDFFIL	L3	625	Kb	21	48.61	1.07
2	NIHLFKQL	L3	331	Kb	22	73.66	1.03
1	SAVLFSPL	L3	187	Kb	23	100.41	0.99
6	PVERYNIL	L3	1228	Kb	21	64.61	0.97
16	ISDVYAPL	M1	127	Kb	22	109.75	0.94
54	RCFMNIQLI	L3	686	Db	21	76.64	0.93
92	MMQTNESSL	S1 (2)	35	Db	25	141.69	0.89
23	TGGFFSCL	S3	47	Kb	22	90.77	0.88

Table 5.1 *continued*

Peptide index	Sequence	Protein	Position	MHC allele	SYFPEITHI score	MHC binding affinity	%IFNγ+, CD8+
14	IPNEFIKL	M1	26	Kb	24	85.86	0.87
25	PNYRFRQS	S1	311	Kb	20	104.15	0.86
5	PVKAFMTL	L3	645	Kb	21	89.45	0.85
20	LSQGYTSL	M3	442	Kb	23	97.48	0.85
56	NHEYNLFGI	L3	1032	Db	21	40.74	0.82
29	RVLKYEVL	L2	91	Kb	23	106.19	0.80
70	QAHPNSTMF	S2	384	Db	22	46.91	0.79
115	EHTANNSTM	L1	690	Db	21	41.65	0.79
30	AVQLFRPL	L2	56	Kb	22	109.55	0.77
103	SSVTGIETI	L2	701	Db	21	110.93	0.76
44	TGINNANEL	L3	125	Db	28	113.88	0.76
78	HSRFNVGTF	M1	199	Db	21	30.31	0.75
19	NANYFGHL	M1	536	Kb	21	68.19	0.75
109	ASIVNDESV	L1	624	Db	27	90.95	0.74
51	MGTPNVSKI	L3	411	Db	22	86.52	0.74
52	STEYNDRSL	L3	1201	Db	22	31.86	0.73
53	PPTENNIHL	L3	326	Db	21	25.71	0.73
105	KESGNTICI	L2	1241	Db	21	79.45	0.73
98	LLIINDTMI	L2	135	Db	23	80.05	0.73
95	LQLLNTITL	L2	1214	Db	25	110.92	0.71
27	HFYRYETL	L2	677	Kb	29	89.87	0.70
102	FVTNNVELF	L2	644	Db	21	39.18	0.70
77	YWKSNPSAI	M1	86	Db	21	26.96	0.69
45	KQLLNTETL	L3	336	Db	28	83.76	0.69
47	TEGANLRSL	L3	386	Db	25	23.27	0.68
106	ICILNSQGF	L2	1247	Db	21	118.29	0.68
99	TEDVNAAMI	L2	1065	Db	23	22.44	0.66
73	SELLNANYF	M1	532	Db	25	83.16	0.65
89	SISNNRMTM	S1	178	Db	23	108.90	0.65
104	ASIRIAELM	L2	1004	Db	21	58.84	0.65
118	SALLRLRTL	L1	1126	Db	21	44.74	0.63
85	AADVNDARL	S3	351	Db	28	49.60	0.62
43	WSFVYWGL	L1	868	Kb	21	102.53	0.61
83	DLYANTQVI	M3	349	Db	21	99.38	0.61
41	LHSMYESL	L1	282	Kb	22	67.06	0.61
62	ALEFNREFL	M2	117	Db	24	48.42	0.60
49	EGGSNQKPM	L3	142	Db	23	106.38	0.57
87	LTGDNGTSL	S1	16	Db	25	62.43	0.57
57	RQYANAWNL	L3	1154	Db	21	114.08	0.57

Table 5.1 *continued*

Peptide index	Sequence	Protein	Position	MHC allele	SYFPEITHI score	MHC binding affinity	%IFNγ+, CD8+
46	TSLENLWDF	L3	621	Db	27	51.64	0.54
96	PFVTNNVEL	L2	643	Db	24	44.17	0.54
116	HTANNSTMM	L1	691	Db	21	135.30	0.54
3	DTEVFSNL	L3	911	Kb	22	74.56	0.53
108	SDLVNLAIL	L1	231	Db	27	112.88	0.53
82	DGIVNRKNV	M3	374	Db	22	49.36	0.53
81	LSTHNGVSL	M3	394	Db	23	108.87	0.52
34	LHDFYSDL	L2	27	Kb	22	70.61	0.52
58	FGDLNYPVM	S4	349	Db	24	59.69	0.52
79	AGVDSLDDL	M1	468	Db	21	33.29	0.52
55	YQQYNGRTF	L3	1001	Db	21	109.30	0.51
94	TLPTNEDLF	L2	1221	Db	26	85.73	0.51
64	LVPYNDEPL	M2	92	Db	24	76.40	0.49
42	GTAEYLKL	L1	777	Kb	22	71.89	0.49
71	KWVLNSDLI	M1	478	Db	26	43.54	0.48
101	LLATNGYQL	L2	306	Db	21	25.80	0.48
91	TLSGNNLAI	S1	193	Db	21	67.78	0.46
107	AGKVNSETI	L1	745	Db	29	113.89	0.46
86	DLAHNAAEL	S3	268	Db	23	18.63	0.46
59	SHAFNGVKL	S4	189	Db	23	44.11	0.45
112	LQDVNTVQL	L1	1164	Db	24	71.45	0.45
97	GSNANPVSL	L2	1106	Db	24	115.42	0.45
60	TRVVNLDQI	M2	365	Db	29	108.23	0.45
35	TSGVYFFL	L2	667	Kb	21	100.35	0.44
80	VTRQNFDVI	M3	154	Db	24	118.07	0.44
88	TAERNIGSL	S1	132	Db	25	90.06	0.43
48	RMNINPTEI	L3	471	Db	25	77.25	0.43
111	ETIQNDLEL	L1	751	Db	24	52.31	0.43
113	IDPLNSDPF	L1	1081	Db	23	50.87	0.42
114	GIIHNPPSL	L1	1001	Db	22	21.04	0.42
110	GYCPNLEWL	L1	292	Db	24	37.90	0.42
37	SDYKFMYM	L1	304	Kb	24	78.64	0.42
31	SNQAFYDL	L2	125	Kb	22	85.92	0.41
50	NIGNNATVI	L3	524	Db	23	120.56	0.41
93	SDGVNETPL	L2	336	Db	27	39.52	0.40
117	AAIATREEL	L1	1023	Db	21	31.12	0.39
84	LGQRNLERI	S3	69	Db	28	153.54	0.39
32	YSDTYEVL	L2	200	Kb	22	68.39	0.39
38	SLPDFKGL	L1	476	Kb	23	109.19	0.38

Table 5.1 *continued*

Peptide index	Sequence	Protein	Position	MHC allele	SYFPEITHI score	MHC binding affinity	%IFNγ+, CD8+
67	SGDVNQLLM	S2	172	Db	27	56.06	0.37
39	SYSSFSKL	L1	1045	Kb	23	90.34	0.37
33	SRLRYLPL	L2	767	Kb	22	94.77	0.37
75	IQNLNRGEI	M1	145	Db	23	89.13	0.35
90	QIVNNNLTL	S1	226	Db	23	58.94	0.35
40	RSDVYKAL	L1	39	Kb	22	103.70	0.34
36	FDAAFQQL	L2	903	Kb	21	97.82	0.31

CHAPTER 6: DISCUSSION

6.1   SUMMARY OF CENTRAL FINDINGS

A new frontier in oncology is approaching due to breakthroughs in cancer immunotherapies and with a particularly immunostimulatory therapeutic agent like oncolytic reovirus, the outcome seems promising. To fully appreciate the efficacy of OV-mediated anti-tumor immune responses, we need a better understanding of how CD8 T cell immunity is generated and maintained. MHC-I peptidomics analysis provides such knowledge since the identification of MHC-I-bound peptides means the identification of CD8 T cell targets. We can then use this information for immunological modulation of CD8 T cell responses and potentiate anti-tumor efficacy. However, despite the huge benefits to be gained, MHC-I peptidomics is not yet a widely used approach as the focus is more on whether TILs are present and functional, rather than the antigenic determinants driving TIL activity. Technological limitations have also hindered advances in the field of tumor MHC-I peptidomics.

To address the current knowledge gap, this thesis presents an elucidation of MHC-I peptides, the expression of which are driven specifically by OV therapy. That is, the amassed MHC-I peptides represent those that are OV-induced on cancer cells or OV-specific, derived from viral proteins. Cutting-edge proteomics technologies were used to discover the reovirus therapy- (*Chapter 3*) and reovirus and ICB combination therapy- (*Chapter 4*) induced changes to the tumor MHC-I peptidome. This provided an insight on how tumors change in response to immunotherapy, as well as an explanation as to how tumors are recognized by therapy-educated CD8 T cells. In addition, an immunoinformatics approach was utilized to determine the MHC-I-restricted epitopes of

reovirus that stimulate anti-viral immunity (*Chapter 5*). Epitope mapping of the whole reovirus genome combined with gold standard immunological assays resulted in the identification and characterization of an immunodominant reovirus epitope and the cognate CD8 T cell responses, respectively. All instances of MHC-I peptide discovery were followed by validation assays to assess immunogenicity. Thus, within the huge datasets of tumor and viral MHC-I peptides identified, the immunogenic epitopes associated with biologically active CD8 T cells were distinguished. We emphasized the importance of identifying immunogenic MHC-I peptides since they serve as the best candidates to study and manipulate CD8 T cell responses (e.g., prime anti-tumor immunity via peptide vaccines or repurpose anti-viral immunity).

6.2 MY CONTRIBUTIONS TO THE LITERATURE

6.2.1 *Publicly Available MHC-I Peptidome Datasets*

From four MHC-I pull-down assays and one *in silico* prediction study, we have identified the sequences of 13,672 MHC-I peptides related to oncolytic reovirus therapy. While there are some overlapping peptides between the multiple datasets, it is nonetheless an impressively high number of T cell epitopes that are unique to these studies in terms of the specific tumor models and treatment regimens including this particular OV. By making our data publicly available, we hope to contribute to the ever-expanding field of MHC-I peptidomics. It is through such scientific practice that epitope prediction and analysis tools (e.g., SYFPEITHI[405], NetMHC[408,409], Immune Epitope Database [IEDB][514]) have been developed and improved. In addition, since not all laboratories are set up to perform the arduous MHC-I peptide IPs, other researchers can take these public datasets, do additional validations, and find novel scientific directions to pursue (e.g., compare MHC-I datasets of

different tumor types and find common epitopes to develop a vaccine targeting multiple cancers). Furthermore, our unique approach of investigating therapy-modulated MHC-I ligands opened up a whole new realm of MHC-I peptidome to explore. That is, even if the MHC-I ligandome of untreated ID8 tumors had already been elucidated, the examination of MHC-I ligands of reovirus-treated ID8 tumors yielded novel epitopes due to the cellular changes that occur in response to OV infection. Also, our demonstration of augmented changes to the tumor MHC-I peptidome mediated by combination immunotherapies suggests that the variety of other combinations yet unexplored means there are still many MHC-I peptides left to be discovered. Our datasets are further strengthened by the use of *in vivo* samples in our MHC-I peptide IP analyses. As shown by the comparison of the MHC-I ligandomes of *in vitro* reovirus-infected ID8 cells and *in vivo* reovirus-treated ID8 tumors in *Chapter 3*, distinct MHC-I ligands were observed in the different contexts. Thus, we highlight the importance of studying MHC-I peptidomes in the presence of a functional immune system. Lastly, T cell epitope mapping of reovirus serotype 3 Dearing has not been previously reported so the huge undertaking of this project has produced an equally big and exclusive dataset of reovirus-specific CD8 T cell epitopes. Overall, as with most '-omics' studies, the amount of MHC-I peptidomics data generated in this work is truly vast and it is important to follow through with the necessary analyses to do the data justice.

6.2.2 *Establishment of an Optimized MHC-I Peptidome Discovery Platform*

While the methods for MHC-I immuno-affinity chromatography have existed for decades, a lot of optimizations was still necessary to establish our version of the MHC-I peptidome discovery platform. Two different techniques of MHC-I peptide IP (for the ID8 model in *Chapter 3* and the MCA205 model in *Chapter 4*) were utilized in this thesis since we

updated our protocols to keep up with the latest advances in the field. To address some of the limitations of the previous approach, we changed many parameters, such as different solid supports for anti-MHC antibody immobilization (cyanogen bromide-activated Sepharose 4B versus Protein A Sepharose 4B), detergents for cell lysis (CHAPS-based versus sodium deoxycholate-based), and separation techniques for MHC-I-eluted peptides (molecular weight cut-off filter versus reverse-phase chromatography). Moreover, one of the greatest contributions our laboratory has made to the MHC-I peptidomics field is the multiplexed analysis approach of MHC-I peptidomes. The method reported by Murphy et al.[434] for TMT-based multiplexed quantitation of MHC-I peptidome was further modified into the improved version utilized here for the MCA205 model in *Chapter 4*. As demonstrated by the analysis of REO+ICB-modulated MHC-I peptidome involving multiple treatment groups (six in total with replicates: PBS, REO, ISO, ICB, REO+ISO, REO+ICB), a multiplexed analysis was necessary and highly advantageous for accurate quantitation. The incorporation of the recently introduced TMTpro 16-plex label reagents will additionally increase the power of future MHC-I peptidome studies. Lastly, our MHC-I discovery pipeline includes a validation step, which is often omitted from other MHC-I peptidomics studies. Integration of this invaluable stage to sift out the immunogenic epitopes from thousands of MHC-I peptides is possible due to in-house expertise and infrastructure facilitating immunological testing studies. As emphasized above, knowledge of immunogenic epitopes is essential for the subsequent therapeutic manipulation of cognate CD8 T cell responses.

6.2.3   *A Paradigm Shift in the Role of Anti-OV Immunity*

Using the knowledge gained from T cell epitope mapping of reovirus, we sought to enhance anti-viral immunity during OV therapy. This paradoxical approach, along with our findings, will instigate others to also reconsider the role of anti-OV immune responses. In certain cases, anti-viral immunity is indeed detrimental to OV therapeutic efficacy and much of the research in this area has focused on selective immune inhibition. In fact, that was the original objective of this project, using reovirus peptide-loaded killer DCs[515] to selectively kill reovirus-specific T cells; but as more evidence came to light in support of anti-tumor benefits of anti-viral immunity, we took a different stance. We proposed that if anti-OV immunity cannot be avoided, then it should be repurposed. To achieve this and have virus-specific T cells target tumors, antigenic reprogramming of the tumor MHC-I peptidome was implemented and the identification of reovirus-specific epitopes was an integral part of this process. Usually, epitope mapping of viruses is done for vaccine development – immunize to generate anti-viral memory immunity and prevent future infections[400,401,490,513]. In the case of repurposing anti-viral immunity, viral peptide vaccines will be administered directly in tumors, essentially treating cancer cells with virus peptides; a knowledge of the role of virus-specific T cells will be necessary to understand the mechanism of action. The use of viral epitopes is advantageous because they stimulate T cells that are not dampened by central tolerance mechanisms and do not display exhausted/dysfunctional phenotypes in the TME, both of which are typical characteristics of anti-tumor T cells[278,503,504]. Thus, as highlighted by our studies, it is equally important to analyze the cognate, virus-specific CD8 T cells following epitope map generation. In doing so, we showed that anti-viral T cells are present in the TME and functionally

competent, thereby strengthening our reason for exploiting them to benefit oncolytic reovirus.

While the therapeutic efficacy of intratumoral reovirus peptide administration remains to be investigated, other studies have demonstrated the feasibility of repurposing virus-specific T cells of different viruses[274–276,483]. The fact that this is an active area of research gives merit to the idea of repurposing anti-viral immunity and especially in an OV context, there are tremendous benefits to be gained therewith. Exploiting anti-viral immunity will also be relatively easier than targeting anti-tumor immunity. Unlike tumor epitopes that need to be identified by MHC-I peptidome analysis of individual tumors, OV epitopes can be predicted in advance for the most common HLA haplotypes across populations and be utilized for any tumor type (i.e., HLA-restricted but not tumor type-restricted). Hence, we advocate for T cell epitope mapping of OVs, along with the necessary immunogenicity assessment and cognate T cell analysis, so that an arsenal of viral peptides is on-hand to repurpose anti-viral immunity during OV therapy.

6.3   FUTURE DIRECTIONS

6.3.1   Integration of Other '-omics' Strategies

For a more comprehensive understanding of MHC-I peptidomes, future studies should incorporate other '-omics' technologies in the experimental design. We did investigate reovirus-induced changes in the proteome when examining the ID8 MHC-I ligandome (*Chapter 3*), but there are many other '-omes' (e.g., genome, transcriptome, epigenome) that we have not explored. For the identification of tumor MHC-I peptides, it would be especially useful to also include whole exome sequencing (WES) which can identify genetic variants within the protein-coding regions of genes[516,517]. Combining WES and

MHC-I peptidomics will result in the discovery of tumor-specific antigens (i.e., neoepitopes), which are more likely to be immunogenic as immunologic tolerance would not apply to their cognate T cells[518]. Of note, the number of immunogenic neoepitopes identified through this method may be low since more selection criteria are being included. As shown by Yadav et al., MHC-I peptidomics analysis of MC38 tumors resulted in 6,239 peptides which was dwindled down to 3 immunogenic neoepitopes after incorporating WES and transcriptome sequencing analyses[519]. Nevertheless, these 3 immunogenic neoepitopes were enough to generate therapeutic T cell responses, underlining the importance of the quality, not quantity, of tumor epitopes. Moreover, single-cell analysis (e.g., single-cell RNA sequencing) is highly advantageous in studying a heterogeneous group of cells such as a tumor[520]. Coupling single-cell analysis with MHC-I peptidomics will be technically challenging but not impossible, as recently demonstrated by Demmers et al. using single-cell derived tumor organoids[521]. With our interest in examining therapy-modulated MHC-I peptidomes, taking tumor clonal diversity into consideration will provide valuable information about new CD8 T cell targets on therapy-resistant clones.

Furthermore, the analyses of anti-tumor and anti-viral T cells can benefit from TCR sequencing. Like MHC genes, polymorphisms in TCR genes exist and along with the random rearrangement of V(D)J gene segments, the resulting TCR repertoire is vast, which is important for T cell function[522–524]. Having focused our attention on elucidating the peptide-MHC complexes, we should also address the other end of the immunological synapse and characterize the corresponding TCRs to gain a greater understanding of antigen specificity. TCR profiling can also help us understand the evolution of a specific T cell pool, which can display varying TCR affinities and clonotype heterogeneity[495,500–]

[502,525]. Whether this translates to functional heterogeneity would be of interest to know for the therapeutic modulation of anti-tumor and anti-viral T cells. Overall, we should take an advantage of the many '-omics' tools available now (and currently being developed) and use a more integrative approach to delve deeper into MHC-I peptidomes and cognate immune repertoire.

6.3.2 *Preclinical to Clinical Translation*

The use of mouse models for *in vivo* analyses of tumor MHC-I peptidomes and immune responses was one of the main strengths of the studies reported here. While this was important for demonstrating proof of concept, we need to move forward and show the feasibility of the approaches in clinical settings. This can be achieved using human biological samples (e.g., tumors, PBMCs) and an anti-human pan-HLA antibody[526], which we already have in-house and have used for HLA peptidomics analysis of human cancer cell lines. Reovirus genome can also be reanalyzed for HLA-restricted epitope mapping. The study of human tumor samples and immune system may reveal novel results that would otherwise not be observed in mice because inbred strains of mice fail to capture the effects of genetic and environmental variability in humans. For example, there are contrasting reports on whether gene expression patterns in mice mimic human inflammatory diseases[527,528]; so even though mouse models have significantly advanced our understanding of the immune system, findings may not successfully translate to human immunity[529,530]. Thus, going forward, we should investigate the tumor MHC-I peptidome and immune responses using human biological samples and determine the implications of the results on anti-tumor and anti-viral immunity.

6.4 CONCLUDING REMARKS

Altogether, we elucidated the MHC-I-restricted epitopes of tumors and reovirus and characterized the cognate anti-tumor and anti-viral immune responses during oncolytic reovirus therapy. We addressed the knowledge gap on the identity of the antigenic determinants dictating these immune responses, the activity of which was well established by previous reports. We showed that the therapy-altered tumor MHC-I peptidomes contain immunogenic epitopes, explaining the mechanism of action of therapy-educated anti-tumor immunity. We also identified an immunodominant epitope of reovirus and used it to establish viral peptide-presenting cancer cells for the repurposing of anti-viral immunity. Ultimately, it was through the identification of MHC-I epitopes that the manipulation of the corresponding CD8 T cells was attainable to enhance OV efficacy.

REFERENCES

(1) Kaufman, H. L.; Kohlhapp, F. J.; Zloza, A. Oncolytic Viruses: A New Class of Immunotherapy Drugs. *Nat Rev Drug Discov* **2015**, *14* (9), 642–662. https://doi.org/10.1038/nrd4663.

(2) Kelly, E.; Russell, S. J. History of Oncolytic Viruses: Genesis to Genetic Engineering. *Mol Ther* **2007**, *15* (4), 651–659. https://doi.org/10.1038/sj.mt.6300108.

(3) Andtbacka, R. H. I.; Kaufman, H. L.; Collichio, F.; Amatruda, T.; Senzer, N.; Chesney, J.; Delman, K. A.; Spitler, L. E.; Puzanov, I.; Agarwala, S. S.; Milhem, M.; Cranmer, L.; Curti, B.; Lewis, K.; Ross, M.; Guthrie, T.; Linette, G. P.; Daniels, G. A.; Harrington, K.; Middleton, M. R.; Jr, W. H. M.; Zager, J. S.; Ye, Y.; Yao, B.; Li, A.; Doleman, S.; VanderWalde, A.; Gansert, J.; Coffin, R. S. Talimogene Laherparepvec Improves Durable Response Rate in Patients With Advanced Melanoma. *J Clin Oncol* **2015**, *33* (25), 2780–2788. https://doi.org/10.1200/JCO.2014.58.3377.

(4) Harrington, K.; Freeman, D. J.; Kelly, B.; Harper, J.; Soria, J.-C. Optimizing Oncolytic Virotherapy in Cancer Treatment. *Nat Rev Drug Discov* **2019**, *18* (9), 689–706. https://doi.org/10.1038/s41573-019-0029-0.

(5) Raja, J.; Ludwig, J. M.; Gettinger, S. N.; Schalper, K. A.; Kim, H. S. Oncolytic Virus Immunotherapy: Future Prospects for Oncology. *J Immunother Cancer* **2018**, *6* (1), 140. https://doi.org/10.1186/s40425-018-0458-z.

(6) Li, L.; Liu, S.; Han, D.; Tang, B.; Ma, J. Delivery and Biosafety of Oncolytic Virotherapy. *Front Oncol* **2020**, *10*. https://doi.org/10.3389/fonc.2020.00475.

(7) Vile, R.; Ando, D.; Kirn, D. The Oncolytic Virotherapy Treatment Platform for Cancer: Unique Biological and Biosafety Points to Consider. *Cancer Gene Ther* **2002**, *9* (12), 1062–1067. https://doi.org/10.1038/sj.cgt.7700548.

(8) Bommareddy, P. K.; Shettigar, M.; Kaufman, H. L. Integrating Oncolytic Viruses in Combination Cancer Immunotherapy. *Nat Rev Immunol* **2018**, *18* (8), 498–513. https://doi.org/10.1038/s41577-018-0014-6.

(9) Twumasi-Boateng, K.; Pettigrew, J. L.; Kwok, Y. Y. E.; Bell, J. C.; Nelson, B. H. Oncolytic Viruses as Engineering Platforms for Combination Immunotherapy. *Nat Rev Cancer* **2018**, *18* (7), 419–432. https://doi.org/10.1038/s41568-018-0009-4.

(10) Martin, N. T.; Bell, J. C. Oncolytic Virus Combination Therapy: Killing One Bird with Two Stones. *Mol Ther* **2018**, *26* (6), 1414–1422. https://doi.org/10.1016/j.ymthe.2018.04.001.

(11) Lemos de Matos, A.; Franco, L. S.; McFadden, G. Oncolytic Viruses and the Immune System: The Dynamic Duo. *Mol Ther Methods Clin Dev* **2020**, *17*, 349–358. https://doi.org/10.1016/j.omtm.2020.01.001.

(12) Lichty, B. D.; Breitbach, C. J.; Stojdl, D. F.; Bell, J. C. Going Viral with Cancer Immunotherapy. *Nat Rev Cancer* **2014**, *14* (8), 559–567. https://doi.org/10.1038/nrc3770.

(13) Vähä-Koskela, M. J. V.; Heikkilä, J. E.; Hinkkanen, A. E. Oncolytic Viruses in Cancer Therapy. *Cancer Lett* **2007**, *254* (2), 178–216. https://doi.org/10.1016/j.canlet.2007.02.002.

(14) Hu, J. C. C.; Coffin, R. S.; Davis, C. J.; Graham, N. J.; Groves, N.; Guest, P. J.; Harrington, K. J.; James, N. D.; Love, C. A.; McNeish, I.; Medley, L. C.; Michael, A.; Nutting, C. M.; Pandha, H. S.; Shorrock, C. A.; Simpson, J.; Steiner, J.; Steven, N. M.; Wright, D.; Coombes, R. C. A Phase I Study of OncoVEXGM-CSF, a Second-Generation Oncolytic Herpes Simplex Virus Expressing Granulocyte Macrophage Colony-Stimulating Factor. *Clin Cancer Res* **2006**, *12* (22), 6737–6747.

(15) Todo, T.; Feigenbaum, F.; Rabkin, S. D.; Lakeman, F.; Newsome, J. T.; Johnson, P. A.; Mitchell, E.; Belliveau, D.; Ostrove, J. M.; Martuza, R. L. Viral Shedding and Biodistribution of G207, a Multimutated, Conditionally Replicating Herpes Simplex Virus Type 1, after Intracerebral Inoculation in Aotus. *Mol Ther* **2000**, *2* (6), 588–595. https://doi.org/10.1006/mthe.2000.0200.

(16) Kimball, K. J.; Preuss, M. A.; Barnes, M. N.; Wang, M.; Siegal, G. P.; Wan, W.; Kuo, H.; Saddekni, S.; Stockard, C. R.; Grizzle, W. E.; Harris, R. D.; Aurigemma, R.; Curiel, D. T.; Alvarez, R. D. A Phase I Study of a Tropism-Modified Conditionally Replicative Adenovirus for Recurrent Malignant Gynecologic Diseases. *Clin Cancer Res* **2010**, *16* (21), 5277–5287.

(17) Angelova, A. L.; Aprahamian, M.; Balboni, G.; Delecluse, H.-J.; Feederle, R.; Kiprianova, I.; Grekova, S. P.; Galabov, A. S.; Witzens-Harig, M.; Ho, A. D.; Rommelaere, J.; Raykov, Z. Oncolytic Rat Parvovirus H-1PV, a Candidate for the Treatment of Human Lymphoma: In Vitro and In Vivo Studies. *Mol Ther* **2009**, *17* (7), 1164–1172. https://doi.org/10.1038/mt.2009.78.

(18) Taneja, S.; MacGregor, J.; Markus, S.; Ha, S.; Mohr, I. Enhanced Antitumor Efficacy of a Herpes Simplex Virus Mutant Isolated by Genetic Selection in Cancer Cells. *PNAS* **2001**, *98* (15), 8804–8808.

(19) Liu, B. L.; Robinson, M.; Han, Z.-Q.; Branston, R. H.; English, C.; Reay, P.; McGrath, Y.; Thomas, S. K.; Thornton, M.; Bullock, P.; Love, C. A.; Coffin, R. S. ICP34.5 Deleted Herpes Simplex Virus with Enhanced Oncolytic, Immune Stimulating, and Anti-Tumour Properties. *Gene Ther* **2003**, *10* (4), 292–303. https://doi.org/10.1038/sj.gt.3301885.

(20) Buller, R. M. L.; Smith, G. L.; Cremer, K.; Notkins, A. L.; Moss, B. Decreased Virulence of Recombinant Vaccinia Virus Expression Vectors Is Associated with a Thymidine Kinase-Negative Phenotype. *Nature* **1985**, *317* (6040), 813–815. https://doi.org/10.1038/317813a0.

(21) Maroun, J.; Muñoz-Alía, M.; Ammayappan, A.; Schulze, A.; Peng, K.-W.; Russell, S. Designing and Building Oncolytic Viruses. *Future Virol* **2017**, *12* (4), 193–213. https://doi.org/10.2217/fvl-2016-0129.

(22) Jung, M.-Y.; Offord, C. P.; Ennis, M. K.; Kemler, I.; Neuhauser, C.; Dingli, D. In Vivo Estimation of Oncolytic Virus Populations within Tumors. *Cancer Res* **2018**, *78* (20), 5992–6000.

(23) Liu, Y.; Cai, J.; Liu, W.; Lin, Y.; Guo, L.; Liu, X.; Qin, Z.; Xu, C.; Zhang, Y.; Su, X.; Deng, K.; Yan, G.; Liang, J. Intravenous Injection of the Oncolytic Virus M1 Awakens Antitumor T Cells and Overcomes Resistance to Checkpoint Blockade. *Cell Death Dis* **2020**, *11* (12), 1–13. https://doi.org/10.1038/s41419-020-03285-0.

(24) Samson, A.; Scott, K. J.; Taggart, D.; West, E. J.; Wilson, E.; Nuovo, G. J.; Thomson, S.; Corns, R.; Mathew, R. K.; Fuller, M. J.; Kottke, T. J.; Thompson, J. M.; Ilett, E. J.; Cockle, J. V.; van Hille, P.; Sivakumar, G.; Polson, E. S.; Turnbull, S. J.; Appleton, E. S.; Migneco, G.; Rose, A. S.; Coffey, M. C.; Beirne, D. A.; Collinson, F. J.; Ralph, C.; Alan Anthoney, D.; Twelves, C. J.; Furness, A. J.; Quezada, S. A.; Wurdak, H.; Errington-Mais, F.; Pandha, H.; Harrington, K. J.; Selby, P. J.; Vile, R. G.; Griffin, S. D.; Stead, L. F.; Short, S. C.; Melcher, A. A. Intravenous Delivery of Oncolytic Reovirus to Brain Tumor Patients Immunologically Primes for Subsequent Checkpoint Blockade. *Sci Transl Med* **2018**, *10* (422), eaam7577. https://doi.org/10.1126/scitranslmed.aam7577.

(25) Hill, C.; Carlisle, R. Achieving Systemic Delivery of Oncolytic Viruses. *Expert Opin Drug Deliv* **2019**, *16* (6), 607–620. https://doi.org/10.1080/17425247.2019.1617269.

(26) Ferguson, M. S.; Lemoine, N. R.; Wang, Y. Systemic Delivery of Oncolytic Viruses: Hopes and Hurdles. *Adv Virol* **2012**, *2012*. https://doi.org/10.1155/2012/805629.

(27) Hadac, E. M.; Kelly, E. J.; Russell, S. J. Myeloma Xenograft Destruction by a Nonviral Vector Delivering Oncolytic Infectious Nucleic Acid. *Mol Ther* **2011**, *19* (6), 1041–1047. https://doi.org/10.1038/mt.2011.68.

(28) Adair, R. A.; Roulstone, V.; Scott, K. J.; Morgan, R.; Nuovo, G. J.; Fuller, M.; Beirne, D.; West, E. J.; Jennings, V. A.; Rose, A.; Kyula, J.; Fraser, S.; Dave, R.; Anthoney, D. A.; Merrick, A.; Prestwich, R.; Aldouri, A.; Donnelly, O.; Pandha, H.; Coffey, M.; Selby, P.; Vile, R.; Toogood, G.; Harrington, K.; Melcher, A. A. Cell Carriage, Delivery, and Selective Replication of an Oncolytic Virus in Tumor in Patients. *Sci Transl Med* **2012**, *4* (138), 138ra77-138ra77. https://doi.org/10.1126/scitranslmed.3003578.

(29) Vanderplasschen, A.; Mathew, E.; Hollinshead, M.; Sim, R. B.; Smith, G. L. Extracellular Enveloped Vaccinia Virus Is Resistant to Complement Because of Incorporation of Host Complement Control Proteins into Its Envelope. *PNAS* **1998**, *95* (13), 7544–7549. https://doi.org/10.1073/pnas.95.13.7544.

(30) Ong, H. T.; Hasegawa, K.; Dietz, A. B.; Russell, S. J.; Peng, K.-W. Evaluation of T Cells as Carriers for Systemic Measles Virotherapy in the Presence of Antiviral Antibodies. *Gene Ther* **2007**, *14* (4), 324–333. https://doi.org/10.1038/sj.gt.3302880.

(31) Thorne, S. H.; Negrin, R. S.; Contag, C. H. Synergistic Antitumor Effects of Immune Cell-Viral Biotherapy. *Science* **2006**, *311* (5768), 1780–1784. https://doi.org/10.1126/science.1121411.

(32) Coukos, G.; Makrigiannakis, A.; Kang, E. H.; Caparelli, D.; Benjamin, I.; Kaiser, L. R.; Rubin, S. C.; Albelda, S. M.; Molnar-Kimber, K. L. Use of Carrier Cells to Deliver a Replication-Selective Herpes Simplex Virus-1 Mutant for the Intraperitoneal Therapy of Epithelial Ovarian Cancer. *Clin Cancer Res* **1999**, *5* (6), 1523–1537.

(33) Iankov, I. D.; Blechacz, B.; Liu, C.; Schmeckpeper, J. D.; Tarara, J. E.; Federspiel, M. J.; Caplice, N.; Russell, S. J. Infected Cell Carriers: A New Strategy for Systemic Delivery of Oncolytic Measles Viruses in Cancer Virotherapy. *Mol Ther* **2007**, *15* (1), 114–122. https://doi.org/10.1038/sj.mt.6300020.

(34) Komarova, S.; Kawakami, Y.; Stoff-Khalili, M. A.; Curiel, D. T.; Pereboeva, L. Mesenchymal Progenitor Cells as Cellular Vehicles for Delivery of Oncolytic Adenoviruses. *Mol Cancer Ther* **2006**, *5* (3), 755–766.

(35) Zheng, M.; Huang, J.; Tong, A.; Yang, H. Oncolytic Viruses for Cancer Therapy: Barriers and Recent Advances. *Mol Ther Oncolytics* **2019**, *15*, 234–247. https://doi.org/10.1016/j.omto.2019.10.007.

(36) Ganesh, S.; Gonzalez-Edick, M.; Gibbons, D.; Van Roey, M.; Jooss, K. Intratumoral Coadministration of Hyaluronidase Enzyme and Oncolytic Adenoviruses Enhances Virus Potency in Metastatic Tumor Models. *Clin Cancer Res* **2008**, *14* (12), 3933–3941. https://doi.org/10.1158/1078-0432.CCR-07-4732.

(37) McKee, T. D.; Grandi, P.; Mok, W.; Alexandrakis, G.; Insin, N.; Zimmer, J. P.; Bawendi, M. G.; Boucher, Y.; Breakefield, X. O.; Jain, R. K. Degradation of Fibrillar Collagen in a Human Melanoma Xenograft Improves the Efficacy of an Oncolytic Herpes Simplex Virus Vector. *Cancer Res* **2006**, *66* (5), 2509–2513. https://doi.org/10.1158/0008-5472.CAN-05-2242.

(38) Bilbao, R.; Bustos, M.; Alzuguren, P.; Pajares, M. J.; Drozdzik, M.; Qian, C.; Prieto, J. A Blood–Tumor Barrier Limits Gene Transfer to Experimental Liver Cancer: The Effect of Vasoactive Compounds. *Gene Ther* **2000**, *7* (21), 1824–1832. https://doi.org/10.1038/sj.gt.3301312.

(39) Guedan, S.; Rojas, J. J.; Gros, A.; Mercade, E.; Cascallo, M.; Alemany, R. Hyaluronidase Expression by an Oncolytic Adenovirus Enhances Its Intratumoral Spread and Suppresses Tumor Growth. *Mol Ther* **2010**, *18* (7), 1275–1283. https://doi.org/10.1038/mt.2010.79.

(40) Guo, Z. S.; Thorne, S. H.; Bartlett, D. L. Oncolytic Virotherapy: Molecular Targets in Tumor-Selective Replication and Carrier Cell-Mediated Delivery of Oncolytic Viruses. *Biochim Biophys Acta* **2008**, *1785* (2), 217–231. https://doi.org/10.1016/j.bbcan.2008.02.001.

(41) Jayawardena, N.; Burga, L. N.; Poirier, J. T.; Bostina, M. Virus–Receptor Interactions: Structural Insights For Oncolytic Virus Development. *Oncolytic Virother* **2019**, *8*, 39–56. https://doi.org/10.2147/OV.S218494.

(42) Finkelshtein, D.; Werman, A.; Novick, D.; Barak, S.; Rubinstein, M. LDL Receptor and Its Family Members Serve as the Cellular Receptors for Vesicular Stomatitis Virus. *PNAS* **2013**, *110* (18), 7306–7311.

(43) Sun, X.; Yau, V. K.; Briggs, B. J.; Whittaker, G. R. Role of Clathrin-Mediated Endocytosis during Vesicular Stomatitis Virus Entry into Host Cells. *Virology* **2005**, *338* (1), 53–60. https://doi.org/10.1016/j.virol.2005.05.006.

(44) Mainou, B. A. The Orchestra of Reovirus Cell Entry. *Curr Clin Microbiol Rep* **2017**, *4* (3), 142–149. https://doi.org/10.1007/s40588-017-0067-5.

(45) Kirchner, E.; Guglielmi, K. M.; Strauss, H. M.; Dermody, T. S.; Stehle, T. Structure of Reovirus Σ1 in Complex with Its Receptor Junctional Adhesion Molecule-A. *PLOS Pathog* **2008**, *4* (12), e1000235. https://doi.org/10.1371/journal.ppat.1000235.

(46) Spear, P. G. Herpes Simplex Virus: Receptors and Ligands for Cell Entry. *Cell Microbiol* **2004**, *6* (5), 401–410. https://doi.org/10.1111/j.1462-5822.2004.00389.x.

(47) Montgomery, R. I.; Warner, M. S.; Lum, B. J.; Spear, P. G. Herpes Simplex Virus-1 Entry into Cells Mediated by a Novel Member of the TNF/NGF Receptor Family. *Cell* **1996**, *87* (3), 427–436. https://doi.org/10.1016/s0092-8674(00)81363-x.

(48) Meier, O.; Greber, U. F. Adenovirus Endocytosis. *J Gene Med* **2004**, *6* (S1), S152–S163. https://doi.org/10.1002/jgm.553.

(49) Aravamudhan, P.; Raghunathan, K.; Konopka-Anstadt, J.; Pathak, A.; Sutherland, D. M.; Carter, B. D.; Dermody, T. S. Reovirus Uses Macropinocytosis-Mediated Entry and Fast Axonal Transport to Infect Neurons. *PLoS Pathog* **2020**, *16* (2), e1008380. https://doi.org/10.1371/journal.ppat.1008380.

(50) Yu, Z.; Chan, M.-K.; O-charoenrat, P.; Eisenberg, D. P.; Shah, J. P.; Singh, B.; Fong, Y.; Wong, R. J. Enhanced Nectin-1 Expression and Herpes Oncolytic Sensitivity in Highly Migratory and Invasive Carcinoma. *Clin Cancer Res* **2005**, *11* (13), 4889–4897.

(51) Malissen, N.; Macagno, N.; Granjeaud, S.; Granier, C.; Moutardier, V.; Gaudy-Marqueste, C.; Habel, N.; Mandavit, M.; Guillot, B.; Pasero, C.; Tartour, E.; Ballotti, R.; Grob, J.-J.; Olive, D. HVEM Has a Broader Expression than PD-L1 and Constitutes a Negative Prognostic Marker and Potential Treatment Target for Melanoma. *Oncoimmunology* **2019**, *8* (12), e1665976. https://doi.org/10.1080/2162402X.2019.1665976.

(52) Guo, P.; Huang, J.; Wang, L.; Jia, D.; Yang, J.; Dillon, D. A.; Zurakowski, D.; Mao, H.; Moses, M. A.; Auguste, D. T. ICAM-1 as a Molecular Target for Triple Negative Breast Cancer. *PNAS* **2014**, *111* (41), 14710–14715. https://doi.org/10.1073/pnas.1408556111.

(53) Au, G. G.; Lincz, L. F.; Enno, A.; Shafren, D. R. Oncolytic Coxsackievirus A21 as a Novel Therapy for Multiple Myeloma. *Br J Haematol* **2007**, *137* (2), 133–141. https://doi.org/10.1111/j.1365-2141.2007.06550.x.

(54) Shafren, D. R.; Au, G. G.; Nguyen, T.; Newcombe, N. G.; Haley, E. S.; Beagley, L.; Johansson, E. S.; Hersey, P.; Barry, R. D. Systemic Therapy of Malignant Human Melanoma Tumors by a Common Cold-Producing Enterovirus, Coxsackievirus A21. *Clin Cancer Res* **2004**, *10* (1), 53–60.

(55) Davola, M. E.; Mossman, K. L. Oncolytic Viruses: How "Lytic" Must They Be for Therapeutic Efficacy? *Oncoimmunology* **2019**, *8* (6). https://doi.org/10.1080/2162402X.2019.1596006.

(56) Guo, Z. S.; Liu, Z.; Kowalsky, S.; Feist, M.; Kalinski, P.; Lu, B.; Storkus, W. J.; Bartlett, D. L. Oncolytic Immunotherapy: Conceptual Evolution, Current Strategies, and Future Perspectives. *Front Immunol* **2017**, *8*. https://doi.org/10.3389/fimmu.2017.00555.

(57) Correa, A. M. S.; Howard-Varona, C.; Coy, S. R.; Buchan, A.; Sullivan, M. B.; Weitz, J. S. Revisiting the Rules of Life for Viruses of Microorganisms. *Nat Rev Microbiol* **2021**, 1–13. https://doi.org/10.1038/s41579-021-00530-x.

(58) Payne, S. Chapter 3 - Virus Interactions With the Cell. In *Viruses*; Payne, S., Ed.; Academic Press, 2017; pp 23–35. https://doi.org/10.1016/B978-0-12-803109-4.00003-9.

(59) Hanahan, D.; Weinberg, R. A. Hallmarks of Cancer: The Next Generation. *Cell* **2011**, *144* (5), 646–674. https://doi.org/10.1016/j.cell.2011.02.013.

(60) Lawler, S. E.; Speranza, M.-C.; Cho, C.-F.; Chiocca, E. A. Oncolytic Viruses in Cancer Treatment: A Review. *JAMA Oncol* **2017**, *3* (6), 841–849. https://doi.org/10.1001/jamaoncol.2016.2064.

(61) Pikor, L. A.; Bell, J. C.; Diallo, J.-S. Oncolytic Viruses: Exploiting Cancer's Deal with the Devil. *Trends Cancer* **2015**, *1* (4), 266–277. https://doi.org/10.1016/j.trecan.2015.10.004.

(62) Prior, I. A.; Hood, F. E.; Hartley, J. L. The Frequency of Ras Mutations in Cancer. *Cancer Res* **2020**, *80* (14), 2969–2974.

(63) Strong, J. E.; Coffey, M. C.; Tang, D.; Sabinin, P.; Lee, P. W. The Molecular Basis of Viral Oncolysis: Usurpation of the Ras Signaling Pathway by Reovirus. *EMBO J* **1998**, *17* (12), 3351–3362. https://doi.org/10.1093/emboj/17.12.3351.

(64) Shmulevitz, M.; Marcato, P.; Lee, P. W. K. Unshackling the Links between Reovirus Oncolysis, Ras Signaling, Translational Control and Cancer. *Oncogene* **2005**, *24* (52), 7720–7728. https://doi.org/10.1038/sj.onc.1209041.

(65) Farassati, F.; Yang, A. D.; Lee, P. W. Oncogenes in Ras Signalling Pathway Dictate Host-Cell Permissiveness to Herpes Simplex Virus 1. *Nat Cell Biol* **2001**, *3* (8), 745–750. https://doi.org/10.1038/35087061.

(66) Lorence, R. M.; Katubig, B. B.; Reichard, K. W.; Reyes, H. M.; Phuangsab, A.; Sassetti, M. D.; Walter, R. J.; Peeples, M. E. Complete Regression of Human Fibrosarcoma Xenografts after Local Newcastle Disease Virus Therapy. *Cancer Res* **1994**, *54* (23), 6017–6021.

(67) Noser, J. A.; Mael, A. A.; Sakuma, R.; Ohmine, S.; Marcato, P.; Lee, P. W.; Ikeda, Y. The RAS/Raf1/MEK/ERK Signaling Pathway Facilitates VSV-Mediated Oncolysis: Implication for the Defective Interferon Response in Cancer Cells. *Mol Ther* **2007**, *15* (8), 1531–1536. https://doi.org/10.1038/sj.mt.6300193.

(68) Schümann, M.; Dobbelstein, M. Adenovirus-Induced Extracellular Signal-Regulated Kinase Phosphorylation during the Late Phase of Infection Enhances Viral Protein Levels and Virus Progeny. *Cancer Res* **2006**, *66* (3), 1282–1288.

(69) Marcato, P.; Shmulevitz, M.; Pan, D.; Stoltz, D.; Lee, P. W. Ras Transformation Mediates Reovirus Oncolysis by Enhancing Virus Uncoating, Particle Infectivity, and Apoptosis-Dependent Release. *Mol Ther* **2007**, *15* (8), 1522–1530. https://doi.org/10.1038/sj.mt.6300179.

(70) Battcock, S. M.; Collier, T. W.; Zu, D.; Hirasawa, K. Negative Regulation of the Alpha Interferon-Induced Antiviral Response by the Ras/Raf/MEK Pathway. *J Virol* **2006**, *80* (9), 4422–4430. https://doi.org/10.1128/JVI.80.9.4422-4430.2006.

(71) Christian, S. L.; Collier, T. W.; Zu, D.; Licursi, M.; Hough, C. M.; Hirasawa, K. Activated Ras/MEK Inhibits the Antiviral Response of Alpha Interferon by Reducing STAT2 Levels. *J Virol* **2009**, *83* (13), 6717–6726. https://doi.org/10.1128/JVI.02213-08.

(72) Shmulevitz, M.; Pan, L.-Z.; Garant, K.; Pan, D.; Lee, P. W. K. Oncogenic Ras Promotes Reovirus Spread by Suppressing IFN-β Production through Negative Regulation of RIG-I Signaling. *Cancer Res* **2010**, *70* (12), 4912–4921.

(73) Sidky, Y. A.; Borden, E. C. Inhibition of Angiogenesis by Interferons: Effects on Tumor- and Lymphocyte-Induced Vascular Responses. *Cancer Res* **1987**, *47* (19), 5155–5161.

(74) Kotredes, K. P.; Gamero, A. M. Interferons as Inducers of Apoptosis in Malignant Cells. *J Interferon Cytokine Res* **2013**, *33* (4), 162–170. https://doi.org/10.1089/jir.2012.0110.

(75) Hervas-Stubbs, S.; Perez-Gracia, J. L.; Rouzaut, A.; Sanmamed, M. F.; Le Bon, A.; Melero, I. Direct Effects of Type I Interferons on Cells of the Immune System. *Clin Cancer Res* **2011**, *17* (9), 2619–2627. https://doi.org/10.1158/1078-0432.CCR-10-1114.

(76) Ilkow, C. S.; Swift, S. L.; Bell, J. C.; Diallo, J.-S. From Scourge to Cure: Tumour-Selective Viral Pathogenesis as a New Strategy against Cancer. *PLoS Pathog* **2014**, *10* (1). https://doi.org/10.1371/journal.ppat.1003836.

(77) Guo, Z. S.; Liu, Z.; Bartlett, D. L. Oncolytic Immunotherapy: Dying the Right Way Is a Key to Eliciting Potent Antitumor Immunity. *Front Oncol* **2014**, *4*. https://doi.org/10.3389/fonc.2014.00074.

(78) Galluzzi, L.; Vitale, I.; Aaronson, S. A.; Abrams, J. M.; Adam, D.; Agostinis, P.; Alnemri, E. S.; Altucci, L.; Amelio, I.; Andrews, D. W.; Annicchiarico-Petruzzelli, M.; Antonov, A. V.; Arama, E.; Baehrecke, E. H.; Barlev, N. A.; Bazan, N. G.; Bernassola, F.; Bertrand, M. J. M.; Bianchi, K.; Blagosklonny, M. V.; Blomgren, K.; Borner, C.; Boya, P.; Brenner, C.; Campanella, M.; Candi, E.; Carmona-Gutierrez, D.; Cecconi, F.; Chan, F. K.-M.; Chandel, N. S.; Cheng, E. H.; Chipuk, J. E.; Cidlowski, J. A.; Ciechanover, A.; Cohen, G. M.; Conrad, M.; Cubillos-Ruiz, J. R.; Czabotar, P. E.; D'Angiolella, V.; Dawson, T. M.; Dawson, V. L.; De Laurenzi, V.; De Maria, R.; Debatin, K.-M.; DeBerardinis, R. J.; Deshmukh, M.; Di Daniele, N.; Di Virgilio, F.; Dixit, V. M.; Dixon, S. J.; Duckett, C. S.; Dynlacht, B. D.; El-Deiry, W. S.; Elrod, J. W.; Fimia, G. M.; Fulda, S.; García-Sáez, A. J.; Garg, A. D.; Garrido, C.; Gavathiotis, E.; Golstein, P.; Gottlieb, E.; Green, D. R.; Greene, L. A.; Gronemeyer, H.; Gross, A.; Hajnoczky, G.; Hardwick, J. M.; Harris, I. S.; Hengartner, M. O.; Hetz, C.; Ichijo, H.; Jäättelä, M.; Joseph, B.; Jost, P. J.; Juin, P. P.; Kaiser, W. J.; Karin, M.; Kaufmann, T.; Kepp, O.; Kimchi, A.; Kitsis, R. N.; Klionsky, D. J.; Knight, R. A.; Kumar, S.; Lee, S. W.; Lemasters, J. J.; Levine, B.; Linkermann, A.; Lipton, S. A.; Lockshin, R. A.; López-Otín, C.; Lowe, S. W.; Luedde, T.; Lugli, E.; MacFarlane, M.; Madeo, F.; Malewicz, M.; Malorni, W.; Manic, G.; Marine, J.-C.; Martin, S. J.; Martinou, J.-C.; Medema, J. P.; Mehlen, P.; Meier, P.; Melino, S.; Miao, E. A.; Molkentin, J. D.; Moll, U. M.; Muñoz-Pinedo, C.; Nagata, S.; Nuñez, G.; Oberst, A.; Oren, M.; Overholtzer, M.; Pagano, M.; Panaretakis, T.; Pasparakis, M.; Penninger, J. M.; Pereira, D. M.; Pervaiz, S.; Peter, M. E.; Piacentini, M.; Pinton, P.; Prehn, J. H. M.; Puthalakath, H.; Rabinovich, G. A.; Rehm, M.; Rizzuto, R.; Rodrigues, C. M. P.; Rubinsztein, D. C.; Rudel, T.; Ryan, K. M.; Sayan, E.; Scorrano, L.; Shao, F.; Shi, Y.; Silke, J.; Simon, H.-U.; Sistigu, A.; Stockwell, B. R.; Strasser, A.; Szabadkai, G.; Tait, S. W. G.; Tang, D.; Tavernarakis, N.; Thorburn, A.;

Tsujimoto, Y.; Turk, B.; Vanden Berghe, T.; Vandenabeele, P.; Vander Heiden, M. G.; Villunger, A.; Virgin, H. W.; Vousden, K. H.; Vucic, D.; Wagner, E. F.; Walczak, H.; Wallach, D.; Wang, Y.; Wells, J. A.; Wood, W.; Yuan, J.; Zakeri, Z.; Zhivotovsky, B.; Zitvogel, L.; Melino, G.; Kroemer, G. Molecular Mechanisms of Cell Death: Recommendations of the Nomenclature Committee on Cell Death 2018. *Cell Death Differ* **2018**, *25* (3), 486–541. https://doi.org/10.1038/s41418-017-0012-4.

(79) Ito, H.; Aoki, H.; Kühnel, F.; Kondo, Y.; Kubicka, S.; Wirth, T.; Iwado, E.; Iwamaru, A.; Fujiwara, K.; Hess, K. R.; Lang, F. F.; Sawaya, R.; Kondo, S. Autophagic Cell Death of Malignant Glioma Cells Induced by a Conditionally Replicating Adenovirus. *J Natl Cancer Inst* **2006**, *98* (9), 625–636. https://doi.org/10.1093/jnci/djj161.

(80) Colunga, A. G.; Laing, J. M.; Aurelian, L. The HSV-2 Mutant ΔPK Induces Melanoma Oncolysis through Nonredundant Death Programs and Associated with Autophagy and Pyroptosis Proteins. *Gene Ther* **2010**, *17* (3), 315–327. https://doi.org/10.1038/gt.2009.126.

(81) Meng, C.; Zhou, Z.; Jiang, K.; Yu, S.; Jia, L.; Wu, Y.; Liu, Y.; Meng, S.; Ding, C. Newcastle Disease Virus Triggers Autophagy in U251 Glioma Cells to Enhance Virus Replication. *Arch Virol* **2012**, *157* (6), 1011–1018. https://doi.org/10.1007/s00705-012-1270-6.

(82) Thirukkumaran, C. M.; Shi, Z. Q.; Luider, J.; Kopciuk, K.; Gao, H.; Bahlis, N.; Neri, P.; Pho, M.; Stewart, D.; Mansoor, A.; Morris, D. G. Reovirus Modulates Autophagy during Oncolysis of Multiple Myeloma. *Autophagy* **2013**, *9* (3), 413–414. https://doi.org/10.4161/auto.22867.

(83) Lowe, S. W.; Ruley, H. E. Stabilization of the P53 Tumor Suppressor Is Induced by Adenovirus 5 E1A and Accompanies Apoptosis. *Genes Dev* **1993**, *7* (4), 535–545. https://doi.org/10.1101/gad.7.4.535.

(84) Kochneva, G.; Zonov, E.; Grazhdantseva, A.; Yunusova, A.; Sibolobova, G.; Popov, E.; Taranov, O.; Netesov, S.; Chumakov, P.; Ryabchikova, E. Apoptin Enhances the Oncolytic Properties of Vaccinia Virus and Modifies Mechanisms of Tumor Regression. *Oncotarget* **2014**, *5* (22), 11269–11282. https://doi.org/10.18632/oncotarget.2579.

(85) Wang, Z.; Yu, B.; Wang, B.; Yan, J.; Feng, X.; Wang, Z.; Wang, L.; Zhang, H.; Wu, H.; Wu, J.; Kong, W.; Yu, X. A Novel Capsid-Modified Oncolytic Recombinant Adenovirus Type 5 for Tumor-Targeting Gene Therapy by Intravenous Route. *Oncotarget* **2016**, *7* (30), 47287–47301. https://doi.org/10.18632/oncotarget.10075.

(86) Angarita, F. A.; Acuna, S. A.; Ottolino-Perry, K.; Zerhouni, S.; McCart, J. A. Mounting a Strategic Offense: Fighting Tumor Vasculature with Oncolytic Viruses. *Trends Mol Med* **2013**, *19* (6), 378–392. https://doi.org/10.1016/j.molmed.2013.02.008.

(87) Bartlett, D. L.; Liu, Z.; Sathaiah, M.; Ravindranathan, R.; Guo, Z.; He, Y.; Guo, Z. S. Oncolytic Viruses as Therapeutic Cancer Vaccines. *Mol Cancer* **2013**, *12* (1), 103. https://doi.org/10.1186/1476-4598-12-103.

(88) Breitbach, C. J.; De Silva, N. S.; Falls, T. J.; Aladl, U.; Evgin, L.; Paterson, J.; Sun, Y. Y.; Roy, D. G.; Rintoul, J. L.; Daneshmand, M.; Parato, K.; Stanford, M. M.; Lichty, B. D.; Fenster, A.; Kirn, D.; Atkins, H.; Bell, J. C. Targeting Tumor Vasculature With an Oncolytic Virus. *Mol Ther* **2011**, *19* (5), 886–894. https://doi.org/10.1038/mt.2011.26.

(89) Breitbach, C. J.; Arulanandam, R.; De Silva, N.; Thorne, S. H.; Patt, R.; Daneshmand, M.; Moon, A.; Ilkow, C.; Burke, J.; Hwang, T.-H.; Heo, J.; Cho, M.; Chen, H.; Angarita, F. A.; Addison, C.; McCart, J. A.; Bell, J. C.; Kirn, D. H. Oncolytic Vaccinia Virus Disrupts Tumor-Associated Vasculature in Humans. *Cancer Res* **2013**, *73* (4), 1265–1275. https://doi.org/10.1158/0008-5472.CAN-12-2687.

(90) Breitbach, C. J.; Paterson, J. M.; Lemay, C. G.; Falls, T. J.; McGuire, A.; Parato, K. A.; Stojdl, D. F.; Daneshmand, M.; Speth, K.; Kirn, D.; McCart, J. A.; Atkins, H.; Bell, J. C. Targeted Inflammation During Oncolytic Virus Therapy Severely Compromises Tumor Blood Flow. *Mol Ther* **2007**, *15* (9), 1686–1693. https://doi.org/10.1038/sj.mt.6300215.

(91) Fu, X.; Tao, L.; Xu, H.; Zhang, X. Virotherapy Induces Massive Infiltration of Neutrophils in a Subset of Tumors Defined by a Strong Endogenous Interferon Response Activity. *Cancer Gene Ther* **2011**, *18* (11), 785–794. https://doi.org/10.1038/cgt.2011.46.

(92) Massberg, S.; Grahl, L.; von Bruehl, M.-L.; Manukyan, D.; Pfeiler, S.; Goosmann, C.; Brinkmann, V.; Lorenz, M.; Bidzhekov, K.; Khandagale, A. B.; Konrad, I.; Kennerknecht, E.; Reges, K.; Holdenrieder, S.; Braun, S.; Reinhardt, C.; Spannagl, M.; Preissner, K. T.; Engelmann, B. Reciprocal Coupling of Coagulation and Innate Immunity via Neutrophil Serine Proteases. *Nat Med* **2010**, *16* (8), 887–896. https://doi.org/10.1038/nm.2184.

(93) Saito, Y.; Sunamura, M.; Motoi, F.; Abe, H.; Egawa, S.; Duda, D. G.; Hoshida, T.; Fukuyama, S.; Hamada, H.; Matsuno, S. Oncolytic Replication-Competent Adenovirus Suppresses Tumor Angiogenesis through Preserved E1A Region. *Cancer Gene Ther* **2006**, *13* (3), 242–252. https://doi.org/10.1038/sj.cgt.7700902.

(94) Kuo, C. J.; Farnebo, F.; Yu, E. Y.; Christofferson, R.; Swearingen, R. A.; Carter, R.; von Recum, H. A.; Yuan, J.; Kamihara, J.; Flynn, E.; D'Amato, R.; Folkman, J.; Mulligan, R. C. Comparative Evaluation of the Antitumor Activity of Antiangiogenic Proteins Delivered by Gene Transfer. *PNAS* **2001**, *98* (8), 4605–4610.

(95) Guse, K.; Sloniecka, M.; Diaconu, I.; Ottolino-Perry, K.; Tang, N.; Ng, C.; Le Boeuf, F.; Bell, J. C.; McCart, J. A.; Ristimäki, A.; Pesonen, S.; Cerullo, V.; Hemminki, A. Antiangiogenic Arming of an Oncolytic Vaccinia Virus Enhances Antitumor Efficacy in Renal Cell Cancer Models. *J Virol* **2010**, *84* (2), 856–866. https://doi.org/10.1128/JVI.00692-09.

(96) Yoo, J. Y.; Kim, J.-H.; Kim, J.; Huang, J.-H.; Zhang, S. N.; Kang, Y.-A.; Kim, H.; Yun, C.-O. Short Hairpin RNA-Expressing Oncolytic Adenovirus-Mediated Inhibition of IL-8: Effects on Antiangiogenesis and Tumor Growth Inhibition. *Gene Ther* **2008**, *15* (9), 635–651. https://doi.org/10.1038/gt.2008.3.

(97) Zhang, G.; Jin, G.; Nie, X.; Mi, R.; Zhu, G.; Jia, W.; Liu, F. Enhanced Antitumor Efficacy of an Oncolytic Herpes Simplex Virus Expressing an Endostatin–Angiostatin Fusion Gene in Human Glioblastoma Stem Cell Xenografts. *PLOS ONE* **2014**, *9* (4), e95872. https://doi.org/10.1371/journal.pone.0095872.

(98) Yoo, J. Y.; Pradarelli, J.; Haseley, A.; Wojton, J.; Kaka, A.; Bratasz, A.; Alvarez-Breckenridge, C. A.; Yu, J.-G.; Powell, K.; Mazar, A. P.; Teknos, T. N.; Chiocca, E. A.; Glorioso, J. C.; Old, M.; Kaur, B. Copper Chelation Enhances Antitumor Efficacy and Systemic Delivery of Oncolytic HSV. *Clin Cancer Res* **2012**, *18* (18), 4931–4941. https://doi.org/10.1158/1078-0432.CCR-12-0697.

(99) Kottke, T.; Hall, G.; Pulido, J.; Diaz, R. M.; Thompson, J.; Chong, H.; Selby, P.; Coffey, M.; Pandha, H.; Chester, J.; Melcher, A.; Harrington, K.; Vile, R. Antiangiogenic Cancer Therapy Combined with Oncolytic Virotherapy Leads to Regression of Established Tumors in Mice. *J Clin Invest* **2010**, *120* (5), 1551–1560. https://doi.org/10.1172/JCI41431.

(100) Arulanandam, R.; Batenchuk, C.; Angarita, F. A.; Ottolino-Perry, K.; Cousineau, S.; Mottashed, A.; Burgess, E.; Falls, T. J.; De Silva, N.; Tsang, J.; Howe, G. A.; Bourgeois-Daigneault, M.-C.; Conrad, D. P.; Daneshmand, M.; Breitbach, C. J.; Kirn, D. H.; Raptis, L.; Sad, S.; Atkins, H.; Huh, M. S.; Diallo, J.-S.; Lichty, B. D.; Ilkow, C. S.; Le Boeuf, F.; Addison, C. L.; McCart, J. A.; Bell, J. C. VEGF-Mediated Induction of PRD1-BF1/Blimp1 Expression Sensitizes Tumor Vasculature to Oncolytic Virus Infection. *Cancer Cell* **2015**, *28* (2), 210–224. https://doi.org/10.1016/j.ccell.2015.06.009.

(101) Schreiber, R. D.; Old, L. J.; Smyth, M. J. Cancer Immunoediting: Integrating Immunity's Roles in Cancer Suppression and Promotion. *Science* **2011**, *331* (6024), 1565–1570. https://doi.org/10.1126/science.1203486.

(102) Binnewies, M.; Roberts, E. W.; Kersten, K.; Chan, V.; Fearon, D. F.; Merad, M.; Coussens, L. M.; Gabrilovich, D. I.; Ostrand-Rosenberg, S.; Hedrick, C. C.; Vonderheide, R. H.; Pittet, M. J.; Jain, R. K.; Zou, W.; Howcroft, T. K.; Woodhouse, E. C.; Weinberg, R. A.; Krummel, M. F. Understanding the Tumor Immune Microenvironment (TIME) for Effective Therapy. *Nat Med* **2018**, *24* (5), 541–550. https://doi.org/10.1038/s41591-018-0014-x.

(103) Murciano-Goroff, Y. R.; Warner, A. B.; Wolchok, J. D. The Future of Cancer Immunotherapy: Microenvironment-Targeting Combinations. *Cell Res* **2020**, *30* (6), 507–519. https://doi.org/10.1038/s41422-020-0337-2.

(104) Nakamura, K.; Smyth, M. J. Myeloid Immunosuppression and Immune Checkpoints in the Tumor Microenvironment. *Cell Mol Immunol* **2020**, *17* (1), 1–12. https://doi.org/10.1038/s41423-019-0306-1.

(105) Labani-Motlagh, A.; Ashja-Mahdavi, M.; Loskog, A. The Tumor Microenvironment: A Milieu Hindering and Obstructing Antitumor Immune Responses. *Front Immunol* **2020**, *11*. https://doi.org/10.3389/fimmu.2020.00940.

(106) Gujar, S.; Pol, J. G.; Kroemer, G. Heating It up: Oncolytic Viruses Make Tumors 'Hot' and Suitable for Checkpoint Blockade Immunotherapies. *OncoImmunology* **2018**, e1442169. https://doi.org/10.1080/2162402X.2018.1442169.

(107) Zhang, Y.; Li, Y.; Chen, K.; Qian, L.; Wang, P. Oncolytic Virotherapy Reverses the Immunosuppressive Tumor Microenvironment and Its Potential in Combination with Immunotherapy. *Cancer Cell Int* **2021**, *21* (1), 262. https://doi.org/10.1186/s12935-021-01972-2.

(108) Paludan, S. R.; Pradeu, T.; Masters, S. L.; Mogensen, T. H. Constitutive Immune Mechanisms: Mediators of Host Defence and Immune Regulation. *Nat Rev Immunol* **2021**, *21* (3), 137–150. https://doi.org/10.1038/s41577-020-0391-5.

(109) Charles A Janeway, J.; Travers, P.; Walport, M.; Shlomchik, M. J. Principles of Innate and Adaptive Immunity. *Immunobiology: The Immune System in Health and Disease. 5th edition* **2001**.

(110) Gujar, S.; Pol, J. G.; Kim, Y.; Lee, P. W.; Kroemer, G. Antitumor Benefits of Antiviral Immunity: An Underappreciated Aspect of Oncolytic Virotherapies. *Trends Immunol* **2018**, *39* (3), 209–221. https://doi.org/10.1016/j.it.2017.11.006.

(111) Marelli, G.; Howells, A.; Lemoine, N. R.; Wang, Y. Oncolytic Viral Therapy and the Immune System: A Double-Edged Sword Against Cancer. *Front Immunol* **2018**, *9*. https://doi.org/10.3389/fimmu.2018.00866.

(112) Akira, S.; Uematsu, S.; Takeuchi, O. Pathogen Recognition and Innate Immunity. *Cell* **2006**, *124* (4), 783–801. https://doi.org/10.1016/j.cell.2006.02.015.

(113) Rommelaere, J.; Bhat, R. Emerging Role of Natural Killer Cells in Oncolytic Virotherapy. *ITT* **2015**, 65. https://doi.org/10.2147/ITT.S55549.

(114) Annels, N. E.; Simpson, G. R.; Denyer, M.; Arif, M.; Coffey, M.; Melcher, A.; Harrington, K.; Vile, R.; Pandha, H. Oncolytic Reovirus-Mediated Recruitment of Early Innate Immune Responses Reverses Immunotherapy Resistance in Prostate Tumors. *Mol Ther Oncolytics* **2021**, *20*, 434–446. https://doi.org/10.1016/j.omto.2020.09.010.

(115) Miyamoto, S.; Inoue, H.; Nakamura, T.; Yamada, M.; Sakamoto, C.; Urata, Y.; Okazaki, T.; Marumoto, T.; Takahashi, A.; Takayama, K.; Nakanishi, Y.; Shimizu, H.; Tani, K. Coxsackievirus B3 Is an Oncolytic Virus with Immunostimulatory Properties That Is Active against Lung Adenocarcinoma. *Cancer Res* **2012**, *72* (10), 2609–2621.

(116) Allen, C.; Vongpunsawad, S.; Nakamura, T.; James, C. D.; Schroeder, M.; Cattaneo, R.; Giannini, C.; Krempski, J.; Peng, K.-W.; Goble, J. M.; Uhm, J. H.; Russell, S. J.; Galanis, E. Retargeted Oncolytic Measles Strains Entering via the EGFRvIII Receptor Maintain Significant Antitumor Activity against Gliomas with Increased Tumor Specificity. *Cancer Res* **2006**, *66* (24), 11840–11850. https://doi.org/10.1158/0008-5472.CAN-06-1200.

(117) Zorn, U.; Dallmann, I.; Grosse, J.; Kirchner, H.; Poliwoda, H.; Atzpodien, J. Induction of Cytokines and Cytotoxicity against Tumor Cells by Newcastle Disease Virus. *Cancer Biother* **1994**, *9* (3), 225–235. https://doi.org/10.1089/cbr.1994.9.225.

(118) Bhat, R.; Rommelaere, J. NK-Cell-Dependent Killing of Colon Carcinoma Cells Is Mediated by Natural Cytotoxicity Receptors (NCRs) and Stimulated by Parvovirus Infection of Target Cells. *BMC Cancer* **2013**, *13*, 367. https://doi.org/10.1186/1471-2407-13-367.

(119) Bhat, R.; Dempe, S.; Dinsart, C.; Rommelaere, J. Enhancement of NK Cell Antitumor Responses Using an Oncolytic Parvovirus. *Int J Cancer* **2011**, *128* (4), 908–919. https://doi.org/10.1002/ijc.25415.

(120) Prestwich, R. J.; Errington, F.; Steele, L. P.; Ilett, E. J.; Morgan, R. S. M.; Harrington, K. J.; Pandha, H. S.; Selby, P. J.; Vile, R. G.; Melcher, A. A. Reciprocal Human Dendritic Cell-Natural Killer Cell Interactions Induce Antitumor Activity Following Tumor Cell Infection by Oncolytic Reovirus. *J Immunol* **2009**, *183* (7), 4312–4321. https://doi.org/10.4049/jimmunol.0901074.

(121) Zhang, J.; Tai, L.-H.; Ilkow, C. S.; Alkayyal, A. A.; Ananth, A. A.; de Souza, C. T.; Wang, J.; Sahi, S.; Ly, L.; Lefebvre, C.; Falls, T. J.; Stephenson, K. B.; Mahmoud, A. B.; Makrigiannis, A. P.; Lichty, B. D.; Bell, J. C.; Stojdl, D. F.; Auer, R. C. Maraba MG1 Virus Enhances Natural Killer Cell Function via Conventional Dendritic Cells to Reduce Postoperative Metastatic Disease. *Mol Ther* **2014**, *22* (7), 1320–1332. https://doi.org/10.1038/mt.2014.60.

(122) Kim, Y.; Clements, D. R.; Sterea, A. M.; Jang, H. W.; Gujar, S. A.; Lee, P. W. K. Dendritic Cells in Oncolytic Virus-Based Anti-Cancer Therapy. *Viruses* **2015**, *7* (12), 6506–6525. https://doi.org/10.3390/v7122953.

(123) DeNardo, D. G.; Ruffell, B. Macrophages as Regulators of Tumour Immunity and Immunotherapy. *Nat Rev Immunol* **2019**, *19* (6), 369–382. https://doi.org/10.1038/s41577-019-0127-6.

(124) Guiducci, C.; Vicari, A. P.; Sangaletti, S.; Trinchieri, G.; Colombo, M. P. Redirecting In Vivo Elicited Tumor Infiltrating Macrophages and Dendritic Cells towards Tumor Rejection. *Cancer Res* **2005**, *65* (8), 3437–3446.

(125) Duan, Z.; Luo, Y. Targeting Macrophages in Cancer Immunotherapy. *Sig Transduct Target Ther* **2021**, *6* (1), 1–21. https://doi.org/10.1038/s41392-021-00506-6.

(126) Chen, D. S.; Mellman, I. Oncology Meets Immunology: The Cancer-Immunity Cycle. *Immunity* **2013**, *39* (1), 1–10. https://doi.org/10.1016/j.immuni.2013.07.012.

(127) Mellman, I.; Coukos, G.; Dranoff, G. Cancer Immunotherapy Comes of Age. *Nature* **2011**, *480* (7378), 480–489. https://doi.org/10.1038/nature10673.

(128) Zamarin, D.; Holmgaard, R. B.; Subudhi, S. K.; Park, J. S.; Mansour, M.; Palese, P.; Merghoub, T.; Wolchok, J. D.; Allison, J. P. Localized Oncolytic Virotherapy Overcomes Systemic Tumor Resistance to Immune Checkpoint Blockade Immunotherapy. *Sci Transl Med* **2014**, *6* (226), 226ra32-226ra32. https://doi.org/10.1126/scitranslmed.3008095.

(129) Fend, L.; Yamazaki, T.; Remy, C.; Fahrner, C.; Gantzer, M.; Nourtier, V.; Préville, X.; Quéméneur, E.; Kepp, O.; Adam, J.; Marabelle, A.; Pitt, J. M.; Kroemer, G.; Zitvogel, L. Immune Checkpoint Blockade, Immunogenic Chemotherapy or IFN-α Blockade Boost the Local and Abscopal Effects of Oncolytic Virotherapy. *Cancer Res* **2017**, *77* (15), 4146–4157. https://doi.org/10.1158/0008-5472.CAN-16-2165.

(130) Gujar, S. A.; Marcato, P.; Pan, D.; Lee, P. W. K. Reovirus Virotherapy Overrides Tumor Antigen Presentation Evasion and Promotes Protective Antitumor Immunity. *Mol Cancer Ther* **2010**, *9* (11), 2924–2933. https://doi.org/10.1158/1535-7163.MCT-10-0590.

(131) Wang, G.; Kang, X.; Chen, K. S.; Jehng, T.; Jones, L.; Chen, J.; Huang, X. F.; Chen, S.-Y. An Engineered Oncolytic Virus Expressing PD-L1 Inhibitors Activates Tumor Neoantigen-Specific T Cell Responses. *Nat Commun* **2020**, *11* (1), 1395. https://doi.org/10.1038/s41467-020-15229-5.

(132) Koks, C. A.; Garg, A. D.; Ehrhardt, M.; Riva, M.; Vandenberk, L.; Boon, L.; Vleeschouwer, S. D.; Agostinis, P.; Graf, N.; Gool, S. W. V. Newcastle Disease Virotherapy Induces Long-Term Survival and Tumor-Specific Immune Memory in Orthotopic Glioma through the Induction of Immunogenic Cell Death. *Int J Cancer* **2015**, *136* (5), E313–E325. https://doi.org/10.1002/ijc.29202.

(133) Garg, A. D.; Agostinis, P. Cell Death and Immunity in Cancer: From Danger Signals to Mimicry of Pathogen Defense Responses. *Immunol Rev* **2017**, *280* (1), 126–148. https://doi.org/10.1111/imr.12574.

(134) Krysko, D. V.; Garg, A. D.; Kaczmarek, A.; Krysko, O.; Agostinis, P.; Vandenabeele, P. Immunogenic Cell Death and DAMPs in Cancer Therapy. *Nat Rev Cancer* **2012**, *12* (12), 860–875. https://doi.org/10.1038/nrc3380.

(135) Obeid, M.; Tesniere, A.; Ghiringhelli, F.; Fimia, G. M.; Apetoh, L.; Perfettini, J.-L.; Castedo, M.; Mignot, G.; Panaretakis, T.; Casares, N.; Métivier, D.; Larochette, N.; van Endert, P.; Ciccosanti, F.; Piacentini, M.; Zitvogel, L.; Kroemer, G. Calreticulin Exposure Dictates the Immunogenicity of Cancer Cell Death. *Nat Med* **2007**, *13* (1), 54–61. https://doi.org/10.1038/nm1523.

(136) Ghiringhelli, F.; Apetoh, L.; Tesniere, A.; Aymeric, L.; Ma, Y.; Ortiz, C.; Vermaelen, K.; Panaretakis, T.; Mignot, G.; Ullrich, E.; Perfettini, J.-L.; Schlemmer, F.; Tasdemir, E.; Uhl, M.; Génin, P.; Civas, A.; Ryffel, B.; Kanellopoulos, J.; Tschopp, J.; André, F.; Lidereau, R.; McLaughlin, N. M.; Haynes, N. M.; Smyth, M. J.; Kroemer, G.; Zitvogel, L. Activation of the NLRP3 Inflammasome in Dendritic Cells Induces IL-1β–Dependent Adaptive Immunity against Tumors. *Nat Med* **2009**, *15* (10), 1170–1178. https://doi.org/10.1038/nm.2028.

(137) Sistigu, A.; Yamazaki, T.; Vacchelli, E.; Chaba, K.; Enot, D. P.; Adam, J.; Vitale, I.; Goubar, A.; Baracco, E. E.; Remédios, C.; Fend, L.; Hannani, D.; Aymeric, L.; Ma, Y.; Niso-Santano, M.; Kepp, O.; Schultze, J. L.; Tüting, T.; Belardelli, F.; Bracci, L.; La Sorsa, V.; Ziccheddu, G.; Sestili, P.; Urbani, F.; Delorenzi, M.; Lacroix-Triki, M.; Quidville, V.; Conforti, R.; Spano, J.-P.; Pusztai, L.; Poirier-Colame, V.; Delaloge, S.; Penault-Llorca, F.; Ladoire, S.; Arnould, L.; Cyrta, J.; Dessoliers, M.-C.; Eggermont, A.; Bianchi, M. E.; Pittet, M.; Engblom, C.; Pfirschke, C.; Préville, X.; Uzè, G.; Schreiber, R. D.; Chow, M. T.; Smyth, M. J.; Proietti, E.; André, F.; Kroemer, G.; Zitvogel, L. Cancer Cell–Autonomous Contribution of Type I Interferon Signaling to the Efficacy of Chemotherapy. *Nat Med* **2014**, *20* (11), 1301–1309. https://doi.org/10.1038/nm.3708.

(138) Apetoh, L.; Ghiringhelli, F.; Tesniere, A.; Obeid, M.; Ortiz, C.; Criollo, A.; Mignot, G.; Maiuri, M. C.; Ullrich, E.; Saulnier, P.; Yang, H.; Amigorena, S.; Ryffel, B.; Barrat, F. J.; Saftig, P.; Levi, F.; Lidereau, R.; Nogues, C.; Mira, J.-P.; Chompret, A.; Joulin, V.; Clavel-Chapelon, F.; Bourhis, J.; André, F.; Delaloge, S.; Tursz, T.; Kroemer, G.; Zitvogel, L. Toll-like Receptor 4–Dependent Contribution of the Immune System to Anticancer Chemotherapy and Radiotherapy. *Nat Med* **2007**, *13* (9), 1050–1059. https://doi.org/10.1038/nm1622.

(139) Bommareddy, P. K.; Zloza, A.; Rabkin, S. D.; Kaufman, H. L. Oncolytic Virus Immunotherapy Induces Immunogenic Cell Death and Overcomes STING Deficiency in Melanoma. *OncoImmunology* **2019**, *8* (7), e1591875. https://doi.org/10.1080/2162402X.2019.1591875.

(140) Ye, T.; Jiang, K.; Wei, L.; Barr, M. P.; Xu, Q.; Zhang, G.; Ding, C.; Meng, S.; Piao, H. Oncolytic Newcastle Disease Virus Induces Autophagy-Dependent Immunogenic Cell Death in Lung Cancer Cells. *Am J Cancer Res* **2018**, *8* (8), 1514–1527.

(141) Shao, X.; Wang, X.; Guo, X.; Jiang, K.; Ye, T.; Chen, J.; Fang, J.; Gu, L.; Wang, S.; Zhang, G.; Meng, S.; Xu, Q. STAT3 Contributes To Oncolytic Newcastle Disease Virus-Induced Immunogenic Cell Death in Melanoma Cells. *Front Oncol* **2019**, *9*. https://doi.org/10.3389/fonc.2019.00436.

(142) Durgeau, A.; Virk, Y.; Corgnac, S.; Mami-Chouaib, F. Recent Advances in Targeting CD8 T-Cell Immunity for More Effective Cancer Immunotherapy. *Front Immunol* **2018**, *9*. https://doi.org/10.3389/fimmu.2018.00014.

(143) Waldman, A. D.; Fritz, J. M.; Lenardo, M. J. A Guide to Cancer Immunotherapy: From T Cell Basic Science to Clinical Practice. *Nat Rev Immunol* **2020**, *20* (11), 651–668. https://doi.org/10.1038/s41577-020-0306-5.

(144) Fehlings, M.; Simoni, Y.; Penny, H. L.; Becht, E.; Loh, C. Y.; Gubin, M. M.; Ward, J. P.; Wong, S. C.; Schreiber, R. D.; Newell, E. W. Checkpoint Blockade Immunotherapy Reshapes the High-Dimensional Phenotypic Heterogeneity of Murine Intratumoural Neoantigen-Specific CD8 + T Cells. *Nat Commun* **2017**, *8* (1), 562. https://doi.org/10.1038/s41467-017-00627-z.

(145) Varn, F. S.; Wang, Y.; Mullins, D. W.; Fiering, S.; Cheng, C. Systematic Pan-Cancer Analysis Reveals Immune Cell Interactions in the Tumor Microenvironment. *Cancer Res* **2017**, *77* (6), 1271–1282. https://doi.org/10.1158/0008-5472.CAN-16-2490.

(146) Wang, Y.; Hallden, G.; Hill, R.; Anand, A.; Liu, T.-C.; Francis, J.; Brooks, G.; Lemoine, N.; Kirn, D. E3 Gene Manipulations Affect Oncolytic Adenovirus Activity in Immunocompetent Tumor Models. *Nat Biotechnol* **2003**, *21* (11), 1328–1335. https://doi.org/10.1038/nbt887.

(147) Niavarani, S.-R.; Lawson, C.; Boudaud, M.; Simard, C.; Tai, L.-H. Oncolytic Vesicular Stomatitis Virus-Based Cellular Vaccine Improves Triple-Negative Breast Cancer Outcome by Enhancing Natural Killer and CD8+ T-Cell Functionality. *J Immunother Cancer* **2020**, *8* (1), e000465. https://doi.org/10.1136/jitc-2019-000465.

(148) Kim, M.; Nitschké, M.; Sennino, B.; Murer, P.; Schriver, B. J.; Bell, A.; Subramanian, A.; McDonald, C. E.; Wang, J.; Cha, H.; Bourgeois-Daigneault, M.-C.; Kirn, D. H.; Bell, J. C.; De Silva, N.; Breitbach, C. J.; McDonald, D. M. Amplification of Oncolytic Vaccinia Virus Widespread Tumor Cell Killing by Sunitinib through Multiple Mechanisms. *Cancer Res* **2018**, *78* (4), 922–937.

(149) Lee, Y. S.; Lee, W. S.; Kim, C. W.; Lee, S. J.; Yang, H.; Kong, S. J.; Ning, J.; Yang, K.-M.; Kang, B.; Kim, W. R.; Chon, H. J.; Kim, C. Oncolytic Vaccinia Virus Reinvigorates Peritoneal Immunity and Cooperates with Immune Checkpoint Inhibitor to Suppress Peritoneal Carcinomatosis in Colon Cancer. *J Immunother Cancer* **2020**, *8* (2), e000857. https://doi.org/10.1136/jitc-2020-000857.

(150) Malvehy, J.; Samoylenko, I.; Schadendorf, D.; Gutzmer, R.; Grob, J.-J.; Sacco, J. J.; Gorski, K. S.; Anderson, A.; Pickett, C. A.; Liu, K.; Gogas, H. Talimogene Laherparepvec Upregulates Immune-Cell Populations in Non-Injected Lesions: Findings from a Phase II, Multicenter, Open-Label Study in Patients with Stage IIIB–IVM1c Melanoma. *J Immunother Cancer* **2021**, *9* (3), e001621. https://doi.org/10.1136/jitc-2020-001621.

(151) Ribas, A.; Dummer, R.; Puzanov, I.; VanderWalde, A.; Andtbacka, R. H. I.; Michielin, O.; Olszanski, A. J.; Malvehy, J.; Cebon, J.; Fernandez, E.; Kirkwood, J. M.; Gajewski, T. F.; Chen, L.; Gorski, K. S.; Anderson, A. A.; Diede, S. J.; Lassman, M. E.; Gansert, J.; Hodi, F. S.; Long, G. V. Oncolytic Virotherapy Promotes Intratumoral T Cell Infiltration and Improves Anti-PD-1 Immunotherapy. *Cell* **2017**, *170* (6), 1109-1119.e10. https://doi.org/10.1016/j.cell.2017.08.027.

(152) Zhang, B.; Cheng, P. Improving Antitumor Efficacy via Combinatorial Regimens of Oncolytic Virotherapy. *Mol Cancer* **2020**, *19* (1), 158. https://doi.org/10.1186/s12943-020-01275-6.

(153) Chen, D. S.; Mellman, I. Elements of Cancer Immunity and the Cancer–Immune Set Point. *Nature* **2017**, *541* (7637), 321–330. https://doi.org/10.1038/nature21349.

(154) Ottolino-Perry, K.; Diallo, J.-S.; Lichty, B. D.; Bell, J. C.; McCart, J. A. Intelligent Design: Combination Therapy with Oncolytic Viruses. *Mol Ther* **2010**, *18* (2), 251–263. https://doi.org/10.1038/mt.2009.283.

(155) Wennier, S. T.; Liu, J.; McFadden, G. Bugs and Drugs: Oncolytic Virotherapy in Combination with Chemotherapy. *Curr Pharm Biotechnol* **2012**, *13* (9), 1817–1833.

(156) Touchefeu, Y.; Vassaux, G.; Harrington, K. J. Oncolytic Viruses in Radiation Oncology. *Radiother Oncol* **2011**, *99* (3), 262–270. https://doi.org/10.1016/j.radonc.2011.05.078.

(157) Shi, T.; Song, X.; Wang, Y.; Liu, F.; Wei, J. Combining Oncolytic Viruses With Cancer Immunotherapy: Establishing a New Generation of Cancer Treatment. *Front Immunol* **2020**, *11*. https://doi.org/10.3389/fimmu.2020.00683.

(158) Zou, W. Immunosuppressive Networks in the Tumour Environment and Their Therapeutic Relevance. *Nat Rev Cancer* **2005**, *5* (4), 263–274. https://doi.org/10.1038/nrc1586.

(159) Achard, C.; Surendran, A.; Wedge, M.-E.; Ungerechts, G.; Bell, J.; Ilkow, C. S. Lighting a Fire in the Tumor Microenvironment Using Oncolytic Immunotherapy. *EBioMedicine* **2018**, *31*, 17–24. https://doi.org/10.1016/j.ebiom.2018.04.020.

(160) Pol, J. G.; Workenhe, S. T.; Konda, P.; Gujar, S.; Kroemer, G. Cytokines in Oncolytic Virotherapy. *Cytokine Growth Factor Rev* **2020**, *56*, 4–27. https://doi.org/10.1016/j.cytogfr.2020.10.007.

(161) Liu, Z.; Ge, Y.; Wang, H.; Ma, C.; Feist, M.; Ju, S.; Guo, Z. S.; Bartlett, D. L. Modifying the Cancer-Immune Set Point Using Vaccinia Virus Expressing Re-Designed Interleukin-2. *Nat Commun* **2018**, *9* (1), 4682. https://doi.org/10.1038/s41467-018-06954-z.

(162) Wang, P.; Li, X.; Wang, J.; Gao, D.; Li, Y.; Li, H.; Chu, Y.; Zhang, Z.; Liu, H.; Jiang, G.; Cheng, Z.; Wang, S.; Dong, J.; Feng, B.; Chard, L. S.; Lemoine, N. R.; Wang, Y. Re-Designing Interleukin-12 to Enhance Its Safety and Potential as an Anti-Tumor Immunotherapeutic Agent. *Nat Commun* **2017**, *8* (1), 1395. https://doi.org/10.1038/s41467-017-01385-8.

(163) Alkayyal, A. A.; Tai, L.-H.; Kennedy, M. A.; de Souza, C. T.; Zhang, J.; Lefebvre, C.; Sahi, S.; Ananth, A. A.; Mahmoud, A. B.; Makrigiannis, A. P.; Cron, G. O.; Macdonald, B.; Marginean, E. C.; Stojdl, D. F.; Bell, J. C.; Auer, R. C. NK-Cell Recruitment Is Necessary for Eradication of Peritoneal Carcinomatosis with an IL12-Expressing Maraba Virus Cellular Vaccine. *Cancer Immunol Res* **2017**, *5* (3), 211–221. https://doi.org/10.1158/2326-6066.CIR-16-0162.

(164) Xu, X.; Sun, Q.; Mei, Y.; Liu, Y.; Zhao, L. Newcastle Disease Virus Co-expressing Interleukin 7 and Interleukin 15 Modified Tumor Cells as a Vaccine for Cancer Immunotherapy. *Cancer Sci* **2018**, *109* (2), 279–288. https://doi.org/10.1111/cas.13468.

(165) Yan, Y.; Li, S.; Jia, T.; Du, X.; Xu, Y.; Zhao, Y.; Li, L.; Liang, K.; Liang, W.; Sun, H.; Li, R. Combined Therapy with CTL Cells and Oncolytic Adenovirus Expressing IL-15-Induced Enhanced Antitumor Activity. *Tumour Biol* **2015**, *36* (6), 4535–4543. https://doi.org/10.1007/s13277-015-3098-7.

(166) Stephenson, K. B.; Barra, N. G.; Davies, E.; Ashkar, A. A.; Lichty, B. D. Expressing Human Interleukin-15 from Oncolytic Vesicular Stomatitis Virus Improves Survival in a Murine Metastatic Colon Adenocarcinoma Model through the Enhancement of Anti-Tumor Immunity. *Cancer Gene Ther* **2012**, *19* (4), 238–246. https://doi.org/10.1038/cgt.2011.81.

(167) Kowalsky, S. J.; Liu, Z.; Feist, M.; Berkey, S. E.; Ma, C.; Ravindranathan, R.; Dai, E.; Roy, E. J.; Guo, Z. S.; Bartlett, D. L. Superagonist IL-15-Armed Oncolytic Virus Elicits Potent Antitumor Immunity and Therapy That Are Enhanced with PD-1 Blockade. *Mol Ther* **2018**, *26* (10), 2476–2486. https://doi.org/10.1016/j.ymthe.2018.07.013.

(168) LaRocca, C. J.; Han, J.; Gavrikova, T.; Armstrong, L.; Oliveira, A. R.; Shanley, R.; Vickers, S. M.; Yamamoto, M.; Davydova, J. Oncolytic Adenovirus Expressing Interferon Alpha in a Syngeneic Syrian Hamster Model for the Treatment of Pancreatic Cancer. *Surgery* **2015**, *157* (5), 888–898. https://doi.org/10.1016/j.surg.2015.01.006.

(169)   Li, H.; Peng, K.-W.; Dingli, D.; Kratzke, R. A.; Russell, S. J. Oncolytic Measles Viruses Encoding Interferon β and the Thyroidal Sodium Iodide Symporter Gene for Mesothelioma Virotherapy. *Cancer Gene Ther* **2010**, *17* (8), 550–558. https://doi.org/10.1038/cgt.2010.10.

(170)   Willmon, C. L.; Saloura, V.; Fridlender, Z. G.; Wongthida, P.; Diaz, R. M.; Thompson, J.; Kottke, T.; Federspiel, M.; Barber, G.; Albelda, S. M.; Vile, R. G. Expression of IFN-β Enhances Both Efficacy and Safety of Oncolytic Vesicular Stomatitis Virus for Therapy of Mesothelioma. *Cancer Res* **2009**, *69* (19), 7713–7720.

(171)   Patel, M. R.; Jacobson, B. A.; Ji, Y.; Drees, J.; Tang, S.; Xiong, K.; Wang, H.; Prigge, J. E.; Dash, A. S.; Kratzke, A. K.; Mesev, E.; Etchison, R.; Federspiel, M. J.; Russell, S. J.; Kratzke, R. A. Vesicular Stomatitis Virus Expressing Interferon-β Is Oncolytic and Promotes Antitumor Immune Responses in a Syngeneic Murine Model of Non-Small Cell Lung Cancer. *Oncotarget* **2015**, *6* (32), 33165–33177.

(172)   Bourgeois-Daigneault, M.-C.; Roy, D. G.; Falls, T.; Twumasi-Boateng, K.; St-Germain, L. E.; Marguerie, M.; Garcia, V.; Selman, M.; Jennings, V. A.; Pettigrew, J.; Amos, S.; Diallo, J.-S.; Nelson, B.; Bell, J. C. Oncolytic Vesicular Stomatitis Virus Expressing Interferon-σ Has Enhanced Therapeutic Activity. *Mol Ther Oncolytics* **2016**, *3*, 16001. https://doi.org/10.1038/mto.2016.1.

(173)   Liu, Z.; Ravindranathan, R.; Li, J.; Kalinski, P.; Guo, Z. S.; Bartlett, D. L. CXCL11-Armed Oncolytic Poxvirus Elicits Potent Antitumor Immunity and Shows Enhanced Therapeutic Efficacy. *OncoImmunology* **2016**, *5* (3), e1091554. https://doi.org/10.1080/2162402X.2015.1091554.

(174)   Eckert, E. C.; Nace, R. A.; Tonne, J. M.; Evgin, L.; Vile, R. G.; Russell, S. J. Generation of a Tumor-Specific Chemokine Gradient Using Oncolytic Vesicular Stomatitis Virus Encoding CXCL9. *Mol Ther Oncolytics* **2020**, *16*, 63–74. https://doi.org/10.1016/j.omto.2019.12.003.

(175)   Lapteva, N.; Aldrich, M.; Weksberg, D.; Rollins, L.; Goltsova, T.; Chen, S.-Y.; Huang, X. F. Targeting the Intratumoral Dendritic Cells by the Oncolytic Adenoviral Vaccine Expressing RANTES Elicits Potent Antitumor Immunity. *J Immunother* **2009**, *32* (2), 145–156. https://doi.org/10.1097/CJI.0b013e318193d31e.

(176)   Li, F.; Sheng, Y.; Hou, W.; Sampath, P.; Byrd, D.; Thorne, S.; Zhang, Y. CCL5-Armed Oncolytic Virus Augments CCR5-Engineered NK Cell Infiltration and Antitumor Efficiency. *J Immunother Cancer* **2020**, *8* (1), e000131. https://doi.org/10.1136/jitc-2019-000131.

(177)   Shi, Y.; Liu, C. H.; Roberts, A. I.; Das, J.; Xu, G.; Ren, G.; Zhang, Y.; Zhang, L.; Yuan, Z. R.; Tan, H. S. W.; Das, G.; Devadas, S. Granulocyte-Macrophage Colony-Stimulating Factor (GM-CSF) and T-Cell Responses: What We Do and Don't Know. *Cell Res* **2006**, *16* (2), 126–133. https://doi.org/10.1038/sj.cr.7310017.

(178)   Chon, H. J.; Lee, W. S.; Yang, H.; Kong, S. J.; Lee, N. K.; Moon, E. S.; Choi, J.; Han, E. C.; Kim, J. H.; Ahn, J. B.; Kim, J.-H.; Kim, C. Tumor Microenvironment Remodeling by Intratumoral Oncolytic Vaccinia Virus Enhances the Efficacy of Immune Checkpoint Blockade. *Clin Cancer Res* **2018**, clincanres.1932.2018. https://doi.org/10.1158/1078-0432.CCR-18-1932.

(179)   Kanerva, A.; Nokisalmi, P.; Diaconu, I.; Koski, A.; Cerullo, V.; Liikanen, I.; Tähtinen, S.; Oksanen, M.; Heiskanen, R.; Pesonen, S.; Joensuu, T.; Alanko, T.; Partanen, K.; Laasonen, L.; Kairemo, K.; Pesonen, S.; Kangasniemi, L.; Hemminki, A. Antiviral and Antitumor T-Cell Immunity in Patients Treated with GM-CSF–Coding Oncolytic Adenovirus. *Clin Cancer Res* **2013**, *19* (10), 2734–2744. https://doi.org/10.1158/1078-0432.CCR-12-2546.

(180)   Chen, L.; Flies, D. B. Molecular Mechanisms of T Cell Co-Stimulation and Co-Inhibition. *Nat Rev Immunol* **2013**, *13* (4), 227–242. https://doi.org/10.1038/nri3405.

(181)   Peggs, K. S.; Quezada, S. A.; Allison, J. P. Cancer Immunotherapy: Co-Stimulatory Agonists and Co-Inhibitory Antagonists. *Clin Exp Immunol* **2009**, *157* (1), 9–19. https://doi.org/10.1111/j.1365-2249.2009.03912.x.

(182)   John, L. B.; Howland, L. J.; Flynn, J. K.; West, A. C.; Devaud, C.; Duong, C. P.; Stewart, T. J.; Westwood, J. A.; Guo, Z. S.; Bartlett, D. L.; Smyth, M. J.; Kershaw, M. H.; Darcy, P. K. Oncolytic Virus and Anti–4-1BB Combination Therapy Elicits Strong Antitumor Immunity against Established Cancer. *Cancer Res* **2012**, *72* (7), 1651–1660. https://doi.org/10.1158/0008-5472.CAN-11-2788.

(183)   Scherwitzl, I.; Opp, S.; Hurtado, A. M.; Pampeno, C.; Loomis, C.; Kannan, K.; Yu, M.; Meruelo, D. Sindbis Virus with Anti-OX40 Overcomes the Immunosuppressive Tumor Microenvironment of Low-Immunogenic Tumors. *Mol Ther Oncolytics* **2020**, *17*, 431–447. https://doi.org/10.1016/j.omto.2020.04.012.

(184)   Rivera-Molina, Y.; Jiang, H.; Fueyo, J.; Nguyen, T.; Shin, D. H.; Youssef, G.; Fan, X.; Gumin, J.; Alonso, M. M.; Phadnis, S.; Lang, F. F.; Gomez-Manzano, C. GITRL-Armed Delta-24-RGD Oncolytic Adenovirus Prolongs Survival and Induces Anti-Glioma Immune Memory. *Neurooncol Adv* **2019**, *1* (1). https://doi.org/10.1093/noajnl/vdz009.

(185)   Zamarin, D.; Holmgaard, R. B.; Ricca, J.; Plitt, T.; Palese, P.; Sharma, P.; Merghoub, T.; Wolchok, J. D.; Allison, J. P. Intratumoral Modulation of the Inducible Co-Stimulator ICOS by Recombinant Oncolytic Virus Promotes Systemic Anti-Tumour Immunity. *Nat Commun* **2017**, *8*, 14340. https://doi.org/10.1038/ncomms14340.

(186)   Bridle, B. W.; Hanson, S.; Lichty, B. D. Combining Oncolytic Virotherapy and Tumour Vaccination. *Cytokine Growth Factor Rev* **2010**, *21* (2–3), 143–148. https://doi.org/10.1016/j.cytogfr.2010.02.009.

(187)   Suksanpaisan, L.; Xu, R.; Tesfay, M. Z.; Bomidi, C.; Hamm, S.; Vandergaast, R.; Jenks, N.; Steele, M. B.; Ota-Setlik, A.; Akhtar, H.; Luckay, A.; Nowak, R.; Peng, K. W.; Eldridge, J. H.; Clarke, D. K.; Russell, S. J.; Diaz, R. M. Preclinical Development of Oncolytic Immunovirotherapy for Treatment of HPVPOS Cancers. *Mol Ther Oncolytics* **2018**, *10*, 1–13. https://doi.org/10.1016/j.omto.2018.05.001.

(188)   Bridle, B. W.; Boudreau, J. E.; Lichty, B. D.; Brunellière, J.; Stephenson, K.; Koshy, S.; Bramson, J. L.; Wan, Y. Vesicular Stomatitis Virus as a Novel Cancer Vaccine Vector to Prime Antitumor Immunity Amenable to Rapid Boosting With Adenovirus. *Mol Ther* **2009**, *17* (10), 1814–1821. https://doi.org/10.1038/mt.2009.154.

(189)   Diaz, R. M.; Galivo, F.; Kottke, T.; Wongthida, P.; Qiao, J.; Thompson, J.; Valdes, M.; Barber, G.; Vile, R. G. Oncolytic Immunovirotherapy for Melanoma Using Vesicular Stomatitis Virus. *Cancer Res* **2007**, *67* (6), 2840–2848. https://doi.org/10.1158/0008-5472.CAN-06-3974.

(190)   Rommelfanger, D. M.; Wongthida, P.; Diaz, R. M.; Kaluza, K. M.; Thompson, J. M.; Kottke, T. J.; Vile, R. G. Systemic Combination Virotherapy for Melanoma with Tumor Antigen-Expressing Vesicular Stomatitis Virus and Adoptive T-Cell Transfer. *Cancer Res* **2012**, *72* (18), 4753–4764. https://doi.org/10.1158/0008-5472.CAN-12-0600.

(191)   McLaughlin, J. P.; Schlom, J.; Kantor, J. A.; Greiner, J. W. Improved Immunotherapy of a Recombinant Carcinoembryonic Antigen Vaccinia Vaccine When given in Combination with Interleukin-2. *Cancer Res* **1996**, *56* (10), 2361–2367.

(192)   Mulryan, K.; Ryan, M. G.; Myers, K. A.; Shaw, D.; Wang, W.; Kingsman, S. M.; Stern, P. L.; Carroll, M. W. Attenuated Recombinant Vaccinia Virus Expressing Oncofetal Antigen (Tumor-Associated Antigen) 5T4 Induces Active Therapy of Established Tumors. *Mol Cancer Ther* **2002**, *1* (12), 1129–1137.

(193)   de Vries, C. R.; Monken, C. E.; Lattime, E. C. The Addition of Recombinant Vaccinia HER2/Neu to Oncolytic Vaccinia-GMCSF given into the Tumor Microenvironment Overcomes MDSC-Mediated Immune Escape and Systemic Anergy. *Cancer Gene Ther* **2015**, *22* (3), 154–162. https://doi.org/10.1038/cgt.2015.2.

(194)   Kottke, T.; Errington, F.; Pulido, J.; Galivo, F.; Thompson, J.; Wongthida, P.; Diaz, R. M.; Chong, H.; Ilett, E.; Chester, J.; Pandha, H.; Harrington, K.; Selby, P.; Melcher, A.; Vile, R. Broad Antigenic Coverage Induced by Vaccination with Virus-Based CDNA Libraries Cures Established Tumors. *Nat Med* **2011**, *17* (7), 854–859. https://doi.org/10.1038/nm.2390.

(195)   Pulido, J.; Kottke, T.; Thompson, J.; Galivo, F.; Wongthida, P.; Diaz, R. M.; Rommelfanger, D.; Ilett, E.; Pease, L.; Pandha, H.; Harrington, K.; Selby, P.; Melcher, A.; Vile, R. Using Virally Expressed Melanoma CDNA Libraries to Identify Tumor-Associated Antigens That Cure Melanoma. *Nat Biotechnol* **2012**, *30* (4), 337–343. https://doi.org/10.1038/nbt.2157.

(196)   Capasso, C.; Hirvinen, M.; Garofalo, M.; Romaniuk, D.; Kuryk, L.; Sarvela, T.; Vitale, A.; Antopolsky, M.; Magarkar, A.; Viitala, T.; Suutari, T.; Bunker, A.; Yliperttula, M.; Urtti, A.; Cerullo, V. Oncolytic Adenoviruses Coated with MHC-I Tumor Epitopes Increase the Antitumor Immunity and Efficacy against Melanoma. *OncoImmunology* **2016**, *5* (4), e1105429. https://doi.org/10.1080/2162402X.2015.1105429.

(197)   Holay, N.; Kim, Y.; Lee, P.; Gujar, S. Sharpening the Edge for Precision Cancer Immunotherapy: Targeting Tumor Antigens through Oncolytic Vaccines. *Front Immunol* **2017**, *8*. https://doi.org/10.3389/fimmu.2017.00800.

(198)   Ring, S. S.; Królik, M.; Hartmann, F.; Schmidt, E.; Hasan Ali, O.; Ludewig, B.; Kochanek, S.; Flatz, L. Heterologous Prime Boost Vaccination Induces Protective Melanoma-Specific CD8+ T Cell Responses. *Mol Ther Oncolytics* **2020**, *19*, 179–187. https://doi.org/10.1016/j.omto.2020.10.001.

(199)   Scott, E. M.; Duffy, M. R.; Freedman, J. D.; Fisher, K. D.; Seymour, L. W. Solid Tumor Immunotherapy with T Cell Engager-Armed Oncolytic Viruses. *Macromol Biosci* **2018**, *18* (1), 1700187. https://doi.org/10.1002/mabi.201700187.

(200)   Fajardo, C. A.; Guedan, S.; Rojas, L. A.; Moreno, R.; Arias-Badia, M.; Sostoa, J. de; June, C. H.; Alemany, R. Oncolytic Adenoviral Delivery of an EGFR-Targeting T-Cell Engager Improves Antitumor Efficacy. *Cancer Res* **2017**, *77* (8), 2052–2063. https://doi.org/10.1158/0008-5472.CAN-16-1708.

(201)   Yu, F.; Wang, X.; Guo, Z. S.; Bartlett, D. L.; Gottschalk, S. M.; Song, X.-T. T-Cell Engager-Armed Oncolytic Vaccinia Virus Significantly Enhances Antitumor Therapy. *Mol Ther* **2014**, *22* (1), 102–111. https://doi.org/10.1038/mt.2013.240.

(202)   Freedman, J. D.; Hagel, J.; Scott, E. M.; Psallidas, I.; Gupta, A.; Spiers, L.; Miller, P.; Kanellakis, N.; Ashfield, R.; Fisher, K. D.; Duffy, M. R.; Seymour, L. W. Oncolytic Adenovirus Expressing Bispecific Antibody Targets T-cell Cytotoxicity in Cancer Biopsies. *EMBO Mol Med* **2017**, *9* (8), 1067–1087. https://doi.org/10.15252/emmm.201707567.

(203)   Morotti, M.; Albukhari, A.; Alsaadi, A.; Artibani, M.; Brenton, J. D.; Curbishley, S. M.; Dong, T.; Dustin, M. L.; Hu, Z.; McGranahan, N.; Miller, M. L.; Santana-Gonzalez, L.; Seymour, L. W.; Shi, T.; Van Loo, P.; Yau, C.; White, H.; Wietek, N.; Church, D. N.; Wedge, D. C.; Ahmed, A. A. Promises and Challenges of Adoptive T-Cell Therapies for Solid Tumours. *Br J Cancer* **2021**, *124* (11), 1759–1776. https://doi.org/10.1038/s41416-021-01353-6.

(204) Nishio, N.; Diaconu, I.; Liu, H.; Cerullo, V.; Caruana, I.; Hoyos, V.; Bouchier-Hayes, L.; Savoldo, B.; Dotti, G. Armed Oncolytic Virus Enhances Immune Functions of Chimeric Antigen Receptor–Modified T Cells in Solid Tumors. *Cancer Res* **2014**, *74* (18), 5195–5205. https://doi.org/10.1158/0008-5472.CAN-14-0697.

(205) Walsh, S. R.; Simovic, B.; Chen, L.; Bastin, D.; Nguyen, A.; Stephenson, K.; Mandur, T. S.; Bramson, J. L.; Lichty, B. D.; Wan, Y. Endogenous T Cells Prevent Tumor Immune Escape Following Adoptive T Cell Therapy. *J Clin Invest* **2019**, *129* (12), 5400–5410. https://doi.org/10.1172/JCI126199.

(206) Robert, C. A Decade of Immune-Checkpoint Inhibitors in Cancer Therapy. *Nat Commun* **2020**, *11* (1), 3801. https://doi.org/10.1038/s41467-020-17670-y.

(207) Darvin, P.; Toor, S. M.; Sasidharan Nair, V.; Elkord, E. Immune Checkpoint Inhibitors: Recent Progress and Potential Biomarkers. *Exp Mol Med* **2018**, *50* (12), 1–11. https://doi.org/10.1038/s12276-018-0191-1.

(208) Diana, A.; Wang, L. M.; D'Costa, Z.; Allen, P.; Azad, A.; Silva, M. A.; Soonawalla, Z.; Liu, S.; McKenna, W. G.; Muschel, R. J.; Fokas, E. Prognostic Value, Localization and Correlation of PD-1/PD-L1, CD8 and FOXP3 with the Desmoplastic Stroma in Pancreatic Ductal Adenocarcinoma. *Oncotarget* **2016**, *7* (27), 40992–41004. https://doi.org/10.18632/oncotarget.10038.

(209) Taube, J. M.; Klein, A.; Brahmer, J. R.; Xu, H.; Pan, X.; Kim, J. H.; Chen, L.; Pardoll, D. M.; Topalian, S. L.; Anders, R. A. Association of PD-1, PD-1 Ligands, and Other Features of the Tumor Immune Microenvironment with Response to Anti-PD-1 Therapy. *Clin Cancer Res* **2014**, *20* (19), 5064–5074. https://doi.org/10.1158/1078-0432.CCR-13-3271.

(210) Klempner, S. J.; Fabrizio, D.; Bane, S.; Reinhart, M.; Peoples, T.; Ali, S. M.; Sokol, E. S.; Frampton, G.; Schrock, A. B.; Anhorn, R.; Reddy, P. Tumor Mutational Burden as a Predictive Biomarker for Response to Immune Checkpoint Inhibitors: A Review of Current Evidence. *Oncologist* **2020**, *25* (1), e147–e159. https://doi.org/10.1634/theoncologist.2019-0244.

(211) Chiu, M.; Armstrong, E. J. L.; Jennings, V.; Foo, S.; Crespo-Rodriguez, E.; Bozhanova, G.; Patin, E. C.; McLaughlin, M.; Mansfield, D.; Baker, G.; Grove, L.; Pedersen, M.; Kyula, J.; Roulstone, V.; Wilkins, A.; McDonald, F.; Harrington, K.; Melcher, A. Combination Therapy with Oncolytic Viruses and Immune Checkpoint Inhibitors. *Expert Opin Biol Ther* **2020**, *20* (6), 635–652. https://doi.org/10.1080/14712598.2020.1729351.

(212) Zamarin, D.; Ricca, J. M.; Sadekova, S.; Oseledchyk, A.; Yu, Y.; Blumenschein, W. M.; Wong, J.; Gigoux, M.; Merghoub, T.; Wolchok, J. D. PD-L1 in Tumor Microenvironment Mediates Resistance to Oncolytic Immunotherapy. *J Clin Invest* **2018**, *128* (4), 1413–1428. https://doi.org/10.1172/JCI98047.

(213) Saha, D.; Martuza, R. L.; Rabkin, S. D. Oncolytic Herpes Simplex Virus Immunovirotherapy in Combination with Immune Checkpoint Blockade to Treat Glioblastoma. *Immunotherapy* **2018**, *10* (9), 779–786. https://doi.org/10.2217/imt-2018-0009.

(214) Rajani, K.; Parrish, C.; Kottke, T.; Thompson, J.; Zaidi, S.; Ilett, L.; Shim, K. G.; Diaz, R.-M.; Pandha, H.; Harrington, K.; Coffey, M.; Melcher, A.; Vile, R. Combination Therapy With Reovirus and Anti-PD-1 Blockade Controls Tumor Growth Through Innate and Adaptive Immune Responses. *Mol Ther* **2016**, *24* (1), 166–174. https://doi.org/10.1038/mt.2015.156.

(215) Bourgeois-Daigneault, M.-C.; Roy, D. G.; Aitken, A. S.; Sayes, N. E.; Martin, N. T.; Varette, O.; Falls, T.; St-Germain, L. E.; Pelin, A.; Lichty, B. D.; Stojdl, D. F.; Ungerechts, G.; Diallo, J.-S.; Bell, J. C. Neoadjuvant Oncolytic Virotherapy before Surgery Sensitizes Triple-Negative Breast Cancer to Immune Checkpoint Therapy. *Sci Transl Med* **2018**, *10* (422), eaao1641. https://doi.org/10.1126/scitranslmed.aao1641.

(216) Ramos-Casals, M.; Brahmer, J. R.; Callahan, M. K.; Flores-Chávez, A.; Keegan, N.; Khamashta, M. A.; Lambotte, O.; Mariette, X.; Prat, A.; Suárez-Almazor, M. E. Immune-Related Adverse Events of Checkpoint Inhibitors. *Nat Rev Dis Primers* **2020**, *6* (1), 1–21. https://doi.org/10.1038/s41572-020-0160-6.

(217) Selby, M. J.; Engelhardt, J. J.; Quigley, M.; Henning, K. A.; Chen, T.; Srinivasan, M.; Korman, A. J. Anti-CTLA-4 Antibodies of IgG2a Isotype Enhance Antitumor Activity through Reduction of Intratumoral Regulatory T Cells. *Cancer Immunol Res* **2013**, *1* (1), 32–42. https://doi.org/10.1158/2326-6066.CIR-13-0013.

(218) Vijayakumar, G.; Palese, P.; Goff, P. H. Oncolytic Newcastle Disease Virus Expressing a Checkpoint Inhibitor as a Radioenhancing Agent for Murine Melanoma. *EBioMedicine* **2019**, *49*, 96–105. https://doi.org/10.1016/j.ebiom.2019.10.032.

(219) Hamilton, J. R.; Vijayakumar, G.; Palese, P. A Recombinant Antibody-Expressing Influenza Virus Delays Tumor Growth in a Mouse Model. *Cell Reports* **2018**, *22* (1), 1–7. https://doi.org/10.1016/j.celrep.2017.12.025.

(220) Shin, D. H.; Nguyen, T.; Ozpolat, B.; Lang, F.; Alonso, M.; Gomez-Manzano, C.; Fueyo, J. Current Strategies to Circumvent the Antiviral Immunity to Optimize Cancer Virotherapy. *J Immunother Cancer* **2021**, *9* (4), e002086. https://doi.org/10.1136/jitc-2020-002086.

(221) Dörner, T.; Radbruch, A. Antibodies and B Cell Memory in Viral Immunity. *Immunity* **2007**, *27* (3), 384–392. https://doi.org/10.1016/j.immuni.2007.09.002.

(222) Murin, C. D.; Wilson, I. A.; Ward, A. B. Antibody Responses to Viral Infections: A Structural Perspective across Three Different Enveloped Viruses. *Nat Microbiol* **2019**, *4* (5), 734–747. https://doi.org/10.1038/s41564-019-0392-y.

(223) Chen, Y.; Yu, D.-C.; Charlton, D.; Henderson, D. R. Pre-Existent Adenovirus Antibody Inhibits Systemic Toxicity and Antitumor Activity of CN706 in the Nude Mouse LNCaP Xenograft Model: Implications and Proposals for Human Therapy. *Hum Gene Ther* **2000**, *11* (11), 1553–1567. https://doi.org/10.1089/10430340050083289.

(224) Harvey, B.-G.; Hackett, N. R.; El-Sawy, T.; Rosengart, T. K.; Hirschowitz, E. A.; Lieberman, M. D.; Lesser, M. L.; Crystal, R. G. Variability of Human Systemic Humoral Immune Responses to Adenovirus Gene Transfer Vectors Administered to Different Organs. *J Virol* **1999**, *73* (8), 6729–6742. https://doi.org/10.1128/JVI.73.8.6729-6742.1999.

(225) Pollard, A. J.; Bijker, E. M. A Guide to Vaccinology: From Basic Principles to New Developments. *Nat Rev Immunol* **2021**, *21* (2), 83–100. https://doi.org/10.1038/s41577-020-00479-7.

(226) Xu, F.; Schillinger, J. A.; Sternberg, M. R.; Johnson, R. E.; Lee, F. K.; Nahmias, A. J.; Markowitz, L. E. Seroprevalence and Coinfection with Herpes Simplex Virus Type 1 and Type 2 in the United States, 1988–1994. *J Infect Dis* **2002**, *185* (8), 1019–1024. https://doi.org/10.1086/340041.

(227) Tai, J. H.; Williams, J. V.; Edwards, K. M.; Wright, P. F.; Crowe, Jr., J. E.; Dermody, T. S. Prevalence of Reovirus-Specific Antibodies in Young Children in Nashville, Tennessee. *J Infect Dis* **2005**, *191* (8), 1221–1224. https://doi.org/10.1086/428911.

(228) Hemminki, O.; Bauerschmitz, G.; Hemmi, S.; Lavilla-Alonso, S.; Diaconu, I.; Guse, K.; Koski, A.; Desmond, R. A.; Lappalainen, M.; Kanerva, A.; Cerullo, V.; Pesonen, S.; Hemminki, A. Oncolytic Adenovirus Based on Serotype 3. *Cancer Gene Ther* **2011**, *18* (4), 288–296. https://doi.org/10.1038/cgt.2010.79.

(229) Xu, C.; Goß, A. V.; Dorneburg, C.; Debatin, K.-M.; Wei, J.; Beltinger, C. Proof-of-Principle That a Decoy Virus Protects Oncolytic Measles Virus against Neutralizing Antibodies. *Oncolytic Virother* **2018**, *7*, 37–41. https://doi.org/10.2147/OV.S150637.

(230) Rojas, J. J.; Sampath, P.; Bonilla, B.; Ashley, A.; Hou, W.; Byrd, D.; Thorne, S. H. Manipulating TLR Signaling Increases the Anti-Tumor T Cell Response Induced by Viral Cancer Therapies. *Cell Reports* **2016**, *15* (2), 264–273. https://doi.org/10.1016/j.celrep.2016.03.017.

(231) Muik, A.; Kneiske, I.; Werbizki, M.; Wilflingseder, D.; Giroglou, T.; Ebert, O.; Kraft, A.; Dietrich, U.; Zimmer, G.; Momma, S.; von Laer, D. Pseudotyping Vesicular Stomatitis Virus with Lymphocytic Choriomeningitis Virus Glycoproteins Enhances Infectivity for Glioma Cells and Minimizes Neurotropism ▿. *J Virol* **2011**, *85* (11), 5679–5684. https://doi.org/10.1128/JVI.02511-10.

(232) Muik, A.; Stubbert, L. J.; Jahedi, R. Z.; Geiß, Y.; Kimpel, J.; Dold, C.; Tober, R.; Volk, A.; Klein, S.; Dietrich, U.; Yadollahi, B.; Falls, T.; Miletic, H.; Stojdl, D.; Bell, J. C.; von Laer, D. Re-Engineering Vesicular Stomatitis Virus to Abrogate Neurotoxicity, Circumvent Humoral Immunity, and Enhance Oncolytic Potency. *Cancer Res* **2014**, *74* (13), 3567–3578. https://doi.org/10.1158/0008-5472.CAN-13-3306.

(233) Pinschewer, D. D.; Perez, M.; Jeetendra, E.; Bächi, T.; Horvath, E.; Hengartner, H.; Whitt, M. A.; de la Torre, J. C.; Zinkernagel, R. M. Kinetics of Protective Antibodies Are Determined by the Viral Surface Antigen. *J Clin Invest* **2004**, *114* (7), 988–993. https://doi.org/10.1172/JCI22374.

(234) Carroll, M. C. The Complement System in Regulation of Adaptive Immunity. *Nat Immunol* **2004**, *5* (10), 981–986. https://doi.org/10.1038/ni1113.

(235) Agrawal, P.; Nawadkar, R.; Ojha, H.; Kumar, J.; Sahu, A. Complement Evasion Strategies of Viruses: An Overview. *Front Microbiol* **2017**, *8*. https://doi.org/10.3389/fmicb.2017.01117.

(236) Wakimoto, H.; Ikeda, K.; Abe, T.; Ichikawa, T.; Hochberg, F. H.; Ezekowitz, R. A. B.; Pasternack, M. S.; Chiocca, E. A. The Complement Response against an Oncolytic Virus Is Species-Specific in Its Activation Pathways. *Mol Ther* **2002**, *5* (3), 275–282. https://doi.org/10.1006/mthe.2002.0547.

(237) Magge, D.; Guo, Z. S.; O'Malley, M. E.; Francis, L.; Ravindranathan, R.; Bartlett, D. L. Inhibitors of C5 Complement Enhance Vaccinia Virus Oncolysis. *Cancer Gene Ther* **2013**, *20* (6), 342–350. https://doi.org/10.1038/cgt.2013.26.

(238) Hook, L. M.; Lubinski, J. M.; Jiang, M.; Pangburn, M. K.; Friedman, H. M. Herpes Simplex Virus Type 1 and 2 Glycoprotein C Prevents Complement-Mediated Neutralization Induced by Natural Immunoglobulin M Antibody. *J Virol* **2006**, *80* (8), 4038–4046. https://doi.org/10.1128/JVI.80.8.4038-4046.2006.

(239) Girgis, N. M.; DeHaven, B. C.; Xiao, Y.; Alexander, E.; Viner, K. M.; Isaacs, S. N. The Vaccinia Virus Complement Control Protein Modulates Adaptive Immune Responses during Infection. *J Virol* **2011**, *85* (6), 2547–2556. https://doi.org/10.1128/JVI.01474-10.

(240) Sahu, A.; Isaacs, S. N.; Soulika, A. M.; Lambris, J. D. Interaction of Vaccinia Virus Complement Control Protein with Human Complement Proteins: Factor I-Mediated Degradation of C3b to IC3b1 Inactivates the Alternative Complement Pathway. *J Immunol* **1998**, *160* (11), 5596–5604.

(241) Ebrahimi, S.; Ghorbani, E.; Khazaei, M.; Avan, A.; Ryzhikov, M.; Azadmanesh, K.; Hassanian, S. M. Interferon-Mediated Tumor Resistance to Oncolytic Virotherapy. *J Cell Biochem* **2017**, *118* (8), 1994–1999. https://doi.org/10.1002/jcb.25917.

(242)   Patel, M. R.; Dash, A.; Jacobson, B. A.; Ji, Y.; Baumann, D.; Ismail, K.; Kratzke, R. A. JAK/STAT Inhibition with Ruxolitinib Enhances Oncolytic Virotherapy in Non-Small Cell Lung Cancer Models. *Cancer Gene Ther* **2019**, *26* (11), 411–418. https://doi.org/10.1038/s41417-018-0074-6.

(243)   Ghonime, M. G.; Cassady, K. A. Combination Therapy Using Ruxolitinib and Oncolytic HSV Renders Resistant MPNSTs Susceptible to Virotherapy. *Cancer Immunol Res* **2018**, *6* (12), 1499–1510. https://doi.org/10.1158/2326-6066.CIR-18-0014.

(244)   Otsuki, A.; Patel, A.; Kasai, K.; Suzuki, M.; Kurozumi, K.; Antonio Chiocca, E.; Saeki, Y. Histone Deacetylase Inhibitors Augment Antitumor Efficacy of Herpes-Based Oncolytic Viruses. *Mol Ther* **2008**, *16* (9), 1546–1555. https://doi.org/10.1038/mt.2008.155.

(245)   Selman, M.; Ou, P.; Rousso, C.; Bergeron, A.; Krishnan, R.; Pikor, L.; Chen, A.; Keller, B. A.; Ilkow, C.; Bell, J. C.; Diallo, J.-S. Dimethyl Fumarate Potentiates Oncolytic Virotherapy through NF-KB Inhibition. *Sci Transl Med* **2018**, *10* (425). https://doi.org/10.1126/scitranslmed.aao1613.

(246)   Arulanandam, R.; Batenchuk, C.; Varette, O.; Zakaria, C.; Garcia, V.; Forbes, N. E.; Davis, C.; Krishnan, R.; Karmacharya, R.; Cox, J.; Sinha, A.; Babawy, A.; Waite, K.; Weinstein, E.; Falls, T.; Chen, A.; Hamill, J.; De Silva, N.; Conrad, D. P.; Atkins, H.; Garson, K.; Ilkow, C.; Kærn, M.; Vanderhyden, B.; Sonenberg, N.; Alain, T.; Le Boeuf, F.; Bell, J. C.; Diallo, J.-S. Microtubule Disruption Synergizes with Oncolytic Virotherapy by Inhibiting Interferon Translation and Potentiating Bystander Killing. *Nat Commun* **2015**, *6* (1), 6410. https://doi.org/10.1038/ncomms7410.

(247)   Fu, X.; Rivera, A.; Tao, L.; Zhang, X. Incorporation of the B18R Gene of Vaccinia Virus Into an Oncolytic Herpes Simplex Virus Improves Antitumor Activity. *Mol Ther* **2012**, *20* (10), 1871–1881. https://doi.org/10.1038/mt.2012.113.

(248)   Alemany, R.; Suzuki, K.; Curiel, D. T. Y. 2000. Blood Clearance Rates of Adenovirus Type 5 in Mice. *J Gen Virol 81* (11), 2605–2609. https://doi.org/10.1099/0022-1317-81-11-2605.

(249)   Moreno, S. G. Depleting Macrophages In Vivo with Clodronate-Liposomes. *Methods Mol Biol* **2018**, *1784*, 259–262. https://doi.org/10.1007/978-1-4939-7837-3_23.

(250)   van Rooijen, N.; Sanders, A.; van den Berg, T. K. Apoptosis of Macrophages Induced by Liposome-Mediated Intracellular Delivery of Clodronate and Propamidine. *J Immunol Methods* **1996**, *193* (1), 93–99. https://doi.org/10.1016/0022-1759(96)00056-7.

(251) Fulci, G.; Dmitrieva, N.; Gianni, D.; Fontana, E. J.; Pan, X.; Lu, Y.; Kaufman, C. S.; Kaur, B.; Lawler, S. E.; Lee, R. J.; Marsh, C. B.; Brat, D. J.; van Rooijen, N.; Rachamimov, A. S.; Hochberg, F. H.; Weissleder, R.; Martuza, R. L.; Chiocca, E. A. Depletion of Peripheral Macrophages and Brain Microglia Increases Brain Tumor Titers of Oncolytic Viruses. *Cancer Res* **2007**, *67* (19), 9398–9406. https://doi.org/10.1158/0008-5472.CAN-07-1063.

(252) Shashkova, E. V.; Doronin, K.; Senac, J. S.; Barry, M. A. Macrophage Depletion Combined with Anticoagulant Therapy Increases Therapeutic Window of Systemic Treatment with Oncolytic Adenovirus. *Cancer Res* **2008**, *68* (14), 5896–5904. https://doi.org/10.1158/0008-5472.CAN-08-0488.

(253) Brandstadter, J. D.; Yang, Y. Natural Killer Cell Responses to Viral Infection. *J Innate Immun* **2011**, *3* (3), 274–279. https://doi.org/10.1159/000324176.

(254) Björkström, N. K.; Strunz, B.; Ljunggren, H.-G. Natural Killer Cells in Antiviral Immunity. *Nat Rev Immunol* **2021**, 1–12. https://doi.org/10.1038/s41577-021-00558-3.

(255) Alvarez-Breckenridge, C. A.; Yu, J.; Kaur, B.; Caligiuri, M. A.; Chiocca, E. A. Deciphering the Multifaceted Relationship between Oncolytic Viruses and Natural Killer Cells. *Adv Virol* **2012**, *2012*, 1–14. https://doi.org/10.1155/2012/702839.

(256) Alvarez-Breckenridge, C. A.; Yu, J.; Price, R.; Wojton, J.; Pradarelli, J.; Mao, H.; Wei, M.; Wang, Y.; He, S.; Hardcastle, J.; Fernandez, S. A.; Kaur, B.; Lawler, S. E.; Vivier, E.; Mandelboim, O.; Moretta, A.; Caligiuri, M. A.; Chiocca, E. A. NK Cells Impede Glioblastoma Virotherapy through NKp30 and NKp46 Natural Cytotoxicity Receptors. *Nat Med* **2012**, *18* (12), 1827–1834. https://doi.org/10.1038/nm.3013.

(257) Han, J.; Chen, X.; Chu, J.; Xu, B.; Meisen, W. H.; Chen, L.; Zhang, L.; Zhang, J.; He, X.; Wang, Q.-E.; Chiocca, E. A.; Kaur, B.; Caligiuri, M. A.; Yu, J. TGFβ Treatment Enhances Glioblastoma Virotherapy by Inhibiting the Innate Immune Response. *Cancer Res* **2015**, *75* (24), 5273–5282. https://doi.org/10.1158/0008-5472.CAN-15-0894.

(258) Xu, B.; Ma, R.; Russell, L.; Yoo, J. Y.; Han, J.; Cui, H.; Yi, P.; Zhang, J.; Nakashima, H.; Dai, H.; Chiocca, E. A.; Kaur, B.; Caligiuri, M. A.; Yu, J. An Oncolytic Herpesvirus Expressing E-Cadherin Improves Survival in Mouse Models of Glioblastoma. *Nat Biotechnol* **2019**, *37* (1), 45–54. https://doi.org/10.1038/nbt.4302.

(259) Selin, L. K.; Welsh, R. M. Plasticity of T Cell Memory Responses to Viruses. *Immunity* **2004**, *20* (1), 5–16. https://doi.org/10.1016/S1074-7613(03)00356-X.

(260) Wiesel, M.; Walton, S.; Richter, K.; Oxenius, A. Virus-Specific CD8 T Cells: Activation, Differentiation and Memory Formation. *APMIS* **2009**, *117* (5–6), 356–381. https://doi.org/10.1111/j.1600-0463.2009.02459.x.

(261) Wherry, E. J.; Ahmed, R. Memory CD8 T-Cell Differentiation during Viral Infection. *J Virol* **2004**, *78* (11), 5535–5545. https://doi.org/10.1128/JVI.78.11.5535-5545.2004.

(262) Kaech, S. M.; Wherry, E. J.; Ahmed, R. Effector and Memory T-Cell Differentiation: Implications for Vaccine Development. *Nat Rev Immunol* **2002**, *2* (4), 251–262. https://doi.org/10.1038/nri778.

(263) Radbruch, A.; Muehlinghaus, G.; Luger, E. O.; Inamine, A.; Smith, K. G. C.; Dörner, T.; Hiepe, F. Competence and Competition: The Challenge of Becoming a Long-Lived Plasma Cell. *Nat Rev Immunol* **2006**, *6* (10), 741–750. https://doi.org/10.1038/nri1886.

(264) Simoni, Y.; Becht, E.; Fehlings, M.; Loh, C. Y.; Koo, S.-L.; Teng, K. W. W.; Yeong, J. P. S.; Nahar, R.; Zhang, T.; Kared, H.; Duan, K.; Ang, N.; Poidinger, M.; Lee, Y. Y.; Larbi, A.; Khng, A. J.; Tan, E.; Fu, C.; Mathew, R.; Teo, M.; Lim, W. T.; Toh, C. K.; Ong, B.-H.; Koh, T.; Hillmer, A. M.; Takano, A.; Lim, T. K. H.; Tan, E. H.; Zhai, W.; Tan, D. S. W.; Tan, I. B.; Newell, E. W. Bystander CD8+ T Cells Are Abundant and Phenotypically Distinct in Human Tumour Infiltrates. *Nature* **2018**, *557* (7706), 575–579. https://doi.org/10.1038/s41586-018-0130-2.

(265) Scheper, W.; Kelderman, S.; Fanchi, L. F.; Linnemann, C.; Bendle, G.; de Rooij, M. A. J.; Hirt, C.; Mezzadra, R.; Slagter, M.; Dijkstra, K.; Kluin, R. J. C.; Snaebjornsson, P.; Milne, K.; Nelson, B. H.; Zijlmans, H.; Kenter, G.; Voest, E. E.; Haanen, J. B. A. G.; Schumacher, T. N. Low and Variable Tumor Reactivity of the Intratumoral TCR Repertoire in Human Cancers. *Nat Med* **2019**, *25* (1), 89–94. https://doi.org/10.1038/s41591-018-0266-5.

(266) Samson, A.; Bentham, M. J.; Scott, K.; Nuovo, G.; Bloy, A.; Appleton, E.; Adair, R. A.; Dave, R.; Peckham-Cooper, A.; Toogood, G.; Nagamori, S.; Coffey, M.; Vile, R.; Harrington, K.; Selby, P.; Errington-Mais, F.; Melcher, A.; Griffin, S. Oncolytic Reovirus as a Combined Antiviral and Anti-Tumour Agent for the Treatment of Liver Cancer. *Gut* **2018**, *67* (3), 562–573. https://doi.org/10.1136/gutjnl-2016-312009.

(267) Ricca, J. M.; Oseledchyk, A.; Walther, T.; Liu, C.; Mangarin, L.; Merghoub, T.; Wolchok, J. D.; Zamarin, D. Pre-Existing Immunity to Oncolytic Virus Potentiates Its Immunotherapeutic Efficacy. *Mol Ther* **2018**, *26* (4), 1008–1019. https://doi.org/10.1016/j.ymthe.2018.01.019.

(268) Alvarez-Breckenridge, C. A.; Choi, B. D.; Suryadevara, C. M.; Chiocca, E. A. Potentiating Oncolytic Viral Therapy through an Understanding of the Initial Immune Responses to Oncolytic Viral Infection. *Curr Opin Virol* **2015**, *13*, 25–32. https://doi.org/10.1016/j.coviro.2015.03.015.

(269) Naik, J. D.; Twelves, C. J.; Selby, P. J.; Vile, R. G.; Chester, J. D. Immune Recruitment and Therapeutic Synergy: Keys to Optimizing Oncolytic Viral Therapy? *Clin Cancer Res* **2011**, *17* (13), 4214–4224. https://doi.org/10.1158/1078-0432.CCR-10-2848.

(270)   Niemann, J.; Woller, N.; Brooks, J.; Fleischmann-Mundt, B.; Martin, N. T.; Kloos, A.; Knocke, S.; Ernst, A. M.; Manns, M. P.; Kubicka, S.; Wirth, T. C.; Gerardy-Schahn, R.; Kühnel, F. Molecular Retargeting of Antibodies Converts Immune Defense against Oncolytic Viruses into Cancer Immunotherapy. *Nat Commun* **2019**, *10* (1), 3236. https://doi.org/10.1038/s41467-019-11137-5.

(271)   Ilett, E.; Kottke, T.; Donnelly, O.; Thompson, J.; Willmon, C.; Diaz, R.; Zaidi, S.; Coffey, M.; Selby, P.; Harrington, K.; Pandha, H.; Melcher, A.; Vile, R. Cytokine Conditioning Enhances Systemic Delivery and Therapy of an Oncolytic Virus. *Mol Ther* **2014**, *22* (10), 1851–1863. https://doi.org/10.1038/mt.2014.118.

(272)   Berkeley, R. A.; Steele, L. P.; Mulder, A. A.; Wollenberg, D. J. M. van den; Kottke, T. J.; Thompson, J.; Coffey, M.; Hoeben, R. C.; Vile, R. G.; Melcher, A.; Ilett, E. J. Antibody-Neutralized Reovirus Is Effective in Oncolytic Virotherapy. *Cancer Immunol Res* **2018**, *6* (10), 1161–1173. https://doi.org/10.1158/2326-6066.CIR-18-0309.

(273)   Iankov, I. D.; Pandey, M.; Harvey, M.; Griesmann, G. E.; Federspiel, M. J.; Russell, S. J. Immunoglobulin G Antibody-Mediated Enhancement of Measles Virus Infection Can Bypass the Protective Antiviral Immune Response. *JVI* **2006**, *80* (17), 8530–8540. https://doi.org/10.1128/JVI.00593-06.

(274)   Millar, D. G.; Ramjiawan, R. R.; Kawaguchi, K.; Gupta, N.; Chen, J.; Zhang, S.; Nojiri, T.; Ho, W. W.; Aoki, S.; Jung, K.; Chen, I.; Shi, F.; Heather, J. M.; Shigeta, K.; Morton, L. T.; Sepulveda, S.; Wan, L.; Joseph, R.; Minogue, E.; Khatri, A.; Bardia, A.; Ellisen, L. W.; Corcoran, R. B.; Hata, A. N.; Pai, S. I.; Jain, R. K.; Fukumura, D.; Duda, D. G.; Cobbold, M. Antibody-Mediated Delivery of Viral Epitopes to Tumors Harnesses CMV-Specific T Cells for Cancer Therapy. *Nat Biotechnol* **2020**. https://doi.org/10.1038/s41587-019-0404-8.

(275)   Rosato, P. C.; Wijeyesinghe, S.; Stolley, J. M.; Nelson, C. E.; Davis, R. L.; Manlove, L. S.; Pennell, C. A.; Blazar, B. R.; Chen, C. C.; Geller, M. A.; Vezys, V.; Masopust, D. Virus-Specific Memory T Cells Populate Tumors and Can Be Repurposed for Tumor Immunotherapy. *Nat Commun* **2019**, *10* (1), 567. https://doi.org/10.1038/s41467-019-08534-1.

(276)   Tähtinen, S.; Feola, S.; Capasso, C.; Laustio, N.; Groeneveldt, C.; Ylösmäki, E. O.; Ylösmäki, L.; Martins, B.; Fusciello, M.; Medeot, M.; Tagliamonte, M.; Chiaro, J.; Hamdan, F.; Peltonen, K.; Ranki, T.; Buonaguro, L.; Cerullo, V. Exploiting Pre-Existing Immunity to Enhance Oncolytic Cancer Immunotherapy. *Cancer Res* **2020**, canres.2062.2019. https://doi.org/10.1158/0008-5472.CAN-19-2062.

(277)   Sobol, P. T.; Boudreau, J. E.; Stephenson, K.; Wan, Y.; Lichty, B. D.; Mossman, K. L. Adaptive Antiviral Immunity Is a Determinant of the Therapeutic Success of Oncolytic Virotherapy. *Mol Ther* **2011**, *19* (2), 335–344. https://doi.org/10.1038/mt.2010.264.

(278)   Nelson, C. E.; Thompson, E. A.; Quarnstrom, C. F.; Fraser, K. A.; Seelig, D. M.; Bhela, S.; Burbach, B. J.; Masopust, D.; Vezys, V. Robust Iterative Stimulation with Self-Antigens Overcomes CD8+ T Cell Tolerance to Self- and Tumor Antigens. *Cell Reports* **2019**, *28* (12), 3092-3104.e5. https://doi.org/10.1016/j.celrep.2019.08.038.

(279)   Neefjes, J.; Jongsma, M. L. M.; Paul, P.; Bakke, O. Towards a Systems Understanding of MHC Class I and MHC Class II Antigen Presentation. *Nat Rev Immunol* **2011**, *11* (12), 823–836. https://doi.org/10.1038/nri3084.

(280)   Vyas, J. M.; Van der Veen, A. G.; Ploegh, H. L. The Known Unknowns of Antigen Processing and Presentation. *Nat Rev Immunol* **2008**, *8* (8), 607–618. https://doi.org/10.1038/nri2368.

(281)   Charles A Janeway, J.; Travers, P.; Walport, M.; Shlomchik, M. J. The Major Histocompatibility Complex and Its Functions. *Immunobiology: The Immune System in Health and Disease. 5th edition* **2001**.

(282)   Vigneron, N. Human Tumor Antigens and Cancer Immunotherapy. *BioMed Res Int* **2015**, *2015*, 1–17. https://doi.org/10.1155/2015/948501.

(283)   Lee, M. Y.; Jeon, J. W.; Sievers, C.; Allen, C. T. Antigen Processing and Presentation in Cancer Immunotherapy. *J Immunother Cancer* **2020**, *8* (2), e001111. https://doi.org/10.1136/jitc-2020-001111.

(284)   Zarour, H. M.; DeLeo, A.; Finn, O. J.; Storkus, W. J. Categories of Tumor Antigens. *Holland-Frei Cancer Medicine. 6th edition* **2003**.

(285)   Berinstein, N. L. Carcinoembryonic Antigen as a Target for Therapeutic Anticancer Vaccines: A Review. *JCO* **2002**, *20* (8), 2197–2207. https://doi.org/10.1200/JCO.2002.08.017.

(286)   Tan, H. L.; Yong, C.; Tan, B. Z.; Fong, W. J.; Padmanabhan, J.; Chin, A.; Ding, V.; Lau, A.; Zheng, L.; Bi, X.; Yang, Y.; Choo, A. Conservation of Oncofetal Antigens on Human Embryonic Stem Cells Enables Discovery of Monoclonal Antibodies against Cancer. *Sci Rep* **2018**, *8* (1), 11608. https://doi.org/10.1038/s41598-018-30070-z.

(287)   Gjerstorff, M. F.; Andersen, M. H.; Ditzel, H. J. Oncogenic Cancer/Testis Antigens: Prime Candidates for Immunotherapy. *Oncotarget* **2015**, *6* (18), 15772–15787.

(288)   Scanlan, M. J.; Gure, A. O.; Jungbluth, A. A.; Old, L. J.; Chen, Y.-T. Cancer/Testis Antigens: An Expanding Family of Targets for Cancer Immunotherapy. *Immunol Rev* **2002**, *188* (1), 22–32. https://doi.org/10.1034/j.1600-065X.2002.18803.x.

(289)   Tashiro, H.; Brenner, M. K. Immunotherapy against Cancer-Related Viruses. *Cell Res* **2017**, *27* (1), 59–73. https://doi.org/10.1038/cr.2016.153.

(290) Lin, C.-T.; Tsai, Y.-C.; He, L.; Calizo, R.; Chou, H.-H.; Chang, T.-C.; Soong, Y.-K.; Hung, C.-F.; Lai, C.-H. A DNA Vaccine Encoding a Codon-Optimized Human Papillomavirus Type 16 E6 Gene Enhances CTL Response and Anti-Tumor Activity. *J Biomed Sci* **2006**, *13* (4), 481–488. https://doi.org/10.1007/s11373-006-9086-6.

(291) Peng, S.; Tomson, T. T.; Trimble, C.; He, L.; Hung, C.-F.; Wu, T.-C. A Combination of DNA Vaccines Targeting Human Papillomavirus Type 16 E6 and E7 Generates Potent Antitumor Effects. *Gene Ther* **2006**, *13* (3), 257–265. https://doi.org/10.1038/sj.gt.3302646.

(292) Swartz, A. M.; Congdon, K. L.; Nair, S. K.; Li, Q.-J.; Herndon, J. E.; Suryadevara, C. M.; Riccione, K. A.; Archer, G. E.; Norberg, P. K.; Sanchez-Perez, L. A.; Sampson, J. H. A Conjoined Universal Helper Epitope Can Unveil Antitumor Effects of a Neoantigen Vaccine Targeting an MHC Class I-Restricted Neoepitope. *npj Vaccines* **2021**, *6* (1), 1–7. https://doi.org/10.1038/s41541-020-00273-5.

(293) Vormehr, M.; Reinhard, K.; Blatnik, R.; Josef, K.; Beck, J. D.; Salomon, N.; Suchan, M.; Selmi, A.; Vascotto, F.; Zerweck, J.; Wenschuh, H.; Diken, M.; Kreiter, S.; Türeci, Ö.; Riemer, A. B.; Sahin, U. A Non-Functional Neoepitope Specific CD8+ T-Cell Response Induced by Tumor Derived Antigen Exposure in Vivo. *OncoImmunology* **2019**, *8* (3), 1553478. https://doi.org/10.1080/2162402X.2018.1553478.

(294) Mylonas, R.; Beer, I.; Iseli, C.; Chong, C.; Pak, H.-S.; Gfeller, D.; Coukos, G.; Xenarios, I.; Müller, M.; Bassani-Sternberg, M. Estimating the Contribution of Proteasomal Spliced Peptides to the HLA-I Ligandome*. *Mol Cell Proteomics* **2018**, *17* (12), 2347–2357. https://doi.org/10.1074/mcp.RA118.000877.

(295) Smart, A. C.; Margolis, C. A.; Pimentel, H.; He, M. X.; Miao, D.; Adeegbe, D.; Fugmann, T.; Wong, K.-K.; Van Allen, E. M. Intron Retention Is a Source of Neoepitopes in Cancer. *Nat Biotechnol* **2018**, *36* (11), 1056–1058. https://doi.org/10.1038/nbt.4239.

(296) Shen, L.; Zhang, J.; Lee, H.; Batista, M. T.; Johnston, S. A. RNA Transcription and Splicing Errors as a Source of Cancer Frameshift Neoantigens for Vaccines. *Sci Rep* **2019**, *9* (1), 14184. https://doi.org/10.1038/s41598-019-50738-4.

(297) Caron, E.; Vincent, K.; Fortier, M.-H.; Laverdure, J.-P.; Bramoulle, A.; Hardy, M.-P.; Voisin, G.; Roux, P. P.; Lemieux, S.; Thibault, P.; Perreault, C. The MHC I Immunopeptidome Conveys to the Cell Surface an Integrative View of Cellular Regulation. *Mol Syst Biol* **2014**, *7* (1), 533–533. https://doi.org/10.1038/msb.2011.68.

(298) Pontarotti, P.; Abi-Rached, L.; Yeh, J.-H.; Paganini, J. Self-Peptidome Variation Shapes Individual Immune Responses. *Trends Genet* **2021**, *37* (5), 414–420. https://doi.org/10.1016/j.tig.2020.10.001.

(299)   Sarkizova, S.; Klaeger, S.; Le, P. M.; Li, L. W.; Oliveira, G.; Keshishian, H.; Hartigan, C. R.; Zhang, W.; Braun, D. A.; Ligon, K. L.; Bachireddy, P.; Zervantonakis, I. K.; Rosenbluth, J. M.; Ouspenskaia, T.; Law, T.; Justesen, S.; Stevens, J.; Lane, W. J.; Eisenhaure, T.; Lan Zhang, G.; Clauser, K. R.; Hacohen, N.; Carr, S. A.; Wu, C. J.; Keskin, D. B. A Large Peptidome Dataset Improves HLA Class I Epitope Prediction across Most of the Human Population. *Nat Biotechnol* **2020**, *38* (2), 199–209. https://doi.org/10.1038/s41587-019-0322-9.

(300)   Li, X. C.; Raghavan, M. Structure and Function of Major Histocompatibility Complex (MHC) Class I Antigens. *Curr Opin Organ Transplant* **2010**, *15* (4), 499–504. https://doi.org/10.1097/MOT.0b013e32833bfb33.

(301)   Zhang, Y.; Williams, D. B. Assembly of MHC Class I Molecules within the Endoplasmic Reticulum. *Immunol Res* **2006**, *35* (1), 151–162. https://doi.org/10.1385/IR:35:1:151.

(302)   Hughes, E. A.; Hammond, C.; Cresswell, P. Misfolded Major Histocompatibility Complex Class I Heavy Chains Are Translocated into the Cytoplasm and Degraded by the Proteasome. *PNAS* **1997**, *94* (5), 1896–1901. https://doi.org/10.1073/pnas.94.5.1896.

(303)   Ljunggren, H.-G.; Stam, N. J.; Öhlén, C.; Neefjes, J. J.; Höglund, P.; Heemels, M.-T.; Bastin, J.; Schumacher, T. N. M.; Townsend, A.; Kärre, K.; Ploegh, H. L. Empty MHC Class I Molecules Come out in the Cold. *Nature* **1990**, *346* (6283), 476–480. https://doi.org/10.1038/346476a0.

(304)   Middleton, D.; Menchaca, L.; Rood, H.; Komerofsky, R. New Allele Frequency Database: Http://Www.Allelefrequencies.Net. *Tissue Antigens* **2003**, *61* (5), 403–407. https://doi.org/10.1034/j.1399-0039.2003.00062.x.

(305)   Crux, N. B.; Elahi, S. Human Leukocyte Antigen (HLA) and Immune Regulation: How Do Classical and Non-Classical HLA Alleles Modulate Immune Response to Human Immunodeficiency Virus and Hepatitis C Virus Infections? *Front Immunol* **2017**, *8*. https://doi.org/10.3389/fimmu.2017.00832.

(306)   Bjorkman, P. J.; Saper, M. A.; Samraoui, B.; Bennett, W. S.; Strominger, J. L.; Wiley, D. C. The Foreign Antigen Binding Site and T Cell Recognition Regions of Class I Histocompatibility Antigens. *Nature* **1987**, *329* (6139), 512–518. https://doi.org/10.1038/329512a0.

(307)   Marty, R.; Kaabinejadian, S.; Rossell, D.; Slifker, M. J.; van de Haar, J.; Engin, H. B.; de Prisco, N.; Ideker, T.; Hildebrand, W. H.; Font-Burgada, J.; Carter, H. MHC-I Genotype Restricts the Oncogenic Mutational Landscape. *Cell* **2017**, *171* (6), 1272-1283.e15. https://doi.org/10.1016/j.cell.2017.09.050.

(308)   La Gruta, N. L.; Gras, S.; Daley, S. R.; Thomas, P. G.; Rossjohn, J. Understanding the Drivers of MHC Restriction of T Cell Receptors. *Nat Rev Immunol* **2018**, *18* (7), 467–478. https://doi.org/10.1038/s41577-018-0007-5.

(309)   Ciechanover, A. Intracellular Protein Degradation: From a Vague Idea Thru the Lysosome and the Ubiquitin–Proteasome System and onto Human Diseases and Drug Targeting. *Cell Death Differ* **2005**, *12* (9), 1178–1190. https://doi.org/10.1038/sj.cdd.4401692.

(310)   Rock, K. L.; Gramm, C.; Rothstein, L.; Clark, K.; Stein, R.; Dick, L.; Hwang, D.; Goldberg, A. L. Inhibitors of the Proteasome Block the Degradation of Most Cell Proteins and the Generation of Peptides Presented on MHC Class I Molecules. *Cell* **1994**, *78* (5), 761–771. https://doi.org/10.1016/S0092-8674(94)90462-6.

(311)   Schubert, U.; Antón, L. C.; Gibbs, J.; Norbury, C. C.; Yewdell, J. W.; Bennink, J. R. Rapid Degradation of a Large Fraction of Newly Synthesized Proteins by Proteasomes. *Nature* **2000**, *404* (6779), 770–774. https://doi.org/10.1038/35008096.

(312)   Murata, S.; Takahama, Y.; Kasahara, M.; Tanaka, K. The Immunoproteasome and Thymoproteasome: Functions, Evolution and Human Disease. *Nat Immunol* **2018**, *19* (9), 923–931. https://doi.org/10.1038/s41590-018-0186-z.

(313)   Huber, E. M.; Basler, M.; Schwab, R.; Heinemeyer, W.; Kirk, C. J.; Groettrup, M.; Groll, M. Immuno- and Constitutive Proteasome Crystal Structures Reveal Differences in Substrate and Inhibitor Specificity. *Cell* **2012**, *148* (4), 727–738. https://doi.org/10.1016/j.cell.2011.12.030.

(314)   Shin, E.-C.; Seifert, U.; Kato, T.; Rice, C. M.; Feinstone, S. M.; Kloetzel, P.-M.; Rehermann, B. Virus-Induced Type I IFN Stimulates Generation of Immunoproteasomes at the Site of Infection. *J Clin Invest* **2006**, *116* (11), 3006–3014. https://doi.org/10.1172/JCI29832.

(315)   Griffin, T. A.; Nandi, D.; Cruz, M.; Fehling, H. J.; Kaer, L. V.; Monaco, J. J.; Colbert, R. A. Immunoproteasome Assembly: Cooperative Incorporation of Interferon γ (IFN-γ)–Inducible Subunits. *J Exp Med* **1998**, *187* (1), 97–104. https://doi.org/10.1084/jem.187.1.97.

(316)   Driscoll, J.; Brown, M. G.; Finley, D.; Monaco, J. J. MHC-Linked LMP Gene Products Specifically Alter Peptidase Activities of the Proteasome. *Nature* **1993**, *365* (6443), 262–264. https://doi.org/10.1038/365262a0.

(317)   Groettrup, M.; Standera, S.; Stohwasser, R.; Kloetzel, P. M. The Subunits MECL-1 and LMP2 Are Mutually Required for Incorporation into the 20S Proteasome. *PNAS* **1997**, *94* (17), 8970–8975.

(318)   Boes, B.; Hengel, H.; Ruppert, T.; Multhaup, G.; Koszinowski, U. H.; Kloetzel, P. M. Interferon Gamma Stimulation Modulates the Proteolytic Activity and Cleavage Site Preference of 20S Mouse Proteasomes. *J Exp Med* **1994**, *179* (3), 901–909. https://doi.org/10.1084/jem.179.3.901.

(319) Suh, W. K.; Cohen-Doyle, M. F.; Fruh, K.; Wang, K.; Peterson, P. A.; Williams, D. B. Interaction of MHC Class I Molecules with the Transporter Associated with Antigen Processing. *Science* **1994**, *264* (5163), 1322–1326. https://doi.org/10.1126/science.8191286.

(320) Peaper, D. R.; Cresswell, P. Regulation of MHC Class I Assembly and Peptide Binding. *Annu Rev Cell Dev Biol* **2008**, *24* (1), 343–368. https://doi.org/10.1146/annurev.cellbio.24.110707.175347.

(321) Schumacher, T. N.; Kantesaria, D. V.; Heemels, M. T.; Ashton-Rickardt, P. G.; Shepherd, J. C.; Fruh, K.; Yang, Y.; Peterson, P. A.; Tonegawa, S.; Ploegh, H. L. Peptide Length and Sequence Specificity of the Mouse TAP1/TAP2 Translocator. *J Exp Med* **1994**, *179* (2), 533–540. https://doi.org/10.1084/jem.179.2.533.

(322) Burgevin, A.; Saveanu, L.; Kim, Y.; Barilleau, É.; Kotturi, M.; Sette, A.; van Endert, P.; Peters, B. A Detailed Analysis of the Murine TAP Transporter Substrate Specificity. *PLoS One* **2008**, *3* (6), e2402. https://doi.org/10.1371/journal.pone.0002402.

(323) Momburg, F.; Roelse, J.; Howard, J. C.; Butcher, G. W.; Hämmerling, G. J.; Neefjes, J. J. Selectivity of MHC-Encoded Peptide Transporters from Human, Mouse and Rat. *Nature* **1994**, *367* (6464), 648–651. https://doi.org/10.1038/367648a0.

(324) Perria, C. L.; Rajamanickam, V.; Lapinski, P. E.; Raghavan, M. Catalytic Site Modifications of TAP1 and TAP2 and Their Functional Consequences. *J Biol Chem* **2006**, *281* (52), 39839–39851. https://doi.org/10.1074/jbc.M605492200.

(325) York, I. A.; Brehm, M. A.; Zendzian, S.; Towne, C. F.; Rock, K. L. Endoplasmic Reticulum Aminopeptidase 1 (ERAP1) Trims MHC Class I-Presented Peptides in Vivo and Plays an Important Role in Immunodominance. *PNAS* **2006**, *103* (24), 9202–9207.

(326) Castro, L. de; A, J. How ERAP1 and ERAP2 Shape the Peptidomes of Disease-Associated MHC-I Proteins. *Front Immunol* **2018**, *9*. https://doi.org/10.3389/fimmu.2018.02463.

(327) Diedrich, G.; Bangia, N.; Pan, M.; Cresswell, P. A Role for Calnexin in the Assembly of the MHC Class I Loading Complex in the Endoplasmic Reticulum. *J Immunol* **2001**, *166* (3), 1703–1709. https://doi.org/10.4049/jimmunol.166.3.1703.

(328) Wada, I.; Imai, S.; Kai, M.; Sakane, F.; Kanoh, H. Chaperone Function of Calreticulin When Expressed in the Endoplasmic Reticulum as the Membrane-Anchored and Soluble Forms. *J Biol Chem* **1995**, *270* (35), 20298–20304. https://doi.org/10.1074/jbc.270.35.20298.

(329) Hughes, E. A.; Cresswell, P. The Thiol Oxidoreductase ERp57 Is a Component of the MHC Class I Peptide-Loading Complex. *Curr Biol* **1998**, *8* (12), 709–713. https://doi.org/10.1016/S0960-9822(98)70278-7.

(330) Morrice, N. A.; Powis, S. J. A Role for the Thiol-Dependent Reductase ERp57 in the Assembly of MHC Class I Molecules. *Curr Biol* **1998**, *8* (12), 713–716. https://doi.org/10.1016/S0960-9822(98)70279-9.

(331) Peaper, D. R.; Wearsch, P. A.; Cresswell, P. Tapasin and ERp57 Form a Stable Disulfide-Linked Dimer within the MHC Class I Peptide-Loading Complex. *The EMBO Journal* **2005**, *24* (20), 3613–3623. https://doi.org/10.1038/sj.emboj.7600814.

(332) Sadasivan, B.; Lehner, P. J.; Ortmann, B.; Spies, T.; Cresswell, P. Roles for Calreticulin and a Novel Glycoprotein, Tapasin, in the Interaction of MHC Class I Molecules with TAP. *Immunity* **1996**, *5* (2), 103–114. https://doi.org/10.1016/S1074-7613(00)80487-2.

(333) Leone, P.; Shin, E.-C.; Perosa, F.; Vacca, A.; Dammacco, F.; Racanelli, V. MHC Class I Antigen Processing and Presenting Machinery: Organization, Function, and Defects in Tumor Cells. *J Natl Cancer Inst* **2013**, *105* (16), 1172–1187. https://doi.org/10.1093/jnci/djt184.

(334) Motal, U. M. A.; Zhou, X.; Joki, A.; Siddiqi, A. R.; Srinivasa, B. R.; Stenvall, K.; Dahmén, J.; Jondal, M. Major Histocompatibility Complex Class I-Binding Peptides Are Recycled to the Cell Surface after Internalization. *Eur J Immunol* **1993**, *23* (12), 3224–3229. https://doi.org/10.1002/eji.1830231227.

(335) Montealegre, S.; van Endert, P. M. Endocytic Recycling of MHC Class I Molecules in Non-Professional Antigen Presenting and Dendritic Cells. *Front Immunol* **2019**, *9*. https://doi.org/10.3389/fimmu.2018.03098.

(336) Mahmutefendić, H.; Blagojević, G.; Kučić, N.; Lučin, P. Constitutive Internalization of Murine MHC Class I Molecules. *J Cell Physiol* **2007**, *210* (2), 445–455. https://doi.org/10.1002/jcp.20877.

(337) Maxfield, F. R.; McGraw, T. E. Endocytic Recycling. *Nat Rev Mol Cell Biol* **2004**, *5* (2), 121–132. https://doi.org/10.1038/nrm1315.

(338) Liu, J.; Gao, G. F. Major Histocompatibility Complex: Interaction with Peptides. In *eLS*; American Cancer Society, 2011. https://doi.org/10.1002/9780470015902.a0000922.pub2.

(339) Liu, J.; Wu, P.; Gao, F.; Qi, J.; Kawana-Tachikawa, A.; Xie, J.; Vavricka, C. J.; Iwamoto, A.; Li, T.; Gao, G. F. Novel Immunodominant Peptide Presentation Strategy: A Featured HLA-A*2402-Restricted Cytotoxic T-Lymphocyte Epitope Stabilized by Intrachain Hydrogen Bonds from Severe Acute Respiratory Syndrome Coronavirus Nucleocapsid Protein. *J Virol* **2010**, *84* (22), 11849–11857. https://doi.org/10.1128/JVI.01464-10.

(340)   Cole, D. K.; Edwards, E. S.; Wynn, K. K.; Clement, M.; Miles, J. J.; Ladell, K.; Ekeruche, J.; Gostick, E.; Adams, K.; Skowera, A.; Peakman, M.; Wooldridge, L.; Price, D. A.; Sewell, A. K. Modification of MHC Anchor Residues Generates Heteroclitic Peptides That Alter TCR Binding and T-Cell Recognition. *J Immunol* **2010**, *185* (4), 2600–2610. https://doi.org/10.4049/jimmunol.1000629.

(341)   van Bleek, G. M.; Nathenson, S. G. The Structure of the Antigen-Binding Groove of Major Histocompatibility Complex Class I Molecules Determines Specific Selection of Self-Peptides. *PNAS* **1991**, *88* (24), 11032–11036. https://doi.org/10.1073/pnas.88.24.11032.

(342)   Zhang, W.; Young, A.; Imarai, M.; Nathenson, S. G.; Sacchettini, J. Crystal Structure of the Major Histocompatibility Complex Class I H-2Kb Molecule Containing a Single Viral Peptide: Implications for Peptide Binding and T-Cell Receptor Recognition. *PNAS 89* (17), 8403–8407.

(343)   Garrett, T. P. J.; Saper, M. A.; Bjorkman, P. J.; Strominger, J. L.; Wiley, D. C. Specificity Pockets for the Side Chains of Peptide Antigens in HLA-Aw68. *Nature* **1989**, *342* (6250), 692–696. https://doi.org/10.1038/342692a0.

(344)   Abastado, J. P.; Casrouge, A.; Kourilsky, P. Differential Role of Conserved and Polymorphic Residues of the Binding Groove of MHC Class I Molecules in the Selection of Peptides. *J Immunol* **1993**, *151* (7), 3569–3575.

(345)   Mitaksov, V.; Fremont, D. H. Structural Definition of the H-2Kd Peptide-Binding Motif. *J Biol Chem* **2006**, *281* (15), 10618–10625. https://doi.org/10.1074/jbc.M510511200.

(346)   Falk, K.; Rötzschke, O.; Stevanovié, S.; Jung, G.; Rammensee, H.-G. Allele-Specific Motifs Revealed by Sequencing of Self-Peptides Eluted from MHC Molecules. *Nature* **1991**, *351* (6324), 290–296. https://doi.org/10.1038/351290a0.

(347)   Rammensee, H. G.; Falk, K.; Rötzschke, O. Peptides Naturally Presented by MHC Class I Molecules. *Annu Rev Immunol* **1993**, *11* (1), 213–244. https://doi.org/10.1146/annurev.iy.11.040193.001241.

(348)   Ruppert, J.; Sidney, J.; Celis, E.; Kubo, R. T.; Grey, H. M.; Sette, A. Prominent Role of Secondary Anchor Residues in Peptide Binding to HLA-A2.1 Molecules. *Cell* **1993**, *74* (5), 929–937. https://doi.org/10.1016/0092-8674(93)90472-3.

(349)   Saito, Y.; Peterson, P. A.; Matsumura, M. Quantitation of Peptide Anchor Residue Contributions to Class I Major Histocompatibility Complex Molecule Binding. *J Biol Chem* **1993**, *268* (28), 21309–21317. https://doi.org/10.1016/S0021-9258(19)36925-X.

(350)   Paul, S.; Weiskopf, D.; Angelo, M. A.; Sidney, J.; Peters, B.; Sette, A. HLA Class I Alleles Are Associated with Peptide-Binding Repertoires of Different Size, Affinity, and Immunogenicity. *J Immunol* **2013**, *191* (12), 5831–5839. https://doi.org/10.4049/jimmunol.1302101.

(351)   Paul, S.; Grifoni, A.; Peters, B.; Sette, A. Major Histocompatibility Complex Binding, Eluted Ligands, and Immunogenicity: Benchmark Testing and Predictions. *Front Immunol* **2020**, *10*. https://doi.org/10.3389/fimmu.2019.03151.

(352)   Wang, S.; Li, J.; Chen, X.; Wang, L.; Liu, W.; Wu, Y. Analyzing the Effect of Peptide-HLA-Binding Ability on the Immunogenicity of Potential CD8+ and CD4+ T Cell Epitopes in a Large Dataset. *Immunol Res* **2016**, *64* (4), 908–918. https://doi.org/10.1007/s12026-016-8795-9.

(353)   Rasmussen, M.; Fenoy, E.; Harndahl, M.; Kristensen, A. B.; Nielsen, I. K.; Nielsen, M.; Buus, S. Pan-Specific Prediction of Peptide-MHC-I Complex Stability; a Correlate of T Cell Immunogenicity. *J Immunol* **2016**, *197* (4), 1517–1524. https://doi.org/10.4049/jimmunol.1600582.

(354)   Wearsch, P. A.; Cresswell, P. Selective Loading of High-Affinity Peptides onto Major Histocompatibility Complex Class I Molecules by the Tapasin-ERp57 Heterodimer. *Nat Immunol* **2007**, *8* (8), 873–881. https://doi.org/10.1038/ni1485.

(355)   Williams, A. P.; Peh, C. A.; Purcell, A. W.; McCluskey, J.; Elliott, T. Optimization of the MHC Class I Peptide Cargo Is Dependent on Tapasin. *Immunity* **2002**, *16* (4), 509–520. https://doi.org/10.1016/S1074-7613(02)00304-7.

(356)   Hammer, G. E.; Gonzalez, F.; James, E.; Nolla, H.; Shastri, N. In the Absence of Aminopeptidase ERAAP, MHC Class I Molecules Present Many Unstable and Highly Immunogenic Peptides. *Nat Immunol* **2007**, *8* (1), 101–108. https://doi.org/10.1038/ni1409.

(357)   Hammer, G. E.; Kanaseki, T.; Shastri, N. The Final Touches Make Perfect the Peptide-MHC Class I Repertoire. *Immunity* **2007**, *26* (4), 397–406. https://doi.org/10.1016/j.immuni.2007.04.003.

(358)   Antunes, D. A.; Devaurs, D.; Moll, M.; Lizée, G.; Kavraki, L. E. General Prediction of Peptide-MHC Binding Modes Using Incremental Docking: A Proof of Concept. *Sci Rep* **2018**, *8* (1), 4327. https://doi.org/10.1038/s41598-018-22173-4.

(359)   Carbone, F. R.; Bevan, M. J. Class I-Restricted Processing and Presentation of Exogenous Cell-Associated Antigen in Vivo. *J Exp Med* **1990**, *171* (2), 377–387. https://doi.org/10.1084/jem.171.2.377.

(360)   Joffre, O. P.; Segura, E.; Savina, A.; Amigorena, S. Cross-Presentation by Dendritic Cells. *Nat Rev Immunol* **2012**, *12* (8), 557–569. https://doi.org/10.1038/nri3254.

(361) Gutiérrez-Martínez, E.; Planès, R.; Anselmi, G.; Reynolds, M.; Menezes, S.; Adiko, A. C.; Saveanu, L.; Guermonprez, P. Cross-Presentation of Cell-Associated Antigens by MHC Class I in Dendritic Cell Subsets. *Front Immunol* **2015**, *6*. https://doi.org/10.3389/fimmu.2015.00363.

(362) Adiko, A. C.; Babdor, J.; Gutiérrez-Martínez, E.; Guermonprez, P.; Saveanu, L. Intracellular Transport Routes for MHC I and Their Relevance for Antigen Cross-Presentation. *Front Immunol* **2015**, *6*. https://doi.org/10.3389/fimmu.2015.00335.

(363) Heath, W. R.; Carbone, F. R. Cross-Presentation in Viral Immunity and Self-Tolerance. *Nat Rev Immunol* **2001**, *1* (2), 126–134. https://doi.org/10.1038/35100512.

(364) Guermonprez, P.; Saveanu, L.; Kleijmeer, M.; Davoust, J.; van Endert, P.; Amigorena, S. ER–Phagosome Fusion Defines an MHC Class I Cross-Presentation Compartment in Dendritic Cells. *Nature* **2003**, *425* (6956), 397–402. https://doi.org/10.1038/nature01911.

(365) Rodriguez, A.; Regnault, A.; Kleijmeer, M.; Ricciardi-Castagnoli, P.; Amigorena, S. Selective Transport of Internalized Antigens to the Cytosol for MHC Class I Presentation in Dendritic Cells. *Nat Cell Biol* **1999**, *1* (6), 362–368. https://doi.org/10.1038/14058.

(366) Pfeifer, J. D.; Wick, M. J.; Roberts, R. L.; Findlay, K.; Normark, S. J.; Harding, C. V. Phagocytic Processing of Bacterial Antigens for Class I MHC Presentation to T Cells. *Nature* **1993**, *361* (6410), 359–362. https://doi.org/10.1038/361359a0.

(367) Shen, L.; Sigal, L. J.; Boes, M.; Rock, K. L. Important Role of Cathepsin S in Generating Peptides for TAP-Independent MHC Class I Crosspresentation In Vivo. *Immunity* **2004**, *21* (2), 155–165. https://doi.org/10.1016/j.immuni.2004.07.004.

(368) Lázaro, S.; Gamarra, D.; Del Val, M. Proteolytic Enzymes Involved in MHC Class I Antigen Processing: A Guerrilla Army That Partners with the Proteasome. *Mol Immunol* **2015**, *68* (2, Part A), 72–76. https://doi.org/10.1016/j.molimm.2015.04.014.

(369) Basha, G.; Omilusik, K.; Chavez-Steenbock, A.; Reinicke, A. T.; Lack, N.; Choi, K. B.; Jefferies, W. A. A CD74-Dependent MHC Class I Endolysosomal Cross-Presentation Pathway. *Nat Immunol* **2012**, *13* (3), 237–245. https://doi.org/10.1038/ni.2225.

(370) Cai, L.; Michelakos, T.; Yamada, T.; Fan, S.; Wang, X.; Schwab, J. H.; Ferrone, C. R.; Ferrone, S. Defective HLA Class I Antigen Processing Machinery in Cancer. *Cancer Immunol Immunother* **2018**, *67* (6), 999–1009. https://doi.org/10.1007/s00262-018-2131-2.

(371) O'Donnell, J. S.; Teng, M. W. L.; Smyth, M. J. Cancer Immunoediting and Resistance to T Cell-Based Immunotherapy. *Nat Rev Clin Oncol* **2019**, *16* (3), 151–167. https://doi.org/10.1038/s41571-018-0142-8.

(372) Dhatchinamoorthy, K.; Colbert, J. D.; Rock, K. L. Cancer Immune Evasion Through Loss of MHC Class I Antigen Presentation. *Front Immunol* **2021**, *12*. https://doi.org/10.3389/fimmu.2021.636568.

(373) Kaer, L. V.; Ashton-Rickardt, P. G.; Ploegh, H. L.; Tonegawa, S. TAP1 Mutant Mice Are Deficient in Antigen Presentation, Surface Class I Molecules, and CD4−8+ T Cells. *Cell* **1992**, *71* (7), 1205–1214. https://doi.org/10.1016/S0092-8674(05)80068-6.

(374) Kincaid, E. Z.; Che, J. W.; York, I.; Escobar, H.; Reyes-Vargas, E.; Delgado, J. C.; Welsh, R. M.; Karow, M. L.; Murphy, A. J.; Valenzuela, D. M.; Yancopoulos, G. D.; Rock, K. L. Mice Completely Lacking Immunoproteasomes Show Major Changes in Antigen Presentation. *Nat Immunol* **2012**, *13* (2), 129–135. https://doi.org/10.1038/ni.2203.

(375) Fridman, W. H.; Pagès, F.; Sautès-Fridman, C.; Galon, J. The Immune Contexture in Human Tumours: Impact on Clinical Outcome. *Nat Rev Cancer* **2012**, *12* (4), 298–306. https://doi.org/10.1038/nrc3245.

(376) Romero, I.; Garrido, C.; Algarra, I.; Chamorro, V.; Collado, A.; Garrido, F.; Garcia-Lora, A. M. MHC Intratumoral Heterogeneity May Predict Cancer Progression and Response to Immunotherapy. *Front Immunol* **2018**, *9*. https://doi.org/10.3389/fimmu.2018.00102.

(377) Schrörs, B.; Lübcke, S.; Lennerz, V.; Fatho, M.; Bicker, A.; Wölfel, C.; Derigs, P.; Hankeln, T.; Schadendorf, D.; Paschen, A.; Wölfel, T. HLA Class I Loss in Metachronous Metastases Prevents Continuous T Cell Recognition of Mutated Neoantigens in a Human Melanoma Model. *Oncotarget* **2017**, *8* (17), 28312–28327. https://doi.org/10.18632/oncotarget.16048.

(378) Campo, A. B. del; Kyte, J. A.; Carretero, J.; Zinchencko, S.; Méndez, R.; González-Aseguinolaza, G.; Ruiz-Cabello, F.; Aamdal, S.; Gaudernack, G.; Garrido, F.; Aptsiauri, N. Immune Escape of Cancer Cells with Beta2-Microglobulin Loss over the Course of Metastatic Melanoma. *Int J Cancer* **2014**, *134* (1), 102–113. https://doi.org/10.1002/ijc.28338.

(379) McGranahan, N.; Rosenthal, R.; Hiley, C. T.; Rowan, A. J.; Watkins, T. B. K.; Wilson, G. A.; Birkbak, N. J.; Veeriah, S.; Van Loo, P.; Herrero, J.; Swanton, C.; Swanton, C.; Jamal-Hanjani, M.; Veeriah, S.; Shafi, S.; Czyzewska-Khan, J.; Johnson, D.; Laycock, J.; Bosshard-Carter, L.; Rosenthal, R.; Gorman, P.; Hynds, R. E.; Wilson, G.; Birkbak, N. J.; Watkins, T. B. K.; McGranahan, N.; Horswell, S.; Mitter, R.; Escudero, M.; Stewart, A.; Van Loo, P.; Rowan, A.; Xu, H.; Turajlic, S.; Hiley, C.; Abbosh, C.; Goldman, J.; Stone, R. K.; Denner, T.; Matthews, N.; Elgar, G.; Ward, S.; Costa, M.; Begum, S.; Phillimore, B.; Chambers, T.; Nye, E.; Graca, S.; Al Bakir, M.; Joshi, K.; Furness, A.; Ben Aissa, A.; Wong, Y. N. S.; Georgiou, A.; Quezada, S.; Hartley, J. A.; Lowe, H. L.; Herrero, J.; Lawrence, D.; Hayward, M.; Panagiotopoulos, N.; Kolvekar, S.; Falzon, M.; Borg, E.; Marafioti, T.; Simeon, C.;

Hector, G.; Smith, A.; Aranda, M.; Novelli, M.; Oukrif, D.; Janes, S. M.; Thakrar, R.; Forster, M.; Ahmad, T.; Lee, S. M.; Papadatos-Pastos, D.; Carnell, D.; Mendes, R.; George, J.; Navani, N.; Ahmed, A.; Taylor, M.; Choudhary, J.; Summers, Y.; Califano, R.; Taylor, P.; Shah, R.; Krysiak, P.; Rammohan, K.; Fontaine, E.; Booton, R.; Evison, M.; Crosbie, P.; Moss, S.; Idries, F.; Joseph, L.; Bishop, P.; Chaturved, A.; Quinn, A. M.; Doran, H.; Leek, A.; Harrison, P.; Moore, K.; Waddington, R.; Novasio, J.; Blackhall, F.; Rogan, J.; Smith, E.; Dive, C.; Tugwood, J.; Brady, G.; Rothwell, D. G.; Chemi, F.; Pierce, J.; Gulati, S.; Naidu, B.; Langman, G.; Trotter, S.; Bellamy, M.; Bancroft, H.; Kerr, A.; Kadiri, S.; Webb, J.; Middleton, G.; Djearaman, M.; Fennell, D.; Shaw, J. A.; Le Quesne, J.; Moore, D.; Nakas, A.; Rathinam, S.; Monteiro, W.; Marshall, H.; Nelson, L.; Bennett, J.; Riley, J.; Primrose, L.; Martinson, L.; Anand, G.; Khan, S.; Amadi, A.; Nicolson, M.; Kerr, K.; Palmer, S.; Remmen, H.; Miller, J.; Buchan, K.; Chetty, M.; Gomersall, L.; Lester, J.; Edwards, A.; Morgan, F.; Adams, H.; Davies, H.; Kornaszewska, M.; Attanoos, R.; Lock, S.; Verjee, A.; MacKenzie, M.; Wilcox, M.; Bell, H.; Hackshaw, A.; Ngai, Y.; Smith, S.; Gower, N.; Ottensmeier, C.; Chee, S.; Johnson, B.; Alzetani, A.; Shaw, E.; Lim, E.; De Sousa, P.; Barbosa, M. T.; Bowman, A.; Jordan, S.; Rice, A.; Raubenheimer, H.; Proli, C.; Cufari, M. E.; Ronquillo, J. C.; Kwayie, A.; Bhayani, H.; Hamilton, M.; Bakar, Y.; Mensah, N.; Ambrose, L.; Devaraj, A.; Buderi, S.; Finch, J.; Azcarate, L.; Chavan, H.; Green, S.; Mashinga, H.; Nicholson, A. G.; Lau, K.; Sheaff, M.; Schmid, P.; Conibear, J.; Ezhil, V.; Ismail, B.; Irvin-sellers, M.; Prakash, V.; Russell, P.; Light, T.; Horey, T.; Danson, S.; Bury, J.; Edwards, J.; Hill, J.; Matthews, S.; Kitsanta, Y.; Suvarna, K.; Fisher, P.; Keerio, A. D.; Shackcloth, M.; Gosney, J.; Postmus, P.; Feeney, S.; Asante-Siaw, J.; Aerts, H. J. W. L.; Dentro, S.; Dessimoz, C. Allele-Specific HLA Loss and Immune Escape in Lung Cancer Evolution. *Cell* **2017**, *171* (6), 1259-1271.e11. https://doi.org/10.1016/j.cell.2017.10.001.

(380) Benitez, R.; Godelaine, D.; Lopez-Nevot, M. A.; Brasseur, F.; Jimenez, P.; Marchand, M.; Oliva, M. R.; Baren, N. van; Cabrera, T.; Andry, G.; Landry, C.; Ruiz-Cabello, F.; Boon, T.; Garrido, F. Mutations of the B2-Microglobulin Gene Result in a Lack of HLA Class I Molecules on Melanoma Cells of Two Patients Immunized with MAGE Peptides. *Tissue Antigens* **1998**, *52* (6), 520–529. https://doi.org/10.1111/j.1399-0039.1998.tb03082.x.

(381) Chang, C.-C.; Pirozzi, G.; Wen, S.-H.; Chung, I.-H.; Chiu, B.-L.; Errico, S.; Luongo, M.; Lombardi, M. L.; Ferrone, S. Multiple Structural and Epigenetic Defects in the Human Leukocyte Antigen Class I Antigen Presentation Pathway in a Recurrent Metastatic Melanoma Following Immunotherapy. *J Biol Chem* **2015**, *290* (44), 26562–26575. https://doi.org/10.1074/jbc.M115.676130.

(382) Montesion, M.; Murugesan, K.; Jin, D. X.; Sharaf, R.; Sanchez, N.; Guria, A.; Minker, M.; Li, G.; Fisher, V.; Sokol, E. S.; Pavlick, D. C.; Moore, J. A.; Braly, A.; Singal, G.; Fabrizio, D.; Comment, L. A.; Rizvi, N. A.; Alexander, B. M.; Frampton, G. M.; Hegde, P. S.; Albacker, L. A. Somatic HLA Class I Loss Is a Widespread Mechanism of Immune Evasion Which Refines the Use of Tumor Mutational Burden as a Biomarker of Checkpoint Inhibitor Response. *Cancer Discov* **2021**, *11* (2), 282–292.

(383) Campoli, M.; Ferrone, S. HLA Antigen Changes in Malignant Cells: Epigenetic Mechanisms and Biologic Significance. *Oncogene* **2008**, *27* (45), 5869–5885. https://doi.org/10.1038/onc.2008.273.

(384) Mari, L.; Hoefnagel, S. J. M.; Zito, D.; van de Meent, M.; van Endert, P.; Calpe, S.; Sancho Serra, M. del C.; Heemskerk, M. H. M.; van Laarhoven, H. W. M.; Hulshof, M. C. C. M.; Gisbertz, S. S.; Medema, J. P.; van Berge Henegouwen, M. I.; Meijer, S. L.; Bergman, J. J. G. H. M.; Milano, F.; Krishnadath, K. K. MicroRNA 125a Regulates MHC-I Expression on Esophageal Adenocarcinoma Cells, Associated With Suppression of Antitumor Immune Response and Poor Outcomes of Patients. *Gastroenterology* **2018**, *155* (3), 784–798. https://doi.org/10.1053/j.gastro.2018.06.030.

(385) Jongsma, M. L. M.; Guarda, G.; Spaapen, R. M. The Regulatory Network behind MHC Class I Expression. *Mol Immunol* **2019**, *113*, 16–21. https://doi.org/10.1016/j.molimm.2017.12.005.

(386) Wang, S.; He, Z.; Wang, X.; Li, H.; Liu, X.-S. Antigen Presentation and Tumor Immunogenicity in Cancer Immunotherapy Response Prediction. *eLife* **2019**, *8*, e49020. https://doi.org/10.7554/eLife.49020.

(387) Ryschich, E.; Nötzel, T.; Hinz, U.; Autschbach, F.; Ferguson, J.; Simon, I.; Weitz, J.; Fröhlich, B.; Klar, E.; Büchler, M. W.; Schmidt, J. Control of T-Cell–Mediated Immune Response by HLA Class I in Human Pancreatic Carcinoma. *Clin Cancer Res* **2005**, *11* (2), 498–504.

(388) Ogino, T.; Shigyo, H.; Ishii, H.; Katayama, A.; Miyokawa, N.; Harabuchi, Y.; Ferrone, S. HLA Class I Antigen Down-Regulation in Primary Laryngeal Squamous Cell Carcinoma Lesions as a Poor Prognostic Marker. *Cancer Res* **2006**, *66* (18), 9281–9289. https://doi.org/10.1158/0008-5472.CAN-06-0488.

(389) Sade-Feldman, M.; Jiao, Y. J.; Chen, J. H.; Rooney, M. S.; Barzily-Rokni, M.; Eliane, J.-P.; Bjorgaard, S. L.; Hammond, M. R.; Vitzthum, H.; Blackmon, S. M.; Frederick, D. T.; Hazar-Rethinam, M.; Nadres, B. A.; Van Seventer, E. E.; Shukla, S. A.; Yizhak, K.; Ray, J. P.; Rosebrock, D.; Livitz, D.; Adalsteinsson, V.; Getz, G.; Duncan, L. M.; Li, B.; Corcoran, R. B.; Lawrence, D. P.; Stemmer-Rachamimov, A.; Boland, G. M.; Landau, D. A.; Flaherty, K. T.; Sullivan, R. J.; Hacohen, N. Resistance to Checkpoint Blockade Therapy through Inactivation of Antigen Presentation. *Nat Commun* **2017**, *8* (1), 1136. https://doi.org/10.1038/s41467-017-01062-w.

(390) Paulson, K. G.; Voillet, V.; McAfee, M. S.; Hunter, D. S.; Wagener, F. D.; Perdicchio, M.; Valente, W. J.; Koelle, S. J.; Church, C. D.; Vandeven, N.; Thomas, H.; Colunga, A. G.; Iyer, J. G.; Yee, C.; Kulikauskas, R.; Koelle, D. M.; Pierce, R. H.; Bielas, J. H.; Greenberg, P. D.; Bhatia, S.; Gottardo, R.; Nghiem, P.; Chapuis, A. G. Acquired Cancer Resistance to Combination Immunotherapy from Transcriptional Loss of Class I HLA. *Nat Commun* **2018**, *9* (1), 3868. https://doi.org/10.1038/s41467-018-06300-3.

(391) Lauss, M.; Donia, M.; Harbst, K.; Andersen, R.; Mitra, S.; Rosengren, F.; Salim, M.; Vallon-Christersson, J.; Törngren, T.; Kvist, A.; Ringnér, M.; Svane, I. M.; Jönsson, G. Mutational and Putative Neoantigen Load Predict Clinical Benefit of Adoptive T Cell Therapy in Melanoma. *Nat Commun* **2017**, *8* (1), 1738. https://doi.org/10.1038/s41467-017-01460-0.

(392) Viatte, S.; Alves, P. M.; Romero, P. Reverse Immunology Approach for the Identification of CD8 T-Cell-Defined Antigens: Advantages and Hurdles. *Immunol Cell Biol* **2006**, *84* (3), 318–330. https://doi.org/10.1111/j.1440-1711.2006.01447.x.

(393) Shraibman, B.; Barnea, E.; Kadosh, D. M.; Haimovich, Y.; Slobodin, G.; Rosner, I.; López-Larrea, C.; Hilf, N.; Kuttruff, S.; Song, C.; Britten, C.; Castle, J.; Kreiter, S.; Frenzel, K.; Tatagiba, M.; Tabatabai, G.; Dietrich, P.-Y.; Dutoit, V.; Wick, W.; Platten, M.; Winkler, F.; von Deimling, A.; Kroep, J.; Sahuquillo, J.; Martinez-Ricarte, F.; Rodon, J.; Lassen, U.; Ottensmeier, C.; van der Burg, S. H.; Thor Straten, P.; Poulsen, H. S.; Ponsati, B.; Okada, H.; Rammensee, H.-G.; Sahin, U.; Singh, H.; Admon, A. Identification of Tumor Antigens Among the HLA Peptidomes of Glioblastoma Tumors and Plasma. *Mol Cell Proteomics* **2019**, *18* (6), 1255–1268. https://doi.org/10.1074/mcp.RA119.001524.

(394) Petricoin, E. F.; Belluco, C.; Araujo, R. P.; Liotta, L. A. The Blood Peptidome: A Higher Dimension of Information Content for Cancer Biomarker Discovery. *Nat Rev Cancer* **2006**, *6* (12), 961–967. https://doi.org/10.1038/nrc2011.

(395) Bassani-Sternberg, M.; Barnea, E.; Beer, I.; Avivi, I.; Katz, T.; Admon, A. Soluble Plasma HLA Peptidome as a Potential Source for Cancer Biomarkers. *PNAS* **2010**, *107* (44), 18769–18776.

(396) Bassani-Sternberg, M.; Bräunlein, E.; Klar, R.; Engleitner, T.; Sinitcyn, P.; Audehm, S.; Straub, M.; Weber, J.; Slotta-Huspenina, J.; Specht, K.; Martignoni, M. E.; Werner, A.; Hein, R.; H. Busch, D.; Peschel, C.; Rad, R.; Cox, J.; Mann, M.; Krackhardt, A. M. Direct Identification of Clinically Relevant Neoepitopes Presented on Native Human Melanoma Tissue by Mass Spectrometry. *Nat Commun* **2016**, *7* (1), 13404. https://doi.org/10.1038/ncomms13404.

(397) Kuznetsov, A.; Voronina, A.; Govorun, V.; Arapidi, G. Critical Review of Existing MHC I Immunopeptidome Isolation Methods. *Molecules* **2020**, *25* (22), 5409. https://doi.org/10.3390/molecules25225409.

(398) Kessler, J. H.; Benckhuijsen, W. E.; Mutis, T.; Melief, C. J. M.; Burg, S. H. van der; Drijfhout, J. W. Competition-Based Cellular Peptide Binding Assay for HLA Class I. *Curr Protoc Immunol* **2004**, *61* (1), 18.12.1-18.12.15. https://doi.org/10.1002/0471142735.im1812s61.

(399) Brusic, V.; Flower, D. R. Bioinformatics Tools for Identifying T-Cell Epitopes. *Drug Discov Today* **2004**, *2* (1), 18–23. https://doi.org/10.1016/S1741-8364(04)02374-1.

(400) Baral, P.; Pavadai, E.; Gerstman, B. S.; Chapagain, P. P. In-Silico Identification of the Vaccine Candidate Epitopes against the Lassa Virus Hemorrhagic Fever. *Sci Rep* **2020**, *10*, 7667. https://doi.org/10.1038/s41598-020-63640-1.

(401) Soria-Guerra, R. E.; Nieto-Gomez, R.; Govea-Alonso, D. O.; Rosales-Mendoza, S. An Overview of Bioinformatics Tools for Epitope Prediction: Implications on Vaccine Development. *J Biol Chem* **2015**, *53*, 405–414. https://doi.org/10.1016/j.jbi.2014.11.003.

(402) Ferrari, G.; Kostyu, D. D.; Cox, J.; Dawson, D. V.; Flores, J.; Weinhold, K. J.; Osmanov, S. Identification of Highly Conserved and Broadly Cross-Reactive HIV Type 1 Cytotoxic T Lymphocyte Epitopes as Candidate Immunogens for Inclusion in Mycobacterium Bovis BCG-Vectored HIV Vaccines. *AIDS Res Hum Retroviruses* **2000**, *16* (14), 1433–1443. https://doi.org/10.1089/08892220050140982.

(403) Falk, K.; Rötzschke, O.; Deres, K.; Metzger, J.; Jung, G.; Rammensee, H. G. Identification of Naturally Processed Viral Nonapeptides Allows Their Quantification in Infected Cells and Suggests an Allele-Specific T Cell Epitope Forecast. *J Exp Med* **1991**, *174* (2), 425–434. https://doi.org/10.1084/jem.174.2.425.

(404) Rötzschke, O.; Falk, K.; Stevanovic, S.; Jung, G.; Walden, P.; Rammensee, H.-G. Exact prediction of a natural T cell epitope. *Eur J Immunol* **1991**, *21* (11), 2891–2894. https://doi.org/10.1002/eji.1830211136.

(405) Rammensee, H.-G.; Bachmann, J.; Emmerich, N. P. N.; Bachor, O. A.; Stevanović, S. SYFPEITHI: Database for MHC Ligands and Peptide Motifs. *Immunogenetics* **1999**, *50* (3), 213–219. https://doi.org/10.1007/s002510050595.

(406) Tong, J. C.; Tan, T. W.; Ranganathan, S. Methods and Protocols for Prediction of Immunogenic Epitopes. *Brief Bioinform* **2007**, *8* (2), 96–108. https://doi.org/10.1093/bib/bbl038.

(407) Milik, M.; Sauer, D.; Brunmark, A. P.; Yuan, L.; Vitiello, A.; Jackson, M. R.; Peterson, P. A.; Skolnick, J.; Glass, C. A. Application of an Artificial Neural Network to Predict Specific Class I MHC Binding Peptide Sequences. *Nat Biotechnol* **1998**, *16* (8), 753–756. https://doi.org/10.1038/nbt0898-753.

(408)   Karosiene, E.; Lundegaard, C.; Lund, O.; Nielsen, M. NetMHCcons: A Consensus Method for the Major Histocompatibility Complex Class I Predictions. *Immunogenetics* **2012**, *64* (3), 177–186. https://doi.org/10.1007/s00251-011-0579-8.

(409)   Lundegaard, C.; Lund, O.; Nielsen, M. Accurate Approximation Method for Prediction of Class I MHC Affinities for Peptides of Length 8, 10 and 11 Using Prediction Tools Trained on 9mers. *Bioinformatics* **2008**, *24* (11), 1397–1398. https://doi.org/10.1093/bioinformatics/btn128.

(410)   Purcell, A. W.; Ramarathinam, S. H.; Ternette, N. Mass Spectrometry–Based Identification of MHC-Bound Peptides for Immunopeptidomics. *Nat Protoc* **2019**, *14* (6), 1687–1707. https://doi.org/10.1038/s41596-019-0133-y.

(411)   Lanoix, J.; Durette, C.; Courcelles, M.; Cossette, É.; Comtois-Marotte, S.; Hardy, M.-P.; Côté, C.; Perreault, C.; Thibault, P. Comparison of the MHC I Immunopeptidome Repertoire of B-Cell Lymphoblasts Using Two Isolation Methods. *Proteomics* **2018**, *18* (12), 1700251. https://doi.org/10.1002/pmic.201700251.

(412)   Shunji Sugawara; Toru Abo; Katsuo Kumagai. A Simple Method to Eliminate the Antigenicity of Surface Class I MHC Molecules from the Membrane of Viable Cells by Acid Treatment at PH 3. *J Immunol Methods* **1987**, *100* (1), 83–90. https://doi.org/10.1016/0022-1759(87)90175-X.

(413)   Lee, J. M.; Watts, T. H. On the Dissociation and Reassociation of MHC Class II-Foreign Peptide Complexes. Evidence That Brief Transit through an Acidic Compartment Is Not Sufficient for Binding Site Regeneration. *The Journal of Immunology 144* (5), 1829–1834.

(414)   Storkus, W. J.; Zen, H. J. I.; Salter, R. D.; Lotze, M. T. Identification of T-Cell Epitopes: Rapid Isolation of Class I-Presented Peptides from Viable Cells by Mild Acid Elution. *J Immunother* **1993**, *14* (2), 94–103.

(415)   Gebreselassie, D.; Spiegel, H.; Vukmanovic, S. Sampling of Major Histocompatibility Complex Class I-Associated Peptidome Suggests Relatively Looser Global Association of HLA-B*5101 With Peptides. *Hum Immunol* **2006**, *67* (11), 894–906. https://doi.org/10.1016/j.humimm.2006.08.294.

(416)   Fortier, M.-H.; Caron, É.; Hardy, M.-P.; Voisin, G.; Lemieux, S.; Perreault, C.; Thibault, P. The MHC Class I Peptide Repertoire Is Molded by the Transcriptome. *J Exp Med* **2008**, *205* (3), 595–610. https://doi.org/10.1084/jem.20071985.

(417)   Rodriguez, E. L.; Poddar, S.; Iftekhar, S.; Suh, K.; Woolfork, A. G.; Ovbude, S.; Pekarek, A.; Walters, M.; Lott, S.; Hage, D. S. Affinity Chromatography: A Review of Trends and Developments over the Past 50 Years. *J Chromatogr B Analyt Technol Biomed Life Sci* **2020**, *1157*, 122332. https://doi.org/10.1016/j.jchromb.2020.122332.

(418) Partridge, T.; Nicastri, A.; Kliszczak, A. E.; Yindom, L.-M.; Kessler, B. M.; Ternette, N.; Borrow, P. Discrimination Between Human Leukocyte Antigen Class I-Bound and Co-Purified HIV-Derived Peptides in Immunopeptidomics Workflows. *Front Immunol* **2018**, *9*. https://doi.org/10.3389/fimmu.2018.00912.

(419) Bassani-Sternberg, M.; Pletscher-Frankild, S.; Jensen, L. J.; Mann, M. Mass Spectrometry of Human Leukocyte Antigen Class I Peptidomes Reveals Strong Effects of Protein Abundance and Turnover on Antigen Presentation. *Mol Cell Proteomics* **2015**, *14* (3), 658–673. https://doi.org/10.1074/mcp.M114.042812.

(420) Ritz, D.; Gloger, A.; Weide, B.; Garbe, C.; Neri, D.; Fugmann, T. High-Sensitivity HLA Class I Peptidome Analysis Enables a Precise Definition of Peptide Motifs and the Identification of Peptides from Cell Lines and Patients' Sera. *Proteomics* **2016**, *16* (10), 1570–1580. https://doi.org/10.1002/pmic.201500445.

(421) Chong, C.; Marino, F.; Pak, H.; Racle, J.; Daniel, R. T.; Müller, M.; Gfeller, D.; Coukos, G.; Bassani-Sternberg, M. High-Throughput and Sensitive Immunopeptidomics Platform Reveals Profound Interferonγ-Mediated Remodeling of the Human Leukocyte Antigen (HLA) Ligandome. *Mol Cell Proteomics* **2018**, *17* (3), 533–548. https://doi.org/10.1074/mcp.TIR117.000383.

(422) Alpízar, A.; Marino, F.; Ramos-Fernández, A.; Lombardía, M.; Jeko, A.; Pazos, F.; Paradela, A.; Santiago, C.; Heck, A. J. R.; Marcilla, M. A Molecular Basis for the Presentation of Phosphorylated Peptides by HLA-B Antigens*. *Mol Cell Proteomics* **2017**, *16* (2), 181–193. https://doi.org/10.1074/mcp.M116.063800.

(423) Caron, E.; Kowalewski, D. J.; Chiek Koh, C.; Sturm, T.; Schuster, H.; Aebersold, R. Analysis of Major Histocompatibility Complex (MHC) Immunopeptidomes Using Mass Spectrometry. *Mol Cell Proteomics* **2015**, *14* (12), 3105–3117. https://doi.org/10.1074/mcp.O115.052431.

(424) Vizcaíno, J. A.; Kubiniok, P.; Kovalchik, K. A.; Ma, Q.; Duquette, J. D.; Mongrain, I.; Deutsch, E. W.; Peters, B.; Sette, A.; Sirois, I.; Caron, E. The Human Immunopeptidome Project: A Roadmap to Predict and Treat Immune Diseases. *Mol Cell Proteomics* **2020**, *19* (1), 31–49. https://doi.org/10.1074/mcp.R119.001743.

(425) Lee, P.; Gujar, S. Potentiating Prostate Cancer Immunotherapy with Oncolytic Viruses. *Nat Rev Urol* **2018**, *15* (4), 235–250. https://doi.org/10.1038/nrurol.2018.10.

(426) Roby, K. F.; Taylor, C. C.; Sweetwood, J. P.; Cheng, Y.; Pace, J. L.; Tawfik, O.; Persons, D. L.; Smith, P. G.; Terranova, P. F. Development of a Syngeneic Mouse Model for Events Related to Ovarian Cancer. *Carcinogenesis* **2000**, *21* (4), 585–591. https://doi.org/10.1093/carcin/21.4.585.

(427)   Michaud, M.; Martins, I.; Sukkurwala, A. Q.; Adjemian, S.; Ma, Y.; Pellegatti, P.; Shen, S.; Kepp, O.; Scoazec, M.; Mignot, G.; Rello-Varona, S.; Tailler, M.; Menger, L.; Vacchelli, E.; Galluzzi, L.; Ghiringhelli, F.; Virgilio, F. di; Zitvogel, L.; Kroemer, G. Autophagy-Dependent Anticancer Immune Responses Induced by Chemotherapeutic Agents in Mice. *Science* **2011**, *334* (6062), 1573–1577. https://doi.org/10.1126/science.1208347.

(428)   Coffey, M. C.; Strong, J. E.; Forsyth, P. A.; Lee, P. W. K. Reovirus Therapy of Tumors with Activated Ras Pathway. *Science* **1998**, *282* (5392), 1332–1334. https://doi.org/10.1126/science.282.5392.1332.

(429)   Helling, F.; Shang, A.; Calves, M.; Zhang, S.; Ren, S.; Yu, R. K.; Oettgen, H. E.; Livingston, P. O. GD3Vaccines for Melanoma: Superior Immunogenicity of Keyhole Limpet Hemocyanin Conjugate Vaccines. *Cancer Res 54* (1), 197–203.

(430)   Kowalewski, D. J.; Stevanović, S. Biochemical Large-Scale Identification of MHC Class I Ligands. *Methods Mol Biol* **2013**, *960*, 145–157. https://doi.org/10.1007/978-1-62703-218-6_12.

(431)   Rappsilber, J.; Ishihama, Y.; Mann, M. Stop and Go Extraction Tips for Matrix-Assisted Laser Desorption/Ionization, Nanoelectrospray, and LC/MS Sample Pretreatment in Proteomics. *Anal Chem* **2003**, *75* (3), 663–670. https://doi.org/10.1021/ac026117i.

(432)   Kowalewski, D. J.; Stevanović, S. Biochemical Large-Scale Identification of MHC Class I Ligands. *Methods Mol Biol* **2013**, 960, 145-157. https://doi.org/10.1007/978-1-62703-218-6_12.

(433)   Murphy, J. P.; Kim, Y.; Clements, D. R.; Konda, P.; Schuster, H.; Kowalewski, D. J.; Paulo, J. A.; Cohen, A. M.; Stevanovic, S.; Gygi, S. P.; Gujar, S. Therapy-Induced MHC I Ligands Shape Neo-Antitumor CD8 T Cell Responses during Oncolytic Virus-Based Cancer Immunotherapy. *J Proteome Res* **2019**, *18* (6), 2666–2675. https://doi.org/10.1021/acs.jproteome.9b00173.

(434)   Murphy, J. P.; Yu, Q.; Konda, P.; Paulo, J. A.; Jedrychowski, M. P.; Kowalewski, D. J.; Schuster, H.; Kim, Y.; Clements, D.; Jain, A.; Stevanovic, S.; Gygi, S. P.; Mancias, J. D.; Gujar, S. Multiplexed Relative Quantitation with Isobaric Tagging Mass Spectrometry Reveals Class I Major Histocompatibility Complex Ligand Dynamics in Response to Doxorubicin. *Anal Chem* **2019**, *91* (8), 5106–5115. https://doi.org/10.1021/acs.analchem.8b05616.

(435)   Murphy, J. P.; Konda, P.; Kowalewski, D. J.; Schuster, H.; Clements, D.; Kim, Y.; Cohen, A. M.; Sharif, T.; Nielsen, M.; Stevanovic, S.; Lee, P. W.; Gujar, S. MHC-I Ligand Discovery Using Targeted Database Searches of Mass Spectrometry Data: Implications for T-Cell Immunotherapies. *J Proteome Res* **2017**, *16* (4), 1806–1816. https://doi.org/10.1021/acs.jproteome.6b00971.

(436) Clements, D. R.; Murphy, J. P.; Sterea, A.; Kennedy, B. E.; Kim, Y.; Helson, E.; Almasi, S.; Holay, N.; Konda, P.; Paulo, J. A.; Sharif, T.; Lee, P. W.; Weekes, M. P.; Gygi, S. P.; Gujar, S. Quantitative Temporal in Vivo Proteomics Deciphers the Transition of Virus-Driven Myeloid Cells into M2 Macrophages. *J Proteome Res* **2017**, *16* (9), 3391–3406. https://doi.org/10.1021/acs.jproteome.7b00425.

(437) Eng, J. K.; McCormack, A. L.; Yates, J. R. An Approach to Correlate Tandem Mass Spectral Data of Peptides with Amino Acid Sequences in a Protein Database. *J Am Soc Mass Spectrom* **1994**, *5* (11), 976–989. https://doi.org/10.1016/1044-0305(94)80016-2.

(438) Elias, J. E.; Gygi, S. P. Target-Decoy Search Strategy for Increased Confidence in Large-Scale Protein Identifications by Mass Spectrometry. *Nat Methods* **2007**, *4* (3), 207–214. https://doi.org/10.1038/nmeth1019.

(439) Classen, D. C.; Morningstar, J. M.; Shanley, J. D. Detection of Antibody to Murine Cytomegalovirus by Enzyme-Linked Immunosorbent and Indirect Immunofluorescence Assays. *J Clin Microbiol* **1987**, *25* (4), 600–604.

(440) Livak, K. J.; Schmittgen, T. D. Analysis of Relative Gene Expression Data Using Real-Time Quantitative PCR and the 2(-Delta Delta C(T)) Method. *Methods* **2001**, *25* (4), 402–408. https://doi.org/10.1006/meth.2001.1262.

(441) Westrop, S. J.; Grageda, N.; Imami, N. Novel Approach to Recognition of Predicted HIV-1 Gag B3501-Restricted CD8 T-Cell Epitopes by HLA-B3501(+) Patients: Confirmation by Quantitative ELISpot Analyses and Characterisation Using Multimers. *J Immunol Methods* **2009**, *341* (1–2), 76–85. https://doi.org/10.1016/j.jim.2008.11.003.

(442) Bland, J. M.; Altman, D. G. Survival Probabilities (the Kaplan-Meier Method). *BMJ* **1998**, *317* (7172), 1572–1580.

(443) Bland, J. M.; Altman, D. G. The Logrank Test. *BMJ* **2004**, *328* (7447), 1073.

(444) Gravitz, L. Cancer Immunotherapy. *Nature* **2013**, *504* (7480), S1–S1. https://doi.org/10.1038/504S1a.

(445) Wei, S. C.; Duffy, C. R.; Allison, J. P. Fundamental Mechanisms of Immune Checkpoint Blockade Therapy. *Cancer Discov* **2018**, *8* (9), 1069–1086. https://doi.org/10.1158/2159-8290.CD-18-0367.

(446) Galluzzi, L.; Buqué, A.; Kepp, O.; Zitvogel, L.; Kroemer, G. Immunogenic Cell Death in Cancer and Infectious Disease. *Nat Rev Immunol* **2017**, *17* (2), 97–111. https://doi.org/10.1038/nri.2016.107.

(447) Sharma, P.; Allison, J. P. Immune Checkpoint Targeting in Cancer Therapy: Toward Combination Strategies with Curative Potential. *Cell* **2015**, *161* (2), 205–214. https://doi.org/10.1016/j.cell.2015.03.030.

(448) Anagnostou, V.; Smith, K. N.; Forde, P. M.; Niknafs, N.; Bhattacharya, R.; White, J.; Zhang, T.; Adleff, V.; Phallen, J.; Wali, N.; Hruban, C.; Guthrie, V. B.; Rodgers, K.; Naidoo, J.; Kang, H.; Sharfman, W.; Georgiades, C.; Verde, F.; Illei, P.; Li, Q. K.; Gabrielson, E.; Brock, M. V.; Zahnow, C. A.; Baylin, S. B.; Scharpf, R. B.; Brahmer, J. R.; Karchin, R.; Pardoll, D. M.; Velculescu, V. E. Evolution of Neoantigen Landscape during Immune Checkpoint Blockade in Non–Small Cell Lung Cancer. *Cancer Discov* **2017**, *7* (3), 264–276. https://doi.org/10.1158/2159-8290.CD-16-0828.

(449) Łuksza, M.; Riaz, N.; Makarov, V.; Balachandran, V. P.; Hellmann, M. D.; Solovyov, A.; Rizvi, N. A.; Merghoub, T.; Levine, A. J.; Chan, T. A.; Wolchok, J. D.; Greenbaum, B. D. A Neoantigen Fitness Model Predicts Tumour Response to Checkpoint Blockade Immunotherapy. *Nature* **2017**, *551* (7681), 517–520. https://doi.org/10.1038/nature24473.

(450) Hirasawa, K.; Nishikawa, S. G.; Norman, K. L.; Alain, T.; Kossakowska, A.; Lee, P. W. K. Oncolytic Reovirus against Ovarian and Colon Cancer. *Cancer Res* **2002**, *62* (6), 1696–1701.

(451) Norman, K. L.; Coffey, M. C.; Hirasawa, K.; Demetrick, D. J.; Nishikawa, S. G.; DiFrancesco, L. M.; Strong, J. E.; Lee, P. W. K. Reovirus Oncolysis of Human Breast Cancer. *Hum Gene Ther* **2002**, *13* (5), 641–652. https://doi.org/10.1089/10430340252837233.

(452) Hirasawa, K.; Nishikawa, S. G.; Norman, K. L.; Coffey, M. C.; Thompson, B. G.; Yoon, C.-S.; Waisman, D. M.; Lee, P. W. K. Systemic Reovirus Therapy of Metastatic Cancer in Immune-Competent Mice. *Cancer Res* **2003**, *63* (2), 348–353.

(453) Wilcox, M. E.; Yang, W.; Senger, D.; Rewcastle, N. B.; Morris, D. G.; Brasher, P. M. A.; Shi, Z. Q.; Johnston, R. N.; Nishikawa, S.; Lee, P. W. K.; Forsyth, P. A. Reovirus as an Oncolytic Agent Against Experimental Human Malignant Gliomas. *J Natl Cancer Inst* **2001**, *93* (12), 903–912. https://doi.org/10.1093/jnci/93.12.903.

(454) Kilani, R. T.; Tamimi, Y.; Hanel, E. G.; Wong, K. K.; Karmali, S.; Lee, P. W. K.; Moore, R. B. Selective Reovirus Killing of Bladder Cancer in a Co-Culture Spheroid Model. *Virus Res* **2003**, *93* (1), 1–12. https://doi.org/10.1016/S0168-1702(03)00045-5.

(455) Alain, T.; Hirasawa, K.; Pon, K. J.; Nishikawa, S. G.; Urbanski, S. J.; Auer, Y.; Luider, J.; Martin, A.; Johnston, R. N.; Janowska-Wieczorek, A.; Lee, P. W. K.; Kossakowska, A. E. Reovirus Therapy of Lymphoid Malignancies. *Blood* **2002**, *100* (12), 4146–4153. https://doi.org/10.1182/blood-2002-02-0503.

(456) Schulz, O.; Diebold, S. S.; Chen, M.; Näslund, T. I.; Nolte, M. A.; Alexopoulou, L.; Azuma, Y.-T.; Flavell, R. A.; Liljeström, P.; Reis e Sousa, C. Toll-like Receptor 3 Promotes Cross-Priming to Virus-Infected Cells. *Nature* **2005**, *433* (7028), 887–892. https://doi.org/10.1038/nature03326.

(457) Benencia, F.; Courrèges, M. C.; Fraser, N. W.; Coukos, G. Herpes Virus Oncolytic Therapy Reverses Tumor Immune Dysfunction and Facilitates Tumor Antigen Presentation. *Cancer Biol Ther* **2008**, *7* (8), 1194–1205. https://doi.org/10.4161/cbt.7.8.6216.

(458) Gujar, S.; Dielschneider, R.; Clements, D.; Helson, E.; Shmulevitz, M.; Marcato, P.; Pan, D.; Pan, L.; Ahn, D.-G.; Alawadhi, A.; Lee, P. W. Multifaceted Therapeutic Targeting of Ovarian Peritoneal Carcinomatosis Through Virus-Induced Immunomodulation. *Mol Ther* **2013**, *21* (2), 338–347. https://doi.org/10.1038/mt.2012.228.

(459) Gujar, S. A.; Clements, D.; Dielschneider, R.; Helson, E.; Marcato, P.; Lee, P. W. K. Gemcitabine Enhances the Efficacy of Reovirus-Based Oncotherapy through Anti-Tumour Immunological Mechanisms. *Br J Cancer* **2014**, *110* (1), 83–93. https://doi.org/10.1038/bjc.2013.695.

(460) Mi, H.; Dong, Q.; Muruganujan, A.; Gaudet, P.; Lewis, S.; Thomas, P. D. PANTHER Version 7: Improved Phylogenetic Trees, Orthologs and Collaboration with the Gene Ontology Consortium. *Nucleic Acids Res* **2010**, *38* (suppl_1), D204–D210. https://doi.org/10.1093/nar/gkp1019.

(461) Thomas, P. D.; Campbell, M. J.; Kejariwal, A.; Mi, H.; Karlak, B.; Daverman, R.; Diemer, K.; Muruganujan, A.; Narechania, A. PANTHER: A Library of Protein Families and Subfamilies Indexed by Function. *Genome Res.* **2003**, *13* (9), 2129–2141. https://doi.org/10.1101/gr.772403.

(462) Spencer, C. T.; Bezbradica, J. S.; Ramos, M. G.; Arico, C. D.; Conant, S. B.; Gilchuk, P.; Gray, J. J.; Zheng, M.; Niu, X.; Hildebrand, W.; Link, A. J.; Joyce, S. Viral Infection Causes a Shift in the Self Peptide Repertoire Presented by Human MHC Class I Molecules. *Proteomics Clin Appl* **2015**, *9* (11–12), 1035–1052. https://doi.org/10.1002/prca.201500106.

(463) Murphy, J. P.; Stepanova, E.; Everley, R. A.; Paulo, J. A.; Gygi, S. P. Comprehensive Temporal Protein Dynamics during the Diauxic Shift in Saccharomyces Cerevisiae. *Mol Cell Proteomics* **2015**, *14* (9), 2454–2465. https://doi.org/10.1074/mcp.M114.045849.

(464) Schuster, H.; Shao, W.; Weiss, T.; Pedrioli, P. G. A.; Roth, P.; Weller, M.; Campbell, D. S.; Deutsch, E. W.; Moritz, R. L.; Planz, O.; Rammensee, H.-G.; Aebersold, R.; Caron, E. A Tissue-Based Draft Map of the Murine MHC Class I Immunopeptidome. *Sci Data* **2018**, *5* (1), 180157. https://doi.org/10.1038/sdata.2018.157.

(465)   Laumont, C. M.; Vincent, K.; Hesnard, L.; Audemard, É.; Bonneil, É.; Laverdure, J.-P.; Gendron, P.; Courcelles, M.; Hardy, M.-P.; Côté, C.; Durette, C.; St-Pierre, C.; Benhammadi, M.; Lanoix, J.; Vobecky, S.; Haddad, E.; Lemieux, S.; Thibault, P.; Perreault, C. Noncoding Regions Are the Main Source of Targetable Tumor-Specific Antigens. *Sci Transl Med* **2018**, *10* (470). https://doi.org/10.1126/scitranslmed.aau5516.

(466)   Zacharakis, N.; Chinnasamy, H.; Black, M.; Xu, H.; Lu, Y.-C.; Zheng, Z.; Pasetto, A.; Langhan, M.; Shelton, T.; Prickett, T.; Gartner, J.; Jia, L.; Trebska-McGowan, K.; Somerville, R. P.; Robbins, P. F.; Rosenberg, S. A.; Goff, S. L.; Feldman, S. A. Immune Recognition of Somatic Mutations Leading to Complete Durable Regression in Metastatic Breast Cancer. *Nat Med* **2018**, *24* (6), 724–730. https://doi.org/10.1038/s41591-018-0040-8.

(467)   Romero, D. Oncolytic Viruses Prime Antitumour Immunity. *Nat Rev Clin Oncol* **2018**, *15* (3), 135–135. https://doi.org/10.1038/nrclinonc.2018.15.

(468)   Yin, J.; Markert, J. M.; Leavenworth, J. W. Modulation of the Intratumoral Immune Landscape by Oncolytic Herpes Simplex Virus Virotherapy. *Front Oncol* **2017**, *7*. https://doi.org/10.3389/fonc.2017.00136.

(469)   Rivadeneira, D. B.; DePeaux, K.; Wang, Y.; Kulkarni, A.; Tabib, T.; Menk, A. V.; Sampath, P.; Lafyatis, R.; Ferris, R. L.; Sarkar, S. N.; Thorne, S. H.; Delgoffe, G. M. Oncolytic Viruses Engineered to Enforce Leptin Expression Reprogram Tumor-Infiltrating T Cell Metabolism and Promote Tumor Clearance. *Immunity* **2019**, *51* (3), 548-560.e4. https://doi.org/10.1016/j.immuni.2019.07.003.

(470)   Engeland, C. E.; Grossardt, C.; Veinalde, R.; Bossow, S.; Lutz, D.; Kaufmann, J. K.; Shevchenko, I.; Umansky, V.; Nettelbeck, D. M.; Weichert, W.; Jäger, D.; von Kalle, C.; Ungerechts, G. CTLA-4 and PD-L1 Checkpoint Blockade Enhances Oncolytic Measles Virus Therapy. *Mol Ther* **2014**, *22* (11), 1949–1959. https://doi.org/10.1038/mt.2014.160.

(471)   Hardcastle, J.; Mills, L.; Malo, C. S.; Jin, F.; Kurokawa, C.; Geekiyanage, H.; Schroeder, M.; Sarkaria, J.; Johnson, A. J.; Galanis, E. Immunovirotherapy with Measles Virus Strains in Combination with Anti–PD-1 Antibody Blockade Enhances Antitumor Activity in Glioblastoma Treatment. *Neuro Oncol* **2017**, *19* (4), 493–502. https://doi.org/10.1093/neuonc/now179.

(472)   Shen, W.; Patnaik, M. M.; Ruiz, A.; Russell, S. J.; Peng, K.-W. Immunovirotherapy with Vesicular Stomatitis Virus and PD-L1 Blockade Enhances Therapeutic Outcome in Murine Acute Myeloid Leukemia. *Blood* **2016**, *127* (11), 1449–1458. https://doi.org/10.1182/blood-2015-06-652503.

(473)   LaRocca, C. J.; Warner, S. G. Oncolytic Viruses and Checkpoint Inhibitors: Combination Therapy in Clinical Trials. *Clin Transl Med* **2018**, *7* (1). https://doi.org/10.1186/s40169-018-0214-5.

(474) Seliger, B.; Maeurer, M. J.; Ferrone, S. Antigen-Processing Machinery Breakdown and Tumor Growth. *Immunol Today* **2000**, *21* (9), 455–464. https://doi.org/10.1016/S0167-5699(00)01692-3.

(475) Dunn, G. P.; Bruce, A. T.; Ikeda, H.; Old, L. J.; Schreiber, R. D. Cancer Immunoediting: From Immunosurveillance to Tumor Escape. *Nat Immunol* **2002**, *3* (11), 991–998. https://doi.org/10.1038/ni1102-991.

(476) Cai, H.; Liu, G.; Zhong, J.; Zheng, K.; Xiao, H.; Li, C.; Song, X.; Li, Y.; Xu, C.; Wu, H.; He, Z.; Zhu, Q. Immune Checkpoints in Viral Infections. *Viruses* **2020**, *12* (9), 1051. https://doi.org/10.3390/v12091051.

(477) Schönrich, G.; Raftery, M. J. The PD-1/PD-L1 Axis and Virus Infections: A Delicate Balance. *Front Cell Infect Microbiol* **2019**, *9*. https://doi.org/10.3389/fcimb.2019.00207.

(478) de Charette, M.; Marabelle, A.; Houot, R. Turning Tumour Cells into Antigen Presenting Cells: The next Step to Improve Cancer Immunotherapy? *Eur J Cancer* **2016**, *68*, 134–147. https://doi.org/10.1016/j.ejca.2016.09.010.

(479) McAlister, G. C.; Huttlin, E. L.; Haas, W.; Ting, L.; Jedrychowski, M. P.; Rogers, J. C.; Kuhn, K.; Pike, I.; Grothe, R. A.; Blethrow, J. D.; Gygi, S. P. Increasing the Multiplexing Capacity of TMTs Using Reporter Ion Isotopologues with Isobaric Masses. *Anal Chem* **2012**, *84* (17), 7469–7478. https://doi.org/10.1021/ac301572t.

(480) Stewart, R.; Hammond, S. A.; Oberst, M.; Wilkinson, R. W. The Role of Fc Gamma Receptors in the Activity of Immunomodulatory Antibodies for Cancer. *J Immunother Cancer* **2014**, *2* (1), 29. https://doi.org/10.1186/s40425-014-0029-x.

(481) Simpson, T. R.; Li, F.; Montalvo-Ortiz, W.; Sepulveda, M. A.; Bergerhoff, K.; Arce, F.; Roddie, C.; Henry, J. Y.; Yagita, H.; Wolchok, J. D.; Peggs, K. S.; Ravetch, J. V.; Allison, J. P.; Quezada, S. A. Fc-Dependent Depletion of Tumor-Infiltrating Regulatory T Cells Co-Defines the Efficacy of Anti–CTLA-4 Therapy against Melanoma. *J Exp Med* **2013**, *210* (9), 1695–1710. https://doi.org/10.1084/jem.20130579.

(482) Bulliard, Y.; Jolicoeur, R.; Windman, M.; Rue, S. M.; Ettenberg, S.; Knee, D. A.; Wilson, N. S.; Dranoff, G.; Brogdon, J. L. Activating Fc γ Receptors Contribute to the Antitumor Activities of Immunoregulatory Receptor-Targeting Antibodies. *J Exp Med* **2013**, *210* (9), 1685–1693. https://doi.org/10.1084/jem.20130573.

(483) Sefrin, J. P.; Hillringhaus, L.; Mundigl, O.; Mann, K.; Ziegler-Landesberger, D.; Seul, H.; Tabares, G.; Knoblauch, D.; Leinenbach, A.; Friligou, I.; Dziadek, S.; Offringa, R.; Lifke, V.; Lifke, A. Sensitization of Tumors for Attack by Virus-Specific CD8+ T-Cells Through Antibody-Mediated Delivery of Immunogenic T-Cell Epitopes. *Front Immunol* **2019**, *10*. https://doi.org/10.3389/fimmu.2019.01962.

(484) Schmidt, M. E.; Varga, S. M. The CD8 T Cell Response to Respiratory Virus Infections. *Front Immunol* **2018**, *9*. https://doi.org/10.3389/fimmu.2018.00678.

(485) He, X.; Xu, C. Immune Checkpoint Signaling and Cancer Immunotherapy. *Cell Res* **2020**, *30* (8), 660–669. https://doi.org/10.1038/s41422-020-0343-4.

(486) Pardoll, D. M. The Blockade of Immune Checkpoints in Cancer Immunotherapy. *Nat Rev Cancer* **2012**, *12* (4), 252–264. https://doi.org/10.1038/nrc3239.

(487) Dersh, D.; Yewdell, J. W.; Wei, J. A SIINFEKL-Based System to Measure MHC Class I Antigen Presentation Efficiency and Kinetics. *Methods Mol Biol* **2019**, *1988*, 109–122. https://doi.org/10.1007/978-1-4939-9450-2_9.

(488) Hanada, K.; Yu, Z.; Chappell, G. R.; Park, A. S.; Restifo, N. P. An Effective Mouse Model for Adoptive Cancer Immunotherapy Targeting Neoantigens. *JCI Insight* **2019**, *4* (10). https://doi.org/10.1172/jci.insight.124405.

(489) Clarke, S. Rm.; Barnden, M.; Kurts, C.; Carbone, F. R.; Miller, J. F.; Heath, W. R. Characterization of the Ovalbumin-Specific TCR Transgenic Line OT-I: MHC Elements for Positive and Negative Selection. *Immunol Cell Biol* **2000**, *78* (2), 110–117. https://doi.org/10.1046/j.1440-1711.2000.00889.x.

(490) Muralidharan, A.; Gravel, C.; Duran, A.; Larocque, L.; Li, C.; Zetner, A.; Van Domselaar, G.; Wang, L.; Li, X. Identification of Immunodominant CD8 Epitope in the Stalk Domain of Influenza B Viral Hemagglutinin. *Biochem Biophys Res Commun* **2018**, *502* (2), 226–231. https://doi.org/10.1016/j.bbrc.2018.05.148.

(491) Wu, C.; Zanker, D.; Valkenburg, S.; Tan, B.; Kedzierska, K.; Zou, Q. M.; Doherty, P. C.; Chen, W. Systematic Identification of Immunodominant CD8 T-Cell Responses to Influenza A Virus in HLA-A2 Individuals. *PNAS* **2011**, *108* (22), 9178–9183.

(492) Mahajan, S.; Kode, V.; Bhojak, K.; Karunakaran, C.; Lee, K.; Manoharan, M.; Ramesh, A.; Hv, S.; Srivastava, A.; Sathian, R.; Khan, T.; Kumar, P.; Gupta, R.; Chakraborty, P.; Chaudhuri, A. Immunodominant T-Cell Epitopes from the SARS-CoV-2 Spike Antigen Reveal Robust Pre-Existing T-Cell Immunity in Unexposed Individuals. *Sci Rep* **2021**, *11* (1), 13164. https://doi.org/10.1038/s41598-021-92521-4.

(493) Dolton, G.; Zervoudi, E.; Rius, C.; Wall, A.; Thomas, H. L.; Fuller, A.; Yeo, L.; Legut, M.; Wheeler, S.; Attaf, M.; Chudakov, D. M.; Choy, E.; Peakman, M.; Sewell, A. K. Optimized Peptide–MHC Multimer Protocols for Detection and Isolation of Autoimmune T-Cells. *Front Immunol* **2018**, *9*. https://doi.org/10.3389/fimmu.2018.01378.

(494) Blattman, J. N.; Antia, R.; Sourdive, D. J. D.; Wang, X.; Kaech, S. M.; Murali-Krishna, K.; Altman, J. D.; Ahmed, R. Estimating the Precursor Frequency of Naive Antigen-Specific CD8 T Cells. *J Exp Med* **2002**, *195* (5), 657–664. https://doi.org/10.1084/jem.20001021.

(495) Gong, C.; Linderman, J. J.; Kirschner, D. Harnessing the Heterogeneity of T Cell Differentiation Fate to Fine-Tune Generation of Effector and Memory T Cells. *Front Immunol* **2014**, *5*, 57. https://doi.org/10.3389/fimmu.2014.00057.

(496) Simon, S.; Labarriere, N. PD-1 Expression on Tumor-Specific T Cells: Friend or Foe for Immunotherapy? *Oncoimmunology* **2017**, *7* (1). https://doi.org/10.1080/2162402X.2017.1364828.

(497) Wolf, Y.; Anderson, A. C.; Kuchroo, V. K. TIM3 Comes of Age as an Inhibitory Receptor. *Nat Rev Immunol* **2020**, *20* (3), 173–185. https://doi.org/10.1038/s41577-019-0224-6.

(498) Jubel, J. M.; Barbati, Z. R.; Burger, C.; Wirtz, D. C.; Schildberg, F. A. The Role of PD-1 in Acute and Chronic Infection. *Front Immunol* **2020**, *11*. https://doi.org/10.3389/fimmu.2020.00487.

(499) Wykes, M. N.; Lewin, S. R. Immune Checkpoint Blockade in Infectious Diseases. *Nat Rev Immunol* **2018**, *18* (2), 91–104. https://doi.org/10.1038/nri.2017.112.

(500) Kohrt, H. E.; Shu, C.-T.; Holmes, S. P.; Weber, J.; Lee, P. P. Heterogeneity within Antigen-Specific T Cell Responses Revealed by Differential Dynamics of TCR Downregulation. *Blood* **2004**, *104* (11), 3851–3851. https://doi.org/10.1182/blood.V104.11.3851.3851.

(501) Meyer-Olson, D.; Brady, K. W.; Bartman, M. T.; O'Sullivan, K. M.; Simons, B. C.; Conrad, J. A.; Duncan, C. B.; Lorey, S.; Siddique, A.; Draenert, R.; Addo, M.; Altfeld, M.; Rosenberg, E.; Allen, T. M.; Walker, B. D.; Kalams, S. A. Fluctuations of Functionally Distinct CD8+ T-Cell Clonotypes Demonstrate Flexibility of the HIV-Specific TCR Repertoire. *Blood* **2006**, *107* (6), 2373–2383. https://doi.org/10.1182/blood-2005-04-1636.

(502) Woolaver, R. A.; Wang, X.; Krinsky, A. L.; Waschke, B. C.; Chen, S. M. Y.; Popolizio, V.; Nicklawsky, A. G.; Gao, D.; Chen, Z.; Jimeno, A.; Wang, X.-J.; Wang, J. H. Differences in TCR Repertoire and T Cell Activation Underlie the Divergent Outcomes of Antitumor Immune Responses in Tumor-Eradicating versus Tumor-Progressing Hosts. *J Immunother Cancer* **2021**, *9* (1), e001615. https://doi.org/10.1136/jitc-2020-001615.

(503) Nurieva, R.; Wang, J.; Sahoo, A. T-Cell Tolerance in Cancer. *Immunotherapy* **2013**, *5* (5), 513–531. https://doi.org/10.2217/imt.13.33.

(504)   Zhang, Z.; Liu, S.; Zhang, B.; Qiao, L.; Zhang, Y.; Zhang, Y. T Cell Dysfunction and Exhaustion in Cancer. *Front Cell Dev Biol* **2020**, *8*. https://doi.org/10.3389/fcell.2020.00017.

(505)   Jensen, P. E.; Weber, D. A.; Thayer, W. P.; Westerman, L. E.; Dao, C. T. Peptide Exchange in MHC Molecules. *Immunol Rev* **1999**, *172*, 229–238. https://doi.org/10.1111/j.1600-065x.1999.tb01368.x.

(506)   Ilca, F. T.; Neerincx, A.; Wills, M. R.; Roche, M. de la; Boyle, L. H. Utilizing TAPBPR to Promote Exogenous Peptide Loading onto Cell Surface MHC I Molecules. *PNAS* **2018**, *115* (40), E9353–E9361. https://doi.org/10.1073/pnas.1809465115.

(507)   Saini, S. K.; Schuster, H.; Ramnarayan, V. R.; Rammensee, H.-G.; Stevanović, S.; Springer, S. Dipeptides Catalyze Rapid Peptide Exchange on MHC Class I Molecules. *PNAS* **2015**, *112* (1), 202–207.

(508)   Olivo Pimentel, V.; Yaromina, A.; Marcus, D.; Dubois, L. J.; Lambin, P. A Novel Co-Culture Assay to Assess Anti-Tumor CD8+ T Cell Cytotoxicity via Luminescence and Multicolor Flow Cytometry. *J Immunol Methods* **2020**, *487*, 112899. https://doi.org/10.1016/j.jim.2020.112899.

(509)   Neubert, N. J.; Soneson, C.; Barras, D.; Baumgaertner, P.; Rimoldi, D.; Delorenzi, M.; Fuertes Marraco, S. A.; Speiser, D. E. A Well-Controlled Experimental System to Study Interactions of Cytotoxic T Lymphocytes with Tumor Cells. *Front Immunol* **2016**, *7*, 326. https://doi.org/10.3389/fimmu.2016.00326.

(510)   Cattaneo, C. M.; Dijkstra, K. K.; Fanchi, L. F.; Kelderman, S.; Kaing, S.; van Rooij, N.; van den Brink, S.; Schumacher, T. N.; Voest, E. E. Tumor Organoid–T-Cell Coculture Systems. *Nat Protoc* **2020**, *15* (1), 15–39. https://doi.org/10.1038/s41596-019-0232-9.

(511)   Zhang, L. Multi-Epitope Vaccines: A Promising Strategy against Tumors and Viral Infections. *Cell Mol Immunol* **2018**, *15* (2), 182–184. https://doi.org/10.1038/cmi.2017.92.

(512)   Dorosti, H.; Eslami, M.; Negahdaripour, M.; Ghoshoon, M. B.; Gholami, A.; Heidari, R.; Dehshahri, A.; Erfani, N.; Nezafat, N.; Ghasemi, Y. Vaccinomics Approach for Developing Multi-Epitope Peptide Pneumococcal Vaccine. *J Biomol Struct Dyn* **2019**, *37* (13), 3524–3535. https://doi.org/10.1080/07391102.2018.1519460.

(513)   Kar, T.; Narsaria, U.; Basak, S.; Deb, D.; Castiglione, F.; Mueller, D. M.; Srivastava, A. P. A Candidate Multi-Epitope Vaccine against SARS-CoV-2. *Sci Rep* **2020**, *10* (1), 10895. https://doi.org/10.1038/s41598-020-67749-1.

(514) Kim, Y.; Ponomarenko, J.; Zhu, Z.; Tamang, D.; Wang, P.; Greenbaum, J.; Lundegaard, C.; Sette, A.; Lund, O.; Bourne, P. E.; Nielsen, M.; Peters, B. Immune Epitope Database Analysis Resource. *Nucleic Acids Res* **2012**, *40* (W1), W525–W530. https://doi.org/10.1093/nar/gks438.

(515) Matsue, H.; Matsue, K.; Walters, M.; Okumura, K.; Yagita, H.; Takashima, A. Induction of Antigen-Specific Immunosuppression by CD95L CDNA-Transfected "killer" Dendritic Cells. *Nat Med* **1999**, *5* (8), 930–937. https://doi.org/10.1038/11375.

(516) Ng, S. B.; Turner, E. H.; Robertson, P. D.; Flygare, S. D.; Bigham, A. W.; Lee, C.; Shaffer, T.; Wong, M.; Bhattacharjee, A.; Eichler, E. E.; Bamshad, M.; Nickerson, D. A.; Shendure, J. Targeted Capture and Massively Parallel Sequencing of Twelve Human Exomes. *Nature* **2009**, *461* (7261), 272–276. https://doi.org/10.1038/nature08250.

(517) Ng, S. B.; Buckingham, K. J.; Lee, C.; Bigham, A. W.; Tabor, H. K.; Dent, K. M.; Huff, C. D.; Shannon, P. T.; Jabs, E. W.; Nickerson, D. A.; Shendure, J.; Bamshad, M. J. Exome Sequencing Identifies the Cause of a Mendelian Disorder. *Nat Genet* **2010**, *42* (1), 30–35. https://doi.org/10.1038/ng.499.

(518) Kisielow, P. How Does the Immune System Learn to Distinguish between Good and Evil? The First Definitive Studies of T Cell Central Tolerance and Positive Selection. *Immunogenetics* **2019**, *71* (8), 513–518. https://doi.org/10.1007/s00251-019-01127-8.

(519) Yadav, M.; Jhunjhunwala, S.; Phung, Q. T.; Lupardus, P.; Tanguay, J.; Bumbaca, S.; Franci, C.; Cheung, T. K.; Fritsche, J.; Weinschenk, T.; Modrusan, Z.; Mellman, I.; Lill, J. R.; Delamarre, L. Predicting Immunogenic Tumour Mutations by Combining Mass Spectrometry and Exome Sequencing. *Nature* **2014**, *515* (7528), 572–576. https://doi.org/10.1038/nature14001.

(520) Wang, D.; Bodovitz, S. Single Cell Analysis: The New Frontier in 'Omics.' *Trends Biotechnol* **2010**, *28* (6), 281–290. https://doi.org/10.1016/j.tibtech.2010.03.002.

(521) Demmers, L. C.; Kretzschmar, K.; Van Hoeck, A.; Bar-Epraïm, Y. E.; van den Toorn, H. W. P.; Koomen, M.; van Son, G.; van Gorp, J.; Pronk, A.; Smakman, N.; Cuppen, E.; Clevers, H.; Heck, A. J. R.; Wu, W. Single-Cell Derived Tumor Organoids Display Diversity in HLA Class I Peptide Presentation. *Nat Commun* **2020**, *11* (1), 5338. https://doi.org/10.1038/s41467-020-19142-9.

(522) Page, D. B.; Yuan, J.; Redmond, D.; Wen, Y. H.; Durack, J. C.; Emerson, R.; Solomon, S.; Dong, Z.; Wong, P.; Comstock, C.; Diab, A.; Sung, J.; Maybody, M.; Morris, E.; Brogi, E.; Morrow, M.; Sacchini, V.; Elemento, O.; Robins, H.; Patil, S.; Allison, J. P.; Wolchok, J. D.; Hudis, C.; Norton, L.; McArthur, H. L. Deep Sequencing of T-Cell Receptor DNA as a Biomarker of Clonally Expanded TILs in Breast Cancer after Immunotherapy. *Cancer Immunol Res* **2016**, *4* (10), 835–844.

(523)   Sims, J. S.; Grinshpun, B.; Feng, Y.; Ung, T. H.; Neira, J. A.; Samanamud, J. L.; Canoll, P.; Shen, Y.; Sims, P. A.; Bruce, J. N. Diversity and Divergence of the Glioma-Infiltrating T-Cell Receptor Repertoire. *PNAS* **2016**, *113* (25), E3529–E3537.

(524)   Gras, S.; Chen, Z.; Miles, J. J.; Liu, Y. C.; Bell, M. J.; Sullivan, L. C.; Kjer-Nielsen, L.; Brennan, R. M.; Burrows, J. M.; Neller, M. A.; Khanna, R.; Purcell, A. W.; Brooks, A. G.; McCluskey, J.; Rossjohn, J.; Burrows, S. R. Allelic Polymorphism in the T Cell Receptor and Its Impact on Immune Responses. *J Exp Med* **2010**, *207* (7), 1555–1567. https://doi.org/10.1084/jem.20100603.

(525)   Redeker, A.; Arens, R. 'Reverse Evolution' in T Cell Biology. *Nat Immunol* **2020**, *21* (4), 360–362. https://doi.org/10.1038/s41590-020-0639-z.

(526)   Tran, T. M.; Ivanyi, P.; Hilgert, I.; Brdicka, T.; Pla, M.; Breur, B.; Flieger, M.; Ivasková, E.; Horejsí, V. The Epitope Recognized by Pan-HLA Class I-Reactive Monoclonal Antibody W6/32 and Its Relationship to Unusual Stability of the HLA-B27/Beta2-Microglobulin Complex. *Immunogenetics* **2001**, *53* (6), 440–446. https://doi.org/10.1007/s002510100353.

(527)   Seok, J.; Warren, H. S.; Cuenca, A. G.; Mindrinos, M. N.; Baker, H. V.; Xu, W.; Richards, D. R.; McDonald-Smith, G. P.; Gao, H.; Hennessy, L.; Finnerty, C. C.; López, C. M.; Honari, S.; Moore, E. E.; Minei, J. P.; Cuschieri, J.; Bankey, P. E.; Johnson, J. L.; Sperry, J.; Nathens, A. B.; Billiar, T. R.; West, M. A.; Jeschke, M. G.; Klein, M. B.; Gamelli, R. L.; Gibran, N. S.; Brownstein, B. H.; Miller-Graziano, C.; Calvano, S. E.; Mason, P. H.; Cobb, J. P.; Rahme, L. G.; Lowry, S. F.; Maier, R. V.; Moldawer, L. L.; Herndon, D. N.; Davis, R. W.; Xiao, W.; Tompkins, R. G.; Abouhamze, A.; Balis, U. G. J.; Camp, D. G.; De, A. K.; Harbrecht, B. G.; Hayden, D. L.; Kaushal, A.; O'Keefe, G. E.; Kotz, K. T.; Qian, W.; Schoenfeld, D. A.; Shapiro, M. B.; Silver, G. M.; Smith, R. D.; Storey, J. D.; Tibshirani, R.; Toner, M.; Wilhelmy, J.; Wispelwey, B.; Wong, W. H. Genomic Responses in Mouse Models Poorly Mimic Human Inflammatory Diseases. *PNAS* **2013**, *110* (9), 3507–3512. https://doi.org/10.1073/pnas.1222878110.

(528)   Takao, K.; Miyakawa, T. Genomic Responses in Mouse Models Greatly Mimic Human Inflammatory Diseases. *PNAS* **2015**, *112* (4), 1167–1172.

(529)   Vandamme, T. F. Use of Rodents as Models of Human Diseases. *J Pharm Bioallied Sci* **2014**, *6* (1), 2–9. https://doi.org/10.4103/0975-7406.124301.

(530)   Godec, J.; Tan, Y.; Liberzon, A.; Tamayo, P.; Bhattacharya, S.; Butte, A. J.; Mesirov, J. P.; Haining, W. N. Compendium of Immune Signatures Identifies Conserved and Species-Specific Biology in Response to Inflammation. *Immunity* **2016**, *44* (1), 194–206. https://doi.org/10.1016/j.immuni.2015.12.006.

APPENDIX A: COPYRIGHT PERMISSIONS

CCC RightsLink®

Home   Help   Email Support   Sign in   Create Account

ACS Publications
Most Trusted. Most Cited. Most Read.

Therapy-Induced MHC I Ligands Shape Neo-Antitumor CD8 T Cell Responses during Oncolytic Virus-Based Cancer Immunotherapy

Author: J. Patrick Murphy, Youra Kim, Derek R. Clements, et al

Publication: Journal of Proteome Research

Publisher: American Chemical Society

Date: Jun 1, 2019

Copyright © 2019, American Chemical Society

PERMISSION/LICENSE IS GRANTED FOR YOUR ORDER AT NO CHARGE

This type of permission/license, instead of the standard Terms and Conditions, is sent to you because no fee is being charged for your order. Please note the following:

- Permission is granted for your request in both print and electronic formats, and translations.
- If figures and/or tables were requested, they may be adapted or used in part.
- Please print this page for your records and send a copy of it to your publisher/graduate school.
- Appropriate credit for the requested material should be given as follows: "Reprinted (adapted) with permission from {COMPLETE REFERENCE CITATION}. Copyright {YEAR} American Chemical Society." Insert appropriate information in place of the capitalized words.
- One-time permission is granted only for the use specified in your RightsLink request. No additional uses are granted (such as derivative works or other editions). For any uses, please submit a new request.

If credit is given to another source for the material you requested from RightsLink, permission must be obtained from that source.

BACK   CLOSE WINDOW